Non-contact Temperature Measurement of Stainless Steel in a TIG Welding Process

William Nichols Pollard, Jr.

Thesis submitted to the faculty of the Virginia Polytechnic Institute and State University in partial fulfillment of the requirements for the degree of

Master of Science
In
Mechanical Engineering

M.A. Pierson
K.S. Ball
A.T. Duggleby

October 9, 2009
College Station, TX

Keywords: Temperature Measurement, Infrared, Non-contact, TIG Welding, One-color, Two-color

Non-contact Temperature Measurement of Stainless Steel in a TIG Welding Process

William Nichols Pollard, Jr.

Abstract

The goal of this research was to design and test an experimental setup capable of performing a TIG welding process and acquiring temperature measurements near the weld with the use of an infrared spot sensor. The data collected can then be used to validate a computer simulation that models the exact same process. An experimental setup was built, and preliminary temperature data were collected. It was determined that infrared measurements taken at the arc contain excessive amounts of interfering radiation emanating from the welding zone. The optimal angle of orientation is normal to the weld line. In this way an infrared spot sensor can be focused on an area just down weld of the arc where the temperatures remain relatively high and thermal gradients, although still large, are at a minimum. Additional data were collected from thermocouples to validate the infrared sensor results and also to provide additional data that can be compared to a computer model. Sources of error were identified and recommendations were made as to how they can be avoided or minimized.

Acknowledgements

I would like to first thank my committee members for all of their guidance, input and support throughout the duration of my postgraduate education at Virginia Tech. Your collective insight was invaluable and the skills I learned from you will remain with me throughout my career. I would like to especially thank Dr. Pierson for helping me secure suitable lab space in which I could conduct my research and also for helping me acquire a teaching assistantship when other options for funding were limited.

I would like to thank Dr. Huxtable for taking me on as a teaching assistant, which allowed me to support myself when a research assistantship was not available. I thoroughly enjoyed my experience working as a TA. I also appreciate you allowing me to borrow equipment from the lab. Without a thermocouple welder on site at my research location, data collection would have been very inconvenient to say the least.

I would also like to thank the entire staff of the Mechanical Engineering Department for all of their assistance in their various capacities. Without your help my day to day tasks would not have flowed as smoothly.

My lab mates deserve special thanks for the excellent company they provided me. Many a laugh were shared in both the $[FT]^2L$ Lab and the Unmanned Systems Lab. Beware of Jimmy's invitations into his office.

I give my utmost thanks to my family, especially my father. Your support and encouragement has served me well over the years.

Special thanks goes to Sua Lee, who knows exactly how to smack motivation into me when I feel like slacking.

Table of Contents

Table of Figures

1 INTRODUCTION

Real-time process control is an important aspect in quality assurance for a variety of manufacturing processes. In welding processes the quality of the weld is dependent on the temperature at which the weld is formed and the speed at which it cools. In order to both provide high quality welds and reduce waste material, accurate real-time temperature monitoring is beneficial.

Temperature measurement generally falls under two categories: contact and non-contact. Many are familiar with contact temperature measurement methods. These methods include thermometers, thermocouples or any other device that is brought into direct physical contact with a material. On the other hand, non-contact temperature measurements do not make physical contact with their targets. These devices typically rely on the transmission of radiative energy, and because of their non-intrusive nature they do not act as a local heat sink which could disrupt thermal profiles.

Both types of temperature measurement techniques have their pros and cons. Direct contact methods are usually less expensive, less complicated and easier to install. However, they tend to respond slowly, absorb thermal energy, and resist ideal thermal contact. Non-contact methods provide superior response times, and ensuring proper thermal contact is a non-issue. Furthermore, they are well suited for applications in hostile environments where there may be relatively high temperatures, or extremely low pressures. For these reasons, a non-contact method of temperature measurement is the preferred mode for monitoring welding processes. The downside is that they are expensive and can be complicated to set up. Additionally, infrared sensors can be difficult to calibrate if the emissivity of the material is unknown.

Most non-contact systems rely on infrared radiation. Infrared radiation is a subset of electromagnetic radiation, obeying the same laws as those for visible light, radio waves and x-rays. The physical difference between these different kinds of radiation is wavelength. The infrared spectrum includes wavelengths from 0.7 μm to 100 μm, which ranges from the longer wave visible region to the shorter microwave region, and it is commonly associated with room temperature thermal radiation. Any object with a temperature above absolute zero emits some level of radiation in the infrared spectrum, and the radiative power, P, emitted by any object above absolute zero is proportional to the fourth power of the absolute temperature, T, of that object, as is shown in Equation 1.

$$P \propto \varepsilon T^4 \qquad 1$$

The intensity of infrared power emitted by an object is further dependent on optical properties of the object. The emissivity, ε, which takes on values $0 \leq \varepsilon \leq 1$, is of central importance in order to accurately determine an object's surface temperature for a detected amount of radiative power. The emissivity of an object is dependent on several factors. These factors include surface material, surface finish, surface color, surface texture, surface temperature, the optical waveband under observation, and also the angle of incidence at which the object is viewed. For instance, organic materials tend to emit better than metallic materials, and oxidized metals tend to emit better than polished materials. Darker surface colors imply better emission than lighter colors, but this is not always true. Surface texture also affects emittance. Given two otherwise similar objects, the rougher of the two will generally appear warmer to an infrared detector. The emissivity for a piece of tungsten at 1600 K can range from $0.1 \leq \varepsilon \leq 0.5$ depending on what wavelength of infrared radiation is being examined. For these particular values, the range of wavelengths is $0.4\ \mu m \leq \lambda \leq 5.0\ \mu m$. [1] Lastly, an everyday

occurrence can be used to show the dependence on angle of incidence. A good example of this is the mirages of puddles that are evident on distant asphalt surfaces, typically seen as we drive down roads on hot days. The watchful observer will notice that these puddles are not present on cool days. However, as we approach them, these puddles never seem to get closer. This is caused by both a rapid temperature gradient in the air and also from viewing the puddle at a shallow angle of viewing incidence. If we were to change the angle at which we saw the puddle, then it would disappear. This is analogous to how the emissivity of a surface changes with its viewed angle of incidence.

As the temperature increases, the radiative power increases and the wavelength at which the greatest radiative flux occurs will shift to smaller wavelengths. This phenomenon is known as Wien's displacement law, and it asserts that the wavelength with the highest radiative intensity is inversely proportional to a blackbody's surface temperature. The term blackbody is elaborated upon in the following paragraph, and Wien's displacement law is shown graphically in Figure 1-1.

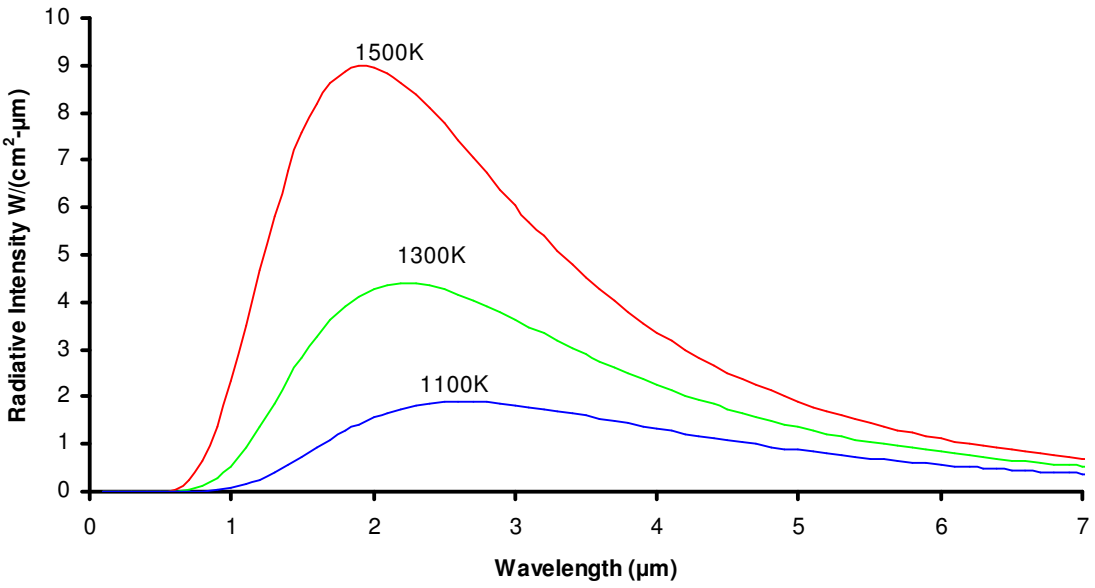

Figure 1-1. Radiative intensity as a function of wavelength and surface temperature. Wien's displacement law is evident as surface temperature increases the peak intensity shifts to the left.

A blackbody is an object that absorbs and emits all energy across all wavelengths. According to the first law of thermodynamics, there are three possible outcomes when radiative energy at a given wavelength strikes the surface of an object. The object will absorb, reflect or transmit the incident radiation. This relationship is shown in Equation 2.

$$\alpha_\lambda + \rho_\lambda + \tau_\lambda = 1 \qquad 2$$

Where α is the absorptance, ρ is the reflectance, and τ is the transmittance. The subscript λ is meant to indicate that each of these parameters is dependent upon the wavelength. These three outcomes are all functions of wavelength. In addition, an object that absorbs a certain proportion of incident radiative energy will also emit the same proportion of radiative energy at that same wavelength. Therefore, absorptivity, α_λ, and emissivity, ε_λ, can be considered equal, making a good absorber a good emitter for a given wavelength.

Infrared sensors use two different approaches to calculate the temperature of an object. Some sensors utilize a one-color approach, whereas other sensors utilize a two-color approach. In one-color thermometry the emissive power at a single wavelength or over a narrow waveband is used to determine temperature. This method requires that the emissivity of the object is both known and constant within the temperature range of the application. If the emissivity of the surface is known, then one-color thermometry can provide satisfactory results. It is evident that variations in emissivity with respect to wavelength, among other factors, can be problematic in determining the emissive power of the surface to be measured. This is the motivation behind two-color thermometry.

Unless spectral tests are performed on a material, the real surface emissivity is usually unknown. By making a graybody assumption, this difficulty can be overcome. A graybody is an object with properties between those of a blackbody and a perfect reflector. That is, a graybody maintains a constant emissivity (<1) across all wavelengths. Objects that exhibit true graybody behavior do not exist in the real world, but if two narrow adjacent wavebands or wavelengths are considered, the graybody assumption is adequate and often used in engineering applications. Graybody behavior is shown graphically in Figure 1-2.

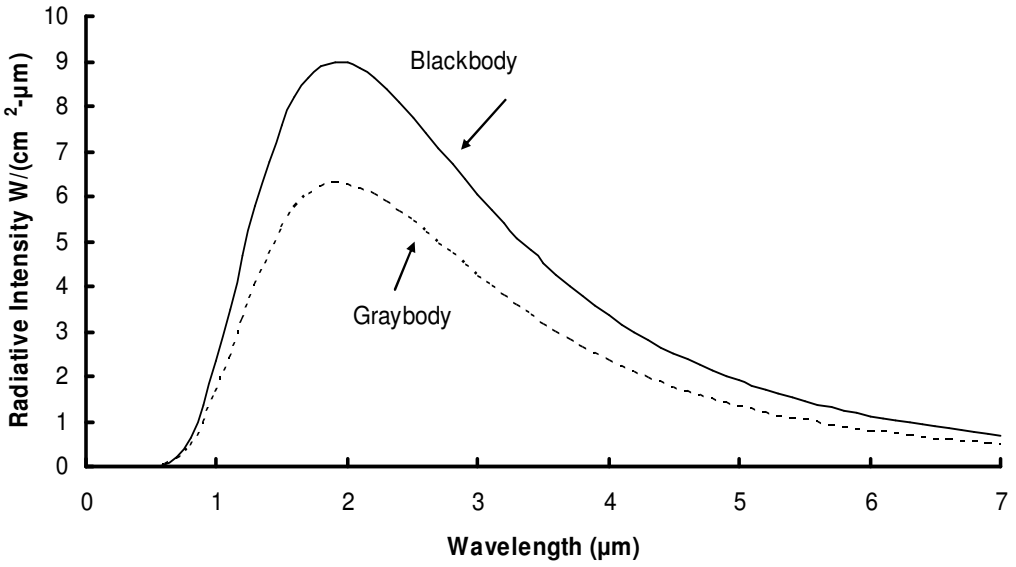

Figure 1-2. Graybody versus blackbody behavior at a constant temperature

A two-color detector measures the emissive output at two wavelengths or two narrow adjacent wavebands and then takes a ratio of the two signals. Using the graybody assumption, the emissivity of both wavelengths or both wavebands is considered approximately equal, and the ratio of the power signals is unaffected by an unknown emissivity, provided that the emissivity is constant for the two wavebands. Considerable error can be introduced when the emissivity of one does not vary at the same rate as the other with respect to changes in surface temperature. Some two-color detectors have the ability to toggle between one and two color modes. This feature can be useful for verifying results and determining which mode works best for an application.

Welding processes can involve complex geometries and extreme conditions, making non-contact temperature measurement an ideal solution for real-time process monitoring. At the same time, however, welding also introduces unique sources of complication due to the process by which materials are joined together. Tungsten inert gas (TIG) welding is a process that passes a

large electrical current from a tungsten electrode, located on the torch tip, through the work piece. Since the torch tip does not make contact with the work piece, an electrical arc forms, and temperatures in excess of 15 000°C may be achieved. This presents two difficulties with respect to non-contact temperature measurement. Both the hot tungsten electrode and the electric arc can reflect radiation off the work piece. The diffuse reflections cause sensors to detect artificially high temperatures, effectively overwhelming the surface temperature of the work piece. In order to properly employ infrared techniques, these effects must be mitigated.

The goal of this research is to design a test rig whereby multiple temperature measurements can be made in real time during a TIG welding process and also to have a computer simulation of the same process that can be validated by the experimental temperature data collected by the infrared sensor and the thermocouples. To achieve this goal, it is imperative that error sources be identified and mitigated so that confidence in the results can be achieved. The computer modeling is a separate research project being carried out concurrently with the experimental counterpart. The modeling will be done using ANSYS and it will utilize a magneto hydrodynamic (MHD) package in order to physically describe all aspects of the molten weld pool. One of the primary benefits of such a model is accurate prediction of weld quality and strength without having to do destructive tests on finished welded components. The goal is that by validating thermal aspects of the 3D model, confidence in the computer modeling can be achieved.

2 LITERATURE REVIEW

Welding engineers have recognized the need for accurate temperature measurements to provide better process control and ensure welds of a higher quality. It is important to make sure that welds occur at a desired temperature and cool appropriately. By monitoring thermal gradients, it is possible to determine several characteristics of the weld, all of which are pertinent to the quality of the weld. Among these characteristics are weld bead width, penetration depth, weld position control, and cooling rates. Some manufacturers do not have adequate methods for monitoring thermal changes, and this inadequacy limits their process control. [2] Due to the demand for tight tolerances and precise components, it is becoming increasingly necessary to examine methods for real-time temperature monitoring in welding processes. It has been shown that the temperature history of a material undergoing a welding process is one aspect that requires further investigation. [3] In the past there has been significant research looking at both predictive heat transfer models and real-time infrared sensing and the benefits each can provide in welding applications.

2.1 Early Weld Modeling and Temperature Measurement

J.M. Barry and his colleagues [4] improved an existing mathematical model for the welding of a steel plate held subject to several requirements. Previous models provided reasonable predictions when a) the temperature was below 1000°F, b) the location of interest was more than 1.5 plate thicknesses away from the weld, and c) the plate was fully penetrated by the weld.

In Barry's set up they took temperature measurements near single pass submerged arc bead-on-plate welds on steel plates with thicknesses of ¼, ½, and 1 inch. Several methods were used to measure the surface temperature. These methods included temperature sensitive lacquers, radiation pyrometry, and thermocouples that were welded directly to the plate. Table 2-1 shows the conditions under which the welding occurred.

Table 2-1. TIG welding conditions used by Barry, et al. Used with permission of Welding Journal editor, Mary Ruth Johnsen, American Welding Society, [4].

Welding Parameters	**¼ inch**	**½ inch**	**1 inch**
Voltage [V]	29	33	33.5
Amperage, [A]	330	550	850
Travel speed, [ipm]	10-65	10-43	60
Filler metal diameter, [in]	⅛	⅛	⅛
Filler metal feed rate, [ipm]	72	114	198
Nozzle height, [in]	¾	¾	¾

It was found that the temperature sensitive lacquers were useful in determining the location of where peak temperatures occurred, but they were not able to tell the magnitude of the peak temperatures. Efforts involving radiation pyrometry were not completely successful because of large variations in the emissivity even after the surface had been treated in an attempt to control the optical properties of the target plate. Radiation pyrometry was useful, however, in showing that the thermocouple did in fact provide an accurate measurement of the surface temperature.

Chromel-alumel, also known as K-type, thermocouples with a 0.004 in. diameter provided the only useful method for collecting data, and they were welded to the top surface and edges of the target plate. Generally, thermocouples are not ideal for arc welding processes because of the

rapid thermal cycles and the high thermal conductivity of the base metal. It has been shown that thermocouples are subject to significant error when arc welding aluminum, but with steel as the base metal, whose thermal conductivity is lower by one order of magnitude, they provide acceptable measurements. Several previous investigations even examined temperature internal to the base metal by drilling holes and inserting the thermocouples. The main problem with this approach is that by altering the geometry of the work piece, the temperature profile is also affected. As a result, the temperatures measured by the thermocouples are not representative of realistic base metal temperatures.

Two useful temperature relationships are presented using point source considerations. Equation 3 models the peak top surface temperature at a point some distance away from a partial penetration weld [5]. The equation is presented below and it is subject to the following assumptions: constant thermal properties, constant torch speed, straight torch travel, no heat transfer from the surface of the metal to the surroundings, edges are far enough away as to not influence the temperature profile, and steady state conditions.

$$\frac{1}{T_p - T_0} = 4.13\rho\ C_p Y\ t\left(\frac{V}{Zq}\right) + \frac{1}{T_m - T_0} \qquad 3$$

Where: T_p is the peak temperature [°F], T_0 is the initial uniform temperature of plate [°F], ρ is the density of the base metal [lb/ft^3], C_p is the specific heat of the base metal [Btu/lb °F], Y is the distance from the weld [ft], t is the thickness of base metal [ft], V is the arc travel speed [ft/hr], Z is the fraction of total arc heat delivered to the base metal [%], q is the arc power [Btu/hr], and T_m is the melting temperature [°F].

A significant source of error in this equation is a direct result of the thermal gradient that exists between where the weld occurs and the point at some distance away from the weld where the temperature is to be determined. Because the thermal properties of steel vary considerably with changes in temperature, approximations of these quantities must be made which in turn introduce error into the model.

Equation 4 models the peak temperature on the bottom side of the base metal. This relationship has been shown to be accurate in instances where the bead width to base metal thickness ratio is less than 1.4.

$$\frac{1}{T_{pB} - T_0} = 2.41\rho\overline{C_p}\left(\frac{Vt^2}{Zq}\right)\left[\frac{b/t}{erf\ b/t}\right] + \frac{0.5}{T_m - T_0} \qquad 4$$

Where: T_{pB} = centerline peak temperature of the base metal bottom face [°F], and b is the effective width of the heat source [ft].

The above equation is an improvement over earlier methods of calculating peak bottom surface temperatures, but it is still rough. It does provide answers that are of the correct magnitude when b is taken as the width of the weld bead. [4]

Using a bead width to base metal thickness ratio between 0.8 and 1.2, Figure 2-1 shows experimental data plotted along curves calculated by Equation 4. The experimental data points fall mostly within the predicted range. This implies that a strip heating source model may be useful for some applications.

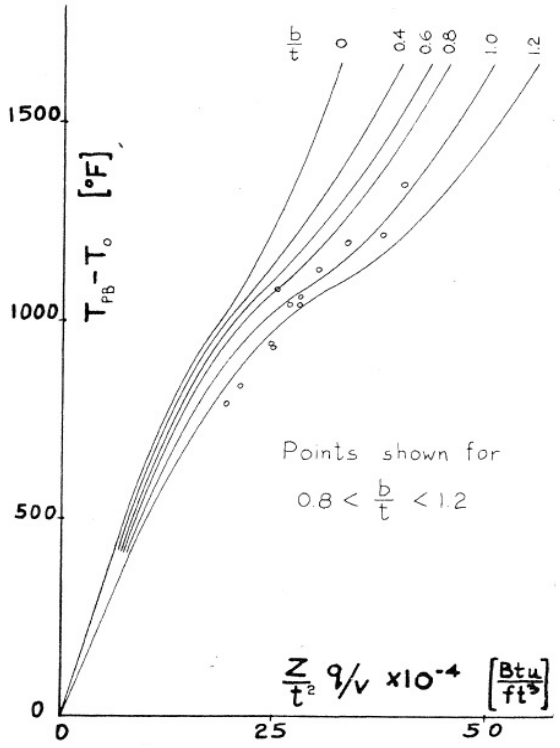

Figure 2-1. Peak temperature rise of base metal bottom face along the weld centerline, using various bead width to base metal thickness ratios. Used with permission of Welding Journal editor, Mary Ruth Johnsen, American Welding Society, [4].

Both of these calculations have limited utility, but are adequate predictors in the absence of more advanced methods or techniques. Each model is subject to its own restrictions, and neither one exactly mirrors a real physical process. In the scope of this project, a more important consideration is that neither method offers real-time feedback of temperatures, temperature changes or temperature gradients.

The following paper is described in detail because it outlines important initial considerations for the development of an experimental setup where a TIG welding process can be monitored with an infrared sensor. Among these initial considerations are where to focus the infrared sensor on the work piece, what type of infrared sensor is best suited for the application, and how to determine an appropriate value of the emissivity of the work piece.

In 1963, Ramsey et al. [6] carried out some of the earliest research on using infrared temperature measurement as applied to welding processes. Their main objective was to determine if in fact infrared radiation could be used reliably to determine the base metal surface temperature profile and from that information further correlate those patterns with changes in welding parameters such as penetration depth and bead width. If such a signal could be accurately acquired, then new methodologies for welding control, manipulation of welding current and welding speed, could be made available.

First, Ramsey et al. deemed it wise to determine the temperature profile of the metal around the weld pool so that the best location for temperature measurement could be located. In welding processes involving thin plates, heat flows parallel to the plane of the base metal and is essentially two dimensional. Figure 2-2 illustrates the welding coordinate systems for this model.

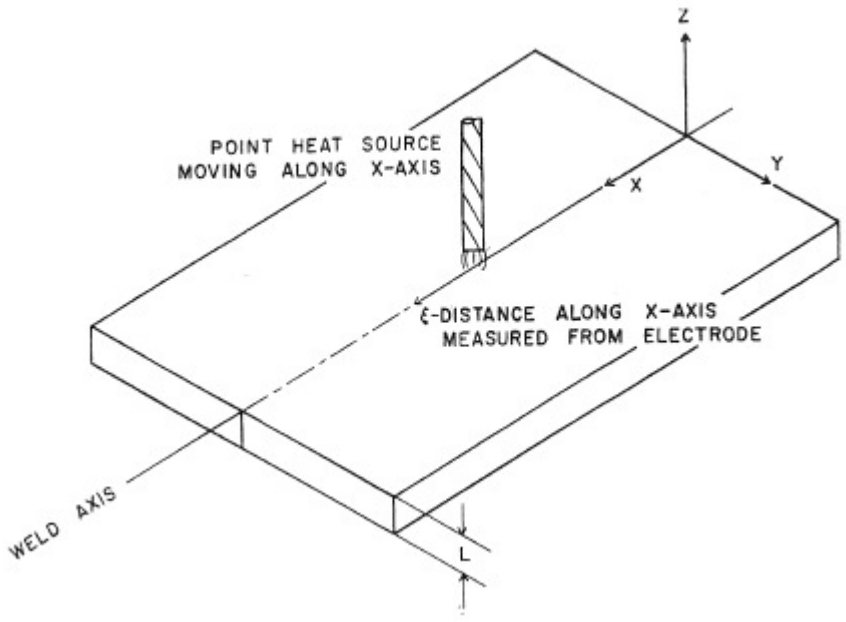

Figure 2-2. Weld coordinate system for heat flow calculations. Used with permission of Welding Journal editor, Mary Ruth Johnsen, American Welding Society, [6].

In the following formulations the arc is considered a moving point source, heat losses are negligible, all pertinent physical properties are considered temperature independent, and latent heat effects associated with phase change are neglected. Equation 5 describes the behavior of such a system.

$$\frac{\partial^2 T}{\partial \xi^2} + \frac{\partial^2 T}{\partial y^2} + \frac{\partial^2 T}{\partial z^2} = -\frac{2\lambda v \partial T}{\partial \xi} + \frac{2\lambda \partial T}{\partial t} \qquad 5$$

Where: $\xi = x\text{-}vt$, or the distance of the point considered from the point source of heat moving in the ¯x direction, y is the coordinate perpendicular to weld axis along surface of base metal, z is the coordinate perpendicular to weld axis and surface of base metal, v is the velocity of point source of heat, t is time, T is the temperature above initial temperature, $\lambda = \rho c/2k$, ρ is the density, c is the specific heat, and k is the thermal conductivity.

The solution to this equation depends on the boundary conditions. In this particular instance the following assumptions will be used: 1) the target plate is considered infinite in length in the x and y direction, 2) the plate is of some finite thickness, 3) there is a point source of heat input, and 4) steady-state is assumed, i.e. $\partial T/\partial t = 0$. For this particular trial the base metal was a ⅛-inch thick aluminum plate. The two-dimensional temperature profile is shown in Figure 2-3.

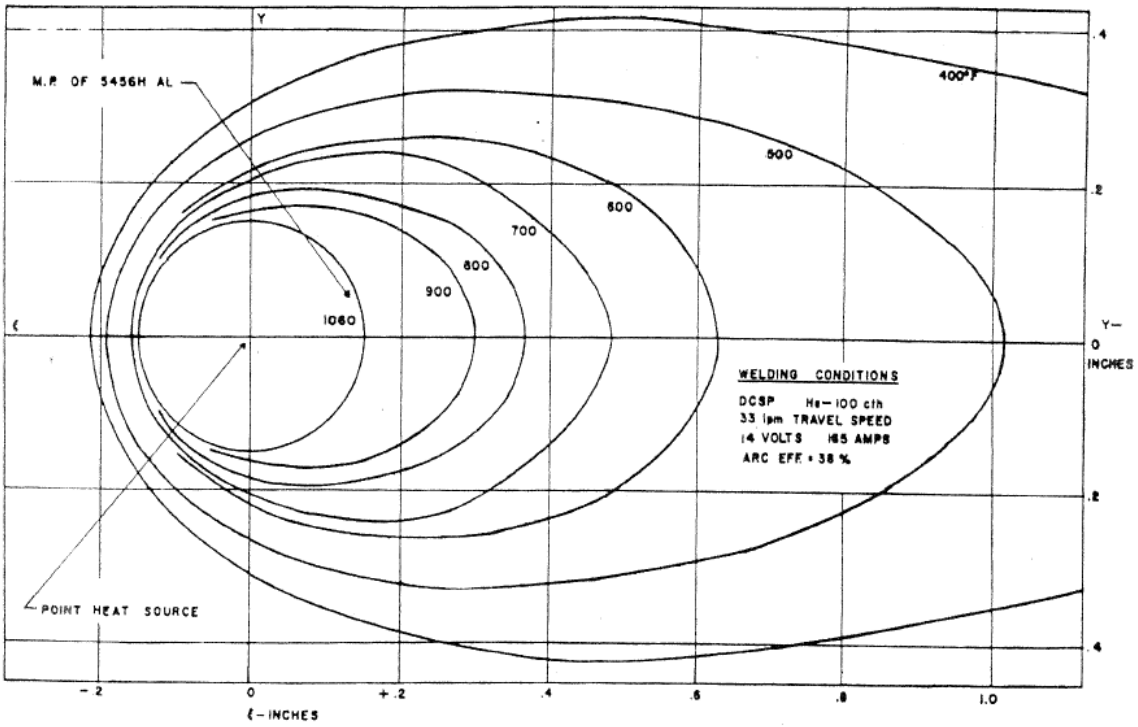

Figure 2-3. Two dimensional temperature profile of 1/8-in. thick aluminum plate. Used with permission of Welding Journal editor, Mary Ruth Johnsen, American Welding Society [6].

From the information gained by this particular solution to Equation 5, two difficulties arose on where to focus the infrared sensor in relation to the welding torch if the infrared signal was to be used for controlling the arc welding process. If the sensor were placed behind the torch the isotherms would be large, but the information provided will in a sense arrive late, limiting the full utility of a proper control system. If the sensor were placed in front of the torch then isotherms would be much smaller, thermal gradients far steeper, and the size of the sensing area would be smaller. Furthermore, since the sensing element will have some finite area a relatively large range of isotherms will exist in the focal area.

In the following experiments, two types of radiometers were used. One radiometer was a fixed position sensor, and the other radiometer performed line scans. For the fixed radiometer experiments the sensor was focused on a target area of ⅛ in. diameter. Large thermal gradients

were expected at locations on and near the weld bead. Large variations in emissivity were also expected. It was thought that by sensing these rapid temperature changes with a scanning radiometer, the weld bead could be identified. The scanning radiometer is essentially a fixed point radiometer traveling along a path and it provides a two dimensional temperature profile. In these experiments the scanning radiometer was held at a focal distance of 30 inches, and it scanned at a rate of 50 inches per second. The viewing area was diamond-shaped with dimensions of 20 x 200 mils with the major axis normal to the scanning direction.

The gas tungsten arc welding (GTAW) tests were carried out with an automatic welding head with arc voltage control, using helium as the shielding gas supplied at a rate of 100 cfm. The radiometer was mounted in such a way that it did not move relative to the welding torch. During the bead-on-plate welds the torch was held stationary while the target plate was allowed to move. The base metal target plates were the same in each trial, and they used a 5456H-343 Aluminum alloy with dimensions of ⅛ x 6 x 20 in.

For the fixed radiometer experiments, the investigators calculated the emissivity of the aluminum plate by using an electrical strip heater and K-type thermocouples mounted to the back of the plate. Various surface treatments were applied to maximize emissivity, thus reducing reflection from the electrode. Depending on the surface treatment applied to the target plate, the emissivity values ranged from 0.31-0.46 for a graphite film treatment or from 0.85-0.90 for a Sicon or Mono-Seal surface treatment, both of which are black enamels. The untreated aluminum stock as it arrived had an emissivity value ranging from 0.05-0.11.

Next, radiation interference experiments were performed. The researchers varied the horizontal and vertical angles at which the radiometer was positioned in relation to the target plate. At a fixed vertical angle of 35° and a focal area 0.28 in. ahead of the arc, the signal was

reduced by a factor of seven as the horizontal angle was increased from 30° to 90°, where a 90° angle is perpendicular to the weld seam. With the horizontal angle fixed at 90°, the vertical angle was varied from 60° to 30°, producing a 50% reduction in the output signal. Moreover, the minimum signal output still corresponded to a surface temperature of 1150°F, which is approximately 100°F above the melting point for aluminum. The calculated temperature as shown previously in Figure 2-3 was less than 400°F. Upon visual inspection of the plate, it was clear that the surface upon which the radiometer was focused had not undergone a phase change. From these trials it is evident that the signal response is very sensitive to the viewing angle, and the temperature measurement error is indicative of radiative interference from the arc area. These effects must be mitigated in order to achieve reliable results.

They also explored targeting areas at distances ranging from 0.28-0.50 in. ahead of the torch with a horizontal angle of 26° and a vertical angle of 37°. The output signal was dramatically reduced as the focus area was moved away from the arc. Even at the furthest distance, the corresponding temperatures measured were too high, a result most likely due to radiative interference. A mechanical shield was introduced to the setup to attenuate the signal noise. With the shield in place the signal output was reduced by a factor of four. Additionally, an indium antimonide filter which is opaque to wavelengths less than 7.5 μm was implemented with the assumption that a large portion of the interfering radiation would be in that region. As it turned out, the signal was attenuated so severely as to render it useless.

The main results of the fixed radiometer trials indicated that although the signal was correlated with welding parameters, it was not a unique function of target plate surface temperature, and reproducibility was poor between trials. These signals were too greatly affected by either varying emissivities or arc interference, and as such were not suitable signals for

controlling the welding process. Figure 2-4 shows a typical output signal from the fixed radiometer experiments. Note that even though all welding parameters were held constant, there remains significant variation in the signal. This variation was as large as ±10%.

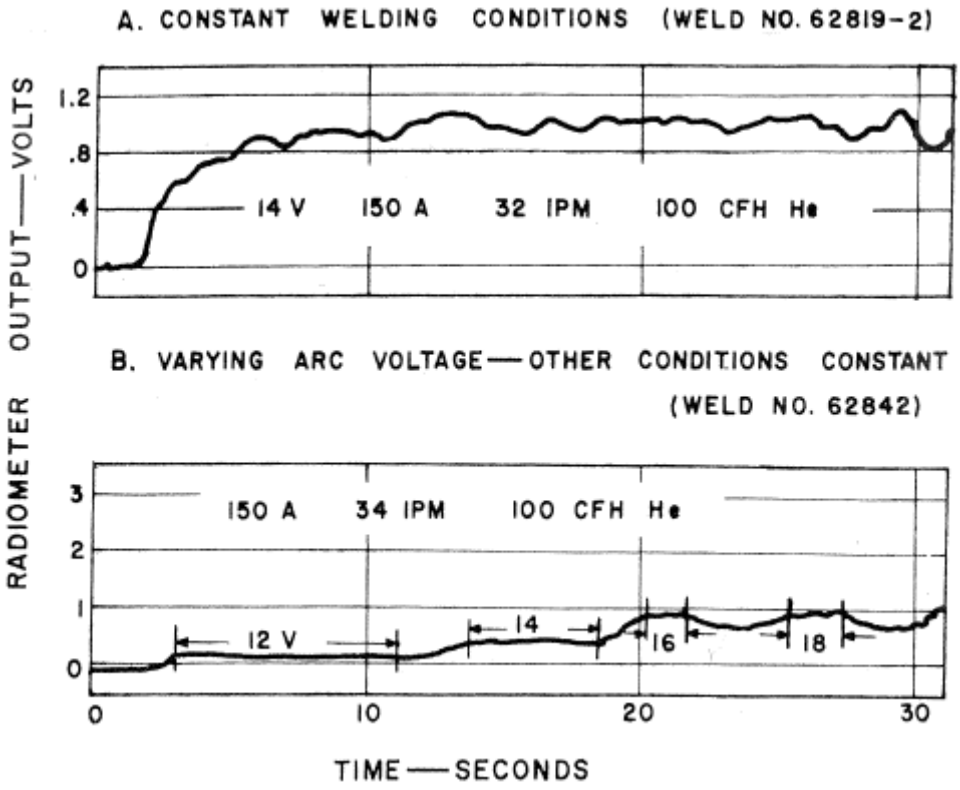

Figure 2-4. Signal output from the fixed radiometer during two trials with the focal area 0.5 inches behind the weld and on the centerline. A) Constant welding conditions; B) Varied voltage as indicated. Used with permission of Welding Journal editor, Mary Ruth Johnsen, American Welding Society, [6].

In the scanning radiometer experiments, the radiometers were first calibrated using heated steel strips and oscillograph recordings of the output pulses. This was done to show that the radiometer was accurately capturing the width of the steel bars. The instrument was attached to the weld torch and focused on a scan line location 0.6 inches behind the weld. If the scanning radiometer was focused any closer to the target than 0.6 inches, then the signal became unusable as a result of the noise from the arc. The scanning radiometer was positioned 30 in. from the plate so that the scan lines could extend 1.5 in. on either side of the weld seam.

The scanning radiometer encounters similar problems as the fixed radiometer in terms of temperature measurement of a specific location. However, the advantage of a scanning radiometer is that it can provide information relating to the width of the weld bead. Oftentimes, the half-height of the scan can be used to determine the width of the scanned object, but in GTAW there is significant interference which affects the signal amplitude. Thus, it makes more sense to assess the width of the scanned object by averaging measurements at the half-height, and at a point 0.3 in. above the signal baseline. A typical series of scan lines is shown in Figure 2-5.

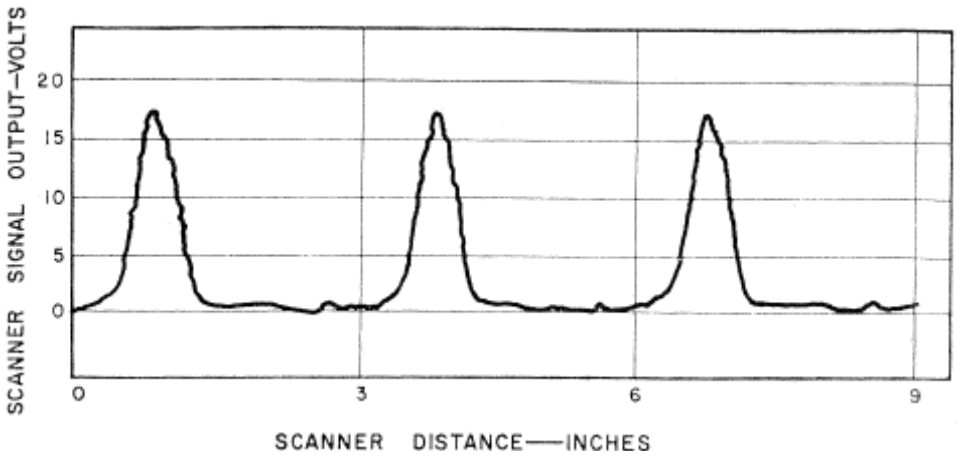

Figure 2-5. Typical series of scan lines obtained with a scanning radiometer during GTAW. The scan line was focused 0.6 inches behind the arc and on the centerline. Used with permission of Welding Journal editor, Mary Ruth Johnsen, American Welding Society, [6].

Welds were then made on ⅛ in. thick 5456H aluminum plates, while each welding parameter was varied independently. For each incremental variation in each parameter, a new weld was made. The results were then averaged and plotted. Results from the scanning radiometer indicated a correlation between the scanner signal dimensions and the weld bead width. Although there was interference from the tungsten electrode, it did not render the signal unusable

as it did in the fixed radiometer tests. Figure 2-6 shows a plot of bead widths as a function of the welding current.

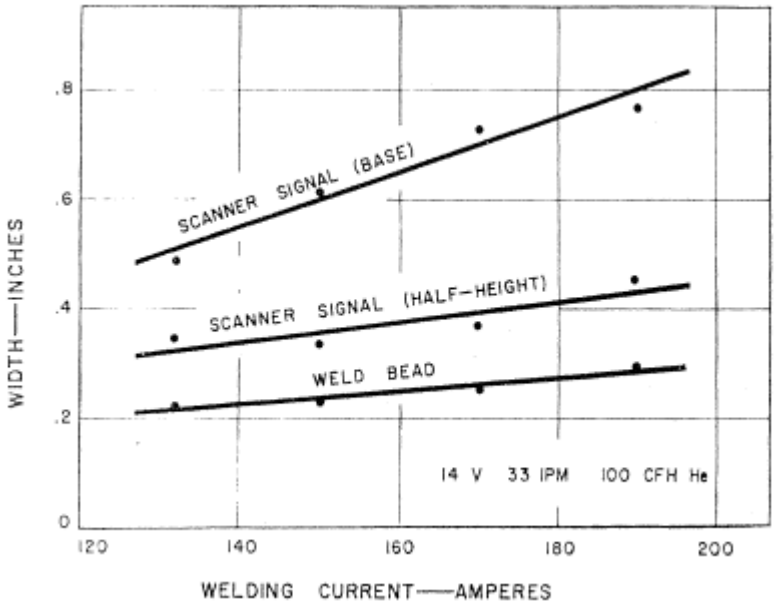

Figure 2-6. Weld bead width and line scan signal width as a function of welding current on a 1/8 inch thick plate of 5456H aluminum. Used with permission of Welding Journal editor, Mary Ruth Johnsen, American Welding Society, [6].

Useful conclusions from this pioneering experiment are that scanning type radiometers show promise in controlling a GTAW process. For the fixed radiometers there was simply too much noise, and no useful signal could be obtained, especially with regards to temperature measurement. It was also shown that GTAW appears more amenable to infrared control because less interfering radiation is emitted by the hot tungsten tip than is emitted from the molten droplets that are involved in the gas metal arc welding process. The research shows that if infrared signals are to be used for a control system, then the best position to focus them is just behind the weld even though this results in a time lag.

Although these experiments do not provide a way of accurately or reliably detecting surface temperatures of base metals with an infrared sensor, they do provide valuable insight as to how

infrared sensors may be implemented in a GTAW process, and how infrared sensors can be expected to behave. For one, it appears that infrared sensors should be oriented so that they focus on an area behind the arc. The thermal gradients in this region are not as severe as they are in front of the arc, providing a more even zone in which to detect radiative intensity. The fixed radiometer experiments undeniably show that interference from the arc zone has a detrimental effect on the instrument's ability to accurately detect radiative emissions that are the sole result of the base metal's surface temperature. In any subsequent research in this area, negative effects from the electrode and the arc should be expected and countermeasures must be taken to minimize their influence. Lastly, scanning radiometers provide seemingly useful information for determining the width of the weld seam. With some calibration these signals, while not yet proven to reliably measure surface temperature, may still be useful for controlling a welding application.

2.2 IR Temperature Measurement of Base Metals

The research described below is discussed in great detail because the current project follows their objectives very closely. The research done by Farson, et al. also proposes a variety of experiments designed to isolate and account for unwanted radiative effects. It is hoped that the final outcome of the current research will provide results that are closer to the true temperature than ±50°F.

In 1998 Farson, Richardson, and Li [7] presented a paper in which they described their methodology as to how they were able to obtain reasonable temperature measurements of the base metal after filtering out extraneous radiation from both the arc and the tungsten electrode. Using various shielding gases during the GTAW process, they made weld beads and used a spectrograph to characterize the arc radiation. A typical arc spectra consists of many sharp peaks

and significant broadband radiation between the wavelengths of 225-850 nm. At wavelengths around 1000 nm, there is almost no radiation. Figure 2-7 shows a typical spectral power distribution from a gas tungsten arc with Argon as the shielding gas.

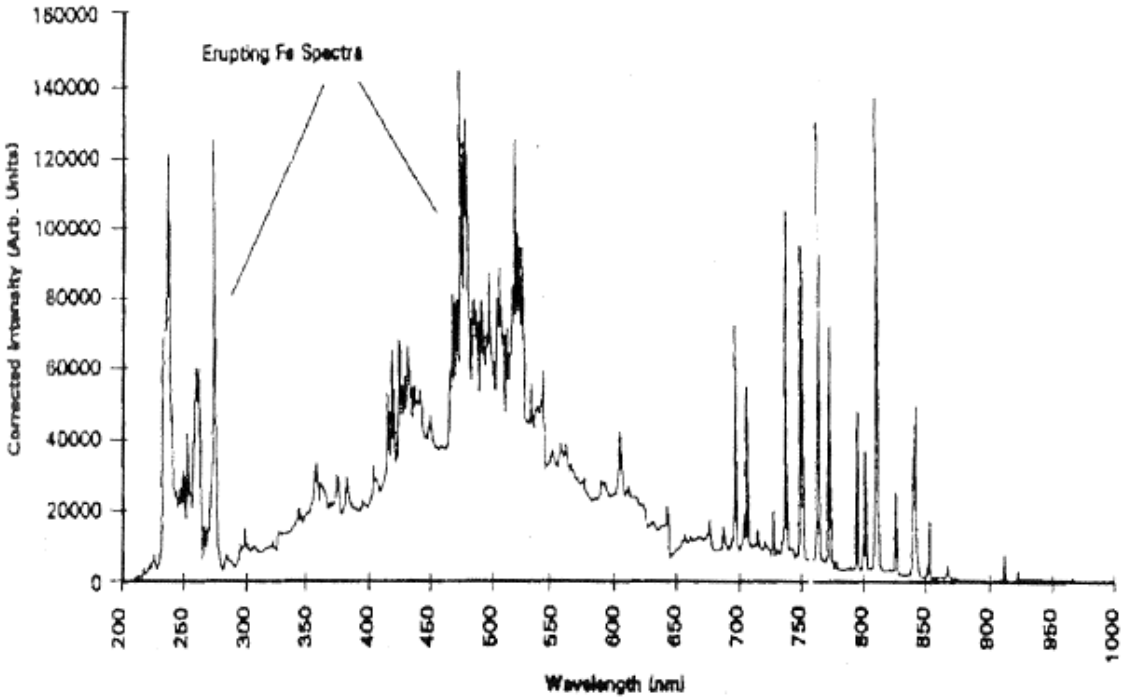

Figure 2-7. Spectral power distribution (in arbitrary units) from a gas tungsten arc using Argon as the shielding gas. Used with permission of Welding Journal editor, Mary Ruth Johnsen, American Welding Society, [7].

Knowing this, an optical band pass filter centered at 1064 nm with a range of 15.2 nm and 45% transmission was incorporated into the experimental set up. A special gas cup was also designed and installed directly on the torch so that it acted as a mechanical shield against unwanted radiation originating from the tungsten electrode. In all, the experimental setup consisted of a gas cup and shield, a focus head with an optical filter connected to the welding torch, a fiber optic cable to transmit the signal, a silicon photodetector, a light power meter, an A/D converter, and a PC unit.

The base metal in this experiment was AISI 1250 sheet metal, which is a carbon steel, with dimensions measuring 6 x 2½ x ⅛ inches, and each target was wire brushed and chemically treated in an effort to reduce surface emissivity variations. The sensing point on the base metal was 0.43 inches behind the arc and 0.20 inches off of the weld centerline. A helium-neon laser was used to line up the infrared sensing device. Welding took place at 100A DC with 25 ft^3/h of Argon and a weld speed of 0.079 in/s.

The first set of experiments investigated the application of an optical band pass filter without the presence of a mechanical shield in order to determine the effectiveness of the filter. Under both the filtered and unfiltered conditions, the response showed four characteristic regions. In the first region there is a characteristic large initial spike which is thought to be predominantly due to arc effects since both the torch and work piece are still cool in comparison. After the initial spike, the response drops considerably. In the second region, the optical power initially rises quickly, reaching a maximum and then leveling off. In this region, the tungsten electrode temperature increases quickly to some maximum value from room temperature. During this time the electrode is rapidly heating and the base metal is heating at a much slower rate, making it difficult to determine how much each component is contributing to the total radiation. In the third region the optical power again increases rapidly to a maximum value. This rise is attributed to the heating of the base metal. The fourth region shows a nearly constant optical power output until shut off time. This is believed to have occurred because the system had reached steady state conditions. Once the welder was shut off an exponential curve, typical of mass undergoing a cooling process, was evident. Two plots are shown in Figure 2-8 comparing the effect of the optical filter on the optical output power of the trials. The four distinct regions previously described are also shown.

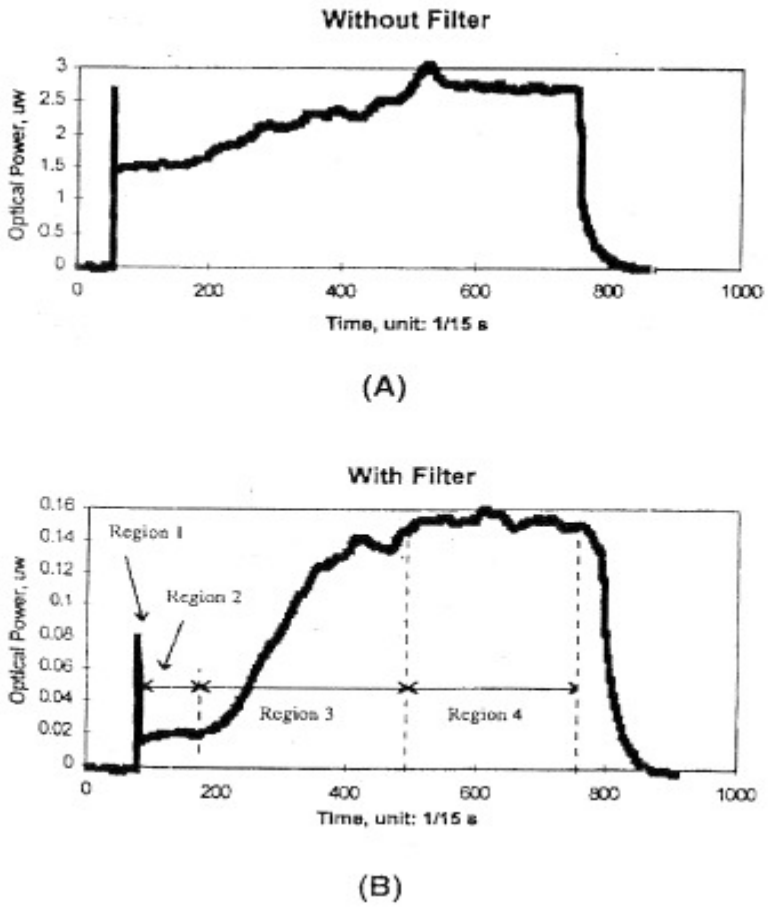

Figure 2-8. Comparison of normal sensor outputs in a GTAW process (A) without and (B) with an optical band-pass filter. Plots (A) and (B) are not to scale. Used with permission of Welding Journal editor, Mary Ruth Johnsen, American Welding Society, [7].

By comparing plots of both of these cases it was determined that the optical filter would attenuate most of the radiation from the arc. Although it was evident that some arc radiation remained, the extent of the arc contribution to the total signal was still unknown. Furthermore, it was still unknown how much of an effect the hot electrode had on the total signal. This uncertainty prompted a set of experiments designed to determine the contribution of each interfering component.

To answer these questions, experiments using the optical band-pass filter were designed in which a water-cooled copper block served as the base metal. Cooling the copper block maintained the base metal at a low enough temperature as to remove its contribution to the total radiative output. By holding all welding parameters constant and varying the length of the weld arc the contribution of arc interference could be measured. To assess the arc interference component the initial transience as shown in Region 1 of Figure 2-8 was measured and taken as the value of arc radiation. Figure 2-9 is a graph of optical power output as a function of time for an arc length of 0.079 in. on a water-cooled copper anode. The plot also shows the arc component and electrode component of the total signal output. The drop in optical output at 20 seconds is believed to be caused by surface changes on the anode.

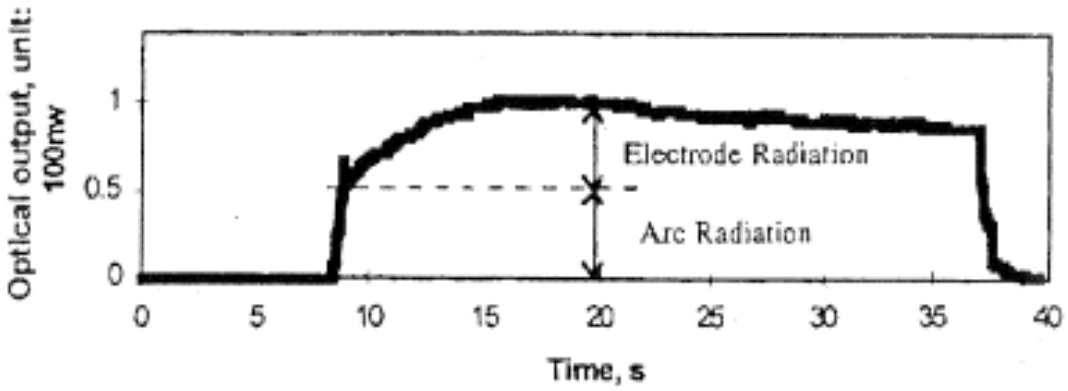

Figure 2-9. Filtered optical power output during a GTAW process on a water-cooled copper anode and arc length of 2mm. Used with permission of Welding Journal editor, Mary Ruth Johnsen, American Welding Society, [7].

It was predicted that as the arc length increases, the signal at arc initiation would increase because at greater arc lengths the sensor captures more diffuse radiation from the arc. The prediction was accurate, and by subtracting the arc component from the total signal, the contribution of the electrode could be indirectly measured, assuming that the copper block was

cooled in such a way that its surface temperature contributed a negligible amount, if at all, to the total signal output. Data were collected at arc lengths of 0.039, 0.079, and 0.118 in. A linear regression was performed on the results and extrapolated to an arc length of 0 in. The total signal output and its two components, arc and electrode, are shown in Figure 2-10.

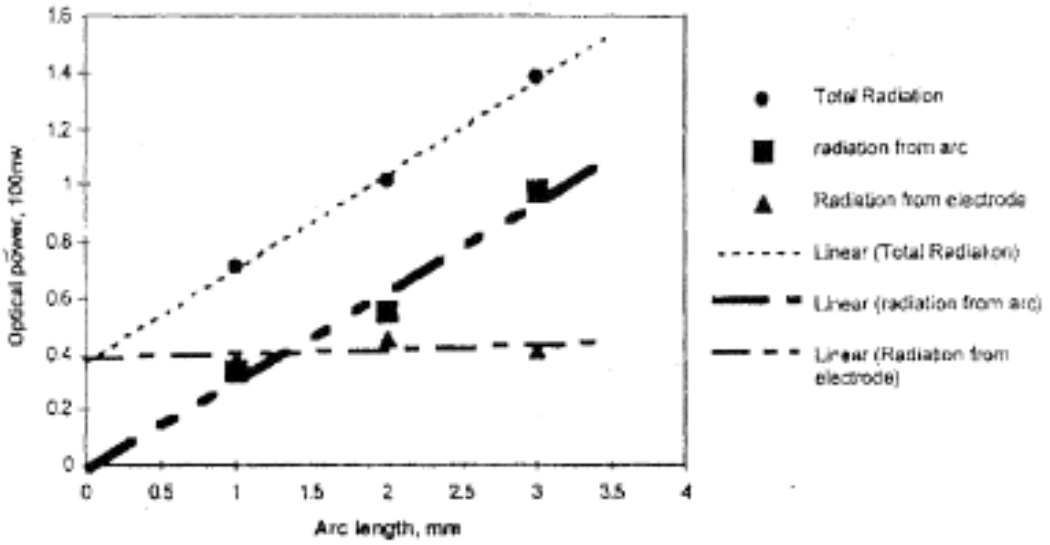

Figure 2-10. Total optical power and its components for arc lengths of 0.039, 0.079, and 0.118 in. Used with permission of Welding Journal editor, Mary Ruth Johnsen, American Welding Society, [7].

The above data show that even with a band-pass filter, interferences from both the arc and the electrode are still significant contributors to the signal output. Knowing this, it is imperative to make an effort to physically block these two interfering sources of radiation. One method by which this can be achieved is to install a mechanical shield between the sensor and torch tip.

The next set of experiments sought to determine how much of the arc and electrode radiation could be blocked by implementing a specially designed gas cup with a radiation shield attached to it. The trials were conducted on the water-cooled copper anode using the optical band-pass filter. All welding parameters were held constant except the height of the shield. After several attempts with the shield at heights ranging from <0.039-0.157 in., the researchers determined

that the shield height must be less than 0.039 in. in order for it to be effectively implemented. At a height of 0.157 in, the arc component of the signal was virtually the same as if no shield were in place, whereas the component from the electrode continued to increase. When the shield was lowered to 0.031 in. the optical power was reduced to 6nW. The total signal output and its components are shown in Figure 2-11 as functions of shield height.

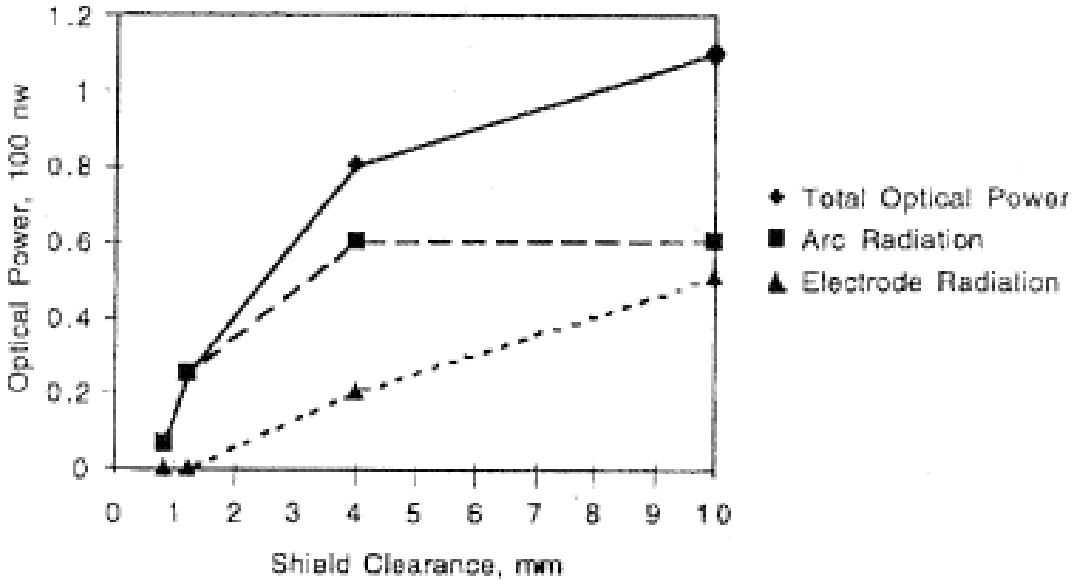

Figure 2-11. Effects of shield height on optical power output. Used with permission by Welding Journal editor, Mary Ruth Johnsen, American Welding Society, [7].

As compared to the output signal in the initial trials shown previously in Figure 2-8 (B), this power, which is believed to have come solely from the arc area, is nearly one order of magnitude smaller. Because of the relatively small contribution of the interference to the overall signal, it was believed that it would not adversely impact a temperature calibration for the optical power output.

In order to calibrate the system, thermocouples were welded to the sensing points using a micro-spot welder. The response of the thermocouples was measured at various welding

currents. Samples were taken at a rate of 10 Hz, and sampling lasted for 60 seconds which was long enough to take the temperature of the target from room temperature up to a maximum value where steady state conditions were achieved. The data from the calibration trials were averaged and a curve of temperature as a function of optical power output was formulated. This calibration was valid only for temperatures above 450°F, at which point the thermal radiation from the sensing spot began to dominate the thermal radiation from the tungsten electrode. Their calibration curve yielded results that were accurate with in ±50°F. These experiments showed that by incorporating a mechanical shield and an optical filter it is possible to measure the base metal temperature near the weld pool using infrared techniques.

Bicknell, Smith and Lucas [8] performed thermal imaging and subsequent image processing in a series of experiments applied to a TIG welding process. As usual, the major obstacle in measuring the top face temperature is overcoming the unwanted affects of both the arc and the tungsten electrode. Knowing the spectral characteristics of both sources of interference, they employed optical filtering techniques to help mitigate these two sources of interference.

In their paper, the weld pool was modeled as a blackbody emitter with an emissivity of less than one. This was done because the emission spectrum of real objects with temperatures above absolute zero is continuous. Furthermore, the melting point of steel was used as a parameter in the Planck equation, and the results indicated that the weld pool emission spectrum peaks around 1300 nm. They also provide a range on the emissivity of steel being from 0.3–0.6. The arc, however, radiates in a different manner which is a result of electron discharge phenomenon. As such, the arc has a line spectrum since energy is released at discrete wavelengths. The arc has radiation spikes up to a wavelength of 1250 nm. Beyond that wavelength there are no emission lines. These results indicate that successful thermal imaging should be possible at wavelengths

just beyond 1300 nm. This was indeed shown to be the case, and as the wavelengths of the high pass optical filters increased from 800 nm to 1500 nm, improvements were noticed.

The experimental setup consisted of the following: a welding rig, a thermal imager, and a computer with all necessary software. The welding rig was fitted with a linear traverse and a rigidly mounted welding torch. In this way the position and speed of the work piece could be controlled relative to the welding torch. The thermal imager used was an Electrophysics 7292 model with a 1500 nm optical band pass filter mounted on the lens assembly. The imager was positioned behind the arc. The computer was used to manipulate the TIG welder and traverse table settings as well as capture and analyze images. The welder used was a Weldcraft TIG welder with a maximum welding current of 300A. For the shielding gas, a mixture of 95% Ar and 5% H_2 was used. The test pieces used were type 304 stainless steel plates of 0.039, 0.079, and 0.118 in. in thickness, and moved at a rate of 0.079 in/s along the traverse table. Experiments were carried out with both a continuous and pulsed TIG weld.

The results of this study concluded that it was possible to use thermal imaging to detect the width of the weld bead even though the reflection of the tungsten electrode in the weld pool itself could not be filtered out. Under both welding operations, continuous and pulsed, the welding process was amenable to real time control by varying welding parameters such as welding current, welding speed, and pulsing signals.

2.3 Applications of Infrared Signals to Control TIG Welding Processes

Using variations on and improvements of the aforementioned technologies, the investigators mentioned below have made efforts to exploit these now reliably measurable signals in order to advance both the capabilities and the overall quality of robotic welding. The welding parameters of greatest interest are joint tracking, weld bead width, and weld penetration. Other aspects of the welding process can now also be observed, measured, and used for control purposes. Among these are cooling rates, part misalignment, and geometric variations. Knowledge of the thermal profile and its behavior as these different aspects vary provides much improved control systems and as a result a more reliable automated welding process.

2.3.1 Joint Tracking

Research investigating how infrared signals could be used to correct for part offsets, specifically in the case of butt joints, has been carried out by several teams [9, 10, 11]. As the process becomes more automated, the welder's insight into the task becomes more limited, reducing the capability of eliminating potential problems in real time. For example, a robot will produce similar welds consistently as it follows its programmed instructions. However, should any unanticipated deviations occur, especially with regard to the placement of the part(s) relative to the torch position, welding defects are likely to occur.

Joint tracking systems are available, but they have their limitations. The first tracking systems used a mechanical device to trace the joint. Not only did the probes wear out after a while, but they were also designed for specific part orientations. Another system used two passes of the torch to store in memory the continuous coordinate locations where the joint was located.

The first pass was made with the arc off and its path of travel was remembered. The second pass was made with the arc on as it followed the path stored in its memory. The drawback of such a system is that it has no ability to correct itself in real time. The preferred method of joint tracking would be to weld and sense simultaneously. The challenge to this method is how to accurately follow the seam, especially in the presence of large amounts of reflected radiation in the vicinity of the weld pool.

This challenge can be overcome by monitoring the temperature distributions around the weld pool, and these observations are typically presented in the form of isothermal contour maps or line scans. Isothermal contour maps are used to give a global picture of the temperature field whereas line scans are used to show how the temperature fluctuates across a line perpendicular to the weld path. Changes in plate alignment affect the thermal distribution. In the case of the butt joint, when the plates are properly aligned there is symmetry in the temperature profile. However, when the plates are misaligned, then the profile is clearly asymmetric. The same is also true should the arc begin to wander away from the joint. As the arc begins to move away from the joint, infrared signal begin to take on a characteristic asymmetrical shape in the vicinity of the arc. This asymmetry is a result of the resistance to heat flow, leading to decreased temperatures on the side of the joint with no direct heat input. In their research they showed that changes in the weld joint could be recognized by changes in the temperature profile, and that these changes in temperature profile could be used as a means for tracking butt joints.

2.3.2 Bead Width and Weld Penetration

It is not currently possible to determine the depth to which a weld pass penetrates its target without subsequently destroying the target and visually inspecting its cross section. As a result, many researchers have correlated the geometry of the weld pool to the weld penetration. Since

the quality of a weld is very dependent on the weld penetration, accurate measurement of the bead width is of the utmost importance.

Banerjee and Chen [12] used weld bead width to predict welding penetration. Different mathematical methods were used, but it was decided that the gradient technique offered the most hope. The gradient technique makes use of the characteristic change in the temperature gradient at the solid-liquid interface as a result of the varying emissivities. These trends are made evident by plotting the temperature gradient versus the x-coordinate. Using infrared line scan measurements and the gradient technique, they calculated the bead width as the distance from the left hand valley to the right hand side peak. The bead width found from the gradient technique shows a linear relation when plotted against the real bead width measured after the welding run, indicating that this technique is reliable.

As an extension of his previous research, Banerjee, et al. [13] showed that infrared detection of bead width, and subsequently penetration depth, can be influenced by shielding gas composition and minor element content in the base metal. In a comparison between 100% pure argon and 100% pure helium shielding gases, they found that the 100% argon shielding gas typically provides a larger macroscopic temperature gradient. The choice of shielding gas also affects the temperature distribution and the depth of the weld penetration. Minor element content refers to the elemental composition of an alloy. To insert different metals into the base metal, full penetrations were made in the base metal and then pieces of aluminum or iron sulfide were forced into the openings. They were able to show that minor elements can alter the temperature gradient. Minor elements change the fluid properties of the molten pool, thus influencing the convective heat transfer process. Metals can have either a positive or negative surface tension coefficient, and this determines the pattern of the flow in the weld pool, which can be either

radially inward or outward. Radial inward flows, associated with metals having a positive surface tension coefficient, tend to produce deeper penetration whereas radial outward flows, associated with metals having a negative surface tension coefficient, tend to produce a wider weld pool.

Similar experiments have been carried out and verified by Menaka, et al [14]. Since the penetration depth is related to the bead width, by manipulating one, it is also possible to manipulate the other, provided all other factors remain constant. The usual modes of increasing bead width are increasing the welding current or decreasing the welding speed.

Wikle [15] made a slight variation to the previously mentioned approach when he implemented a point infrared sensor to an automated welding rig. He controlled this system with National Instruments LabVIEW package. Feedback control with the infrared system was used to monitor the process. Wikle used a proportional-integral control process to ensure that the point of interest was receiving heat from the torch at the desired rate. To adjust the heat flux, the current was varied. Wikle found that by using the infrared sensor and computer controls, he could maintain a constant penetration depth profile, even in the presence of increasing gaps between two plates in a butt joint.

Sometimes welds are of a more complicated geometry. For example, parts may be tapered or contain sections in which the thickness varies along the path of the welding torch. Nagarajan et al. [10, 16] determined that it was possible to control the depth of weld penetration in real time even if the thickness of the target varied. They specially made steel components that exhibited both gradually changing thicknesses and step changing thicknesses. These parts were then welded and the output from the infrared sensors was subsequently analyzed.

The top face temperature varied inversely with the plate thickness. As the plate got thinner the temperature increased. This makes sense because the same heat input is being applied to a smaller volume of material, in effect providing less mass that needs to be heated. As the plate thickness decreased gradually, there was a corresponding gradual increase in the signal output from the infrared sensor. As the plate thickness changed suddenly, there was an abrupt increase in signal output. Similarly, when the plate thickness suddenly increased, a sudden decrease in temperature was evident.

They verified that the temperature profile changes when plate thickness varies, and from this information it is also possible to exercise some control on welding penetration. They further noted that geometric patterns of isotherms provide the best signals to study changes in joint penetration and variations in plate thicknesses.

The welding parameters of joint tracking, bead width and weld penetration all play important roles in producing quality welds. Nagarajan, et al. [17] showed that all three measurements could be controlled with one infrared sensor. When there are imperfections in the joints, their presence manifests itself as asymmetries clearly noticeable in the outer edges of the temperature profile. On the other hand, in order to measure the weld bead width, attention is directed towards the center nearer the weld pool, which is largely unaffected by reasonable changes in joint alignment. Since weld penetration is related to the weld bead width, this information is also known. Furthermore, any variations in plate thickness can also be detected and used as a control parameter.

Oftentimes welding occurs on a base metal that rests on a relatively horizontal surface. However in some applications this orientation may not be possible resulting in the need to weld base metals that have some angle in inclination. Fan, et al. [18] conducted research investigating

the feasibility of using infrared thermography to monitor the uphand welding process with particular attention to weld bead width and weld penetration. They found that it was possible to use infrared techniques with such a part orientation, and they also showed that bead width and weld penetration were affected by the inclination angle of the work piece. As the angle of inclination of the work piece increased the bead width decreased and the weld penetration increased. The implication of this is that the shape of the weld pool changes with varying base metal inclination angles. Therefore, in order to maintain a uniform weld penetration, the heat input to the work piece must be reduced.

2.3.3 Sensing of Cooling Rates

When high strength steels are initially fabricated, they undergo very specific heating cycles in order to create a specific microstructure that provides optimal mechanical properties. During a welding process, rapid heating and cooling can result in solid-state changes that may destroy the metal's original microstructure, deteriorating its mechanical properties. If control over welding cooling rates could be exercised, this would allow an increase in the capability of the operator to produce welds that maintain the original microstructure and mechanical properties. Infrared sensors are ideal for such an application because of their sensitivity, fast response time, and non-intrusive nature [19].

In 1982, Lukens and Morris [20] pioneered research in this field with the use of infrared sensors. They concluded that it might be possible to use infrared sensors to control cooling rates in GTAW and gas metal arc welding (GMAW) processes because of the reproducibility and sensitivity of the instruments while varying the operating voltage and current as well as the torch speed.

Over the past 50 years, extensive research has been conducted in the areas of temperature distribution and temperature measurement in various welding processes. Solutions to the governing equations of the physical processes occurring in the base metal initially suggested ideal locations and orientations from which infrared measurement techniques could be applied. Using infrared spot sensors and infrared line scanning instruments, thermal signals have been accurately and reliably obtained during a welding process. Spot sensors have been shown to provide accurate absolute temperature measurements, and line scanning methods have been shown to provide extremely useful information, especially with regard to feedback loops and process control. Information from infrared sensors has helped automate the welding process by being able to simultaneously monitor joint tracking, weld penetration depth, and cooling rates, all three of which are crucial to the fabrication of strong, high quality welds.

3 EXPERIMENTAL SETUP

The experimental setup consists of six functional groups which are the support structure, the welding unit, the target plate motion system, the data acquisition (DAQ) system, the thermocouple modules, and the infrared sensor. A laptop PC is used to communicate with the target plate motion system and the DAQ. The other groups operate on their own without the need for computer communication. The experimental set up is described in the paragraphs below, and it is also discussed in detail with pictures in Appendix A. In addition, schematics of the target plate and its accessories are provided in Appendix G.

The support structure holds the target plate motion system which is a linear x-direction slide table with a steel plate mounted to its carriage. The support structure also holds the welding torch in a fixed position. In this way, the target plate is allowed to move at a constant predetermined velocity along the length of the slide table while the welding torch remains rigidly held, allowing a weld line to be burned on to the target plate. The laptop PC is used to control the velocity of the target plate. Configuration of the servo driver is shown in Appendix B, and a calibration curve for the velocity of the servo motor is shown in Appendix D.

As the target plate passes under the welding arc the temperatures of both the top and bottom faces of the plate are measured with the infrared sensor and K-type thermocouples, respectively. The infrared sensor is manually focused on the top face of the plate at a location determined a priori, and the thermocouples are individually spot welded directly to the bottom face of the plate to ensure the best thermal contact. Furthermore, the thermocouples are welded in a straight line directly above which the welding torch should ideally pass. Each of these temperature

transducers ultimately feeds into the DAQ, but each thermocouple signal must first pass through an optical isolation unit to prevent damage to the circuitry on board the DAQ.

The DAQ system consists of the hardware that reads the signals from both the infrared sensor and the thermocouples and the software that is used to read the signals that are captured by the hardware. The laptop PC is used to configure the DAQ system, initialize data acquisition, and receive data. The software program that is used to capture the signals is LabVIEW 8.5.1. The program plots all incoming signals in real time while writing the data to .txt files for subsequent analysis and post-processing. The configuration of the LabVIEW program is shown in Appendix C. A block diagram of the experimental setup is shown in Figure 3-1.

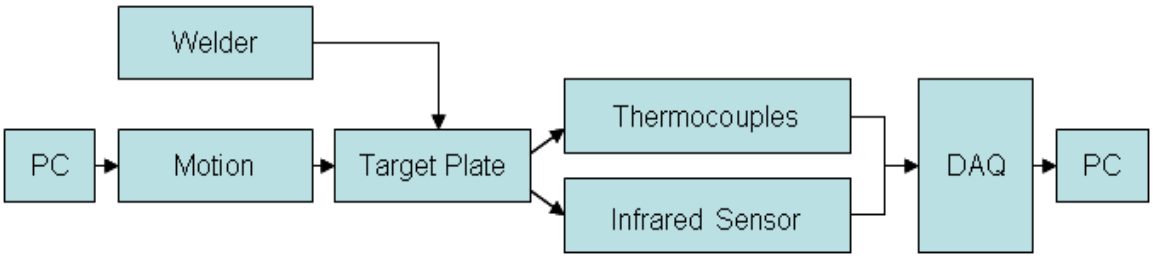

Figure 3-1. Block diagram of experimental setup.

Prior to starting a trial, certain tasks must be completed to prepare the setup. Appendix E lists this process in full detail, but the prep work will only be discussed briefly in this section. Firstly, five K-type thermocouples must be spot welded to the bottom face of the target plate in a straight line. The plate is then mounted on the carriage of the slide table using the ceramic spacers. The welding torch is then ideally aligned such that it remains directly above the thermocouples throughout the travel length of the plate. Next the target plate is moved to its starting position, and the infrared sensor is focused at a point of interest on the top face of the target plate. The welder is then powered on and set to a predetermined welding current. Once both the servo

driver and DAQ have been configured, data acquisition is begun, the motor is initiated, and the arc start switch on the welder is flipped to the “on” position.

At this point the welder, the DAQ, and the motor should all be operating. Target plate motion should be readily apparent, and temperature rises due to welding should make themselves known through the plots on the front panel of the LabVIEW program. It is important to ensure that the target plate is in motion. If it is not in motion then there is a risk of burning through the target plate, which has the potential of damaging the slide table.

After the last thermocouple has passed under the welding torch and had approximately 10 seconds to cool, it is time to shut down the set up. First, the arc start switch is flipped to the “off” position. Then the velocity of the motor is reset to 0 in/sec, and finally, data acquisition can be stopped. The target plate should be moved to a position along the slide table such that it can be removed without the welding torch obstructing it. The plate should be dismounted and allowed to cool before the thermocouples are detached.

The goals of this research are twofold. For one, it is desired that enough data be collected to fully characterize the setup under a variety of operating conditions and infrared sensor configurations in an effort to discover the most suitable orientation from which infrared temperature measurements can be made with a minimum amount of interference from both the welding arc and the hot tungsten electrode. The other goal of this experiment is to provide accurate temperature data at known locations so that they can be subsequently compared with the output of a computational model in order to validate its accuracy.

There were many variables of interest in this experiment. All the experimental variables and their values are listed in Table 3-1. The Cartesian coordinate system used to determine the values of some of these variables is shown in Figure 3-2. Furthermore, because of a breakdown in the

Graybody assumption, the IR sensor was not used in its two color mode. Instead, it was operated in the single color mode utilizing the long waveband in all trials.

Table 3-1. Experimental variables and the values that they may take on. The values for those variables marked with an (*) experienced tremendous fluctuations in several trials due to bending in the target plate, but the value listed is the nominal value.

Variable	Values
Horizontal Angle, θ_H [°]	0, 45, 90
Vertical Angle, θ_V [°]	45, 90
Shield Presence	Yes, No
*Shield Height [in]**	0.08
*Torch Height [in]**	0.05
Weld Position	Side, Middle
Emissivity	0.3, 0.5, 0.55, 0.6
Focus Distance [in]	0.2, 0.4
Weld Current [A]	100, 130
Weld Speed [in/min]	2.47
Gas Flow [SCFH]	20,30,40,50

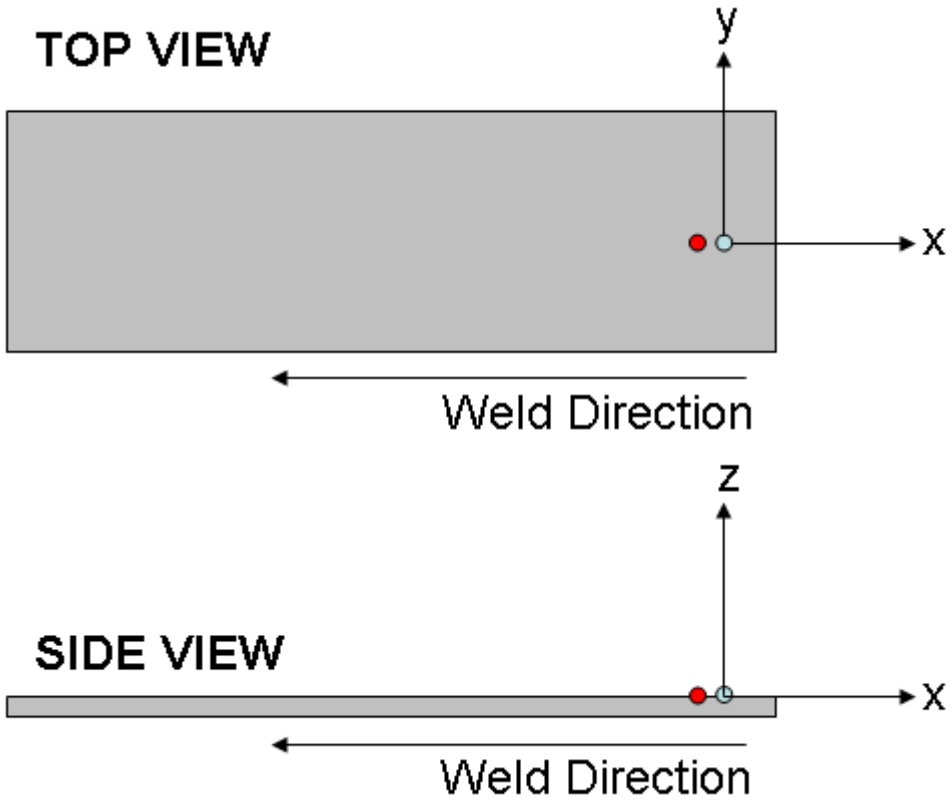

Figure 3-2. Cartesian coordinate system of experimental setup. The red indicator marks the location of the welding torch, and the blue indicator marks the location of the point upon which the infrared sensor is focused.

In terms of a spherical coordinate system, the horizontal angle is similar to the azimuth angle, and the vertical angle is akin to the inclination angle. The coordinate (0,0,0) corresponds to that point on the plates surface at which the infrared sensor is focused, and the y-coordinate is always taken as positive and in the direction of the infrared sensor. From the origin the (x,y,z) position of the lens of the infrared sensor could readily be measured, and with the coordinate system defined as such, the horizontal and vertical viewing angles could be calculated.

In some of the trials, a stainless steel foil was secured around the welding torch to serve as a mechanical shield. The presence of the shield was recorded as either “Yes” or “No,” and if used, the distance between the top face of the target plate and the bottom edge of the shield was

recorded. The torch height was measured in the same manner and was recorded. Every effort was made to keep these distances constant throughout all trials.

Because welding on the same target plate multiple times caused gradual deformation to the target plate, namely extensive bowing where the change in height of the plate relative to the welding torch differed by as much as ¼ inch over a 6 inch length, two of the experimental parameters varied uncontrollably. As the target plate followed its path, the torch height and shield height would initially both be relatively far away from the target plate, but as it traversed its path, that distance would gradually decrease to the nominal value as indicated in Table 3-1, and then slowly increase again.

Depending on where the row of thermocouples were located on the bottom face of the target plate, an entry of “Side” or “Middle” was recorded for the weld position. Because of possible edge effects and the pooling of thermal energy on the “Side” trials, this information was important as elevated temperatures on both the top and bottom face of the target plate were anticipated.

Two variables relating to the configuration of the infrared sensor were recorded. The variables were emissivity and focus distance. Since there were no readily available data for the emissivity of a type 304 stainless steel plate undergoing a welding process, best guesses were made as to what that value might be. Also, the focus distance was recorded. The focus distance was defined as the distance directly behind the welding arc at which the infrared sensor was focused.

Lastly, three welding parameters were recorded. The welding current is the current at which the welding occurred and it essentially adjusts the heat flux to the target plate. The weld speed is the speed at which the target plate moves beneath the welding torch, by increasing or decreasing

the weld speed, the heat flux is either decreased or increased. These two variables are the only means by which the heat flux to the target plate can be effectively manipulated. Also, the gas flow was recorded. The gas flow is controlled by opening or closing the regulator valve on the regulator attached to the gas cylinder.

To reduce the number of trials in the experiments, some of the variables listed above were held constant. The variables that were held constant were torch height, shield height, and weld speed. The main variables of interest in these experiments were horizontal viewing angle, vertical viewing angle, shield presence, weld position, emissivity, weld current, and gas flow.

The first sets of trials aimed to determine the optimal viewing angle at which the infrared sensor could be oriented to minimize interference emanating from the welding torch. Holding all other variables constant, the horizontal angle was adjusted to 0°, 45°, and 90° with three trials taken at each setting. After reviewing the data, the horizontal angle with the least apparent interference was chosen, and then the vertical viewing angle was increased to 90°. Three more trials were then taken at this configuration.

After the optimum viewing angle had been determined, the infrared sensor was repositioned in that particular orientation and then a shield was installed around the end of the welding torch to investigate to what extent interference from the arc area could be attenuated. At this point in the experiments, both the emissivity and the welding current were increased. The emissivity was gradually increased to a final value of 0.60, and the welding current was changed from 100 A to 130 A.

Up to this point in the trials, the thermocouple array on the bottom face of the target plate was a straight line. Now that the response of the infrared sensor had been sufficiently explored, it was necessary to begin adjusting the placement of the thermocouples. By placing thermocouples

at offsets from the typical centerline of the weld the surface temperature profile is better understood and it supplies additional points that can be used to validate the computer simulation.

There were two typical types of thermocouple offsets. The first type of offset is where each thermocouple is offset from the weld centerline by some distance. In the thermocouple offset tests, the offsets used were 0.1, 0.2, and 0.5 inches. Of the five thermocouples in the row, four were offset by the same amount while one remained fixed on the centerline as a control. Three trials were taken for each offset distance.

The second type of thermocouple offset used was called a Figure-5 offset because it resembled the "5" on a standard die. The arrangement of the Figure-5 offset is shown in Figure 3-3. The Figure-5 configuration was placed between thermocouples B and C so that the plate had enough time to reach steady state, and since only five thermocouple channels could be utilized simultaneously, there were no thermocouples in their standard positions while temperature profile data were being collected with the Figure-5 offset.

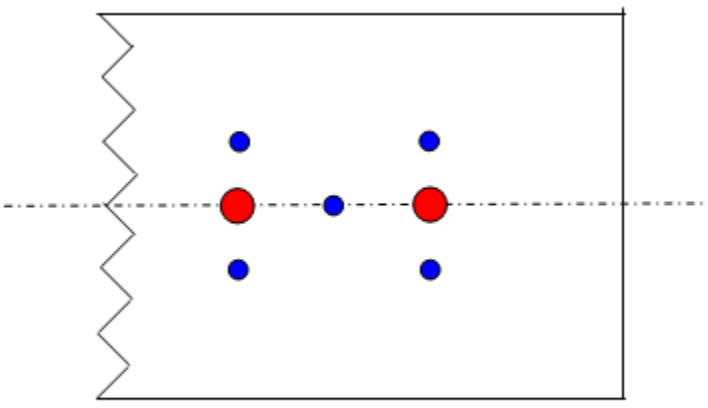

Figure 3-3. Configuration for Figure-5 offset for thermocouples. Red spots indicate location of standard thermocouples, and the blue spots indicate the Figure-5 configuration. Each corner is offset by 0.3 inches.

The last set of tests sought to determine how much of an effect the gas flow had on the surface temperature of the plate during the welding process. Using three similar target plates trials were started with a typical gas flow rate of approximately 30 SCFH. As the welding torch approached the middle of the target plate, the gas flow was instantaneously changed to either 20, 40, or 50 SCFH, and the trial was allowed to continue until completion at the new gas flow rate.

4 RESULTS AND DISCUSSION

Upon examining the results below, it is important to bear in mind that the emissivity of the target plate was unknown, rendering the temperature output of the infrared sensor inherently inaccurate. A large degree of uncertainty is also introduced because the position on the target plate upon which the IR sensor focuses relative to the torch is not exactly the same in each trial. The infrared sensor takes an average temperature of the surface in its targeting reticle. Since it is aimed in an area where large thermal gradients are known to exist, any variation in relative position can have large impacts on the output temperature. In summary, not only are the IR temperature data inaccurate, but the process contains a high degree of uncertainty far beyond those as specified for the instrument itself. Because of these facts, it makes sense to analyze the IR data using a qualitative framework. To this effect, relative changes and characteristic behavior of the IR data were examined.

The thermocouples, because they do accurately measure the temperature of the location at which they were welded, lent themselves more readily to quantitative analysis. The thermocouple data are believed to be accurate, but there is considerable uncertainty associated with the thermocouples real position and its ideal position. This uncertainty is discussed in the following section.

Several trials of each experimental condition were run. Since there was such a large amount of data collected, only one trial of each condition is shown in the figures below except where otherwise noted. In this way, the figures maintain their clarity while presenting an adequate amount of information. APPENDIX H contains a table showing the values of the experimental

variables for all trials, and it also presents graphical illustrations of the data collected from each trial.

4.1 Preliminary Thermocouple Analysis

The results from the thermocouple data will serve as reference points for the computer model. If the model adequately accounts for all of the physical processes occurring under a certain set of welding conditions, then confidence in the computer model can be realized. The difficulty of doing this in a real world application is that very slight deviation in thermocouple placement can lead to relatively large changes in the temperature output. Variability in thermocouple placement includes, but is not limited to, the following: 1) distance between thermocouple leads, 2) depth of spot weld penetration, and 3) placement of thermocouple. As the distance between the thermocouple leads increases, the temperature that the thermocouple reads becomes more of an average temperature between the leads rather than the ideally exact temperature in the middle of the leads. If the thermocouples penetrate the surface of the plate in a given range of depths when they are spot welded to it, then this will affect the temperature output, too. Perhaps the most significant impact on thermocouple output comes from the location on the plate to which they are welded. A decimal ruler was used to mark locations for thermocouples and to align prepped plates beneath the welding torch. Any deviation from perfect alignment with respect to the welding torch and thermocouples will reduce the temperature, and since thermal gradients are large in the vicinity of the arc slight misalignments will have profound impacts on the output.

Of the variables manipulated, only welding position, welding current, and offset distance had any effect on the thermocouple output, so once all of the trials had been completed, it was

possible to examine the distribution of the temperature for the more common welding configurations, which were 1) 100 A, side weld, and 0 in. offset, and 2) 130 A, middle weld, and 0 in. offset. Histograms of the peak thermocouple temperature output for these two conditions are shown in Figure 4-1 and Figure 4-2, respectively.

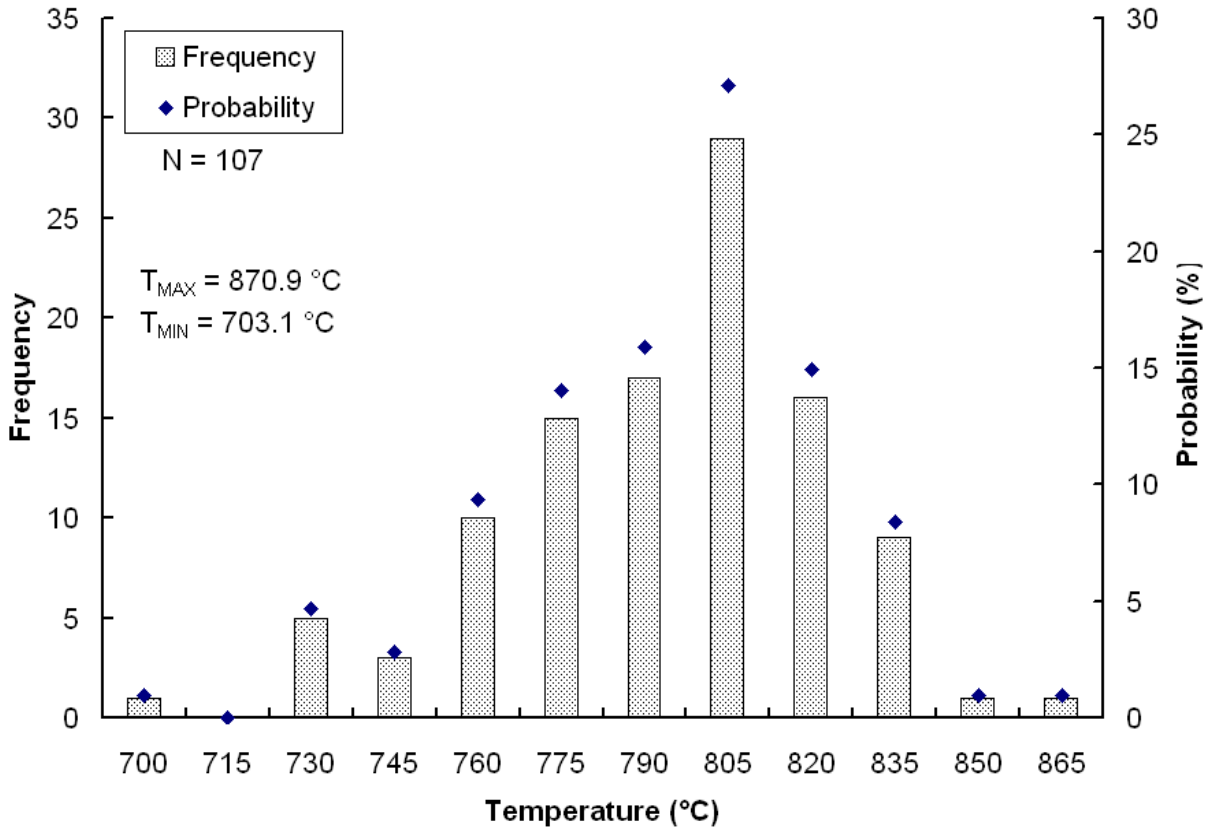

Figure 4-1. Peak thermocouple temperature distribution with N = 107 trials. Parameters: 100 A, side weld, no offset.

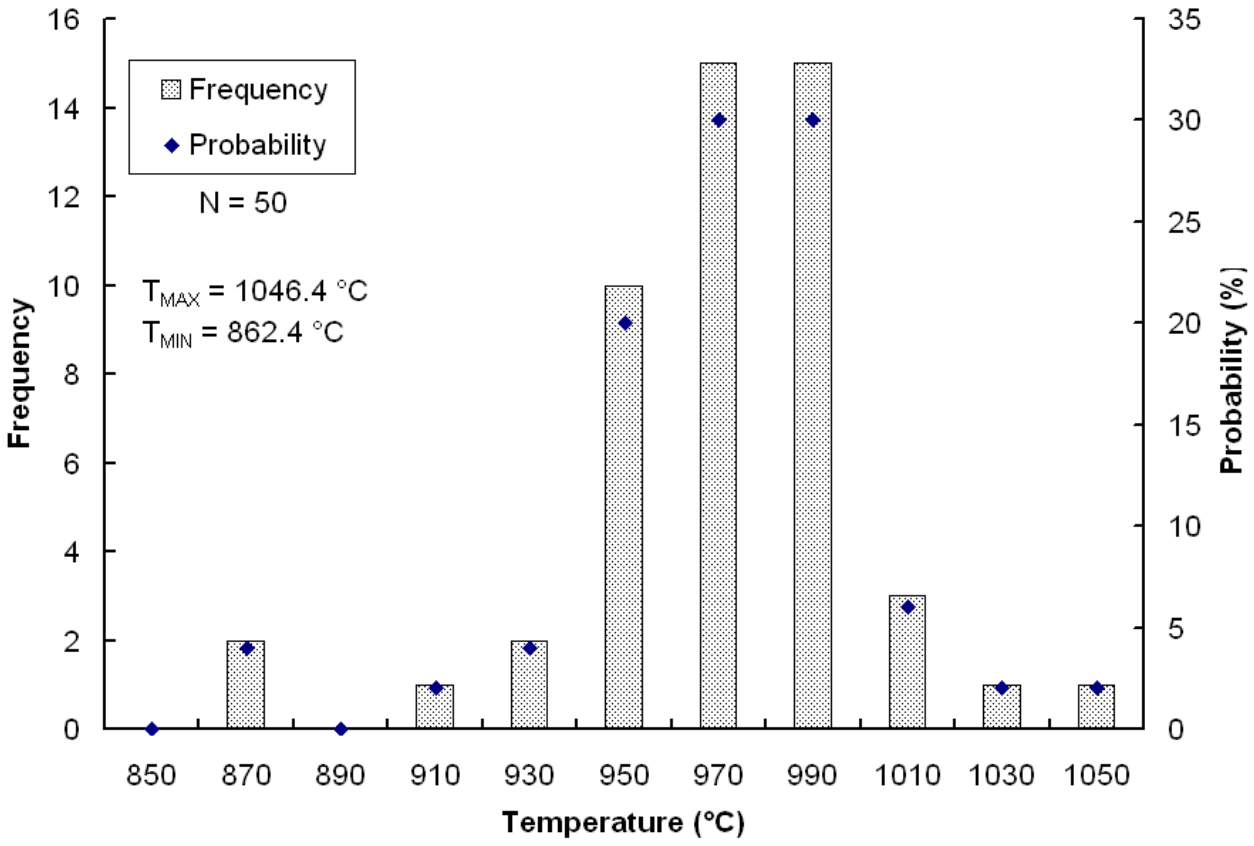

Figure 4-2. Peak thermocouple temperature distribution with N = 50 trials. Parameters: 130 A, middle weld, no offset.

The above histograms show left-skewed distributions of peak temperatures as recorded by thermocouples aligned directly under the centerline of the weld. The distribution is not normal, and therefore it cannot be quantitatively analyzed using means and standard deviations. Instead the data can be analyzed in terms of T_{MAX} and T_{MIN}, which are the maximum and minimum temperatures recorded in a distribution.

If the weld line is thought of as the $x = 0$ line, then a thermocouple placed exactly on that line will measure the highest possible temperature during a welding process, holding all other variables constant. Any deviation away from the weld line will measure a lower temperature. Furthermore, with sharp temperature gradients near the arc, very small deviations can result in

relatively large departures from the true maximum temperature on the bottom face of the target plate. For these reasons that is why the temperature distribution of the thermocouples does not follow a normal distribution. However, it seems reasonable to assume that T_{MAX} for a given set of welding parameters is very close to the true temperature of the bottom surface of the target plate directly beneath the arc. Also noticeable in both histograms is that the temperature difference of the most probable temperature bin and T_{MAX} is approximately 60 °C.

It is also useful to compare T_{MAX} and T_{MIN}. Assuming enough data points have been collected, taking the difference of these two values provides a range of detected temperatures. While this is of little use in data analysis, it may be an indicator of how repeatable is the process by which the thermocouples are welded to the plate and aligned with the welding torch. The difference of T_{MAX} and T_{MIN} provides a feel for how sensitive the thermocouple response is to the quality of the thermocouple weld. Unless an individual is highly skilled, the process of spot welding thermocouples to the target plate is far from ideal and is not truly repeatable when done manually. There will always exist some level of variability which will most likely serve to drive down the measured temperature.

4.2 Infrared Sensor Results

Several different trials were conducted with the infrared sensor in an effort to characterize its output during a welding process. The most important factors investigated were viewing angle, shield presence, and repeatability. In addition to these three main points of interest, another unforeseen condition presented itself and showed a limitation of this experimental setup. This condition concerned the number of trials a single plate could be used before the data became

useless to achieve the goals of this research. These conditions are each discussed below. It is also worth mentioning again that the IR sensor was only used in the one color mode utilizing the long waveband.

4.2.1 Viewing Angle

One of the primary goals of this research was to determine what steps could be taken to provide reliable infrared temperature data whereby the interference from both the arc and electrode was minimized. The first set of experiments sought to discover the optimum orientation of the infrared sensor with respect to the target plate. With θ_V fixed at 45°, θ_H was investigated at values of 0°, 45°, and 90°, where 0° is parallel to the weld line and 90° is normal to it. After analyzing the data from the variable θ_H trials, the optimum orientation was applied, and θ_V was increased to ~90°. The thermocouples were located as best as possible directly under the weld line. Aside from the viewing angles, the values of the other experimental variables are shown in Table 4-1. Figure 4-3 shows the temperature response from both the infrared sensor and the thermocouples of one trial from each viewing angle condition.

Table 4-1. Experimental variables for viewing angle comparisons.

EXPERIMENTAL VARIABLES								
Shield Presence	*Shield Height (mm)*	*Torch Height (in)*	*Weld Position*	*Emissivity*	*Focus Distance (in.)*	*Weld Current (A)*	*Weld Speed (in/min)*	*Gas Flow (SCFH)*
No	N/A	0.05	Side	0.3	0.4	100	2.47	30

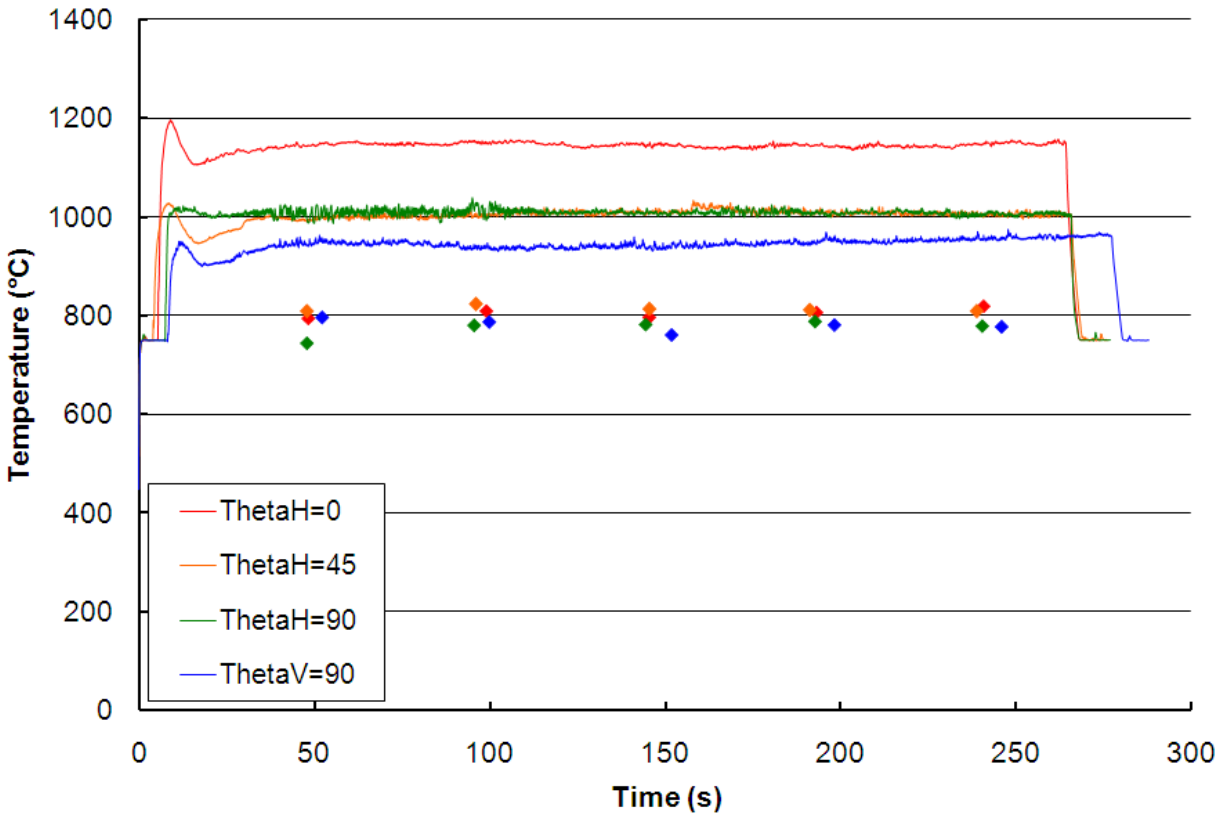

Figure 4-3. Comparison of viewing angles and IR response. IR signals shown with lines; thermocouples shown with points. The thermocouple data points shown were the maximum values as recorded by that thermocouple, ie. when the torch is directly above the thermocouple.

From the above figure it can be seen that while holding all other variables constant, viewing the target plate from horizontal angles away from 0° decreases the detected surface temperature, which was expected. At $\theta_H = 0°$ the temperature as detected from the IR sensor hovered around 1145 °C. With the IR sensor oriented at $\theta_H = 0°$, the line of sight is directly in line with the arc and the electrode. Although the IR sensor sees only what is inside the targeting reticle, significant amounts of radiation originating from the arc and the hot electrode are reflected from this area and subsequently detected by the IR sensor.

At viewing angles where $\theta_H \geq 45°$, it appears that the temperature response of the infrared sensor is largely unchanged. As the IR sensor is rotated around the welding torch, the line of

sight includes a decreasing component of arc and electrode effects. The output temperature of both the $\theta_H = 45°$ and the $\theta_H = 90°$ conditions was approximately 1010 °C. The results for all trials in both of these conditions were similar, but because the $\theta_V = 45°$ orientation provided a more repeatable setup than the $\theta_V = 90°$, the $\theta_V = 45°/\theta_H = 90°$ orientation was used in all subsequent trials.

The $\theta_V = 90°$ orientation had an overall lower average temperature output. For the trial shown above the temperature was approximately 945 °C. However, it also appeared to contain more variation, and it was not as repeatable. Much of this was due to the difficulty encountered when attempting to position the IR sensor in an orientation such that it could see straight down. The dimensions of the support structure did not readily allow for the sensor mounted on a tripod to overlook the target plate.

Also noticeable in Figure 4-3 is that as the horizontal angle is increased, the initial abrupt rise in temperature tends to become less pronounced. In all cases the temperature rises sharply and peaks at some value. Then the temperature typically decreases and then slowly increases to a somewhat steady value which is generally lower than the initial spike. These results are similar to those observed by Farson, et al. in their research which was described previously.

In the $\theta_H = 90°$ case, the temperature profile follows a similar pattern but the initial spike is very small compared to its steady value. The height of the spike in relation to the settling temperature likely indicates the degree of interference. Experience would also support this hypothesis. When the arc is initially struck, the temperature may jump as high as 1000+ °C, but if the arc is immediately turned off the area of the plate upon which the infrared sensor is focused remains cool to the touch. It is very unlikely under these welding conditions that in this small amount of time the target plate has been heated to such a temperature. What is more likely is that

IR sensor is seeing radiation from the arc or electrode, both of which may reasonably experience such abrupt temperature changes.

Oftentimes, incident radiation is classified as "diffuse," which means that the incident radiation on a surface is reflected equally in all directions. If these spikes do correspond to levels of interference, then it seems that a diffuse assumption is not valid, and the reflected radiation has some straight line directional preference. This would further support the decision to orient the infrared sensor at a horizontal angle normal to the weld line, and at a vertical angle of 45°.

The thermocouple data in Figure 4-3 are relatively consistent, considering their distributions. With all thermocouples aligned in the same fashion and experiencing the same thermal history, they should all give similar results since the output of the thermocouples is independent of the angle at which the infrared sensor views the target plate, and this is shown in the data. Granted the thermocouples and infrared sensor are detecting temperatures at different points with respect to the torch, but what remains important to consider is that the top face of the target plate is simultaneously undergoing its own thermal history, which is also independent of the viewing angle of the infrared sensor. Using this line of reason, it becomes more apparent that the viewing angle does impact the accuracy of the infrared sensor.

4.2.2 Shield Testing

After determining that the viewing angle of θ_H =90° and θ_V = 45° afforded an orientation with the least amount of interference, the effect of employing a mechanical shield to attenuate more of the interfering component of the radiation was investigated. Trials were conducted at the experimentally determined optimal viewing angle using the same experimental variables

provided in Table 4-1 for the unshielded trials. The values of the experimental variables shown in Table 4-2 were the same for the unshielded trials with the exception of the presence of a shield

Table 4-2. Experimental variable values for the shielded condition.

EXPERIMENTAL VARIABLES								
Shield Presence	*Shield Height (mm)*	*Torch Height (in)*	*Weld Position*	*Emissivity*	*Focus Distance (in.)*	*Weld Current (A)*	*Weld Speed (in/min)*	*Gas Flow (SCFH)*
Yes	2	0.05	Side	0.3	0.4	100	2.47	30

A comparison of the unshielded and shielded trials is shown graphically in Figure 4-4. It is worth explicitly mentioning that the unshielded trial shown in the figure below is for all intents and purposes the same as the θ_H =90° trial in Figure 4-3. The reason that trial is not used in the graph below is because it was not collected on the same day as the shielded trial. Knowing that very small differences in IR position have a noticeable impact on the output temperature, it was considered more appropriate to compare two trials that were taken on the same day so that bulk movement of the IR sensor could be eliminated as a confounding variable. As a side note, due to time constraints it was not always possible to collect all similar trials in one session. Furthermore, by breaking down the experimental setup and then reassembling it, the repeatability of the experiments can be assessed.

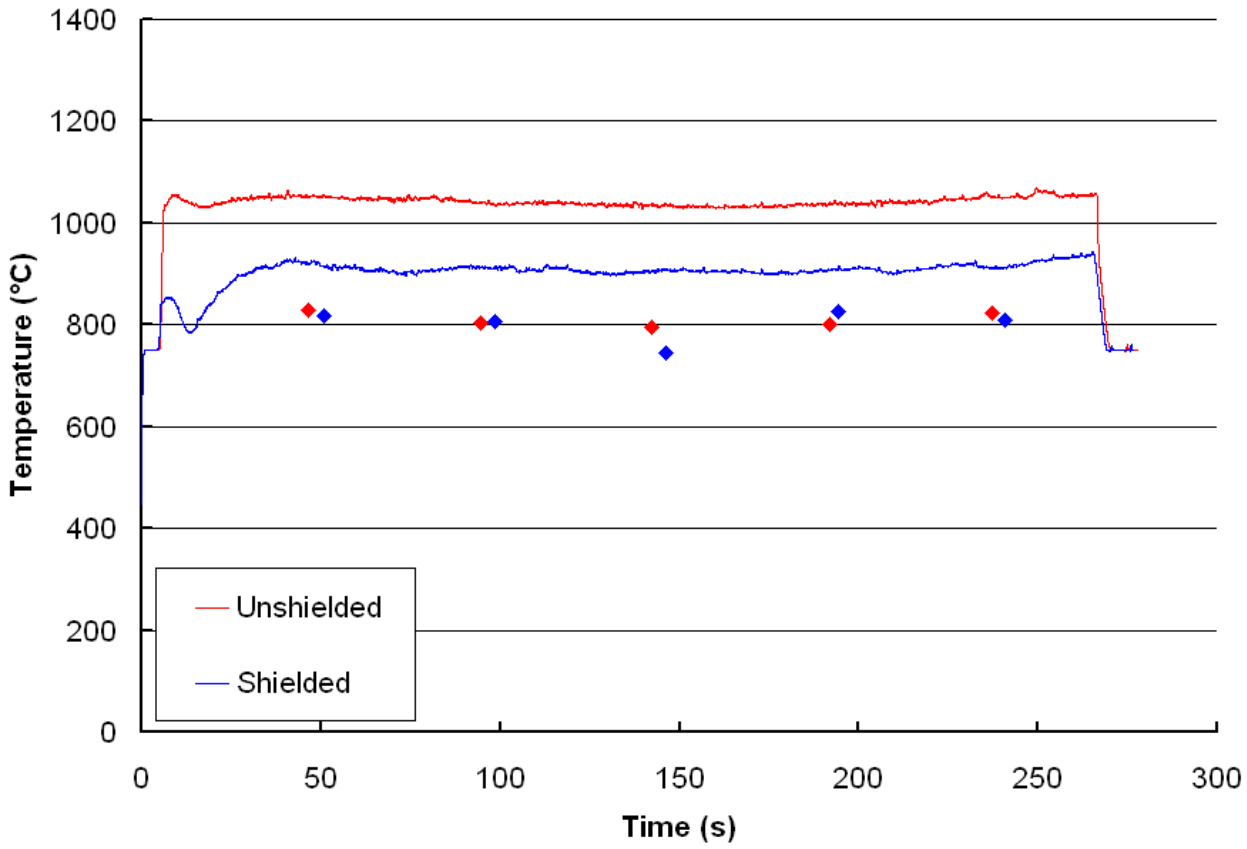

Figure 4-4. Comparison of unshielded and shielded trials. IR signals shown with lines; thermocouples shown with points. The thermocouple data points shown are the maximum values as recorded by that thermocouple, ie. when the torch is directly above the thermocouple.

In Figure 4-4 it is shown that the temperature as detected by the infrared sensor in the unshielded trial is approximately 1050 °C whereas during the shielded trial, the temperature is around 900 °C. The thermocouple measurements from both trials are all in close agreement, except those taken at time t = 145 s. As in the previous section this indicates that the temperature on the top surface of the target plate should be the same between trials as well, but the top face temperature in the shielded trial is about 14% lower. It appears that utilizing a mechanical shield positioned at a height of 2 mm above the target plate reduces more interference in addition to that amount eliminated by viewing the target plate at a 90° horizontal angle.

Another noticeable feature in this figure is the different behavior of the initial temperature spike. In the unshielded case, the temperature spikes to a maximum value and then decreases slightly, eventually leveling off at a temperature that is close to its initial peak. This same behavior was also seen in the θ_H =90° trial in Figure 4-3. However, what is interesting to observe in the shielded case is the temperature response after the initial spike. After the temperature spikes, it decreases slowly as it does in the other trials, but after some time it begins to rise again, passing the initial spike in the temperature. This may indicate that while, yes, there may still be some remaining interfering radiation, the signal to noise ratio is improving and a more representative thermal history of the plate is shown as it approaches steady state conditions.

4.2.3 Variability Between Similar Trials

According to the experimental data, the optimum configuration for eliminating interference from the arc and electrode was obtained by implementing a mechanical shield and orienting the infrared sensor such that θ_H =90° and θ_V =45°. The next important question is how repeatable is the infrared temperature response between similar trials. To investigate this question multiple trials were taken under exactly the same experimental conditions and then compared. The experimental variables for these trials are shown in Table 4-3.

Table 4-3. Experimental variables for variability trials.

EXPERIMENTAL VARIABLES								
Shield Presence	*Shield Height (mm)*	*Torch Height (in)*	*Weld Position*	*Emissivity*	*Focus Distance (in.)*	*Weld Current (A)*	*Weld Speed (in/min)*	*Gas Flow (SCFH)*
Yes	2	0.05	Middle	0.6	0.4	130	2.47	30

A few of the experimental variables were changed during these trials, namely the weld position, emissivity, and welding current. In this series of trials, the emissivity was increased to more accurately represent the surface characteristics of the target plate during the welding process. Prior to welding, the target plates were smooth and had no finishing or polishing treatments applied to them, so they appeared somewhat dull. In Figure 12.20 in *Fundamentals of Heat and Mass Transfer* (5ed.) by Incropera and DeWitt [1], typical emissivity values for such a material are shown as ranging from 0.10-0.40. Upon visual inspection of the target plate after the welding process, the plate was dark in color as it had been oxidized. For oxidized metals this same figure gives a range of 0.25-0.70 for the emissivity. As such, there was a short series of trials where the emissivity of the infrared sensor was increased to a value of ε =0.60. The results of these trials serve only to ensure that the target plate surface temperature falls within the range of the infrared sensor. Since these trials do not address the objectives of this research directly, they have been omitted from this section. They can, however, be found with the rest of the experimental data in Appendix H.

Increasing the emissivity decreased the temperature output of the instrument to a level that fell outside the lower range detectable by the sensor. In order to bring the temperature of the target plate back within the measurable range of the sensor, the heat flux had to be increased. Therefore, the welding current was increased to 130 A. Alternatively, the welding speed could

have been reduced but that would have resulted in longer trial times and an excessive amount of data.

With these new experimental variables set, several trials were taken to investigate the repeatability of the infrared temperature sensor. The results from these trials are shown in Figure 4-5.

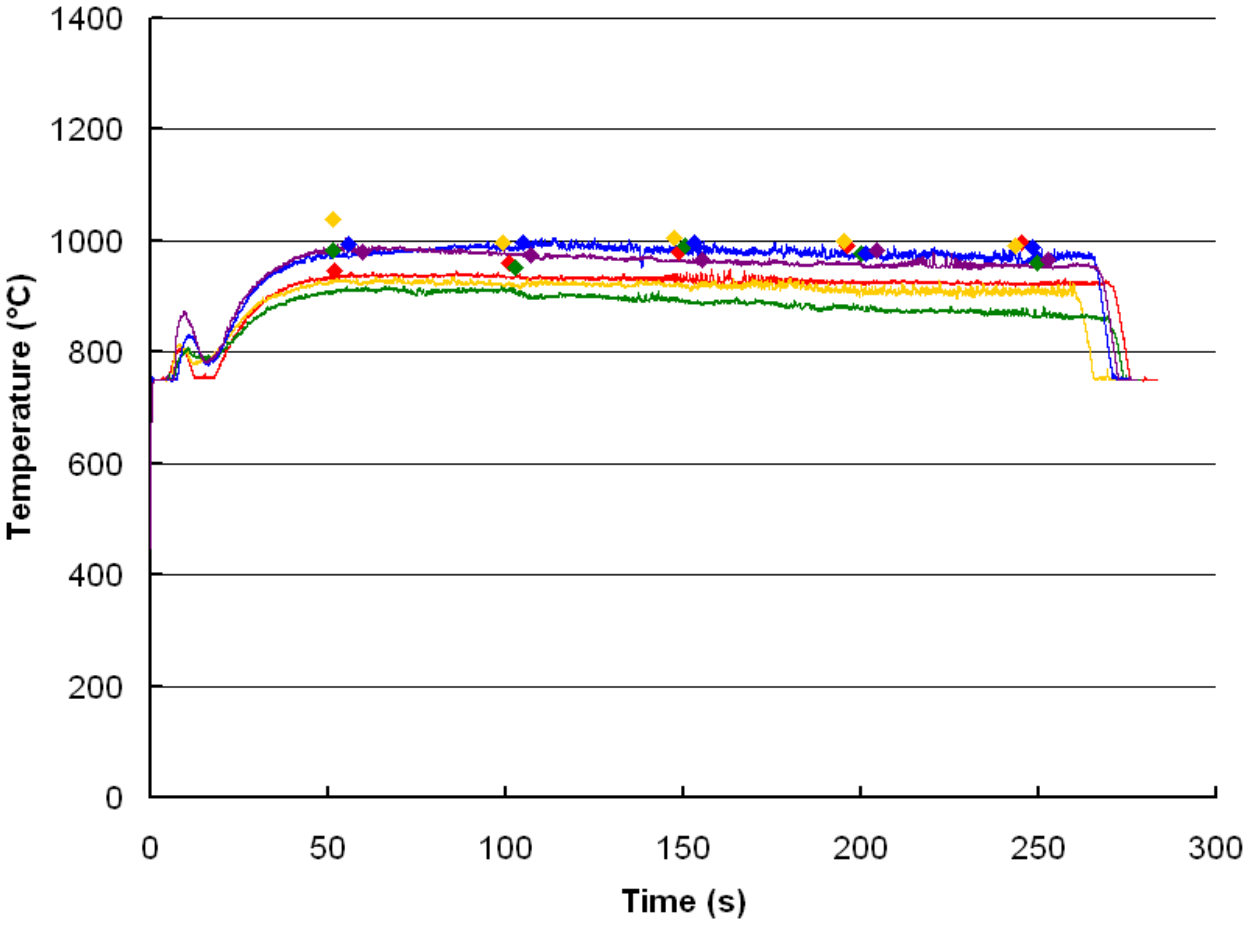

Figure 4-5. Variability of infrared temperature sensor under the experimentally determined optimal configuration. Infrared signals are shown as solid lines and maximum thermocouple temperatures are shown as points.

Each of the trials show the characteristic spike followed by a larger gradual temperature increase associated with the use of a mechanical shield. The thermocouple data all very closely

match each other, indicating that the top face surface temperature should be nearly the same for all trials. However, this is not what is shown in the data.

The importance of Figure 4-5 is to graphically show the extent and types of variation encountered while taking IR data with the current experimental setup. The three trials marked by the blue, purple, and green lines, show a steadily decreasing temperature trend as the target plate traverses its full length while the red and orange trend lines remain relatively constant throughout their trials, which is what should ideally be expected. In the region of the data after the gradual increase in temperature, there is also considerable difference in the detected temperature values between trials. At $t \approx 55$ s, the difference between the highest and lowest temperatures between trials is about 85 °C, which gives an error of about 8.5%. At $t \approx 260$ s, the temperature difference has increased to about 120 °C, which gives an error of about 12%.

The reason for the steady decline in temperatures as shown by three of the trend lines is most likely due to the infrared sensor wandering away from the intended focal area on the target plate. Assuming the shield remains in a fixed position, this can happen in three ways. For one, it is possible that the mounting plate on the tripod has not settled into a steady resting place after aiming the IR sensor on the target plate. The tripod is not a truly rigid component. Some play exists in the IR mounting plate, and it is possible that after maneuvering the IR sensor it continues to settle slowly. Secondly, there could be some motion of the welding torch or arc. Forces generated when the arc is struck may be strong enough to slowly move the arc in one direction. Lastly, the target plate itself may have a warped profile that would change the distance between the target plate and the bottom of the shield. Also, as a bent plate traverses its path, the surface upon which the infrared sensor is focused takes on higher (or lower) elevations. This

change in height changes the position at which the IR sensor is focused. The following plot in Figure 4-6 shows how sensitive the IR temperature output is to the position of the focus point.

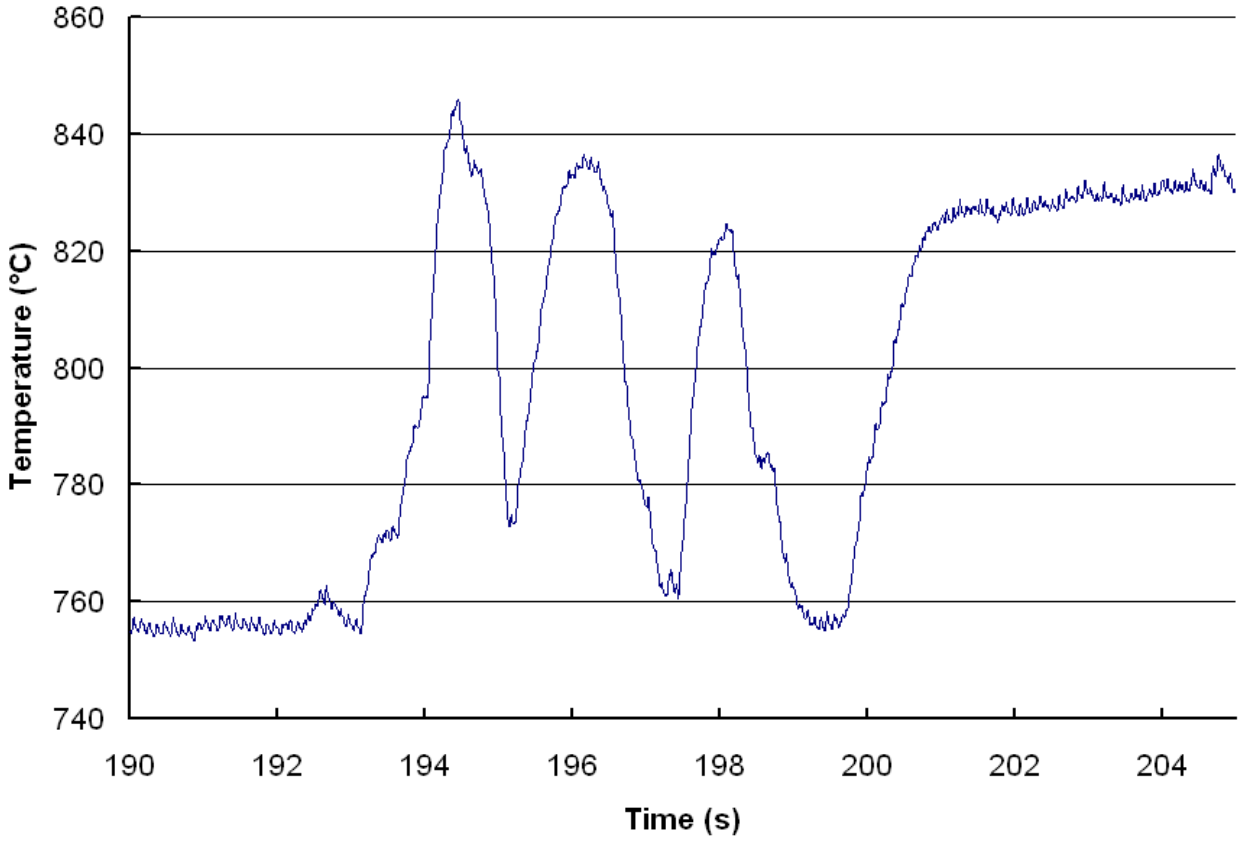

Figure 4-6. IR sensor response to very small changes in position.

During the trial from which the data in Figure 4-6 were taken, the IR sensor was lightly tapped several times to see how sensitive the instrument was to very small changes in position. Due to a lack of a reliable standard of measurement in this instance, it is estimated that when tapped the sensor moved less than 0.05 in. in a direction normal to and towards the weld line. The temperature change associated with this small variation in position was approximately 75 °C. At this particular time interval during the trial, the temperature variation due to the small change in position was ~10%.

4.2.4 Multiple Runs on a Single Target Plate

The way the experiment was designed, three trials could be performed on a single plate. Ordinarily, once oriented on the support structure, the welding torch remained fixed until it needed to be moved, which was determined by the availability of remaining target plates that had not yet been welded in that particular welding position. Towards the end of the research it was noticed that as the target plates underwent multiple trials, they began to warp and in some cases showed extensive curvature. Perhaps most importantly, on a single target plate the order in which the three different welding positions were used seemed to have the most impact. After two trials, most plates showed some degree of warping. Those plates whose third trial was on the side welding position showed extreme bowing, and those plates whose third trial was on the middle welding position showed bowing but to a lesser extent. These observations are show graphically in Figure 4-7 below.

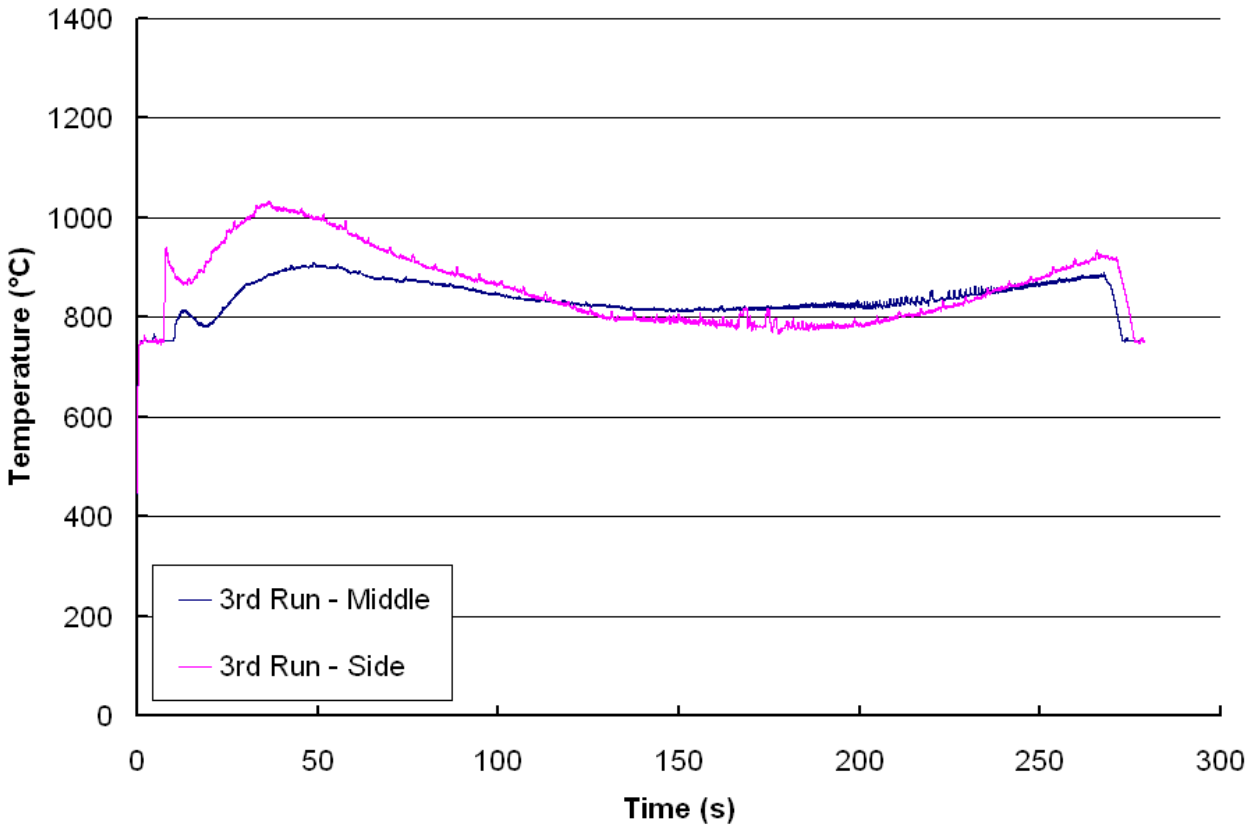

Figure 4-7. IR temperature dependence on weld position of a target plate's final run.

The curves in the temperature data shown in Figure 4-7 are related to the amount of bowing in the target plate that is present before the run occurs, so it seems that welding down the middle of the plate causes more deflection. For the trial where the third run was in the middle the temperature changed by more that 200 °C, whereas for the trial where the third run was on the side, the temperature change was nearly half that.

The deflection is problematic for the welding set up because it eliminates experimental control for the "torch height" and "shield height" variables. Because the plate is bowed so severely, all alignment measurements made during the set up phase of the run must be taken from the point on the target plate at which the distance between the target plate and the welding torch is a minimum. This means that along the weld line the distance between the shield and the

target plate is constantly changing. Typically, the target plate bent in such a way that the ends along the long dimension were lower than the middle section. Therefore, the shield was not effectively used at the beginning and ends of these trials, hence the high temperatures at the beginning and the lower temperatures in the middle of the trial. Also, as was mentioned in the previous section, such bowing in the plate can make the IR sensor appear to wander from the focal point on the target plate, causing large changes in the detected surface temperature.

4.3 Thermocouple Results

In general, there were two variations on the thermocouple arrangement on the target plates. In most cases the thermocouples were arranged on the bottom surface of the target plate in a straight line directly below the weld line. In other trials, the thermocouples were arranged with some type of offset from the weld line. In the previous section in-line thermocouples were used to show that the plates maintained an approximately uniform temperature on the bottom surface while the response of the IR sensor changed with the imposed experimental conditions. The thermocouples can also be used to validate a computer simulation. Comparing the thermocouple data to the output of a computer simulation can serve to either support the simulation if the temperatures are in close agreement, or it can serve to indicate that perhaps the simulation is not taking all physical processes into account and requires modification. To provide more of a scalar temperature field of the bottom surface of the target plate, it was necessary to take temperature readings at points away from the weld line. The values for the experimental variables used in the offset tests are provided in Table 4-4.

Table 4-4. Experimental parameters for offset tests.

EXPERIMENTAL VARIABLES								
Shield Presence	*Shield Height (mm)*	*Torch Height (in)*	*Weld Position*	*Emissivity*	*Focus Distance (in.)*	*Weld Current (A)*	*Weld Speed (in/min)*	*Gas Flow (SCFH)*
Yes	2	0.05	Middle	0.6	0.4	130	2.47	30

For the offset tests, thermocouples were placed some distance away from the weld centerline. In each of the three trials for a particular offset, at least one thermocouple was always placed on the weld line to serve as a control. Representative plots for each of these configurations are shown below in Figure 4-8, Figure 4-9, Figure 4-10, and Figure 4-11.

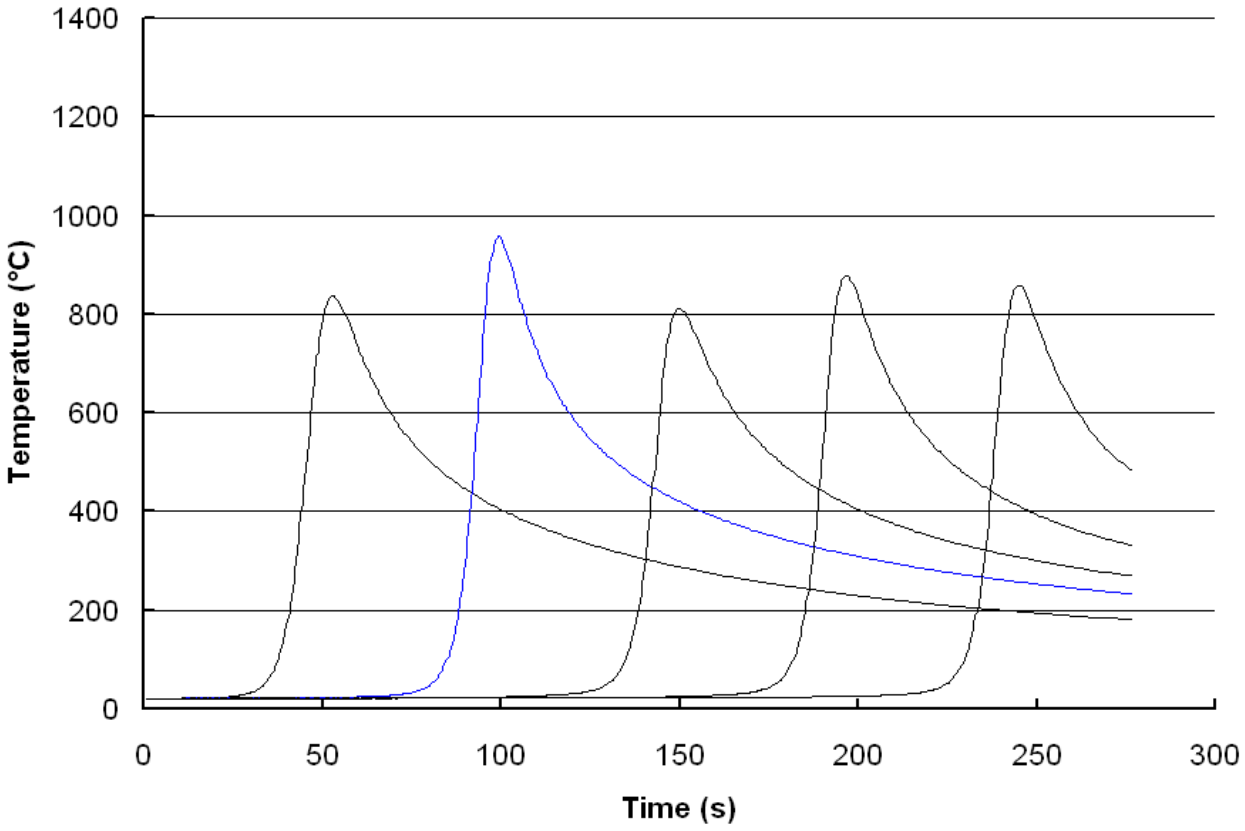

Figure 4-8. Maximum thermocouple temperatures for 0.1 inch offset. Control thermocouple shown in blue.

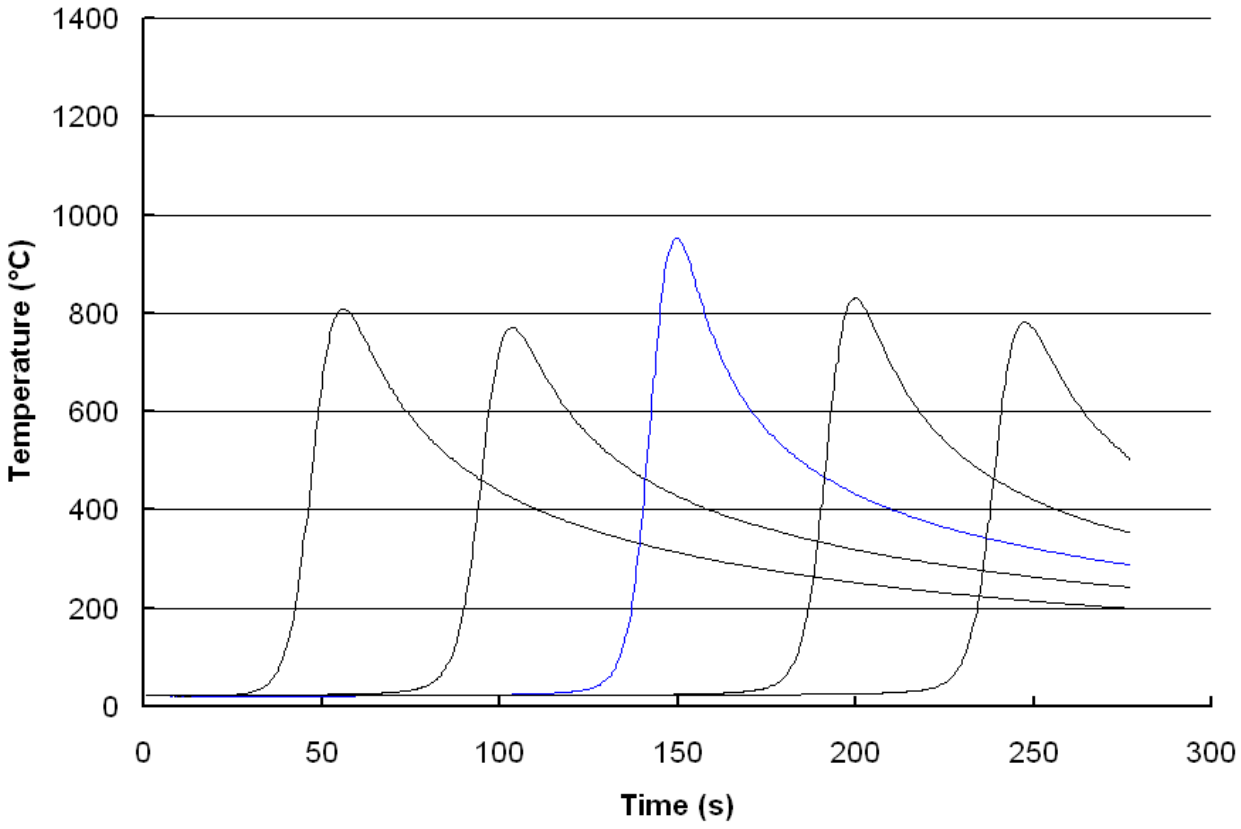

Figure 4-9. Maximum thermocouple temperatures for 0.2 inch offset. Control thermocouple shown in blue.

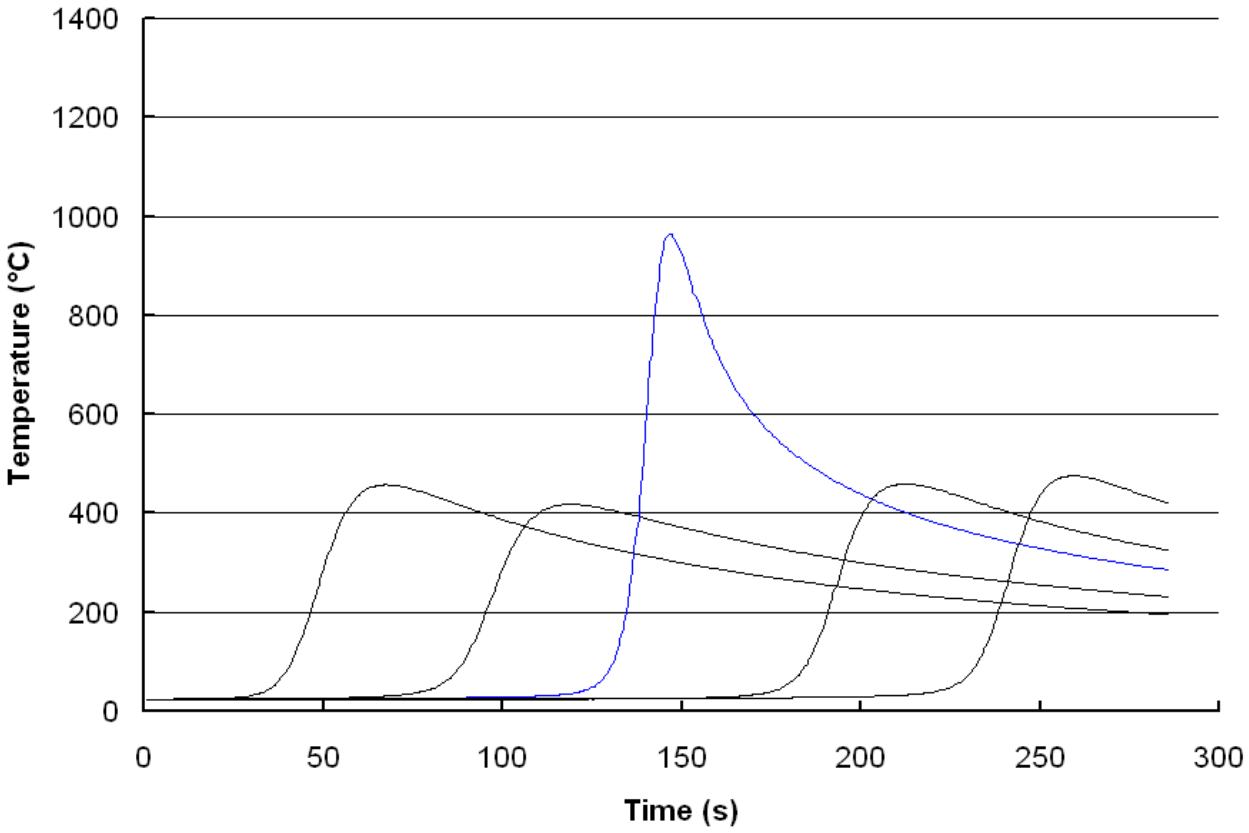

Figure 4-10. Maximum thermocouple temperatures for 0.5 inch offset. Control thermocouple shown in blue.

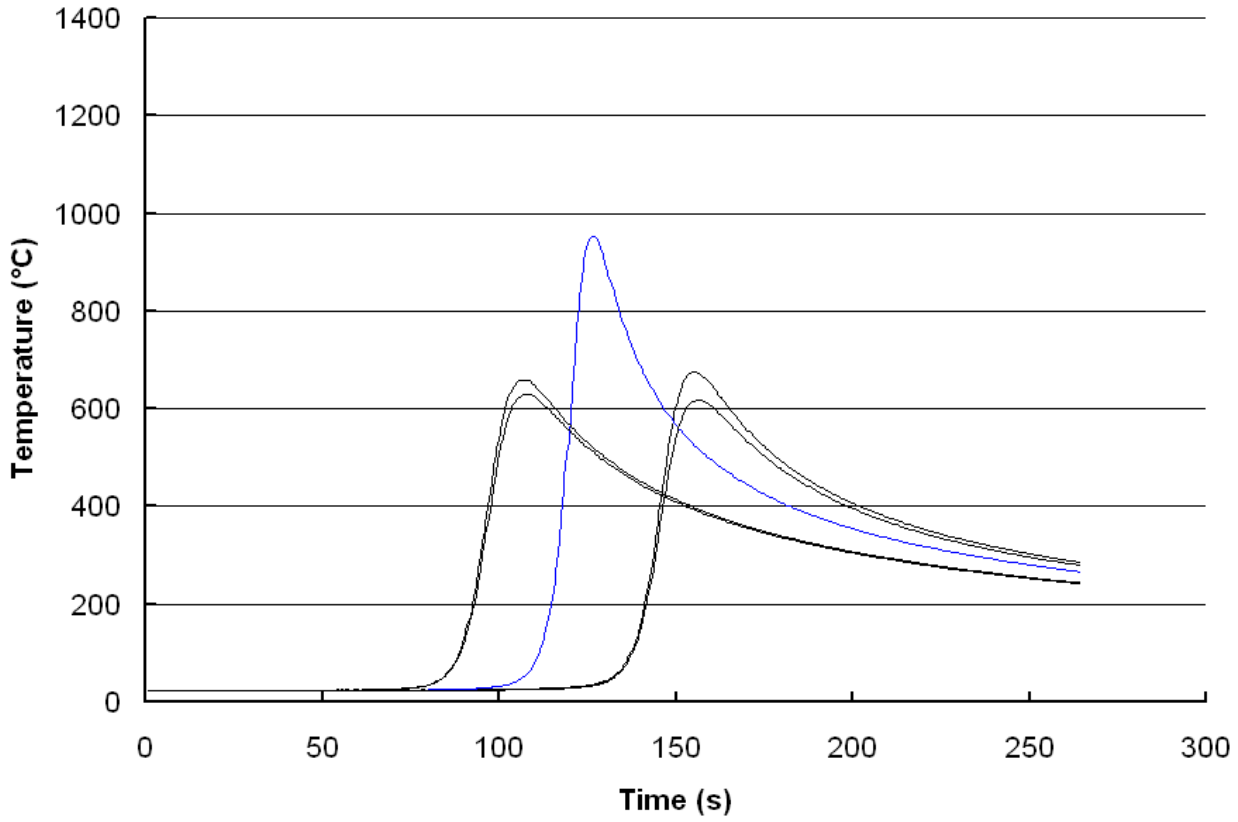

Figure 4-11. Maximum thermocouple temperatures for Figure-5 offset. Control thermocouple shown in blue.

In the above four plots, the maximum temperature of the control thermocouples is roughly the same. As the offset of the thermocouple increases the temperature decreases rapidly. At a distance of 0.5 inches away from the weld line, the temperature has dropped by as much as 50%. One caveat of these data points, however, is that they are more susceptible to error than the thermocouples arranged in a straight line. The reason for this is that it is possible that the control thermocouple and the offset thermocouples lie on opposite sides of the weld line. The error effect of this is two fold. First, the control thermocouple will read lower than it should because it is not directly underneath the weld line. Secondly, the offset thermocouples will read an artificially high temperature because in reality it is closer than the offset distance prescribes.

The misalignment effect is especially pronounced in the Figure-5 trials, and to some extent this is shown in the data. The control thermocouple reads a temperature that would be expected, based on the temperature distribution given in Figure 4-2. However, any misalignment now causes one side of the weld line to exhibit increased temperature while simultaneously decreasing the temperatures on the opposite side of the weld line. Since the data points from the offset tests may be useful for comparison to a computer model, they have been presented below in Table 4-5.

Table 4-5. Maximum thermocouple temperatures for all trials of each offset condition. Those temperatures marked with an * denote a control thermocouple. Trial 1 data were taken from Figure 4-8 – Figure 4-11.

Offset	Trial	Maximum Temperature (°C)				
		TC_A	TC_B	TC_C	TC_D	TC_E
0.1 inches	1	863.5	957.6*	811.6	878.9	858.5
	2	857.8	837.8	962.2*	731.4	819.9
	3	857.3	950.1	982.5*	951	886.8
0.2 inches	1	809.3	770.4	953.4*	830.9	782.2
	2	822	764.3	958*	857.7	830.3
	3	951*	686.7	973*	749.4	802
0.5 inches	1	457.7	417.8	965.1*	458.8	475.3
	2	414.9	421.5	985.8*	442.4	460.2
	3	592.3	531	1046.4*	509.7	492.7
Fig-5	1	659.3	629.7	953.8*	675.1	617.3
	2	670.2	594.9	862.4*	656.2	568.7
	3	736	632.7	957.2*	703.1	592.9

In summary, it was clear in all measurements, both infrared and thermocouple, that there was a large component of error. However, from preliminary data it appeared that some of the interference error associated with infrared temperature measurements can be eliminated by choosing a strategic viewing orientation and implementing a mechanical shield. These results from these tests are summarized in Figure 4-12 below.

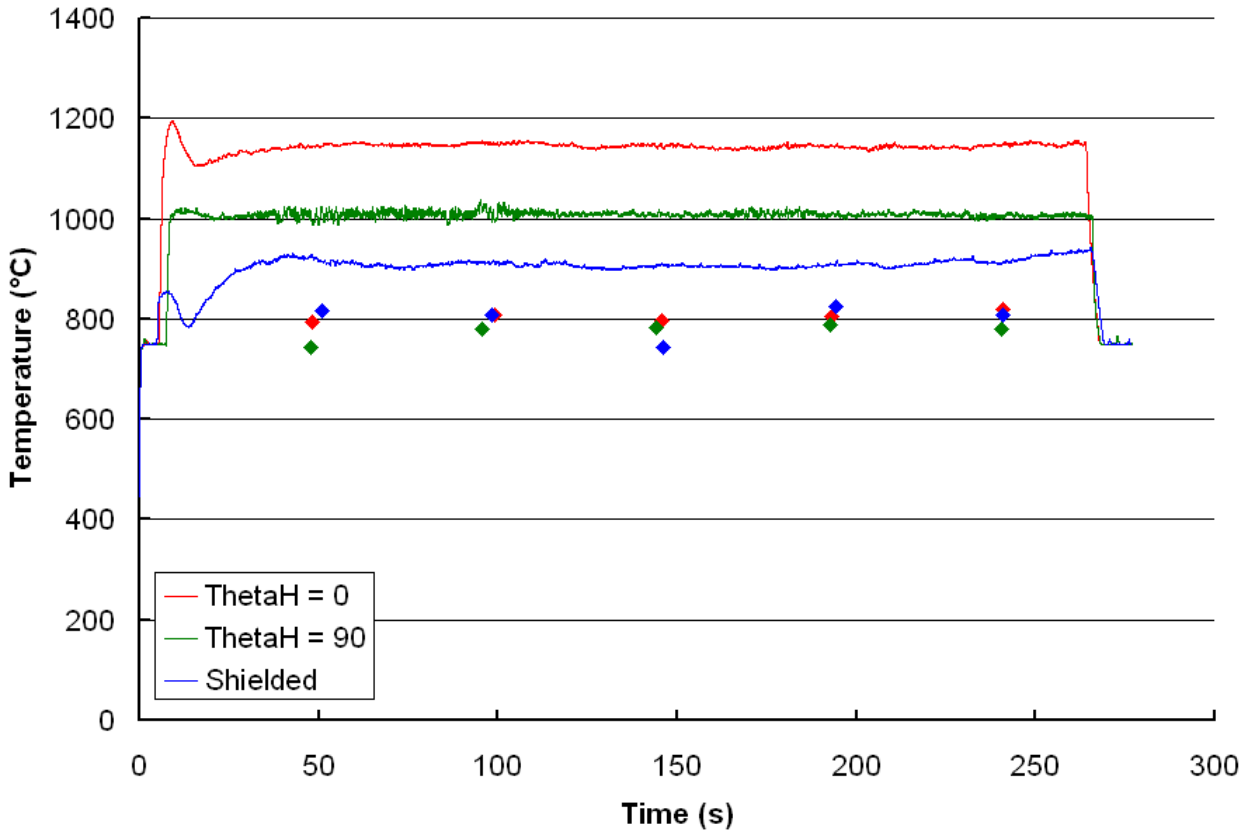

Figure 4-12. Improvement of infrared temperature measurements by partial removal of interfering sources.

Like the infrared temperature data, the thermocouple data also suffered from a component of error that can be attributed to misalignment. By way of reason, the maximum temperature sensed by all thermocouples for all similar trials can be regarded as the closest to the true bottom face surface temperature. However, because each thermocouple weld varied slightly in its position and its quality, the best analytical approach that can be taken at this point is to describe the distribution of the temperatures using minimum, maximum, and most probable values.

5 CONCLUSION AND RECOMMENDATIONS

The objective of this research was to design, build and test an experimental setup capable of simulating a TIG welding process and recording reliable infrared temperature measurements for the comparison and validation of a computer simulation. The test rig was successfully designed and preliminary data were collected. The data characterized optimal orientations for infrared temperature measurement so that interference was reduced. Infrared temperature data are best captured when viewing the welding process from a direction normal to the weld line using one color pyrometry. The data also indicated other sources of considerable error, which will be elaborated upon shortly.

Based on the results presented in the previous section, it has been shown that infrared temperature measurements in a TIG welding process are highly susceptible to two sources of error. The more difficult of the two error sources to eliminate is the interference of radiation coming from the arc and the hot tungsten electrode. It is possible to eliminate some of this interference by orienting the infrared sensor perpendicular to the weld line and focusing on a point behind the torch. Viewing the target in this manner removes the source of the interference from the instrument's line of sight, and as a result some component of the interfering radiation that is reflected off the target plate is removed also. Furthermore, it appears that attempts to use a mechanical shield to block additional radiation were successful. The infrared sensor measured a temperature decrease of roughly 250 °C between the baseline trial of $\theta_H = 0°$, unshielded and the trial $\theta_H = 90°$, shielded while the thermocouple on the opposite side of the plate maintained a temperature centered around 800 °C on the same two trials. Subsequent tests showed that large temperature variations in the infrared sensor are likely, even when comparing similar trials, but

the range of the temperature variations in these tests was ~120 °C. The fact that the thermocouple temperatures remained relatively constant coupled with the observed decrease in temperature, which was twice as large as the expected variation, is a strong indicator that some component of the interfering radiation had been removed. Having determined this, it is still uncertain as to how much interference was still contained in the captured infrared temperature signal.

The second source of error for the IR sensor was the consistency of its alignment relative to the welding torch. Although every effort was made to make sure the IR sensor focused on the same spot in each trial, it is highly improbable that the sensor focused on exactly the same position each time. It is known that large thermal gradients exist in the vicinity of the welding zone, so small changes in position in any direction will lead to very different temperature data. Furthermore, the data showed how sensitive the infrared sensor's temperature response was to slight perturbations in position. Gently tapping on the infrared sensor resulted in temperature fluctuations of 75 °C, so it is understandable how realigning the infrared sensor for each individual trial introduces a high level of uncertainty in the temperature measurements.

With respect to alignment, the thermocouples suffer a similar drawback. Although they are reliable temperature sensors, they only measure the temperature of the point in space at which they are located. Because the thermocouples were welded and aligned manually it is impossible to say that all thermocouples were identically welded and positioned in precisely the same location with respect to the center of the weld line. As has been previously stated, the influence of large temperature gradients exacerbates this error effect.

Presently, an experimental set up exists that has the capability to simulate a straight line TIG welding process and simultaneously record temperature data from two different types of sensors.

There were several problems encountered in the development of the set up which rendered it non-functional, but each of them was successfully overcome. The effects of and solutions to each problem are given in Appendix F.

The set up has been tested under a variety of configurations, and data have been generated that characterizes its behavior, particularly with respect to the infrared sensor whose application is of primary interest. The work accomplished provides a good starting point for the continuation of this research. Known issues still exist, but with an improved design it is hoped that they their effects will be minimized.

There are several recommendations that can be made that will potentially improve the accuracy and precision of the experimental set up. First, in order to achieve accuracy in the infrared temperature measurements, the emissivity of the plate must be determined. The best way to accomplish this is by sending several samples to a lab. Prior to welding the samples, it would be beneficial to apply a consistent surface treatment to each plate. At a minimum this treatment should include abrading the surface with rough sandpaper and cleaning contaminants such as grease or oils from the surface with acetone. The samples should be taken from welds that have the same experimental parameters as those that will be investigated. Different weld speeds and welding currents change the heat flux and also the level of oxidation. The other critical variable is gas flow. Lower gas flows have been observed to produce welds that are duller and darker in appearance than those welds created with higher gas flows at the same welding current. For reasons that will be discussed later, it may also be useful to determine the spectral properties of a piece of target material that has not been welded.

One accessory that is sometimes used with an infrared sensor, and the M770S in particular, is a sight tube, which is an 18 inch long aluminum cylinder with the inside coated in a flat black

finish. These are often used in harsh environments, especially where particles in the air may obstruct the line of sight. The sight tube, if positioned very close to the area of interest, may also serve as a secondary mechanical shield, possibly removing additional interference. A housing unit for the M770S is available, but it is cost prohibitive. While the housing unit is not necessary for the implementation of the sight tube, it does provide rigid support. An alternative approach would be to design a component attached to the support structure that would rigidly secure the sight tube. Because of geometry of the sight tube, it would be best implemented such that the infrared sensor was oriented at $\theta_V = 90°$. In this way it could be mounted and remain a fixed distance from the target plate. Another option would be to machine the end of the sight tube to an angle that would suit some other preferred vertical angle. One remaining problem with the use of a sight tube is that as the sight tube gets closer to the target plate, less visible light is allowed in, and proper aiming of the infrared sensor becomes problematic; however, it may be possible to install an LED partially surrounded by a reflective material inside the sight tube to provide enough light by which to aim the instrument. Fitting the open end of the sight tube with an aperture may also reduce interference even more. An additional benefit of using the sight tube is that it maintains the infrared sensor at a fixed distance away from the target, thus removing a source of experimental variation. Since the M770S takes an average temperature of the surface seen in the viewing reticle, a shorter line of sight necessarily results in a smaller target area. As this area approaches zero, the temperature at a point in space is approached. Since the viewing area has some finite value over a large temperature gradient, the maximum temperature on the weld line will never be measured by the infrared sensor, but by keeping the viewing area at a minimum, which is determined by the minimum focus distance, it is at least possible to approach a best case scenario. However, because of the likelihood of the presence of EMI, this may not be

feasible as damage to the infrared sensor may result. Another problem with using a sight tube is that a minimum distance of the radius of the sight tube between the focus area and welding torch is imposed, which may put the focus area outside the area of interest.

The focus area on the target plate is also worth reconsidering. All trials were taken with the focus area at 0.4 inches directly down weld of the torch. While viewing this area from an angle of $\theta_H = 90°$ had the apparent effect of reducing interference from the weld zone when compared to $\theta_H = 0°$, further reductions of interference may be possible by moving the focus area just beyond the weld line. In this way, the line of sight a) does not pass through the welding zone, and b) is focused at a point beyond the torch. Assuming that radiation originating from the welding zone and reflected by the target plate has some forward directional preference, this may have the effect of reducing unwanted reflected radiation. Since the focus area is no longer on the weld line, in this instance knowing the emissivity of a clean target plate surface is crucial for accurate temperature measurement. Because of the obstructing presence of a mechanical shield, at a position removed from the weld line it becomes possible to attach thermocouples to the top face of the target plate. Using a low welding current of about 80 A for a ¼ inch thick target plate so that burn through is not achieved, it becomes possible to compare the temperature readings of the infrared sensor and a thermocouple when the infrared sensor is focused on the area where a thermocouple is located. Choosing a new focus area may also carry with it the obligation to reconsider thermocouple placement on the bottom face of the target plate.

With respect to the infrared sensor, yet another consideration is to purchase a more versatile instrument, preferably one that allows the attachment of a fiber optic cable and is sensitive to temperatures below 750 °C. Attaching a fiber optic cable presents two distinct advantages. Firstly, the instrument itself can be remotely located so that it is not in the immediate presence of

strong EMI which may damage it or at the very least corrupt its sensors. Secondly, more certainty in its position can be attained. The tip of the fiber optic cable could be rigidly positioned with respect to the torch, and it could also be mounted at a fixed height above the plate. These improvements will help minimize the uncertainty in the measurements that arise from continuous realignment between trials, and it may serve to minimize interference by fact of its close proximity to the plate. Fiber optic cables can be specified by their acceptance angle. Knowing this angle, the diameter of the fiber optic cable, and its height from the target plate, the focus area can be calculated. A narrow acceptance angle and short height above the plate result in a small target area, thus the maximum temperature detected can be further refined. If the height above the target plate is very small, as it should be to decrease both interference and focus area, precautions must be taken to ensure that unevenness in the target plate will not cause the two to scrape against each other over the course of a trial, scratching and ruining the tip of the fiber optic cable. It should also be made certain that no damage to the fiber optic cable will occur as a result of its proximity to the torch.

Purchasing a new infrared sensor and using the sight tube have one thing in common. The use of either of these implementations facilitate measuring the target area from an orientation where $\theta_V = 90°$. The cost of a new sensor may not be affordable, and it may be undesirable to effect permanent changes to the sight tube, but a design could be imagined where the M770S is rigidly supported such that it can reliably acquire measurements from such a vertical viewing angle. Previous data suggested that this might not be the optimal orientation because it did not have the least amount of variation. However, the tripod on which the infrared sensor was mounted was not conducive to such an orientation. Further exploration of this viewing angle is worthwhile provided that a change in design allows for secure positioning of the infrared sensor.

In previous trials the infrared sensor tripod did not comply to this orientation, allowing an opportunity for the infrared sensor to wander from the intended target area.

Changes can also be made to the target plate to ensure proper alignment and thermocouple placement. If the target plate is not lined up squarely with the carriage on the slide table, then a weld line is created at an angle that is not perfectly parallel with the edges of the target plate. This small deviation is enough to cause relatively large changes in temperatures as detected by the thermocouples. For this reason, guides can be installed that secure to the safety plate. These guides need be little more than vertical rails that extend just above the target plate between which the target plate can rest, keeping it properly aligned. At this point it becomes necessary to question the alignment of the safety plate, which is a valid concern. Although the process of ensuring that the safety plate is squarely aligned can be tedious, it should only need to be done once because it is never removed unlike the target plates which are removed and replaced after every trial. This will offer an additional layer of consistency with respect to the passage of thermocouples beneath the torch, provided that the thermocouples are all ideally positioned. A potential problem with this design is that the guide rails will act as local heat sinks, affecting the thermal profile of the target plate. To minimize such effects, the guide rails can be made relatively thin so that the contact area is reduced to a sufficient amount.

When aligning thermocouples, it is not only important to make sure that they fall in line parallel with the direction of travel, but it is also important that they fall in line with the welding torch. Since the thermocouple array is located on the bottom face of the target plate, it is difficult to determine how accurately they are positioned. To this effect, two very shallow paths can be machined into the target plate. Removing a small amount of material on the top and bottom surfaces of the target plate can serve as a guide for welding thermocouples as well as boundaries

for visibly witnessing in real time the complete trajectory of the target plate with respect to the welding torch. Choosing appropriate width dimensions for each path can help ensure that the thermocouples fall very closely in line with the welding torch. A dimension of 1.5 times the electrode diameter centered above a width dimension appropriate for the gauge of the thermocouple wire can help ensure that the torch will pass very close to the vertical plane of the thermocouples. With the thermocouples welded along their path, a trial run of the welding path is all that is required to make sure the torch tip stays within its path, and by extension very closely above the thermocouples. There will still be some error involved, especially with regard to the quality of the weld of individual thermocouples, but it may help impose some thermocouple distance limits on the horizontal distance away from the torch. However, removing material from the plate clearly changes its geometry, and this should be accounted for in any computer simulation.

Just as the variation of placement affects thermocouple measurements, the quality of the thermocouple weld is largely dependent on how close the leads are to one another. Ideally, the two leads fuse together and attach to the target plate. If the leads are relatively far away, then the thermocouple measures an average temperature for the two points. In this particular application, 0.1 inches is considered far away. Unless the user is already proficient at welding thermocouples, this skill should be practiced until confidence in the weld quality is attained prior to welding thermocouples to the target plate. Suggestions on how to create a quality thermocouple weld are provided in Appendix E.

The target plates were designed with the intention of using each one three times, meaning that each plate would undergo three separate welding events in three different locations. As it turned out, multiple trials on a single target caused severe deformation, rendering the plates unfit

for experimental investigation. It is important that the mechanical shield height maintains a constant value throughout the length of the weld line. The plates need to be redesigned so that each plate receives only one trial. Presumably, this will only involve reducing the width dimension of the plate. As the plate becomes narrower, edge effects become more pronounced, and increased surface temperatures should be expected. Also, since it appears that the target plate reaches a steady state condition at $t \approx 50$ s, the length of the trials can be reduced. This is not to be misunderstood with making the target plates shorter. Decreasing the length dimension may cause unwanted heat loss through conduction on the support end of the target plate. Reducing the length of the trials offers two benefits. For a given velocity, trial times will be shorter, and with shorter lengths, the thermocouples can be placed in closer proximity to one another, which can help reduce the effects of potential misalignment.

Final suggestions for improvement of the experimental set up involve mounting two components more rigidly to the support structure. Both the torch and the shield need to be secured more permanently. Any movement in either of these two components can drastically affect the temperature results, and under the current design, they are both zip-tied to the support structure. Initially, metal worm drive clamps were used to secure the torch to the welding arm, but electricity was observed arcing between the clamps. This did not appear safe, so plastic zip-ties were used in their place. Perhaps a worm drive clamp can be used with proper insulation surrounding the section of the welding arm and torch to where the clamp will fasten. The situation is similar with the shield, but zip-ties had to be strategically located to avoid melting. If the zip-ties were placed too close to the target plate, heat conducted through the shield would melt the zip-tie, and the shield would fail.

The present experimental setup is functional, and preliminary data seem to suggest that it is possible to use a one color infrared sensor to acquire temperature data in the vicinity of the welding zone. Future tests may also involve further investigation of the Graybody assumption and its potential breakdown. Present tests in the two-color mode show immediate wash out of the IR sensor, meaning that the detected temperature lies above the maximum value recorded by the instrument. While in two-color mode, the detected temperature is above 2000 °C which is well above the ~1500 °C melting point of the material. To test the validity of the Graybody assumption, it may be useful to simulate two identical welding conditions while recording the temperature output of the IR sensor from both the short waveband and long waveband modes of one color detection. If the Graybody assumption is valid then the two temperatures in both wavebands should be the same. However, this experimental setup is especially problematic to this approach given the high degree of variation inherent in the repeatability associated with the exactness of the location of the IR focus area.

There is no doubt that the data collected thus far is susceptible to error. Several ideas have been presented as to how it may be possible to reduce some of these error sources, improving the signal to noise ratio, and these recommendations provide a good starting point for continued research in this area.

References

[1] Incropera, F., DeWitt, D.P., "Fundamentals of heat and mass transfer, 5 ed." John Wiley & Sons, Inc., Hoboken, NJ, p. 724, 2002.

[2] Doumanidis, C.C., Hardt, D.E., "Multivariable adaptive control of thermal properties during welding," *Journal of Dynamic Systems, Measurement and Control, Transactions of the ASME*, Vol. 113, No. 1, p. 82-92, 1991.

[3] Kannatey-Asibu, Elijah, Jr., Kikuchi, N., Jallad, A.R., "Experimental finite element analysis of temperature distribution during arc welding," *Journal of Engineering Materials and Technology, Transactions of the ASME*, Vol. 111, No. 1, p. 9-18, 1989.

[4] Barry, J.M., Paley, Zvi, Adams, C.M., "Heat Conduction from Moving Arcs in Welding," *Welding Journal*, Vol. 42, No. 3, p. 97S-104S, 1963.

[5] Rosenthal, D., "Mathematical theory of heat distribution during welding and cutting," *Welding Journal*, Vol. 20, No. 5, p. 220s-225s.

[6] Ramsey, P.W., Chyle, J.J., Kuhr, J.N., Myers, P.S., Weiss, M., and Groth, W., "Infrared Temperature Sensing Systems for Automatic Fusion Welding," *Welding Journal*, Vol. 42, No. 8, p. 337S-346S, 1963.

[7] Farson, D., Richardson, R., Li, X., "Infrared temperature measurement of base metal temperature in gas tungsten arc welding," *Welding Journal*, Vol. 77, No. 9, p. 396S-401S, 1998.

[8] Bicknell, A., Smith, J.S., Lucas, J., "Infrared sensor for top face monitoring of weld pools," *Measurement Science & Technology*, Vol. 5, No. 4, p. 371-378, 1994.

[9] Govardhan, S.M., Wikle, H.C., Nagarajan, S., and Chin, B.A., "Real-time welding process control using infrared sensing," *Proceedings of the American Control Conference*, Vol. 3, p. 1712-1716, 1995.

[10] Nagarajan, S., Chen, W.H., Chin, B.A., "Infrared sensing for adaptive arc welding," *Welding Journal*, Vol. 68, No. 11, p. 462S-466S, 1989.

[11] Khan, Mansoor A., Madsen, N.H., Goodling, J.S., and Chin, B.A., "Infrared thermography as a control for the welding process," *Optical Engineering*, Vol. 25, No. 6, p. 799-805, 1986.

[12] Banerjee, Probal, Chin, B.A., "Infrared sensor-based on-line weld penetration control," Proceedings of SPIE - The International Society for Optical Engineering, Vol. 1933, THERMOSENSE XV, 1993, p. 83-92.

[13] Banerjee, P., Govardhan, S., Wikle, H.C., Liu, J.Y., and Chin, B.A., "Infrared sensing for on-line weld geometry monitoring and control," *Journal of Engineering for Industry, Transactions of the ASME*, Vol. 117, No. 3, p. 323-330, 1995.

[14] Menaka, M., Vasudevan, M., Venkatraman, B., and Raj, B., "Estimating bead width and depth of penetration during welding by infrared thermal imaging," *Insight*, Vol. 47, No. 9, p. 564-568, 2005.

[15] Wikle, H.C. III, Kottilingam, S., Zee, R.H., and Chin, B.A., "Infrared sensing techniques for penetration depth control of the submerged arc welding process," *Journal of Materials Processing Technology*, Vo. 113, No. 1-3, p. 228-233, 2001.

[16] Raghavan, S., Wikle, H.C. III, Chin, B.A., "Adaptive control of arc welding using infrared sensing," Proceedings of SPIE - The International Society for Optical Engineering, Vol. 1933, THERMOSENSE XV, 1993, p. 76-82.

[17] Nagarajan, Sundaram, Banerjee, P., Chen W.H., and Chin, B.A., "Control of the welding process using infrared sensors," *IEEE Transactions on Robotics and Automation*, Vol. 8, No. 1, p. 86-93, 1992.

[18] Fan, H., Ravala, N.K., Wikle, H.C., and Chin, B.A., "Low-cost infrared sensing system for monitoring the welding process in the presence of plate inclination angle," *Journal of Materials Processing Technology*, Vol. 140, Special Issue, p. 668-675, 2003.

[19] Zhang, YuMing, "Real-time weld process monitoring," CRC Press LLC, Boca Raton, FL, p. 74-99, 2008.

[20] Lukens, W.E., Morris, R.A., "Infrared temperature sensing of cooling rates for arc welding control," *Welding Journal*, Vol. 61, No. 1, p. 27-33, 1982.

Appendix A: Experimental Setup

The goal of this research is to determine whether or not surface temperatures can be accurately measured by detecting infrared radiation emanating from the top face of a work piece undergoing a TIG welding process. In order to accomplish this goal it is necessary to design an experimental setup that can both simulate a welding operation and measure temperatures. The current design is composed of six different functional groups. The functional groups are the support structure, the welding unit, the target plate motion system, the data acquisition system, the thermocouple modules, and the infrared instrument. Each of these functional groups will be elaborated upon in the following sections.

A.1 Support Structure

The support structure was designed as a free standing assembly whose main purpose was to hold the welding unit and motion system in a fixed position relative to one another. It was constructed using one inch square steel perforated square tubing. The perforations are one inch apart from one another, allowing for ample flexibility in the support structure's configuration. The base of the support structure consists of eight interconnected legs to provide a sturdy foundation and minimize any wobbling or unwanted motion. A picture of the support structure is shown in Figure A-1.

Figure A-1. Support structure for welding experimental setup. A – welding arm, B – guide screws. The welding torch secures to the welding arm so that it remains in a fixed position, and the guide screws are used to ensure that the slide table moves the target in a

Halfway up the support structure there are cross beam on which a slide table, which is part of the motion system, rests. It is held in place by two screws that pin it against the rails running the length of the support structure. This is done to ensure that there is no side to side movement of the target plates as they undergo welding. Any motion perpendicular to the direction of the weld will misalign the arc with respect to the various temperature sensors.

Moving up the structure, there are two other cross beams with a section of tubing bolted to them and oriented normal to the plane of travel as indicated by the layout of the slide table. This section is the torch support. The torch support holds the welding torch in a fixed position and the torch is secured to the torch support using two slotted banding clamps. The banding clamps are affixed to the top and bottom of the welding torch so as to minimize any unwanted motion that

might be caused by the presence of the arc. The use of banding clamps facilitates manipulation of possible experimental variables associated with the torch. For one, the banding clamps allow for the torch height to be changed rather easily. Also, the bottom banding clamp can be fitted with a strip of steel foil that can serve as a radiation shield, whose height can also be manipulated quickly.

The open areas to either side of the torch support are meant to be used as viewing windows so that the infrared sensor, when positioned at horizontal angles greater than 0°, has an unobstructed field of vision on the target plates. The tube stock as shipped had no finish on it and appeared as if it would be a good reflector. In order to reduce undesirable reflections from the arc area, the entire support structure has been painted in flat black.

A.2 The Welding Unit

In an effort to keep the experimental setup as consistent with the industrial application as possible, a TIG welding unit was purchased. The TIG welding unit is a Lincoln Invertec V160-T, and it has an operating range of 5-160 ADC. The V160-T can be operated in either TIG mode or stick mode, and the arc can be struck using either a scratch start or a high frequency start. Additional features of the V160-T include downslope control, 2-step or 4-step trigger sequences, postflow control, pulse mode and pulse frequency control. Some of these features will not be used, but in future research having the ability to manipulate these parameters may be important.

Other specialized and necessary items were ordered in addition to just the basic welding unit. These specialized items are a remote arc start switch and a straight TIG torch. The arc start

switch which is a pressure switch plugs into the front of the welding unit and must be in the depressed position in order to initiate and maintain a welding arc. A modification was made to this control device to allow greater motility to those using the experimental setup. The pressure switch was cut from the cable, leaving approximately 6 inches of wire on the switch side. At the end of the cable still connected to the V160-T, a standard light switch was installed. Now the arc start switch could be held in the "on" position without having to apply constant pressure to the original switch. Visual inspections were made of the new installment to ensure that there were no exposed live surfaces. The straight torch was ordered to provide and easier fit to the torch support of support structure. Straight torches are more amenable to mounting than are standard hand torches, and they are commonly used in industrial applications. In addition to these upgrades, other necessary equipment was purchased. This equipment includes different sized work clamps, 2% thoriated tungsten electrodes with diameters of 1/16 and 3/32 inches, face masks, welding helmets, and welding gloves. The welding unit is shown in Figure A-2.

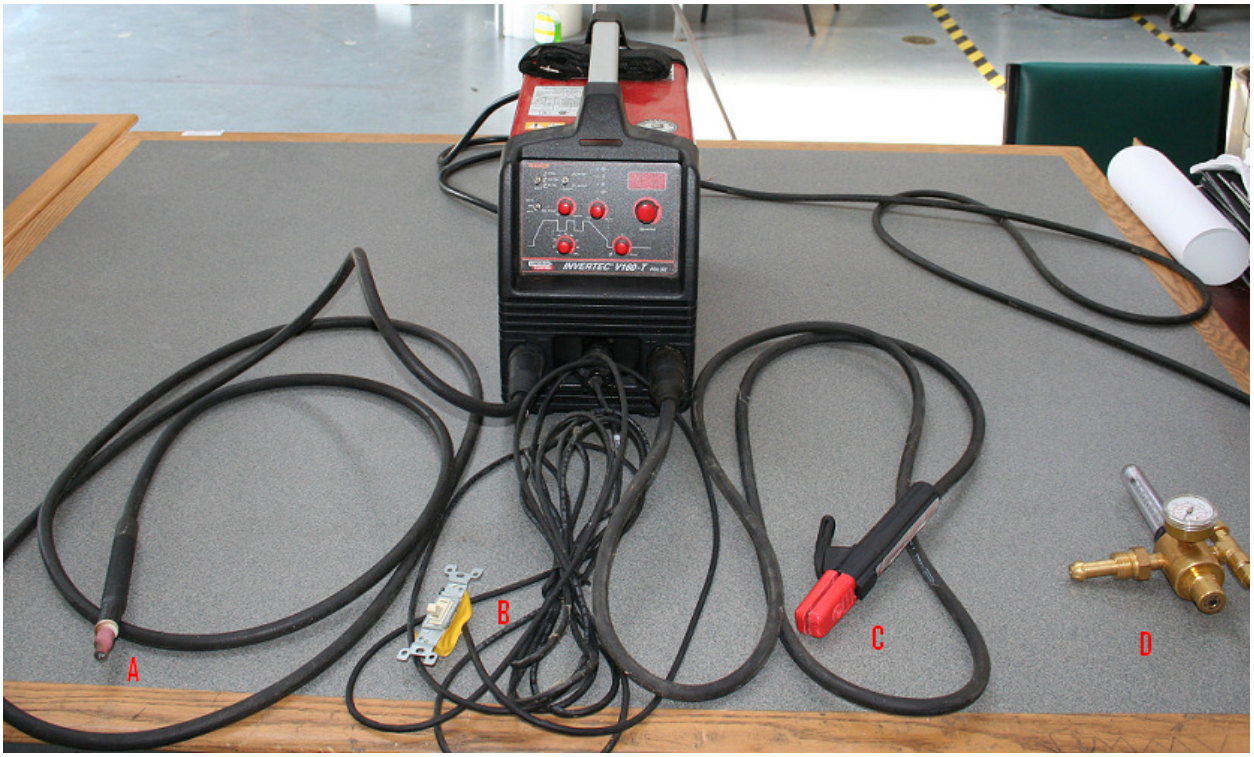

Figure A-2. Lincoln Invertec V160-T TIG welder base unit showing A – torch, B – modified arc start switch, C – ground clamp, and D – shielding gas regulator.

The tungsten electrodes must be prepped and properly placed in the torch before use. The tip of the electrode must be shaped to a point with a grinder in such a way that the grinding lines are in line with the length of the electrode. The pointed tip keeps the arc straight and prevents it from wandering. The sharpened electrode should be inserted into the torch so that it extends no more than ⅛" past the gas cup. Should an electrode become contaminated or need reshaping, the electrode should be removed from the torch and the tip broken off. Since tungsten is very brittle, simply pressing down on the tip at an angle will result in a clean square break. The tip can then be reshaped with the grinder.

Since TIG welding requires an inert shielding gas, a 336 ft^3 tank of Argon was purchased along with the Harris model 355-AR-58010 Argon flow meter and 10 ft hose. The regulator attaches to the top of the tank next to the valve. The 10' hose then connects the regulator to the

gas inlet port on the rear of the V160-T. Once the valve on the tank is opened, the regulator can be adjusted to provide the desired amount of air flow. Because the Argon tank is under tremendous pressure, extreme care is taken so that it does not sustain any damage whatsoever, particularly with respect to the valve area, as this is the weakest point on the cylinder. To this end, the tank is always stored out of the way in an upright position and securely chained to a large, sturdy, and rigid fixture. Figure A-3 shows a picture of the shielding gas cylinder and its connections.

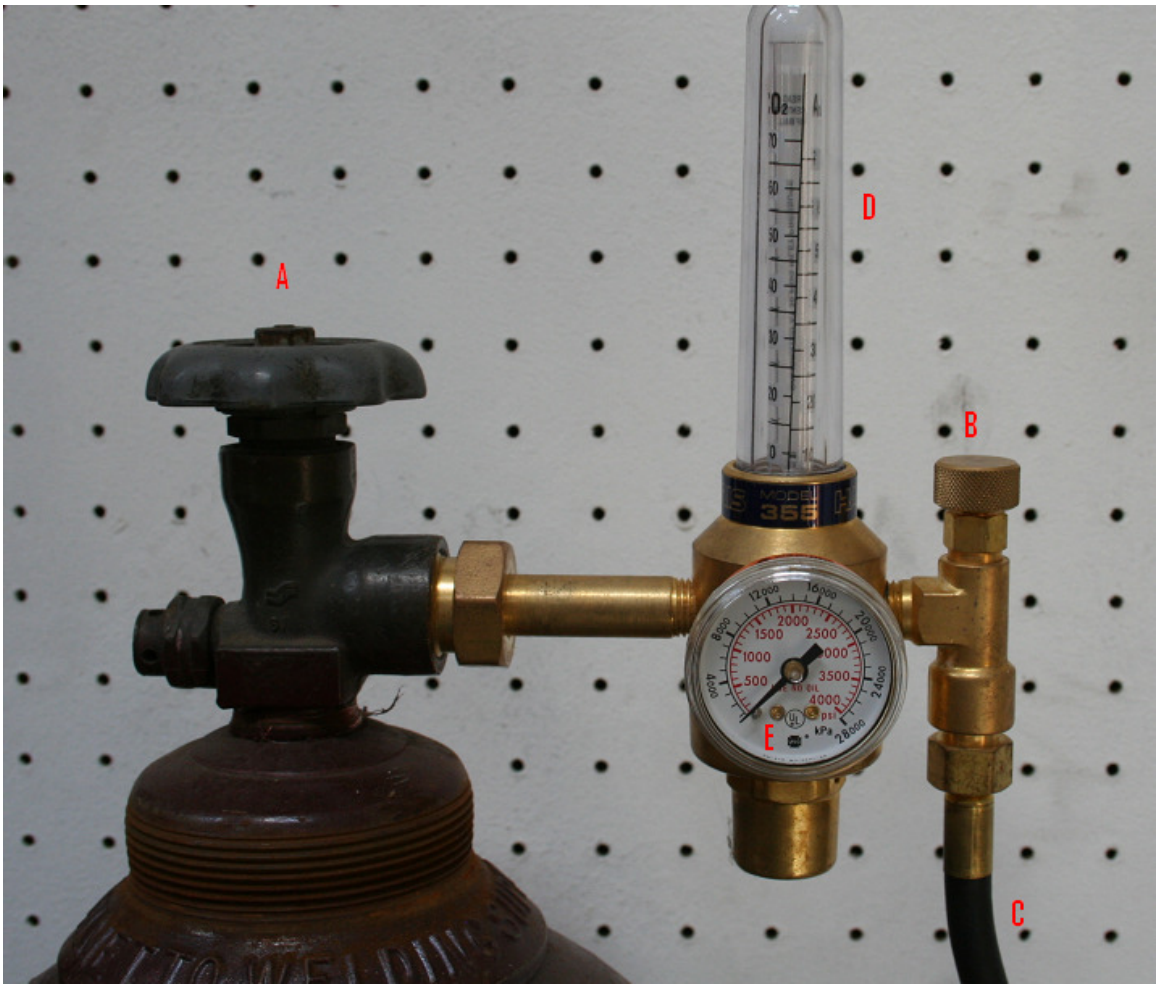

Figure A-3. Shielding gas cylinder. A – main cylinder valve, B – flow regulator, C – shielding gas supply line to welding unit, D – flowmeter, E – cylinder pressure gage. Although not shown, the cylinder is chained to the wall for safety purposes.

During testing, the welding unit must be configured and operated properly to ensure repeatability and safety. Since no filler wire will be used in the experiments, the V160-T must be set to operate in TIG mode. Furthermore, the torch cable must be connected to the (-) terminal, and the work clamp must be connected to the (+) terminal. Both of these terminals are located on the front face of the V160-T. The torch is then secured to the torch support at a predetermined height above the work piece, and the work clamp is attached to the backside of the work piece. The V160-T can then be powered on, and the current can be set by using a variable current select dial. After opening the valve on the Argon tank, the flow regulator can be adjusted to provide the appropriate amount of shielding gas. Only after these steps have been taken is the welding system ready for use.

In addition to the setup steps all safety guidelines must be followed. A welding helmet should be worn at all times when the welder is in use. Welding gloves must always be worn to avoid electric shock. Clothing should cover any exposed skin, and shirttails should not be tucked in. Work boots are the most appropriate footwear, but any closed toe shoe will suffice. A welding curtain should contain the work area to prevent others from inadvertently looking directly at the arc. The work piece should be clear of any debris, and all cables should be checked for excessive wear or exposed wires. Ventilation should be used to help remove any harmful fumes that result from the welding process. For this setup, a large floor fan and an open door are used to remove these fumes. Welding of any type is a potentially dangerous process. It is imperative that these regulations are followed to avoid damage caused to the eyes and skin as a result of ultraviolet radiation, extremely hot metal, and/or electrocution. When welding certain types of metals, like stainless steels, an exhaust system must be used to avoid inhaling toxic fumes.

As previously mentioned, there are two ways to start the arc when the arc start switch is in the “on” position. To initiate the arc with a scratch start, the work piece is simply scratched with the electrode, taking care to quickly back away from the work piece. If the torch is pulled too far from the work piece, then the arc cannot sustain itself and the sequence must be repeated. If the torch is not pulled away quickly enough, the electrode will stick to the work piece and become contaminated. However, within the scope of these experiments the torch is always maintained in a fixed position that is not in physical contact with the work piece and an alternate method of scratch starting must be used. Given these conditions, a scratch start can also be initiated by taking a spare tungsten electrode and touching it to the torch electrode and work piece simultaneously. Welding gloves MUST be used to avoid severe electric shock while executing this procedure. As an extra precaution, electrical tape can also be liberally applied to one end of the spare electrode.

Initiating the arc in the high frequency mode is much simpler in comparison. In order to strike the arc, direct contact between electrode and work piece is not required. The torch can be held just above the work piece and high frequency pulses are sent to the torch initiating the arc. Once the welder has detected the presence of the arc, the high frequency pulses cease, and it returns to normal operation. To terminate the arc in either scratch start or high frequency start modes, the user only needs to set the arc start switch to the “off” position.

A.3 Target Plate and Motion System

The target plate motion system consists of a one meter x-direction slide table, a brushless DC servomotor, a DC servo drive, and target plate assembly. The purpose of this functional group is to provide a consistent weld path for the target plate to follow at a speed that can be controlled.

The slide table is made by Thomson, and its part number is 2RB12G0N1200. It is a total of 1200mm long, and its stroke length is 1 meter. Throughout the stroke length, the carriage is continuously supported so that there is no flexion on the lead ball screw. Within the screw cavity of the slide table there are three limit switches that can be used for precision position control. On one end of the slide table there is a mount for a motor to drive the ball screw.

The motor chosen for this application is an AKM24D-ANDNC brushless servomotor available from Integrated Motion. This motor is capable of a peak torque of 4.76N-m and a maximum rotational speed of 8000rpm. These specifications are sufficient to move the ~7kg target assembly up to the maximum desired speed of 15cm/min. The servomotor attaches to the slide table via a collar that is part of the slide table. Power to the motor and feedback are provided by the servo drive. The servomotor and slide table are shown in Figure A-4.

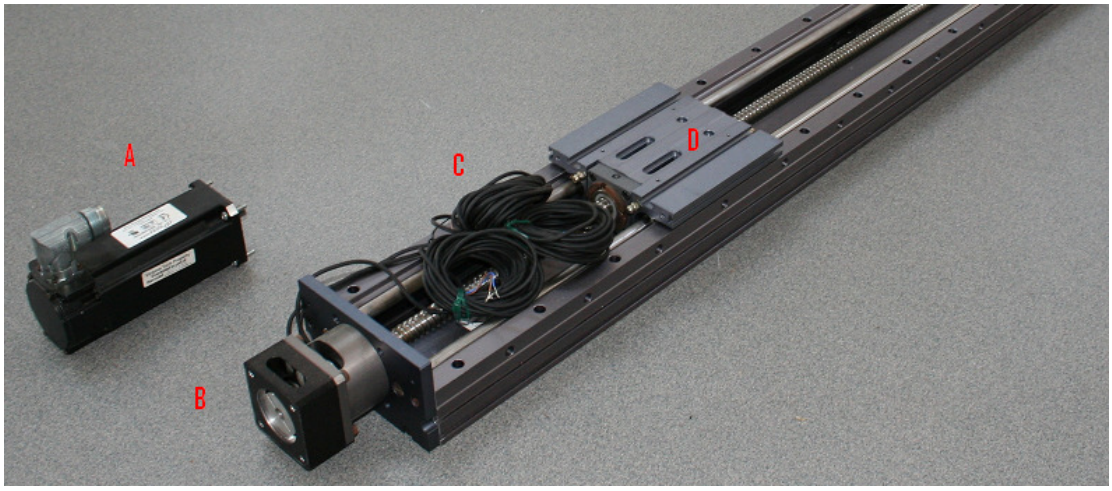

Figure A-4. Slide table and servomotor. A – servomotor, B – connection for servomotor, C – limit switches for smart feedback control (3), D – carriage.

The servo drive, also available from Integrated Motion, is an S200 base unit with part number of S20360-VTS. It is a brushless servo drive operating on 120/240 VAC, and it is rated at 3A. It is capable of working in either continuous velocity or continuous torque modes. The servo drive also has Smart Feedback Device (SFD) capabilities. Figure A-5 shows the servo drive and its connecting cables and power supplies.

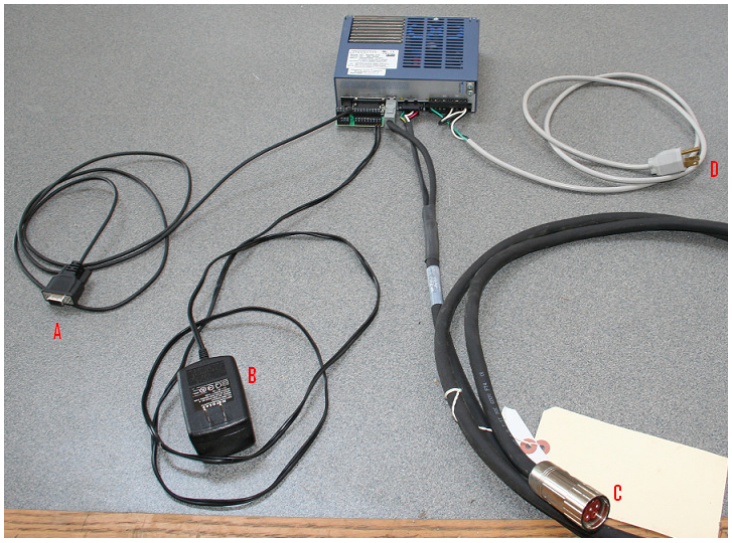

Figure A-5. S200 Series servo drive. A – RS232 connection to PC, B – power supply, C – power supply and SFD to servomotor, and D – power supply.

The motor connects to the S200 by way of a 3m composite cable from Kollmorgen that carries power and feedback. The feedback control connects to terminal J3 on the front of the S200, and the motor control connects to terminal J2. The S200 receives 120VAC power from a standard 3-prong cable. One end of the 3-prong cable plugs into an outlet, and the other end is clipped so that the wires can be connected to terminals L1 and L2 on the J1 AC Power terminal block. Terminals L1 and L2 must then have jumpers between C1 and C2, respectively. The L terminals provide power to the unit and motor while the C terminals provide power to the control system. The S200 then connects to a laptop computer with a RS232 serial communication cable. The mod jack terminal connects to the J5 terminal on the S200, and the DB-9 terminal connects to a serial port on the laptop. These connections are shown in Figure A-6.

Figure A-6. Close up of S200 series servo driver showing all connections.

Once power has been established to the S200 unit, a laptop computer controls the motor using S200 Tools, a software program provided by Integrated Motion. In S200 Tools the drive

must be configured to allow SFD and to operate in a constant velocity mode. To adjust the velocity of the carriage on the slide table, the CmdGain and CmdOffset values on the Command Control tab need to be varied. Screen shots for properly configuring the S200 series servo driver are shown in Appendix B. A series of tests were run to calibrate the voltages and carriage velocity. During these tests, the CmdOffset was held constant at 0 V, and the CmdGain was varied between 0.25 and 2 kRPM/V. The motor was allowed to move for an interval of 1 minute. Knowing the starting point and ending point, the distance could readily be measured, and the speed calculated. Data from the servomotor speed calibration can be found in Appendix D.

Depending on the load applied to the carriage on the slide table, the motor may need to be tuned. If the slide table hums while in use, tuning is necessary. Tuning the motor is accomplished merely by adjusting the KVP, KVI, ARF0 and ARF1 values found on the Loop Gains tab, and it is an iterative process. The gains should be slightly adjusted one at a time while the slide table is in motion. Care needs to be taken so that the carriage does not force itself against either end of the slide table while the operator is adjusting the gain values. This may cause catastrophic and permanent damage to both the slide table and the motor.

The target plates are made of type 304 stainless steel. The dimensions of the plate are 18”x6”x¼”. On one end, the plates have four penetrations that are arranged in a rectangular formation which are used for support and mounting it to the carriage on the slide table. On the opposite end of the support penetrations, there are four penetrations in a line along the edge. These penetrations help secure a small steel bar to the bottom side of the target plate. The purpose of this steel bar is to provide strain relief for thermocouples that are spot welded to the bottom side of the plate. Without the strain relief bar in place, the thermocouples would detach

themselves from the target plate as it is moved along the slide table. A typical line of thermocouples secured by the strain relief bar is shown in Figure A-7.

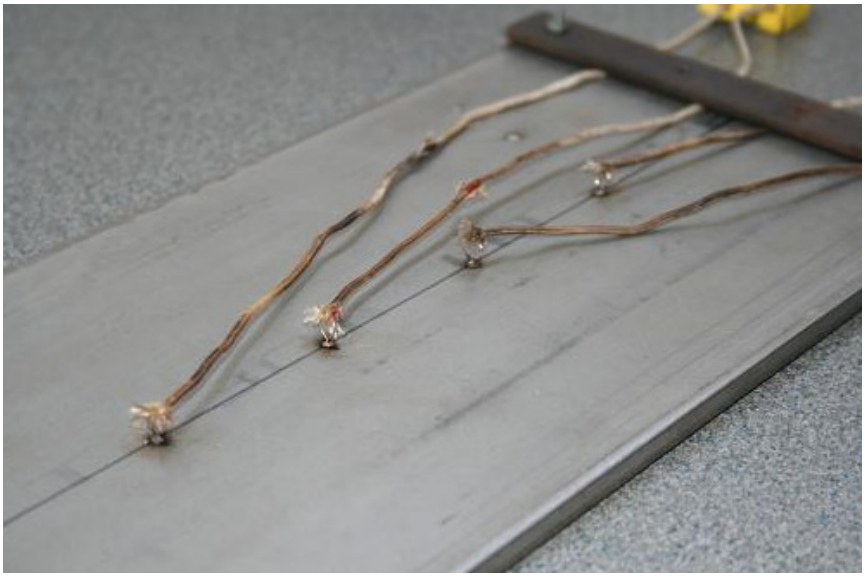

Figure A-7. Bottom side of target plate with spot welded array of thermocouples secured by the strain relief bar.

The target plates mount to the carriage on the slide table. The carriage has two T-slots that run along the length of the slide table. Four T-slot bolts were purchased and machined so that they fit securely in the carriage. The T-slot bolts are shown in place on the slide table carriage in Figure A-8.

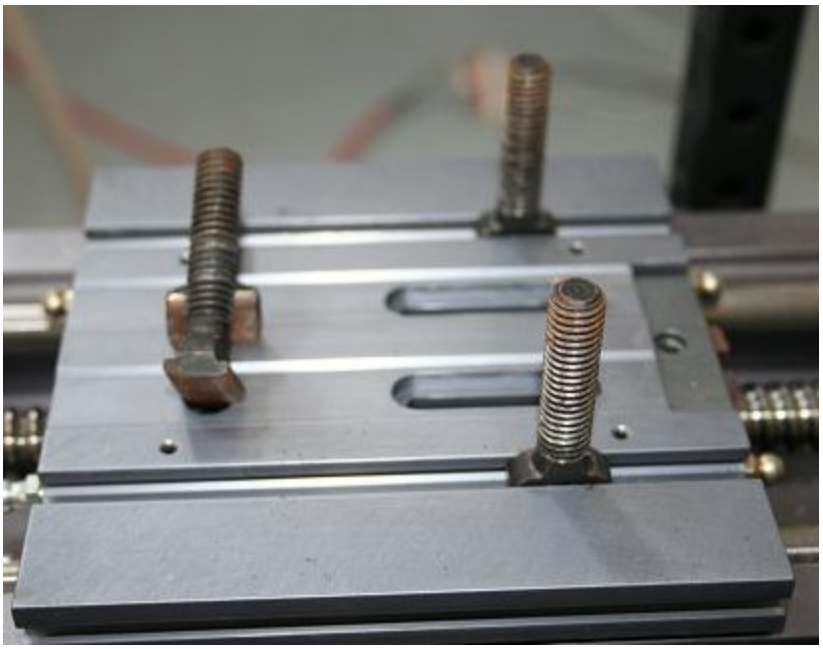

Figure A-8. Slide table carriage and T-slot bolts.

The target plate area actually consists of two identical steel plates. The bottom plate serves as a protective plate should any slag fall from the target plate above. The protective plate is held in position by two nuts on each of the four T-slot bolts. These nuts also serve as spacers to provide some distance between the target plate and the protective plate. Above these spacers are a series of three high temperature, electrically insulating glass-mica ceramic discs. The first outside spacer prevents any metal to metal contact between the bottom side of the target plate and the spacing nut below. The next spacer prevents any metal to metal contact between the target plate and the T-slot bolt inside the penetration of the target plate. The top outside spacer prevents any metal to metal contact between the top side of the target plate and the nut above, which is used to hold the target plate in a fixed position. This configuration is shown in Figure A-9.

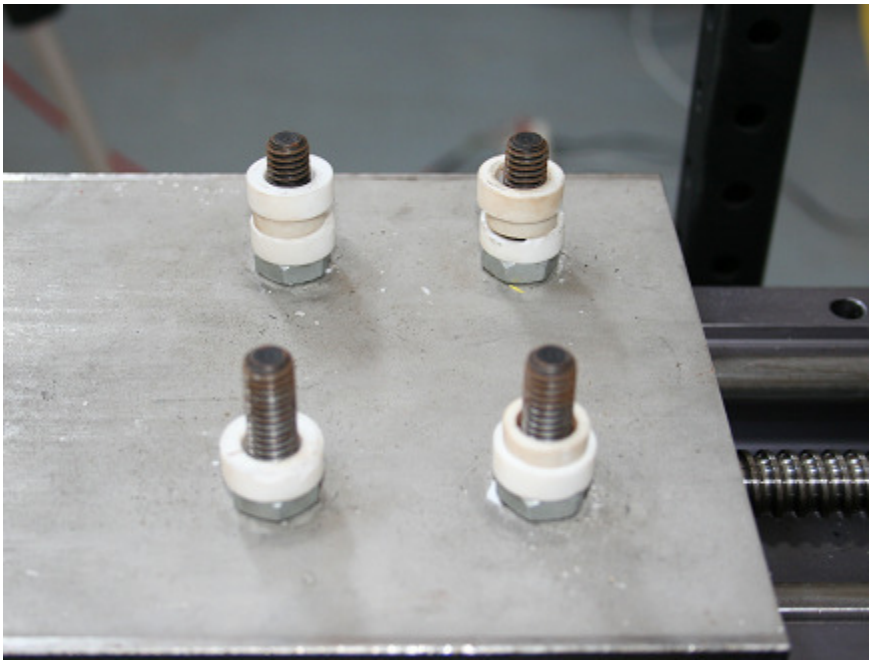

Figure A-9. Slide table carriage with safety plate and electrically insulating ceramic spacers.

The ceramic discs electrically insulate the target plate, keeping unwanted electrical charge from reaching the motor. If excessive electrical charge reaches the motor, the drive will fault and target plate motion will cease. Another view of a target plate with the ceramic spacers positioned on it is shown in Figure A-10. Also visible in this figure is the grounding strap attached to the target plate. The grounding strap was attached to the plate because there is not enough clearance between the safety plate and the target plate for the grounding clamp of the welder.

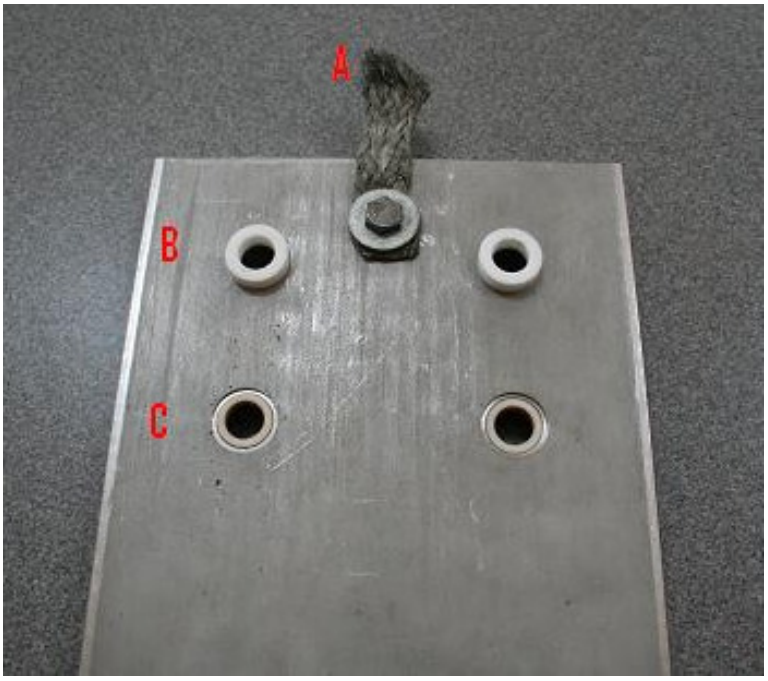

Figure A-10. Support side of target plate. A – grounding strap for welder, B – outside ceramic spacer, C – inside ceramic spacer.

Figure A-11 shows a completely installed target plate on the carriage of the slide table. The welding ground clamp has been secured to the grounding strap and the welding torch has been secured to the welding arm of the support structure. Also visible in this figure is the steel foil that was used as the mechanical shield to prevent interference from both the arc and the electrode. Both the torch and the shield are secured to the welding arm with standard zip ties.

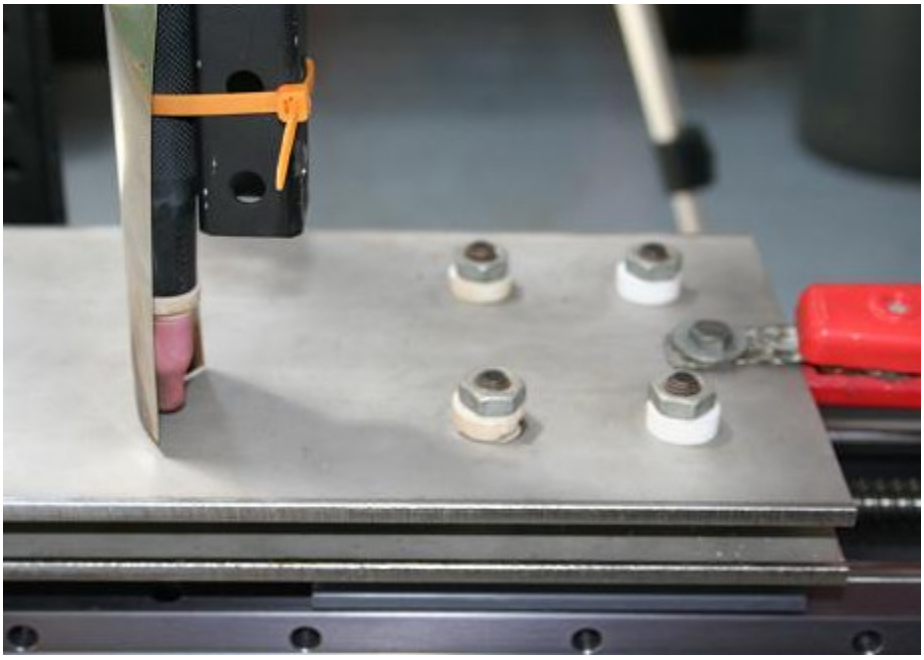

Figure A-11. Support end of completely installed target plate. Also visible are the welding torch and welding shield, both of which are secured to the welding arm of the support structure with standard zip ties. The welding safety plate is also visible below the target plate.

A.4 Data Acquisition System

The data acquisition system (DAQ) consists of a chassis, a high precision temperature/voltage logger, an input/output (I/O) connector block, and an input current module. The chassis is an NI PXI-1033, and it functions as a gateway between a laptop computer and any other peripheral instruments that might be used. The laptop communicates with the PXI-1033 through a NI Express Card 8360. The chassis has inputs for five boards that can be used to digitize signals from a wide variety of other instruments. The boards installed on the PXI-1033 are the PXI-4351, the PXI-6221, and the PXI-7340. The PXI-7340 is a motion controller, and was originally intended to control the S200 through a LabVIEW interface. However due to complications configuring third party components, it is not used, and the preferred method of

motion control is by interfacing the laptop directly with the S200, as was previously described. The DAQ chassis is shown in Figure A-12.

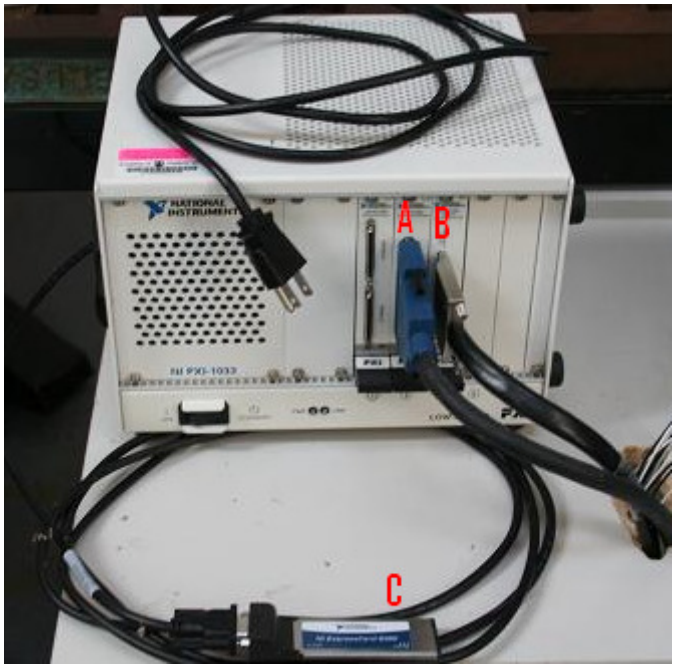

Figure A-12. DAQ chassis NI-PXI 1033. A – connection to TBX-68T, B – connection to SCC-68, C – express card connection to laptop PC.

The PXI-4351 is a high precision temperature/voltage logger. This board is installed in slot 3 of the PXI-1033, and it is connected to a TBX-68T by a 68-pin shielded cable. The TBX-68T supplies 14 unconditioned channels that can be used to measure thermocouples, voltages, or resistances, and it also has internal cold junction compensation. The TBX-68T is used to acquire voltage signals from five thermocouple modules that incorporate optical isolation. These modules will be described in a later section. The PXI-4351 has the capability to sample at an aggregate rate of 60Hz; however, since 5 channels will be sampled at one time, a much lower sample rate should be expected. The error associated with voltage measurements taken from the PXI-4351/TBX-68T is in the range of 0.01-0.02% of the reading. The TBX-68T is shown in Figure A-13.

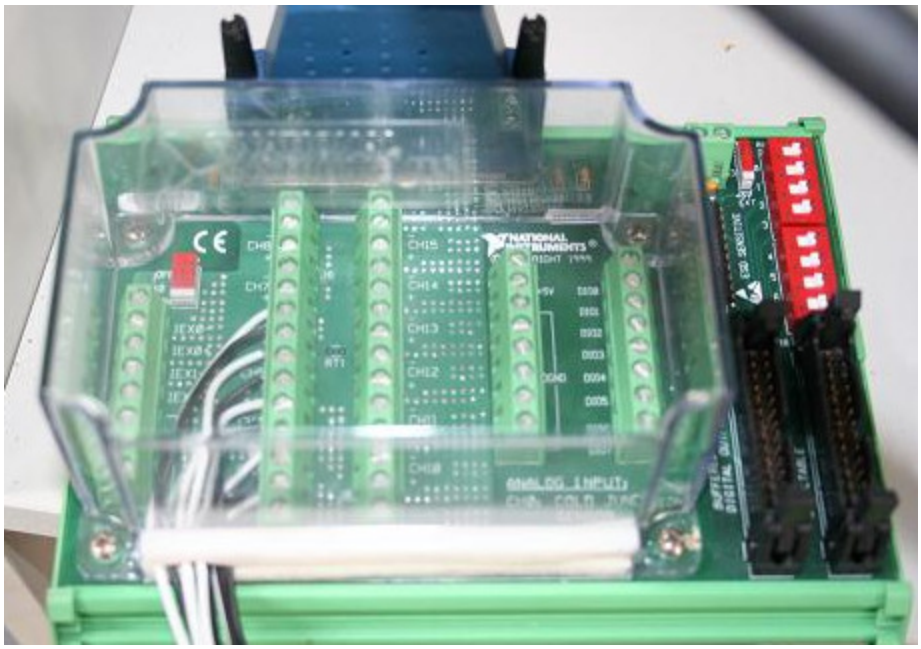

Figure A-13. TBX-68T temperature/voltage logger. The black and white wires connected to the TBX-68T carry voltage signals from the thermocouple modules to their respective channels.

The PXI-6221 is a 16-bit M series multifunction DAQ board that is connected to the SCC-68 terminal block by a shielded 68-D-type to 68 VHDCI cable. The SCC-68 is quite robust in utility. It has the capability to sample at a rate of 250kHz, and it has 84 screw terminals, a small breadboard, and four expansion slots for SCC modules. In this application only one of the expansion slots is in use. An SCC-CI20 is installed in expansion slot MOD1. This set up is shown in Figure A-14.

Figure A-14. SCC-68 multifunction DAQ device and SCC-CI20 current input module. Also shown are terminals 62 and 67 with an orange jumper wire connecting them.

The SCC-CI20 is a current input module that can measure the 4-20mA output signal from the infrared sensor. When using analog input SCC modules in the SCC-68, the AI SENSE, screw terminal 62, must be connected to AI GND, screw terminal 67. The SCC-CI20, or any other analog input module, will not work unless this connection is made.

The LabVIEW program that was used to capture data was built off of a pre-existing file titled "Continuous Multiple Transducer Measurements" that is readily available in the archived examples in the LabVIEW program. Several additions were made to the example file. These additions as well as their respective configurations are discussed in Appendix C.

A.5 Thermocouples

Since the melting point of type 304 stainless steel is roughly 1500°C, K-type thermocouples have been selected for use in this application because they can operate at temperatures up to 1372°C.Other types of thermocouples, such as R, S, and B-types, can measure temperatures up to 1800°C, but they are prohibitively expensive. Because of the interest in collecting temperature measurements from several locations in each trial and because electrical interference from the welding arc is anticipated, a 15' length of shielded bundled K-type thermocouple wire was purchased and terminated with thermocouple plugs. On the bottom side of the target plate fifteen individual glass braid insulated unshielded K-type thermocouples were spot welded using a Hot Spot Thermocouple welder shown in Figure A-15.

Figure A-15. Hot Spot thermocouple welder.

The placement of the thermocouples on the bottom face of the target plate is shown in Figure A-16.

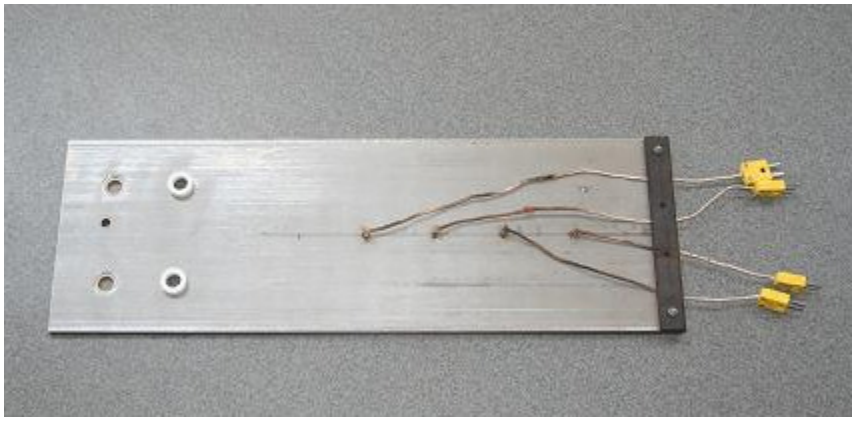

Figure A-16. Thermocouples spot welded to the bottom face of the target plate.

The thermocouples run down the length of the target plate and are secured at the end using the strain relief bar. The ends of the unshielded thermocouples are also terminated with plugs so that they can be easily connected to the corresponding wires on the bundled cable. This connection is shown in Figure A-17. The bundled thermocouple cable then connects to a battery of five thermocouple modules.

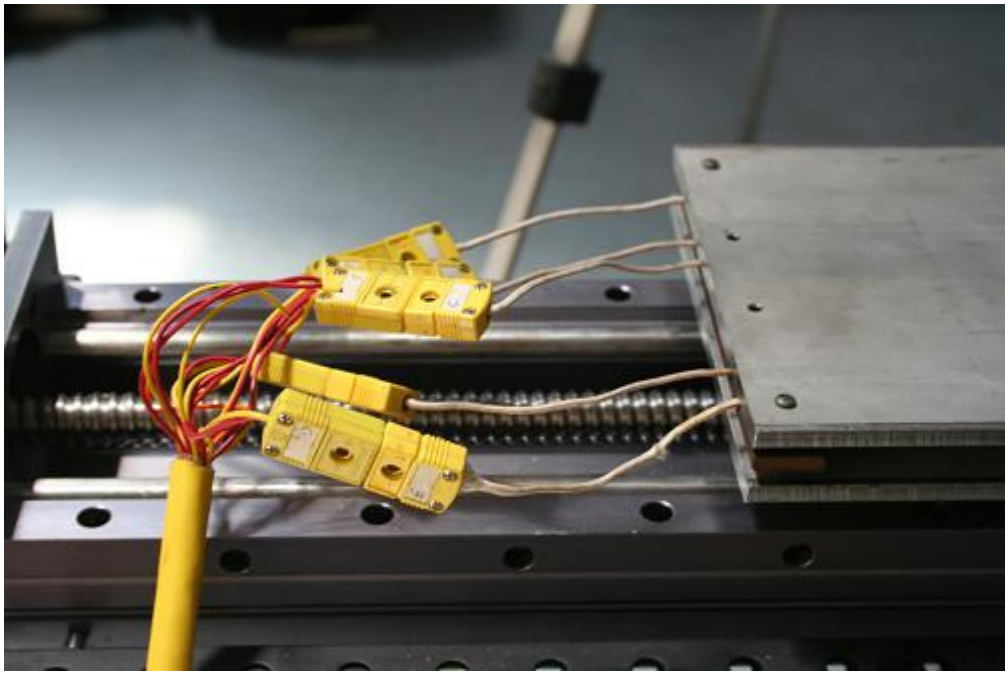

Figure A-17. K-type thermocouples terminated with plugs connecting to shielded bundled thermocouple cable.

The thermocouple modules were purchased from Phoenix Contact, and their part number is MCR/T-UI-E. A power supply, also purchased from Phoenix Contact, powers the thermocouple modules with 24VDC. By connecting the hot (black) wire to the L(+) terminal and the neutral (white) wire to the N(-) terminal on AC in terminals of the power supply, power can be delivered to the unit. Power is then distributed to the five thermocouple modules by connecting the positive and negative output signals to terminals 10 and 12, respectively, on the thermocouple modules. The positive and negative output signals from the thermocouple modules correspond to terminals 8 and 9, respectively. Figure A-18 shows the power supply and thermocouple modules and their respective connections.

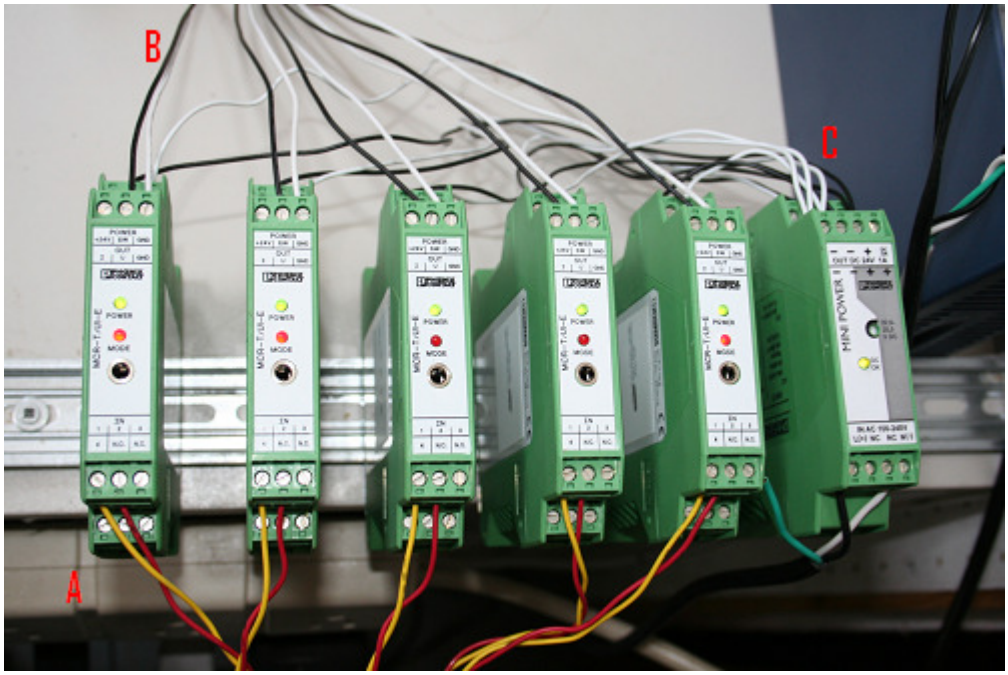

Figure A-18. Thermocouple modules and power supply. A – connection to bundled thermocouple cable, B – voltage output signal to TBX-68T, connections to power supply (module on far right).

These units are specially calibrated to operate with K-type thermocouples over a temperature range of -200°C to 1372°C. The thermocouple modules take the input analog voltage from the K-type thermocouples and amplify it. Next the amplified analog signal is converted to a digital signal The module then optically isolates the signal by pulsing light across a gap to a detector on the other side. The detector then converts the digital signal back to an analog 0-10 V signal which is linearly proportional to the input temperature. A calibration curve of this signal is provided in Appendix D. The measurement error in the thermocouple modules is less than 0.1% of the end value, and the cold junction compensation has an error of less than 3°C.

The optically isolated and amplified voltage is finally fed to the appropriate channels of the TBX-68T on the DAQ system as shown in Figure A-18. The optical isolation is necessary

because without it, the current can follow a direct path to the PXI-4351 in the DAQ chassis, and it is very likely that this will cause damage to the board.

A.6 Infrared Sensor

The infrared sensor selected for this application is the M770s made by Mikron. The M770s is a two color spot sensor with two narrow adjacent wavebands near 1μm and variable emissivity from 0.1-1.0. Note that this instrument is only a spot sensor. It is not a thermal imager, and it is not capable of providing a two dimensional temperature field. A side view of the instrument is shown in Figure A-19.

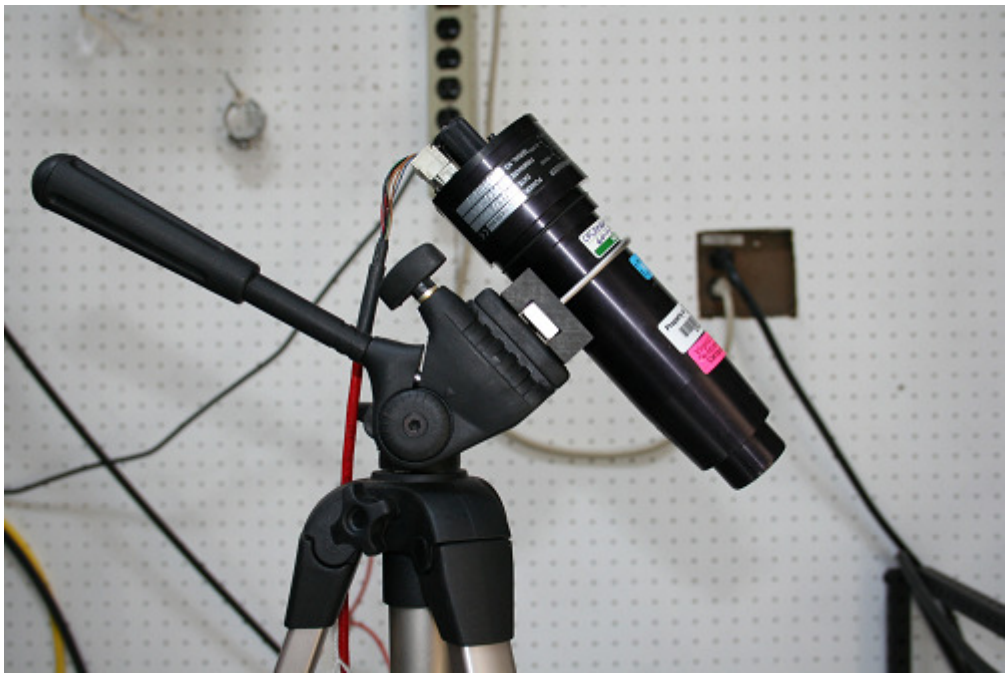

Figure A-19. Mikron M770s infrared spot sensor mounted on a tripod.

Focusing the M770s on its desired target is accomplished by simply looking through the viewing port on the rear of the instrument and locating the desired area so that it is within the targeting reticle. This particular M770s has been configured to have an operating distance from the target of 15”-infinity, and it has an aspect ratio of 90:1. The minimum diameter of a target can be found by using the formula presented in Equation 6,

$$d = \frac{D}{AR} \qquad 6$$

Where: d is the target diameter as viewed by the M770s, D is the distance away from the M770s, and AR is the aspect ratio.

Therefore, with a minimum distance of 15” and an aspect ratio of 90, the minimum diameter of a viewed target is 0.167”. A sturdy adjustable tripod is used to mount the M770s and provide a fixed position from which data may be collected.

The M770s is powered by a 24VDC power supply that connects to terminal 1 (+), and terminal 2 (-). Terminal 3 can be used as a ground. To send the current signal from the M770s to the SCC-CI20, connections must be made from terminals 4 (+) and terminals 5 (-) on the IR sensor to the corresponding (+) and (-) terminals on the SCC-CI20 module in the SCC-68, which are terminals 4 and 3 or 2 and 1, respectively. These connections are shown in Figure A-20.

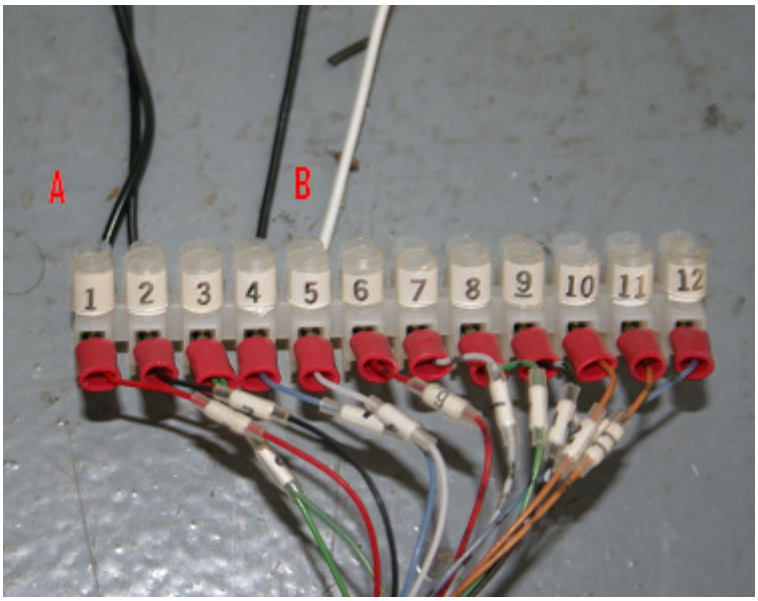

Figure A-20. Connections to Mikron M770s. A – 24V power supply, B – current output signal to SCC-CI20 module.

The output of the M770s is a 4-20mA signal, and it is designed to sense infrared radiation from target between 750°C and 2000°C. The output signal is linearly related to the surface temperature of the target. An exact calibration, as performed by NIST, is shown in Appendix D. The maximum sampling rate of the M770s is 1kHz. The temperature resolution is 1°C or 2°F. It can report data with an accuracy of 0.5% of full scale, and it has a repeatability of 0.3%of full scale temperature.

Appendix B: Motion Control Configuration

In order for all the components in the target plate motion system to communicate with each other, it was necessary to properly configure the servo driver. It was also learned that in order for them to all work efficiently together, then the servo driver required tuning as well. In Figure B-1 through Figure B-6 screen shots of the S200 Tools program are shown with the proper configurations for each setting. Figure B-7 shows the Summary tab as it should look once all the other tabs have been configured as indicated by the previous figures.

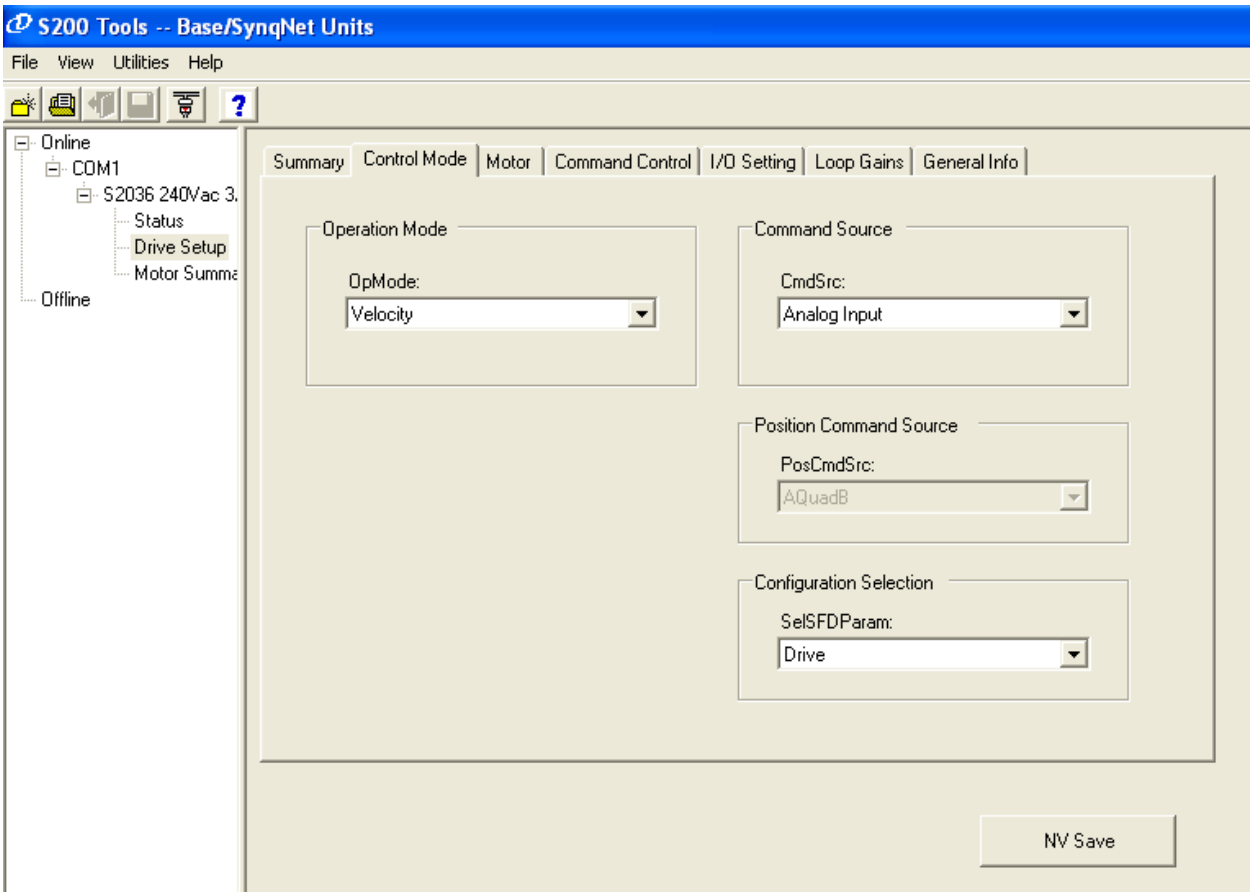

Figure B-1. Screen shot of the Control Mode tab in S200 Tools.

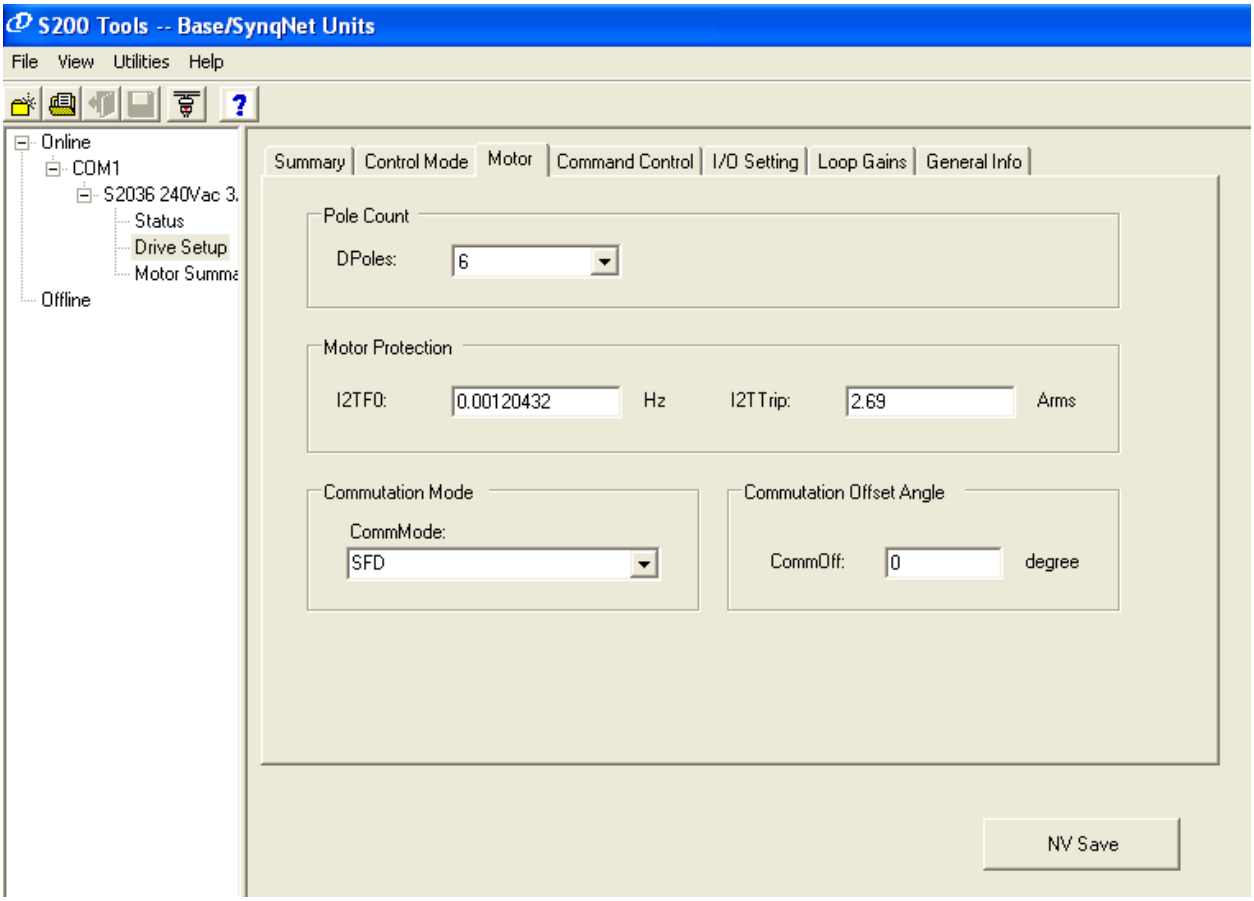

Figure B-2. Screen shot of the Motor tab in S200 Tools.

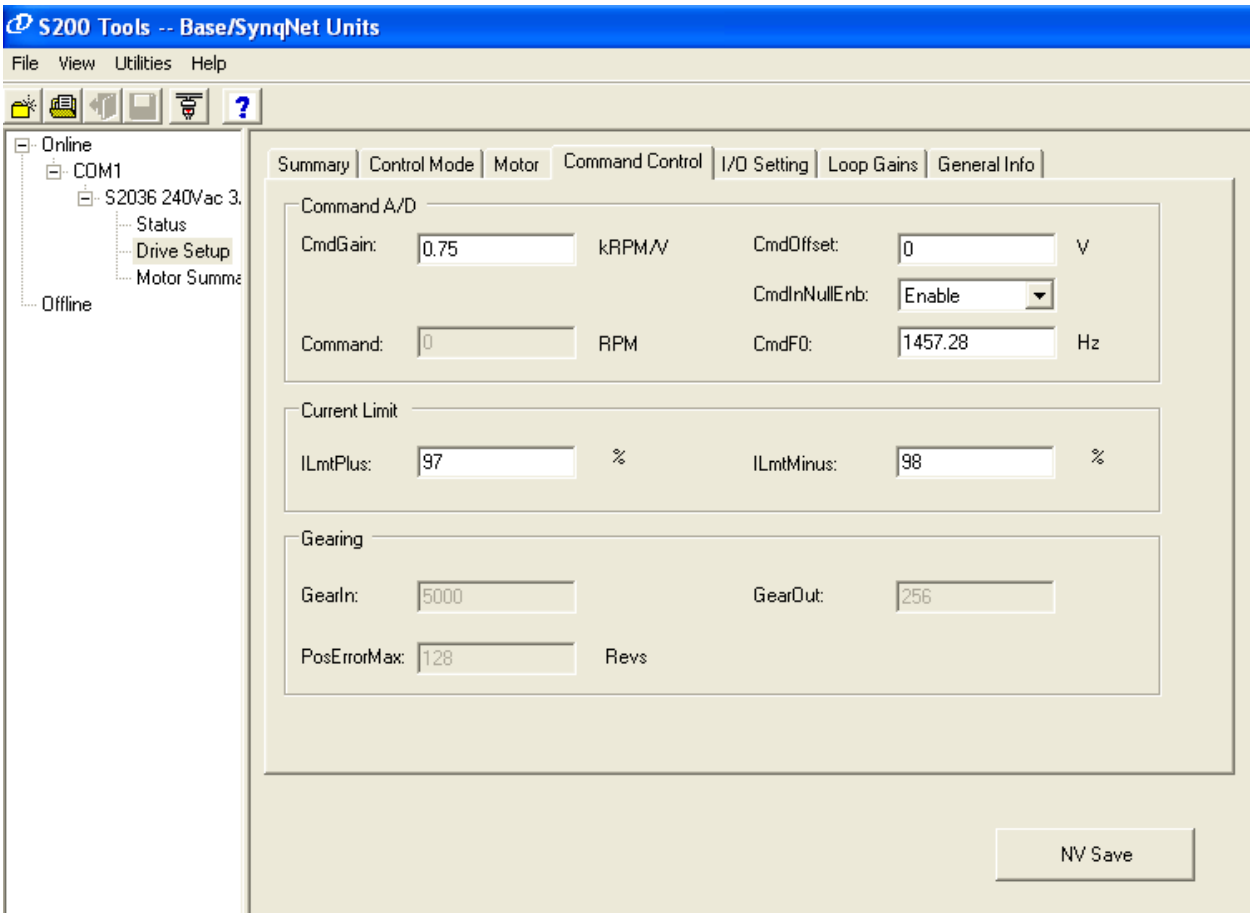

Figure B-3. Screen shot of the Command Control tab in S200 Tools.

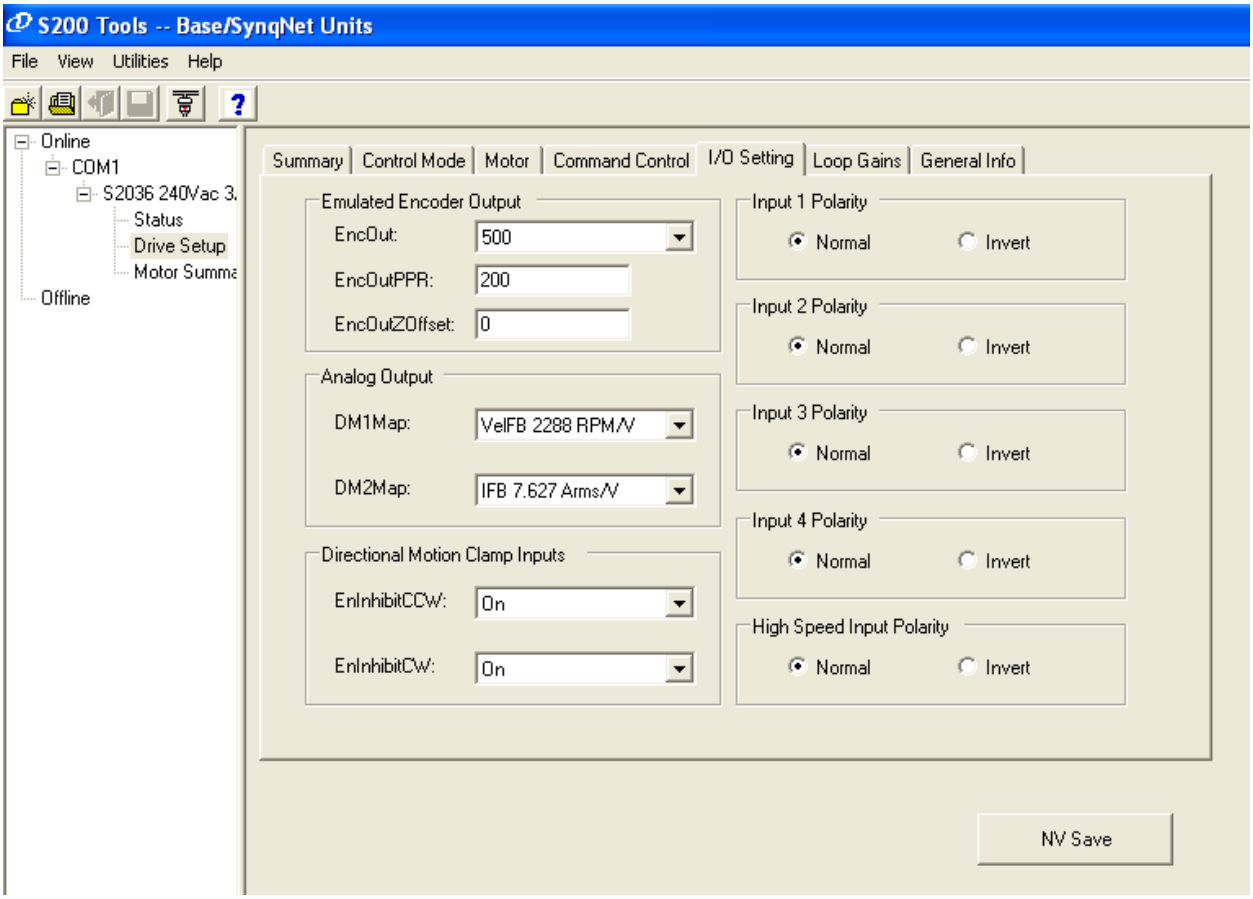

Figure B-4. Screen shot of I/O Setting tab in S200 Tools.

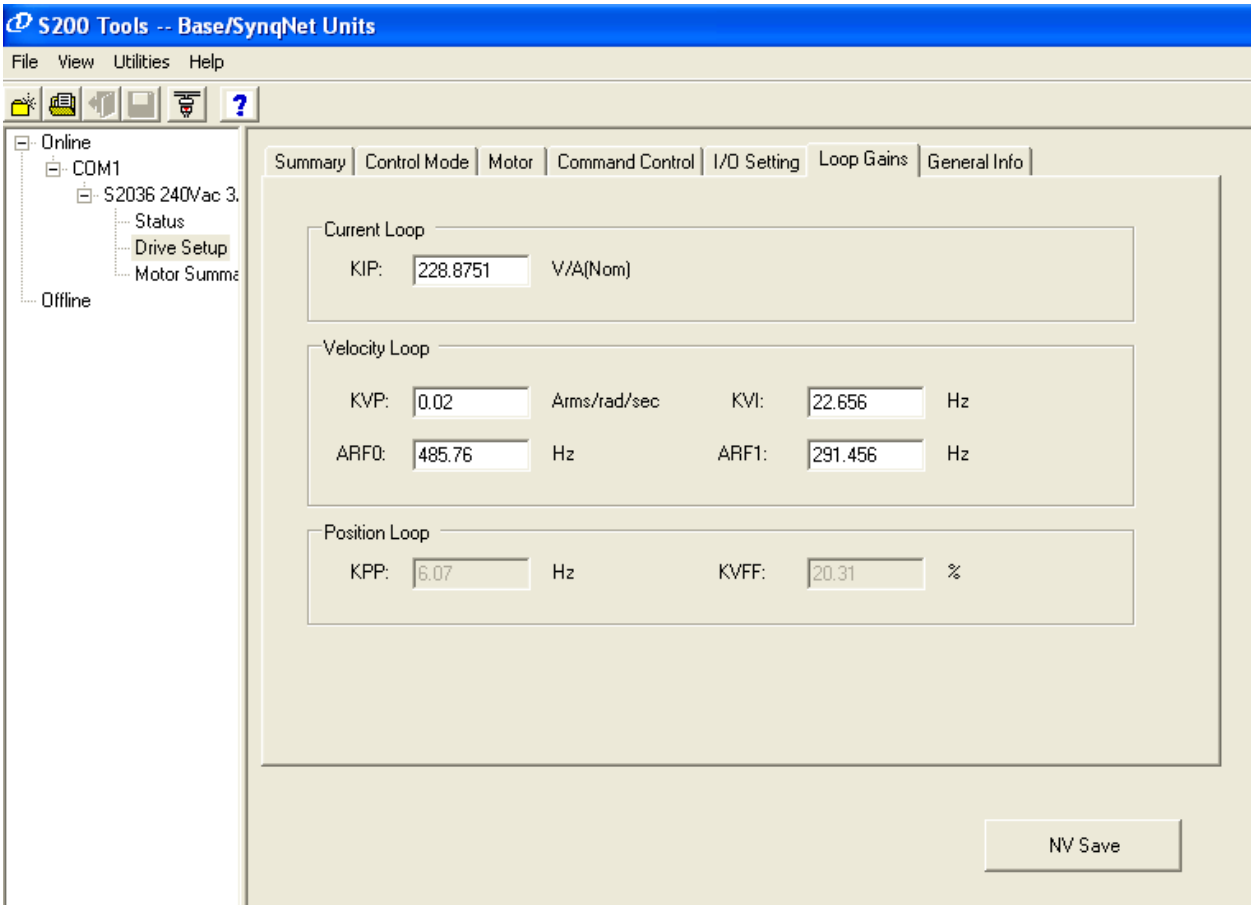

Figure B-5. Screen shot of Loop Gains tab in S200 Tools.

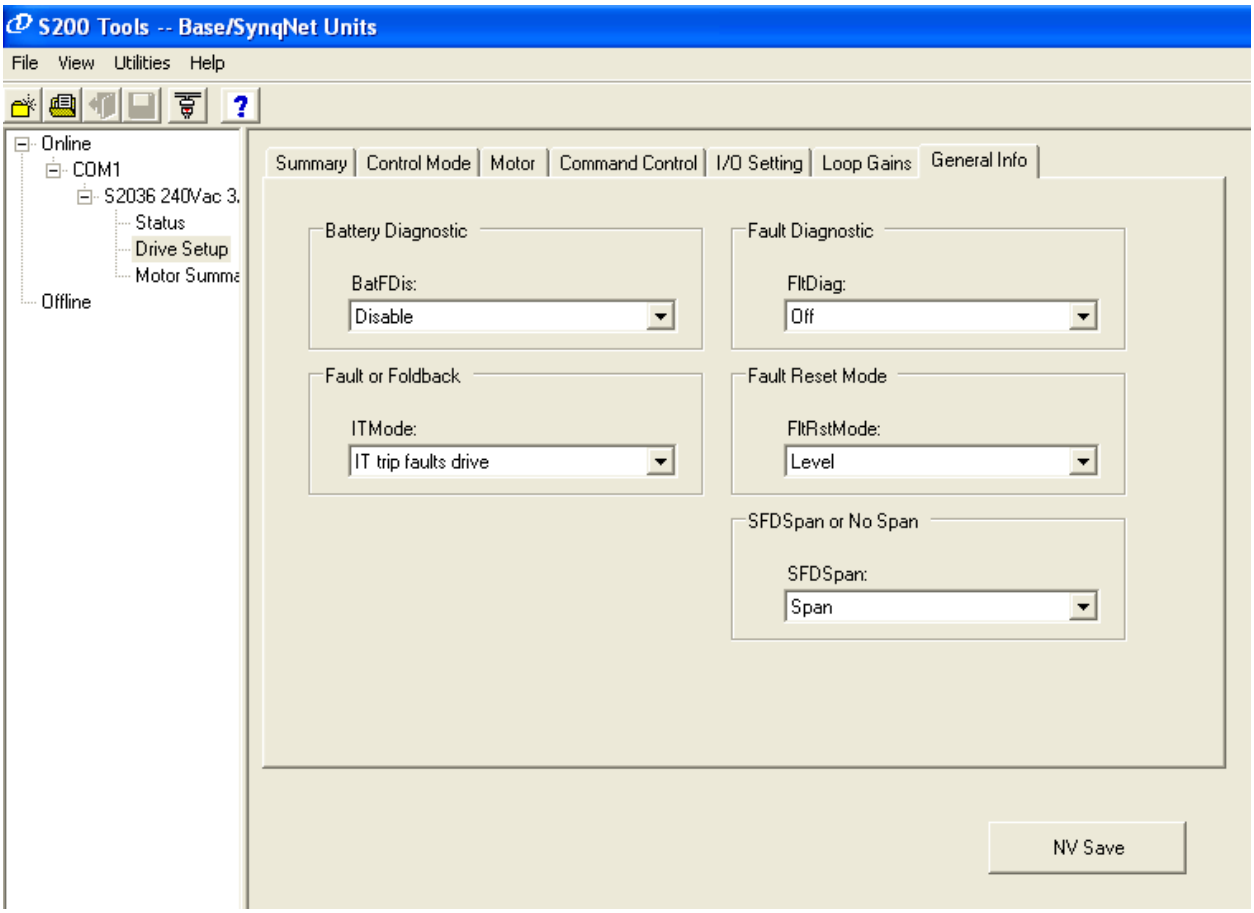

Figure B-6. Screen shot of General Info tab in S200 Tools.

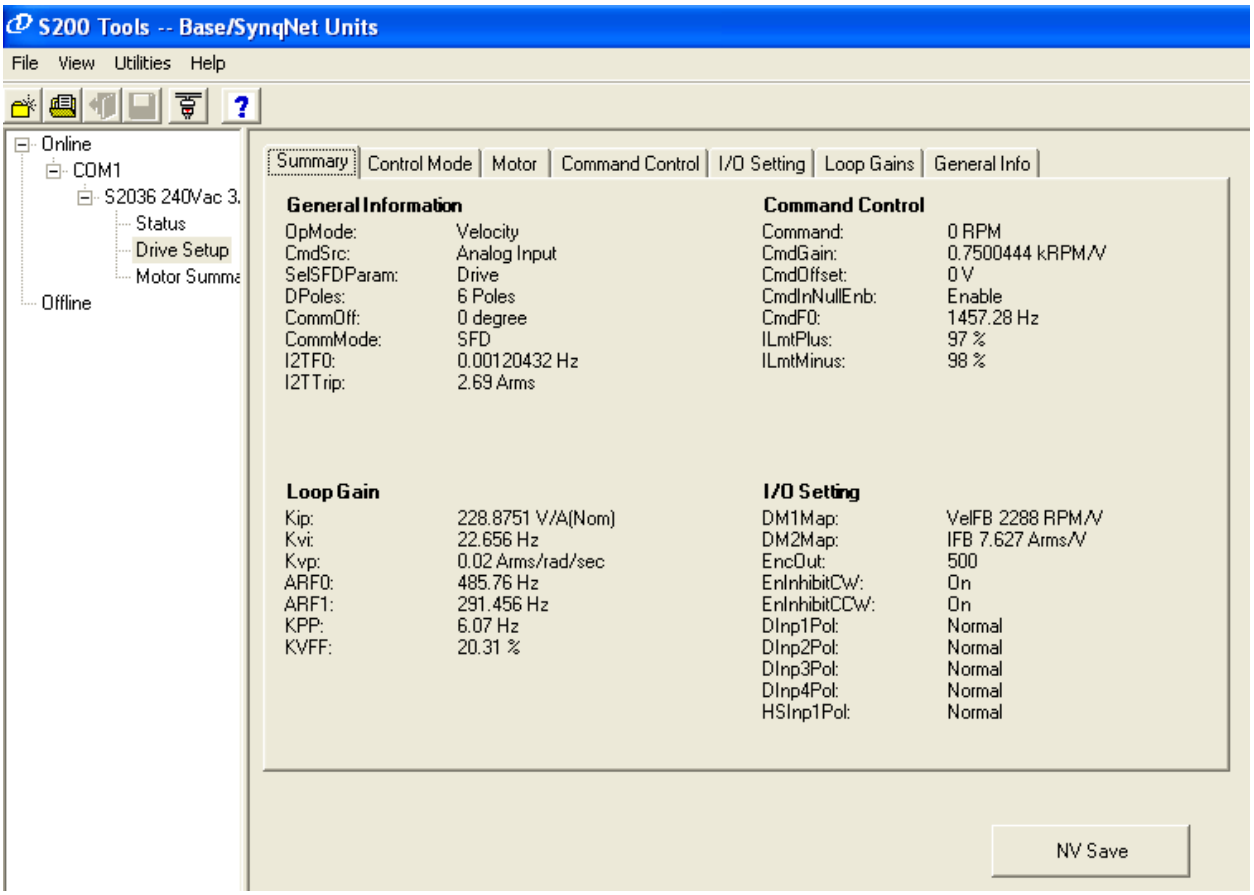

Figure B-7. Drive Setup Summary tab in S200 Tools after configuration.

With the servo driver properly configured, it is now possible to vary the rotational speed of the motor and the translational speed of the carriage on the slide table. The method used to adjust the velocity throughout this experiment was to keep the CmdOffset value set at 0 V, and adjust the CmdGain. By adjusting the CmdGain value a calibration curve was generated for the motor velocity. This curve is shown in Figure D-1 in Appendix D. However, in these trials the weld speed was held constant at a speed of 2.47 in/min, corresponding to a CmdGain value of 0.75 kRPM/V.

Tuning the motor is accomplished by adjusting the gains on the Loop Gains tab shown in Figure B-5. This is a largely iterative process, done mostly using a guess and check

methodology. Following the order 1) KVP, 2) KVI, 3) ARF0, 4) ARF1, the individual loop gains should be reduced while the motor is operating under typical conditions of its intended use, which include applied load and speed. If the motor is not well-tuned then the user will hear an audible humming sound emanating from the slide table. When the motor is not tuned, feedback loops cause the 1 m screw in the slide table to vibrate. As adjustments are made to the loop gains during motor operation, the humming will gradually cease and the slide table will operate smoothly and silently.

Appendix C: LabVIEW Configuration

Even with the benefit of being able to use a pre-existing LabVIEW program, some additional features were required to process signals, plot instrument responses, and write captured data to .txt files. In addition, for the LabVIEW program to recognize what hardware components had been installed and were in use, some configuration was needed. Figure C-1 shows the front panel of the .vi file. The areas marked in red are described in the figure caption.

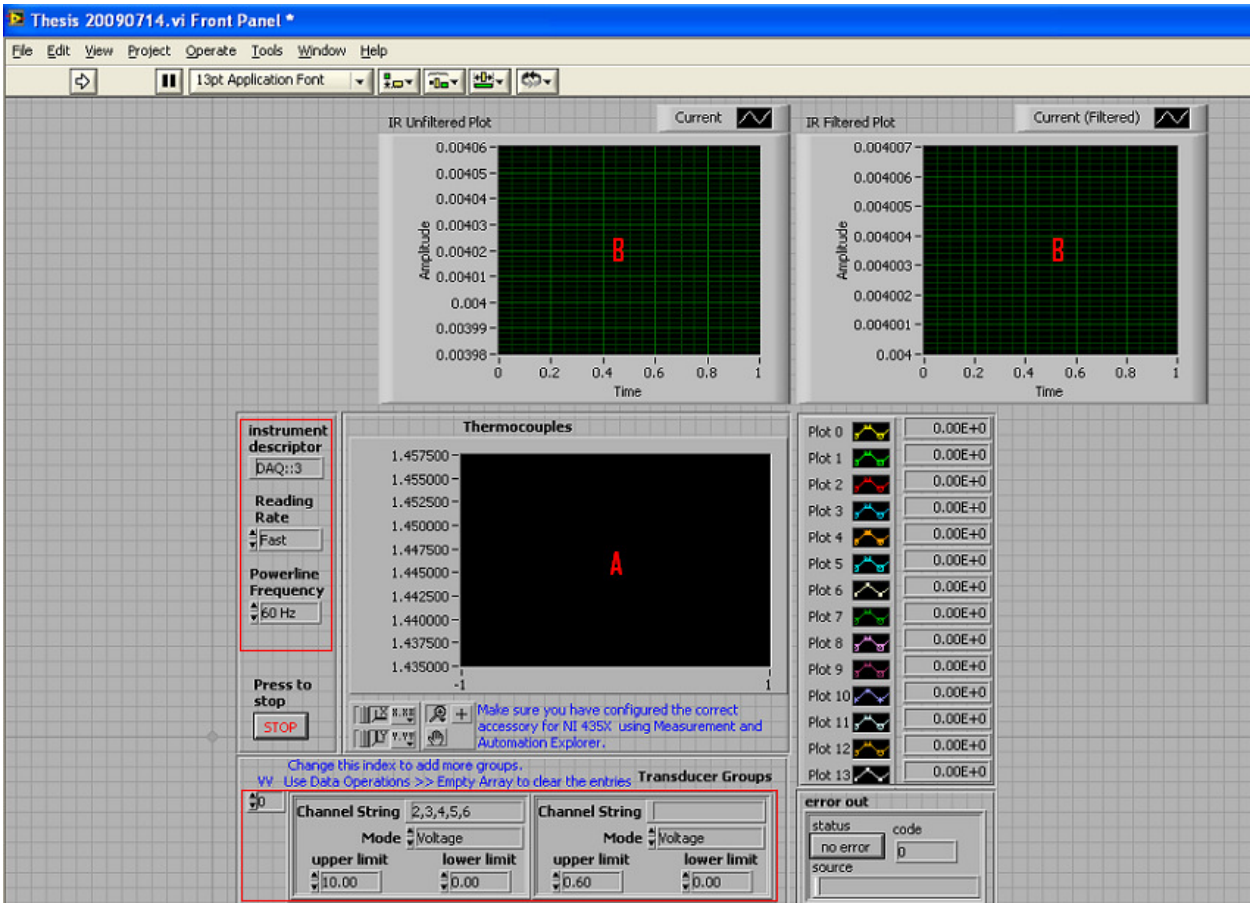

Figure C-1. Front Panel of LabVIEW .vi file. A – plot that came with the pre-existing LabVIEW file, B – additional plots installed to view signal from the infrared sensor. The fields enclosed in the red box are those that must be configured as shown before initializing data acquisition.

Figure C-2 shows the back panel of the LabVIEW .vi file. It is essentially a block diagram/flow chart of how the .vi file operates. In Figure C-3 through Figure C-7, the configurations for all additional controls and devices are shown. These items are numbered in red in Figure C-2.

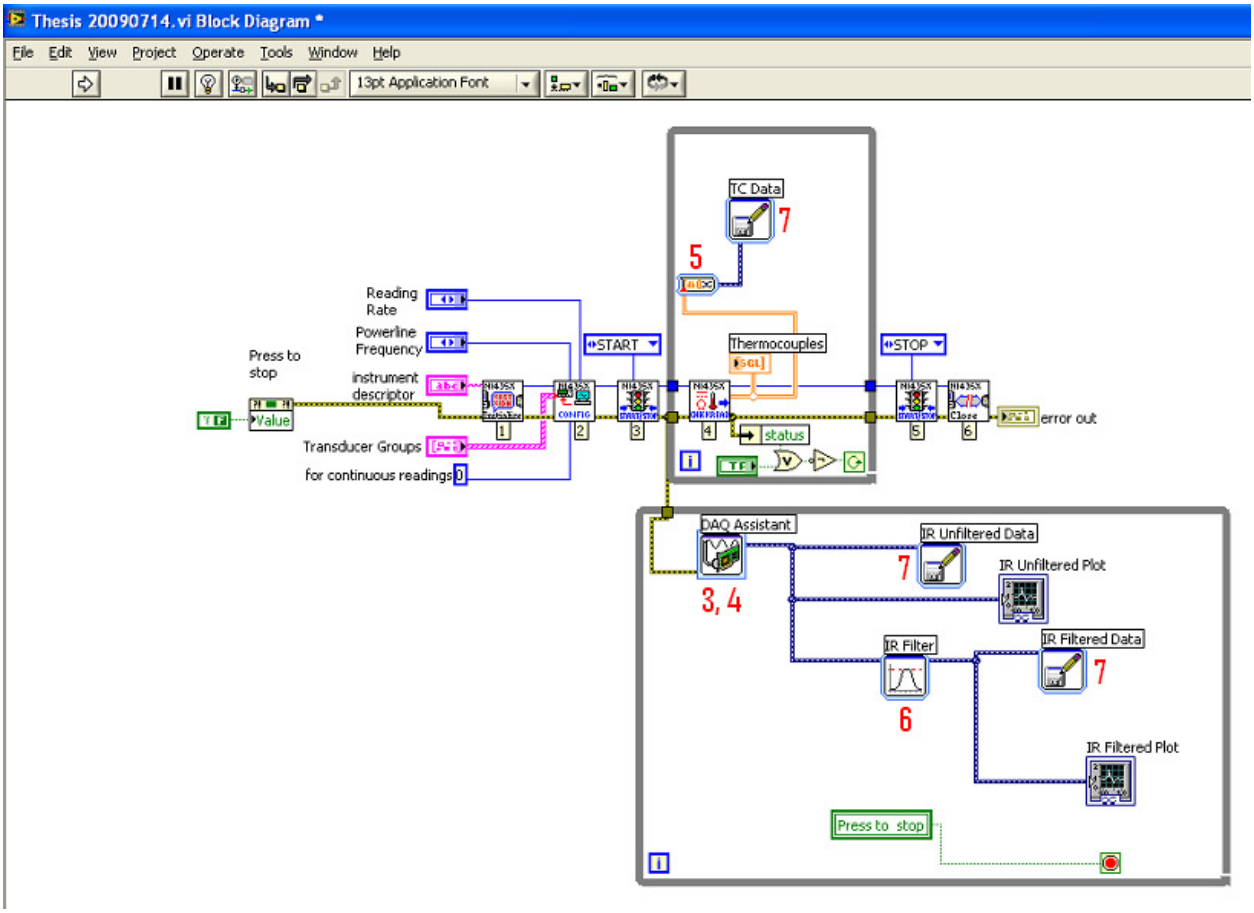

Figure C-2. Back panel of LabVIEW .vi file. The numbers in red correspond to the figures in Appendix C in which the configuration for that particular control or device is shown.

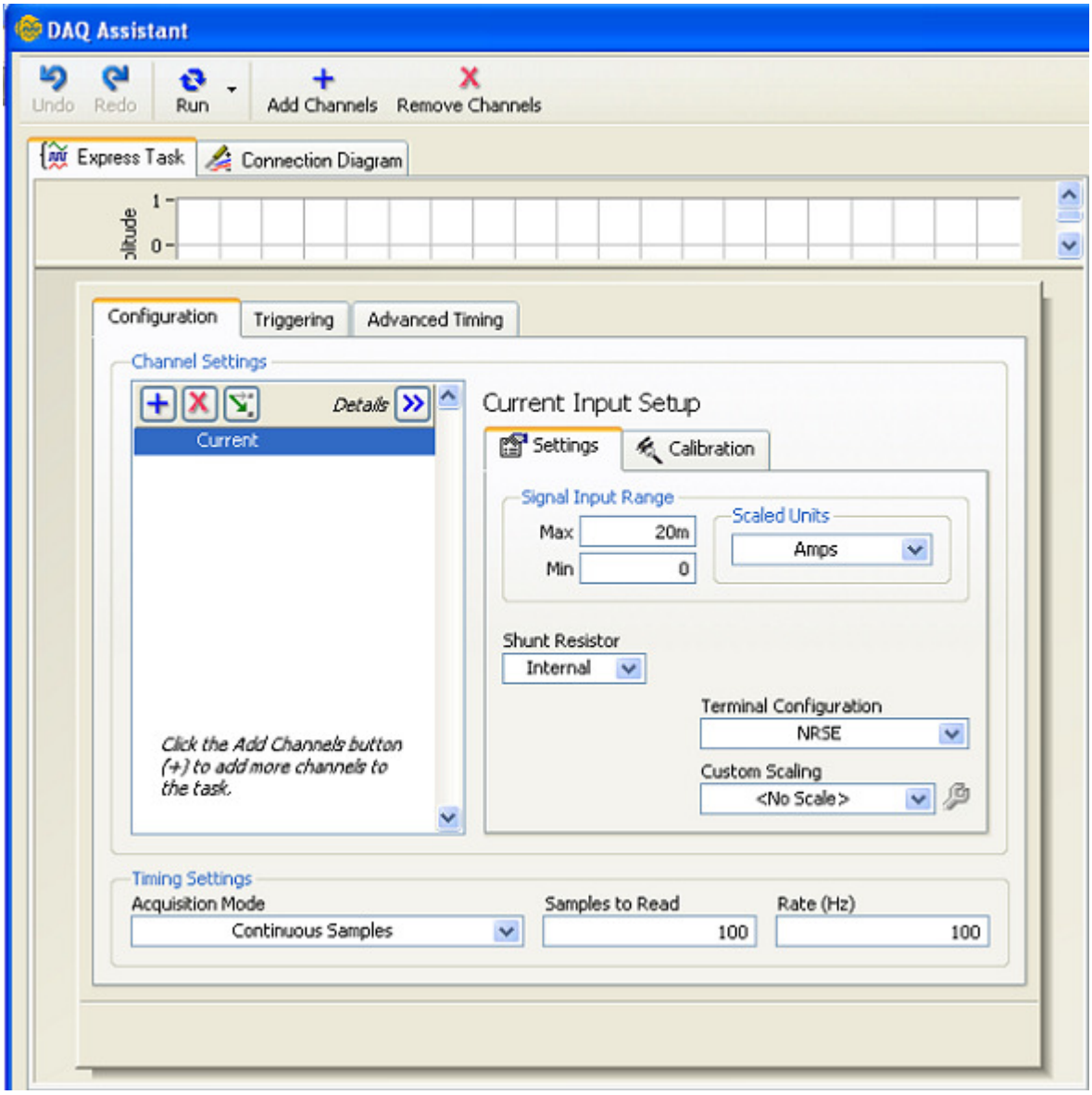

Figure C-3. DAQ Assistant configuration window.

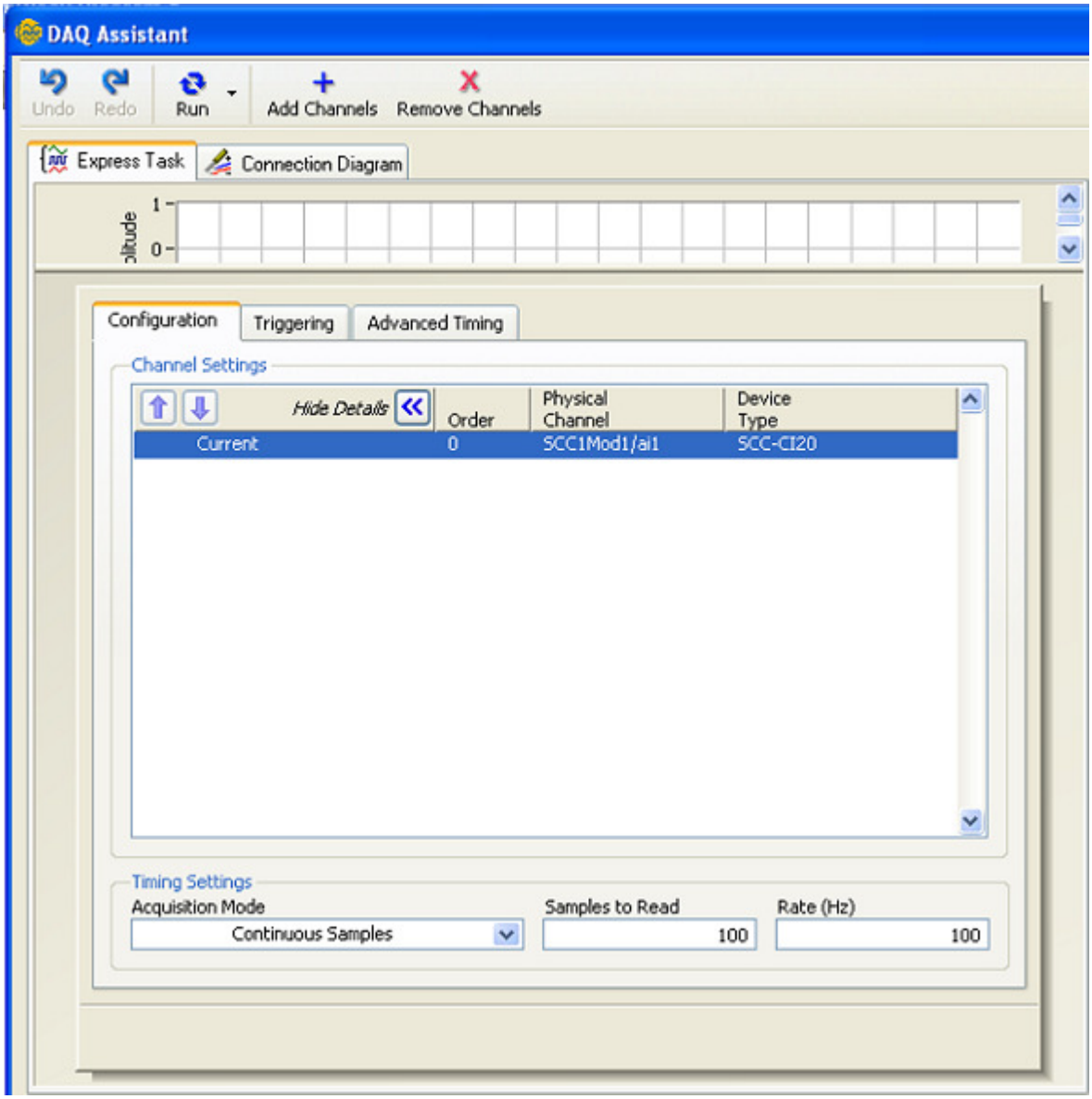

Figure C-4. DAQ Assistant configuration window showing details.

Note that in Figure C-4 shown above the physical channel and device type are listed as "SCC1Mod1/ai1" and "SCC-CI20," respectively, but with no obvious means of changing the setting. When the "DAQ Assistant" block is introduced to the .vi file for the first time, a window appears asking what type of signal should be captured and with what device and channel.

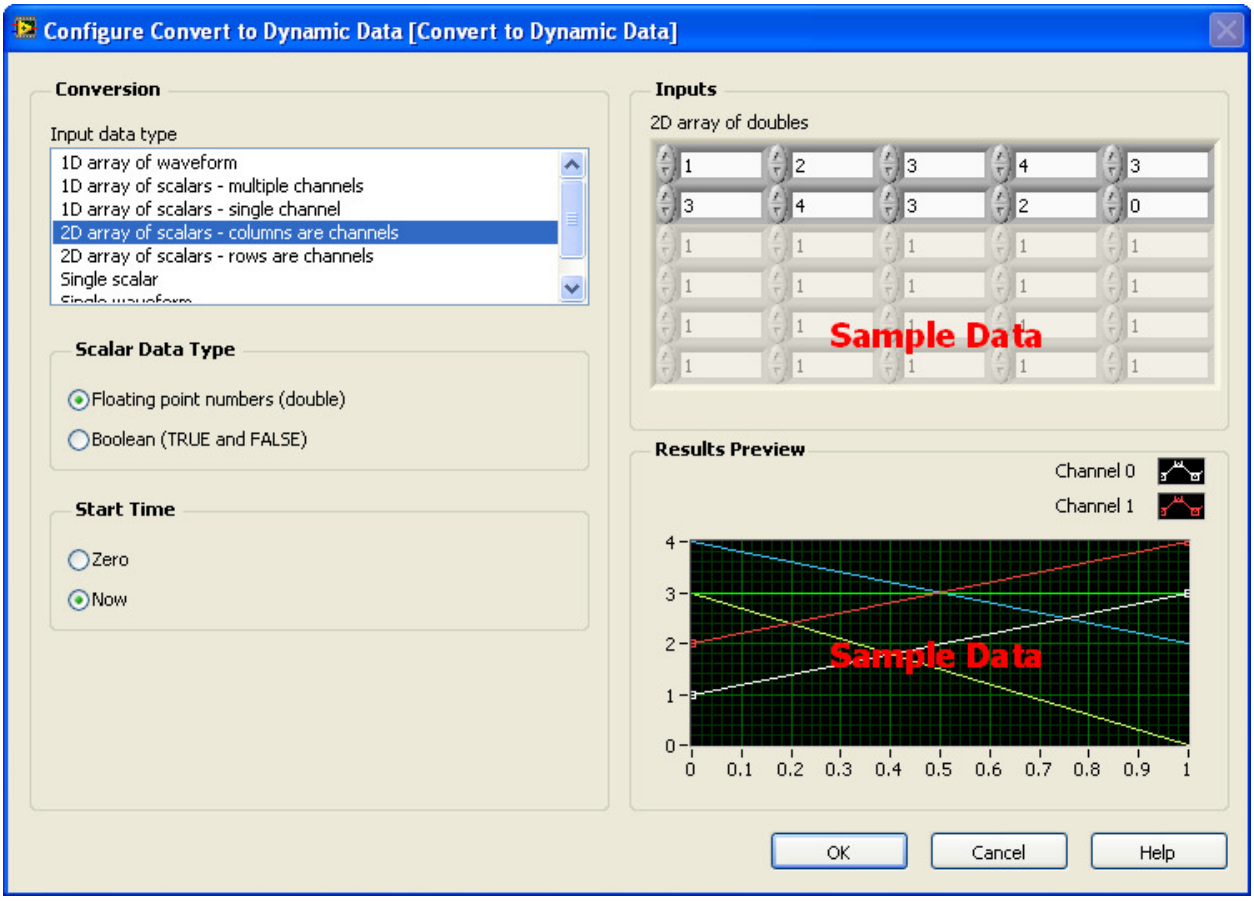

Figure C-5. Thermocouple data conversion configuration screen shot.

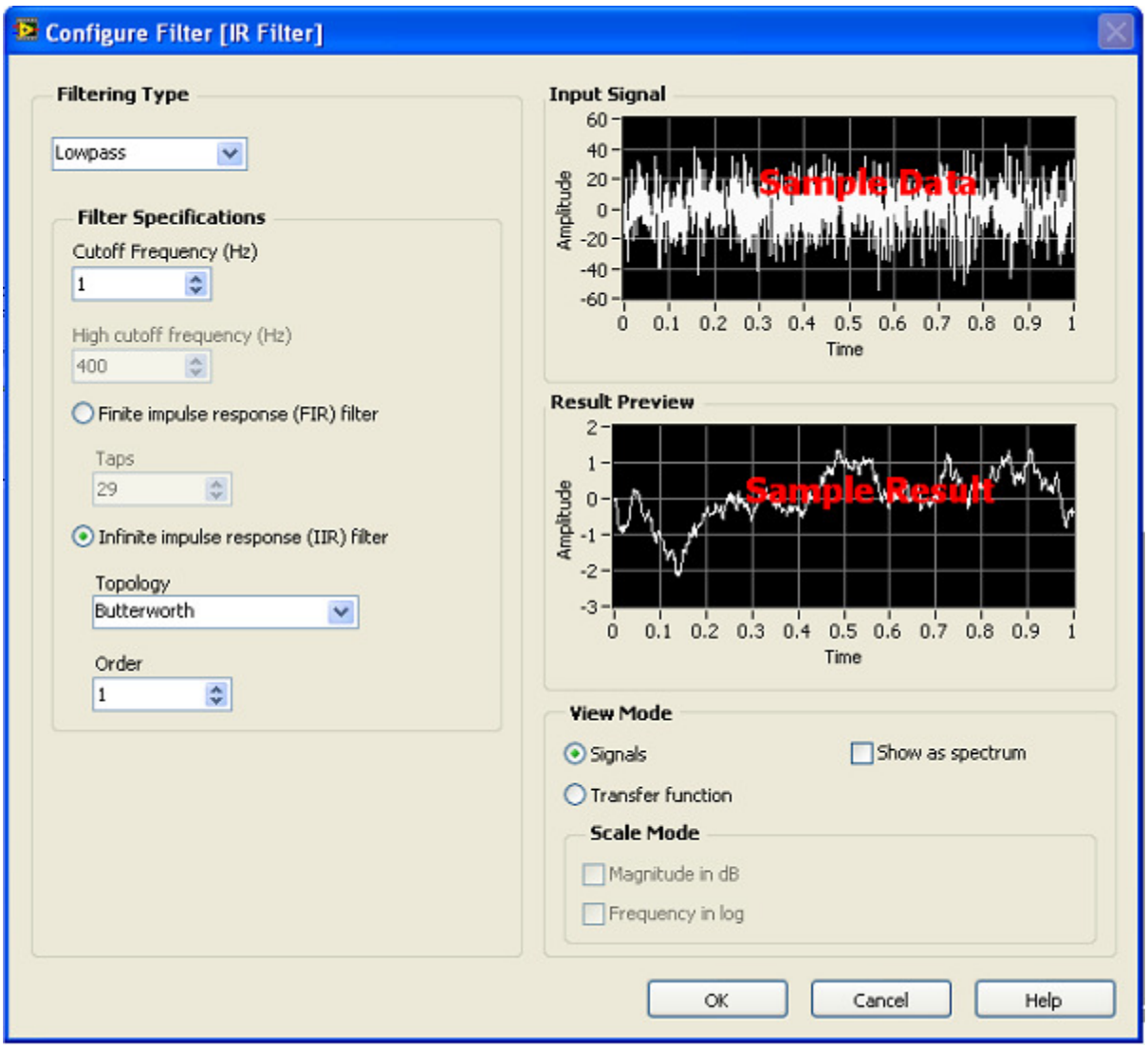

Figure C-6. Infrared sensor filter configuration screen shot.

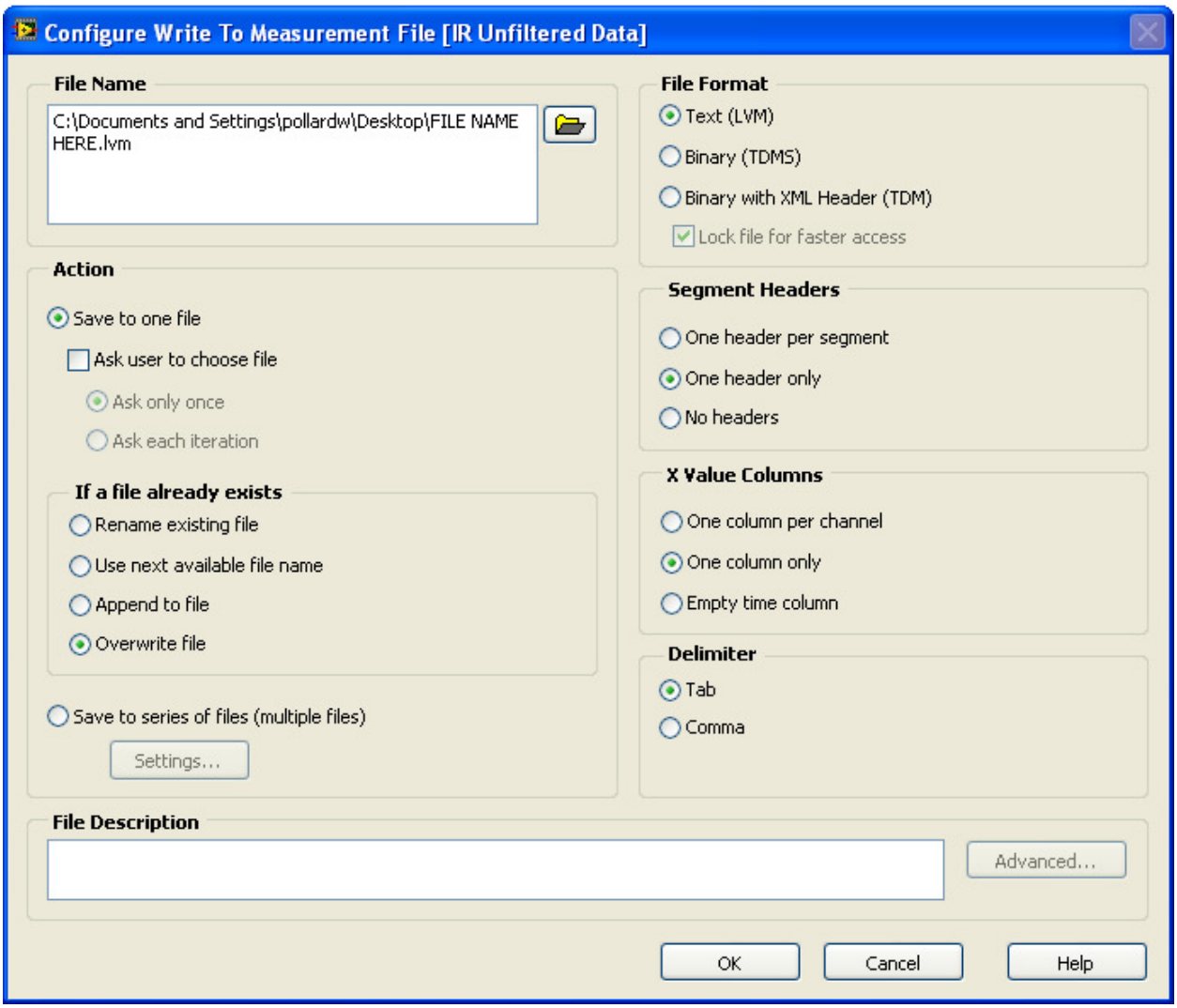

Figure C-7. Write to file configuration screen shot.

Under the "File Name" textbox in Figure C-7, the path for saving the file ends with "FILE NAME HERE." For these experiments it was necessary to have three separate "Write to..." commands – one for the thermocouples, one for the unfiltered infrared sensor, and one for the filtered infrared sensor. Most of these setting depend solely on the user's preference, but caution should be exercised if the "Overwrite file" button is selected.

Appendix D: Motion Control, Thermocouple and M770s Calibration

Several components in this experimental set up required calibration because either the input signal or the output signal was in units such as volts or amps. The velocity of some servo motors can be adjusted by varying the applied voltage, and a wide variety of temperature sensors output either a voltage or current signal that can readily be converted into conventional temperature units such as degrees Celsius.

D.1 Servo Motor Calibration

The servo driver had to be calibrated so that a useful relationship between the CmdGain value [kRPM/V] in the S200 Tools program and the translational target plate velocity could be established. In this experiment the only welding speed used was 2.47 in/min, but in future research it may be desirable to adjust the heat flux by increasing or decreasing the welding speed. It should also be noted that the heat flux can also be varied by either increasing or decreasing the welding current. The data from the velocity calibration are shown in Table D-1, and a graphical depiction complete with a calibration curve is shown in Figure D-1.

Table D-1. Data from velocity calibration.

CmdGain (kRPM/V)	*Distance (in)*	*Time (min)*	*Velocity (in/min)*	*Average Velocity (in/min)*
0.25	0.81	1.00	0.81	0.81
0.25	0.81	1.00	0.81	
0.25	0.81	1.00	0.81	
0.50	1.64	1.00	1.64	1.64
0.50	1.64	1.00	1.64	
0.50	1.65	1.00	1.65	
0.75	2.47	1.00	2.47	2.47
0.75	2.46	1.00	2.46	
0.75	2.47	1.00	2.47	
1.00	3.25	1.00	3.26	3.26
1.00	3.26	1.00	3.26	
1.00	3.25	1.00	3.26	
1.50	4.91	1.00	4.91	4.91
1.50	4.92	1.00	4.92	
1.50	4.91	1.00	4.91	
2.00	3.28	0.50	6.56	6.56
2.00	3.28	0.50	6.56	
2.00	3.27	0.50	6.55	

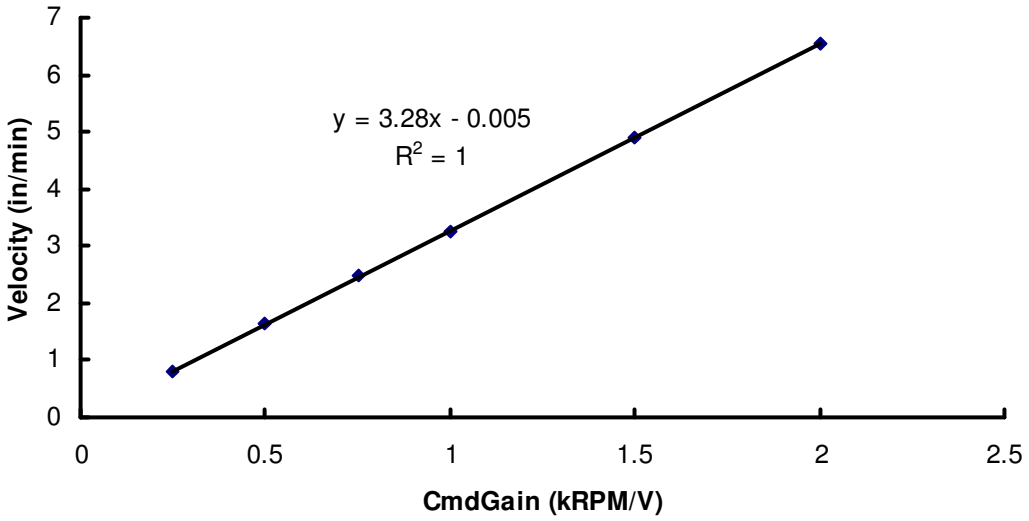

Figure D-1. Calibration curve for servo motor velocity.

D.2 Thermocouple Calibration

The LabVIEW program that was used for in this project has the capability of directly converting the input voltage from a user specified thermocouple type directly to a temperature in degrees Celsius. These direct conversions usually involve detecting very small voltages – usually on the order of mV. However, because it was necessary to have an intermediary device, the optical isolator, between the thermocouple bead and the DAQ, a calibration of the intermediary signal was required. As was described previously in Appendix A, the optical isolators transform the raw thermocouple input signal into one that spans the range of 0-10V with 0V corresponding to the minimum detectable temperature and 10V corresponding to the highest detectable temperature, which is in the case of a K-type thermocouple is -200°C and 1372°C, respectively; furthermore, with respect to the optical isolator, a linear relationship exists between the output voltage and the detected temperature. The calibration curve for the thermocouple modules is given in Figure D-2. The thermocouple modules can be programmed to detect a narrower range of temperatures if more precision is needed by the end user.

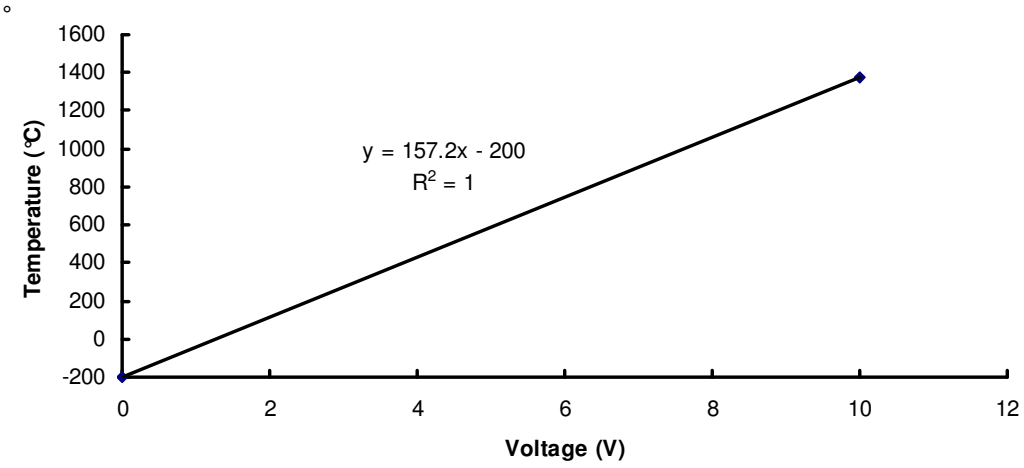

Figure D-2. Optical isolation module temperature calibration.

D.3 M770s Calibration

Like the thermocouples, the M770s also senses temperature, but its raw output signal is a 4-20 mA signal as opposed to a voltage. The temperature range of the sensor is 750 °C-2000 °C. Before the each unit is delivered for the first time to the customer, Mikron sends the instrument to NIST for a certified calibration. If for any reason the M770s requires servicing, the sensor will need to be recalibrated. Mikron can do the calibration themselves, or alternatively a request can be made, at the expense of time and money, to have the M770s shipped to NIST for a certified calibration. Whenever the instrument is delivered it should always contain calibration data and a certificate if it was NIST calibrated. The data in Table D-2 contain the most recent calibration data, and in Figure D-3 the data are graphed and fit with a linear regression.

Table D-2. M770s temperature calibration data.

Blackbody Source	*Blackbody Temp (°C)*	*SW Temp (°C)*	*LW Temp (°C)*	*Ratio Temp (°C)*	*Ratio Output (mA)*	*Exact Output (mA)*
M390	800	801	801	799	4.627	4.627
M390	1000	1000	1001	1001	7.214	7.213
M390	1200	1201	1201	1202	9.787	9.786
M390	1400	1401	1401	1401	12.33	12.333
M390	1600	1601	1601	1601	14.902	14.893
M390	1800	1803	1804	1804	17.493	17.491
M390	1950	1954	1954	1954	19.413	19.411

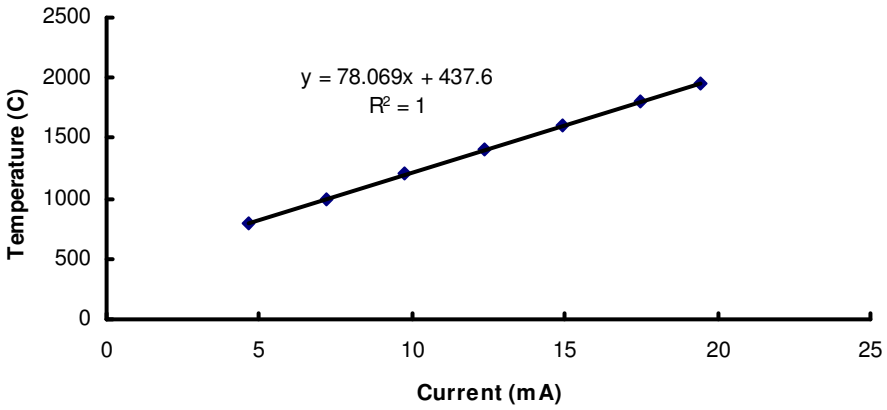

Figure D-3. Temperature calibration for M770s infrared spot sensor.

Appendix E: Experimental Procedures

1) TARGET PLATE PREPARATION

a) Cut five lengths of K-type thermocouple wire to 21, 23, 25, 27, and 29 inches.

b) Terminate one end of each length with the appropriate thermocouple plug.

c) Label them A, B, C, D, and E, respectively. Thermocouple A, the shortest one, will be located closest to the leading edge, whereas thermocouple E will be located closest to the support end of the target plate.

d) Make three lines, equally spaced at 1.5 inches, down the length of the plate. The two outside lines should go directly through the support holes, and the middle line should be along the centerline of the plate.

e) Starting three inches from the leading edge (end with strain relief bar) and along each of the lines just drawn, make five marks spaced 2 inches from each other. This will mark where you spot weld the thermocouples.

f) Supply power to the HOTSPOT TC welder.

g) Strip the thermocouple wire down about 0.5 inches and cross the exposed leads to make a wide X shape.

h) With the welding pliers, firmly grab both thermocouple leads just below the point at which they cross and give the top end a small twist.

i) With a second pair of pliers, snip the excess wire from the leads so that there is approximately half of a twist holding the two wires together. It is important to make sure that this is the only point at which the wires are in direct contact with each other.

j) Place the graphite electrode on top of the target plate, but out of the way of where the thermocouple is to be attached.

k) Turn the power dial on the HOTSPOT TC Welder to an appropriate power setting. (80% works well for 26 gauge wire)

l) Touch the half-twisted exposed thermocouple leads to the desired location on the plate making sure that the thermocouple wire is the only material (other than the graphite electrode and insulated work table) in contact with the target plate.

m) Press the "Fire" button when the machine buzzes and the red light becomes lit.

n) Inspect the weld. If the weld is satisfactory, continue to the next. If the weld is not satisfactory, remove the thermocouple wire from the target plate, snip off the damaged ends with pliers, and restart at step g).

o) Once all five thermocouples have been welded in their appropriate positions, align thermocouple wires so that they extend beyond the leading edge of the target plate and secure them in place with the strain relief bar.

p) Attach the grounding strap.

q) Connect target plate thermocouples to the corresponding thermocouple plugs on the shielded bundled thermocouple cable, i.e. A goes to A, B goes to B, etc.

NOTE: It is recommended that only one row of thermocouples be spot welded to the bottom face of the target plate at one time. Doing so eliminates the need for unnecessary adjustment of the welding arm on the support structure. This will become more evident in the next series of steps.

2) ALIGNMENT OF THE WELDING TORCH

a) Move the welding arm on the support structure so that it is roughly above the line of thermocouples.

b) Using the motion control system, move the target plate so that the welding torch is approximately 1 inch past the leading edge and directly above the plate.

c) Manually change the height of the welding torch so that it is hovering 0.10 inches above the target plate and.

d) If a mechanical shield is being used the clearance between the shield and the target plate should also be measured and adjusted if needed.

e) Set the motion system CmdGain for 0.2 kRPM/V and allow the plate to move slowly.

f) Place a very thin ruler on the top face of the target plate and allow the ruler to move with the plate such that the ruler is perpendicular to the direction. Use the long edges that run parallel to the weld direction as your reference points.

g) As the ruler passes under the welding torch, adjust the position of the torch so that it corresponds to the location of the line of thermocouples below. For example if the thermocouples were placed 1.5 inches from one side of the target plate, the welding torch should be manipulated so that it, too, is 1.5 inches from the same side of the target plate.

h) This process should be done as many times as possible along the full length of the target plate's travel distance. If the welding torch seems to steadily shift towards one direction, it is likely that the plate is not square. Rotate the plate so that the leading edge is square with the weld path.

i) If the target plate is one that is undergoing its second or third trial, it is very likely that the once flat plate will now have some degree of curvature. Measure the torch's lateral position as best as possible to ensure that it stays above the thermocouples, and measure the torch height and shield height from the "highest" spot on the plate. This will ensure that the neither the tungsten electrode nor the foil shield catch on the target plate as it traverses its path.

j) Once the position of the welding torch has been set, make sure that it has been secured well enough so that it does not drift during the actual welding process.

3) POSITIONING OF THE INFRARED SENSOR

a) Position the target plate as described in part 2b). The welding torch should already be positioned as best as possible above the line of thermocouples.

b) Power on the welding unit and set the welding current to 130A.

c) Open the main valve to the shielding gas.

d) Open the regulator valve to the shielding gas slowly until the indicator ball drops out of sight.

e) Connect the welder grounding clamp to the grounding strap on the target plate.

f) Turn the arc start switch to the "on" position, and then quickly turn it off once the arc strikes. The smaller the burned spot is the better. Also, take notice of the reading provided by the indicator ball in the regulator. Adjust regulator as needed. Leave main power to welding unit on.

g) Use the motion system to move the freshly burned spot a predetermined distance down-weld of the welding torch. For most cases in these experiments, a distance of 0.4 inches was used.

h) Setup the M770s on the tripod, making sure that the geometric orientation of the tripod is approximately as is desired, i.e. direct view, side view, etc.

i) Looking through the see-through sighting aperture on the M770s, align the targeting reticle up so that the burned spot is completely within the focus area. In low level light the aperture can be difficult to see through, so a flashlight may be necessary.

j) Once the M770s has been focused on the target plate, use a tape measure and record the x, y, and z distances between the focus location and the lens of the instrument. This will allow calculations for distance as well as horizontal and vertical viewing angles. Attempts should be made to maintain distances and viewing angles as consistent as possible.

4) COLLECTING DATA

a) Make sure the shielding gas is being delivered at the desired rate.

b) Ensure that all LabVIEW and S200 Tools configurations are set appropriately.

c) Start data acquisition.

d) Initiate motion to target plate.

e) Turn the arc start switch to the “on” position. Sometimes, especially when there is a large deflection in the plate, the arc will not start. This obstacle can be overcome by touching a

spare electrode to the torch tip and the target plate. DANGER! WELDING GLOVES **MUST** BE WORN FOR THIS PROCEDURE.

f) Wait until the welding torch has passed the last thermocouple.

g) Turn arc start switch to the "off" position.

h) Cease target plate motion.

i) Stop data acquisition.

j) Reverse motion to motion system. This can be done by simply entering a negative value in the CmdGain field in S200 Tools. Cease motion when the target plate is clear of the welding arm on the support structure.

k) Disconnect the grounding clamp from the grounding strap and disconnect all thermocouple plugs.

l) Remove target plate from slide table. It may be necessary to allow the plate to cool, or protective gloves can be worn.

m) Remove the thermocouples from the bottom face of the plate with pliers.

This describes one complete cycle of data collection. To perform another trial these steps should all be followed again as necessary, making adjustments to configurations when appropriate.

Appendix F: Problems Encountered

Table F-1. Problems encountered during experimental testing.

PROBLEM	CAUSE	SOLUTION	STATUS
DAQ not responding properly to known thermocouple inputs.	Circuits on DAQ card damaged by direct electrical connection to welding circuit	Optical isolation of each thermocouple signal prior to reaching the DAQ system.	*RESOLVED*
S200 Driver faults (Blink code 13) when welding arc is struck	Excess voltage leaking into SFD as a result of electrical contact with welding circuit	Electrically and thermally insulating ceramic spacers separating target plate and slide table.	*RESOLVED*
Slide table hums when motor is started	S200 Driver not tuned for the application	Adjusted loop gains in S200 Tools.	*RESOLVED*
Guide rails on slide table suffered excessive pitting	Anodic corrosion due to electrical contact with welding circuit	Electrically and thermally insulating ceramic spacers separating target plate and slide table.	*RESOLVED*
Terminals 1 & 2 on SCC-CI20 do not detect current input	Unknown	1) Replace internal shunt resistor (spare resistor inside unit) 2) Purchase new module 3) Use terminals 3 & 4	*UNRESOLVED*
M770S occasionally faults and reboots, not especially problematic but inconvenient	1) EMI Interference 2) Faulty unit – has been serviced twice.	1) Acquire new unit 2)	*UNRESOLVED*

Table F-1 (cont). Problems encountered during experimental testing.

PROBLEM	CAUSE	SOLUTION	STATUS
DAQ measures periodic interference for current signals.	Possible damage to DAQ from direct electrical contact with welding circuit	Send DAQ multifunction card in for diagnosis/repair.	*UNRESOLVED*

Appendix G: Part Diagrams for Target Plate and Ceramic Spacers

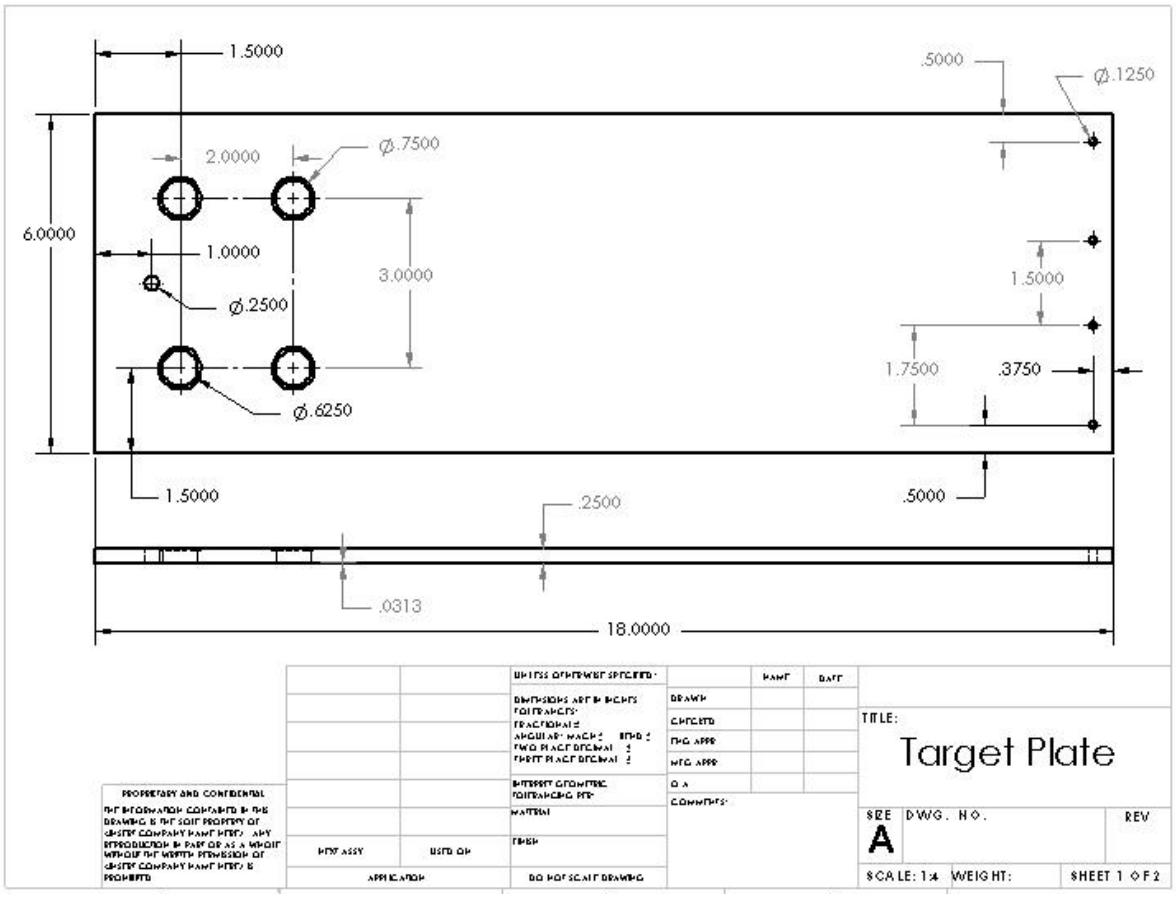

Figure G-1. Dimensional schematic of target plate.

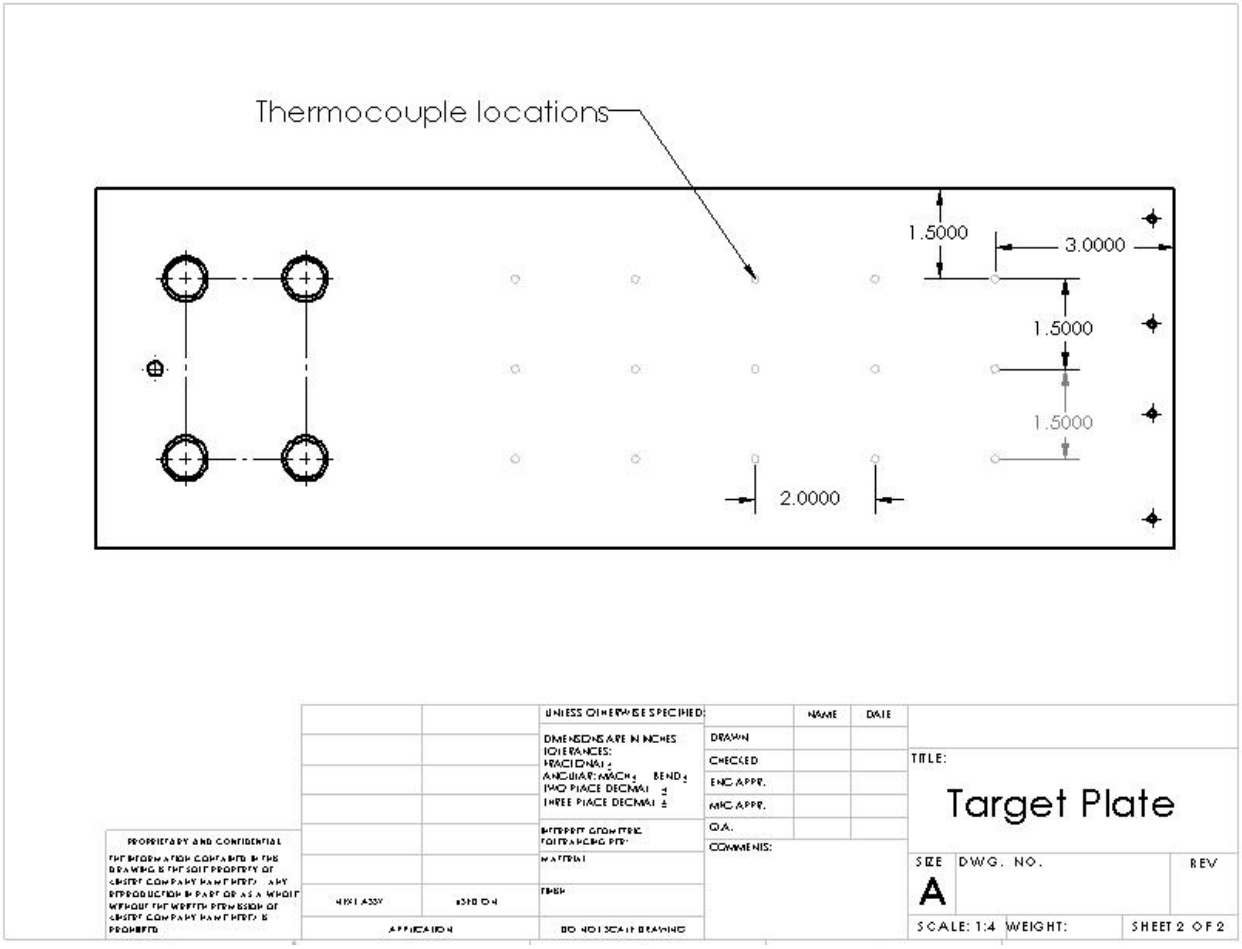

Figure G-2. Dimensional schematic of target plate with thermocouple locations.

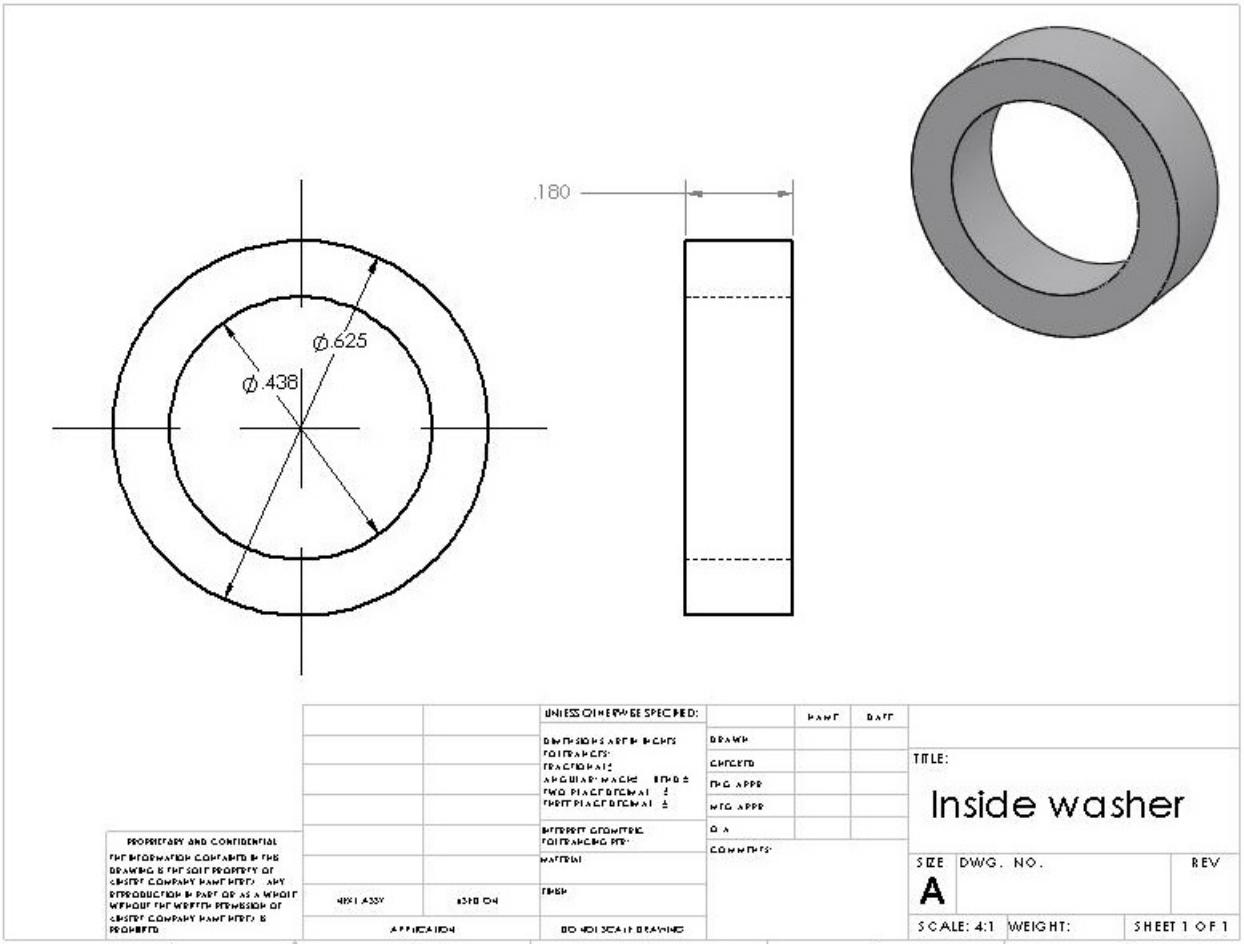

Figure G-3. Dimensional schematic of inside ceramic washer.

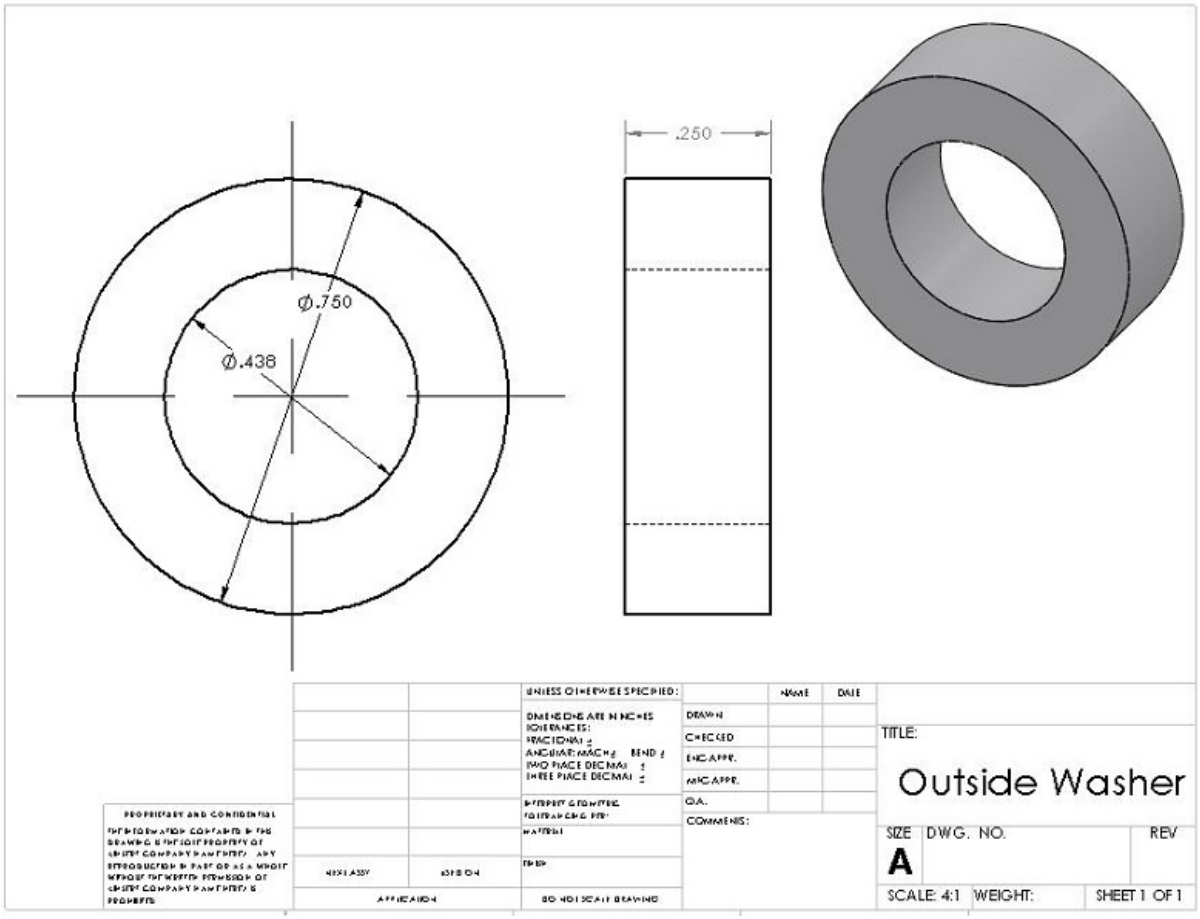

Figure G-4. Dimensional schematic of outside ceramic washer (spacer).

Appendix H: Trial Description and Plots

Table H-1. Summary of trial conditions

Trial #	Plate #	Run #	θ_H(degrees)	θ_V (degrees)	Shield	Shield Height (mm)	Torch Height (in)	Position	Emissivity.	Focus Distance (in)	Current (A)	Gas Flow (SCFH)	Electrode	TC Offset
2	6	1	0	41	No	N/A	0.05	Side	0.3	0.4	100	30	1/16; 2%	0
3	6	2	0	38	No	N/A	0.05	Side	0.3	0.4	100	30	1/16; 2%	0
4	8	1	0	40	No	N/A	0.05	Side	0.3	0.4	100	30	1/16; 2%	0
5	21	1	90	40	No	N/A	0.05	Side	0.3	0.4	100	30	1/16; 2%	0
6	22	1	90	40	No	N/A	0.05	Side	0.3	0.4	100	30	1/16; 2%	0
7	7	1	90	40	No	N/A	0.05	Side	0.3	0.4	100	30	1/16; 2%	0
8	9	1	90	40	No	N/A	0.05	Side	0.3	0.2	100	30	1/16; 2%	0
9	7	2	90	40	No	N/A	0.05	Side	0.3	0.2	100	30	1/16; 2%	0
10	9	2	90	40	No	N/A	0.05	Side	0.3	0.2	100	30	1/16; 2%	0
11	8	2	79	0	No	N/A	0.05	Side	0.3	0.4	100	30	1/16; 2%	0
12	22	2	79	0	No	N/A	0.05	Side	0.3	0.4	100	30	1/16; 2%	0
14	5	1	43	42	No	N/A	0.05	Side	0.3	0.4	100	30	3/32; 2%	0
15	4	1	43	42	No	N/A	0.05	Side	0.3	0.4	100	30	3/32; 2%	0
16	17	1	43	42	No	N/A	0.05	Side	0.3	0.4	100	30	3/32; 2%	0
17	15	1	90	0	No	N/A	0.05	Side	0.3	0.4	100	30	3/32; 2%	0
18	14	1	90	0	No	N/A	0.05	Side	0.3	0.4	100	30	3/32; 2%	0
19	13	1	90	0	No	N/A	0.05	Side	0.3	0.4	100	30	3/32; 2%	0
20	19	1	0	44	No	N/A	0.05	Side	0.3	0.4	100	30	3/32; 2%	0
21	18	1	0	44	No	N/A	0.05	Side	0.3	0.4	100	30	3/32; 2%	0
22	20	1	0	44	No	N/A	0.05	Side	0.3	0.4	100	30	3/32; 2%	0
23	12	1	90	44	No	N/A	0.05	Side	0.3	0.4	100	30	3/32; 2%	0
24	11	1	90	44	No	N/A	0.05	Side	0.3	0.4	100	30	3/32; 2%	0

Table H-1 (cont). Summary of trial conditions.

Trial #	Plate #	Run #	θ_H(degrees)	θ_V (degrees)	Shield	Shield Height (mm)	Torch Height (in)	Position	Emissivity.	Focus Distance (in)	Current (A)	Gas Flow (SCFH)	Electrode	TC Offset
25	10	1	90	44	No	N/A	0.05	Side	0.3	0.4	100	30	3/32; 2%	0
26	10	2	90	45	No	N/A	0.05	Side	0.3	0.4	100	30	3/32; 2%	0
27	11	2	90	45	No	N/A	0.05	Side	0.3	0.4	100	30	3/32; 2%	0
28	12	2	90	45	Yes	2	0.05	Side	0.3	0.4	100	30	3/32; 2%	0
29	20	2	90	45	Yes	2	0.05	Side	0.3	0.4	100	30	3/32; 2%	0
30	18	2	90	44	Yes	2-5	0.05	Side	0.3	0.4	100	30	3/32; 2%	0
31	1	1	90	41	Yes	2	0.05	Side	0.3	0.4	100	30	3/32; 2%	0
32	2	1	90	41	Yes	2	0.05	Side	0.5	0.4	100	30	3/32; 2%	0
33	3	1	90	41	Yes	2	0.05	Side	0.5	0.4	100	30	3/32; 2%	0
34	19	2	90	41	Yes	4-2	0.05	Side	0.3	0.4	100	30	3/32; 2%	0
35	13	2	90	46	Yes	2	0.05	Side	0.55	0.4	100	30	3/32; 2%	0
36	14	2	90	44	Yes	2	0.05	Side	0.55	0.4	130	30	3/32; 2%	0
37	15	2	90	46	Yes	2	0.05	Side	0.6	0.4	130	30	3/32; 2%	0
38	17	2	90	46	Yes	2	0.05	Side	0.6	0.4	130	30	3/32; 2%	0
39	20	3	90	46	Yes	2	0.05	Middle	0.6	0.4	130	30	3/32; 2%	0
40	19	3	90	45	Yes	5-2	0.05	Middle	0.6	0.4	130	30	3/32; 2%	0
41	4	2	90	46	Yes	2	0.05	Middle	0.6	0.4	130	30	3/32; 2%	0
42	5	2	90	46	Yes	2	0.05	Middle	0.6	0.4	130	30	3/32; 2%	0
43	18	3	90	46	Yes	5-2	0.05	Middle	0.6	0.4	130	30	3/32; 2%	0.2
44	17	3	90	46	Yes	2	0.05	Middle	0.6	0.4	130	30	3/32; 2%	0.1
45	15	3	90	45	Yes	5-2	0.05	Middle	0.6	0.4	130	30	3/32; 2%	0.2
46	14	3	90	45	Yes	5-2	0.05	Middle	0.6	0.4	130	30	3/32; 2%	0.1

Table H-1 (cont). Summary of trial conditions.

Trial #	Plate #	Run #	θ_H(degrees)	θ_V (degrees)	Shield	Shield Height (mm)	Torch Height (in)	Position	Emissivity.	Focus Distance (in)	Current (A)	Gas Flow (SCFH)	Electrode	TC Offset
47	13	3	90	45	Yes	5-2	0.05	Middle	0.6	0.4	130	30	3/32; 2%	0.1
48	12	3	90	45	Yes	5-2	0.05	Middle	0.6	0.4	130	30	3/32; 2%	0.2
49	11	3	90	44	Yes	5-2	0.05	Middle	0.6	0.4	130	30	3/32; 2%	0.5
50	10	3	90	44	Yes	5-2	0.05	Middle	0.6	0.4	130	30	3/32; 2%	0.5
51	9	3	90	44	Yes	5-2	0.05	Middle	0.6	0.4	130	30	3/32; 2%	0.5
52	3	2	90	44	Yes	2	0.05	Middle	0.6	0.4	130	30	3/32; 2%	0
53	2	2	90	44	Yes	2	0.05	Middle	0.6	0.4	130	30	3/32; 2%	0
54	1	2	90	44	Yes	2	0.05	Middle	0.6	0.4	130	30	3/32; 2%	0
55	16	2	90	44	Yes	2	0.05	Middle	0.6	0.4	130	30	3/32; 2%	0
56	8	3	90	44	Yes	5-2	0.05	Middle	0.6	0.4	130	30	3/32; 2%	Fig-5
57	7	3	90	44	Yes	5-2	0.05	Middle	0.6	0.4	130	30	3/32; 2%	Fig-5
58	6	3	90	44	Yes	5-2	0.05	Middle	0.6	0.4	130	30	3/32; 2%	Fig-5
59	5	3	90	45	Yes	12-2	0.3-0.05-0.2	Side	0.6	0.4	130	30	3/32; 2%	Fig-5
60	4	3	90	45	Yes	11-2	0.3-0.05-0.2	Side	0.6	0.4	130	30	3/32; 2%	Fig-5
61	3	3	90	45	Yes	10-2	0.2-0.05	Side	0.6	0.4	130	30	32/; 2%	Fig-5
62	2	3	90	45	Yes	10-2	0.2-0.05	Side	0.6	0.4	130	30-20	3/32; 2%	No TC
63	1	3	90	45	Yes	10-2	0.2-0.05	Side	0.6	0.4	130	30-40	3/32; 2%	No TC
64	16	3	90	45	Yes	10-2	0.2-0.05	Side	0.6	0.4	130	30-50	3/32; 2%	No Tc

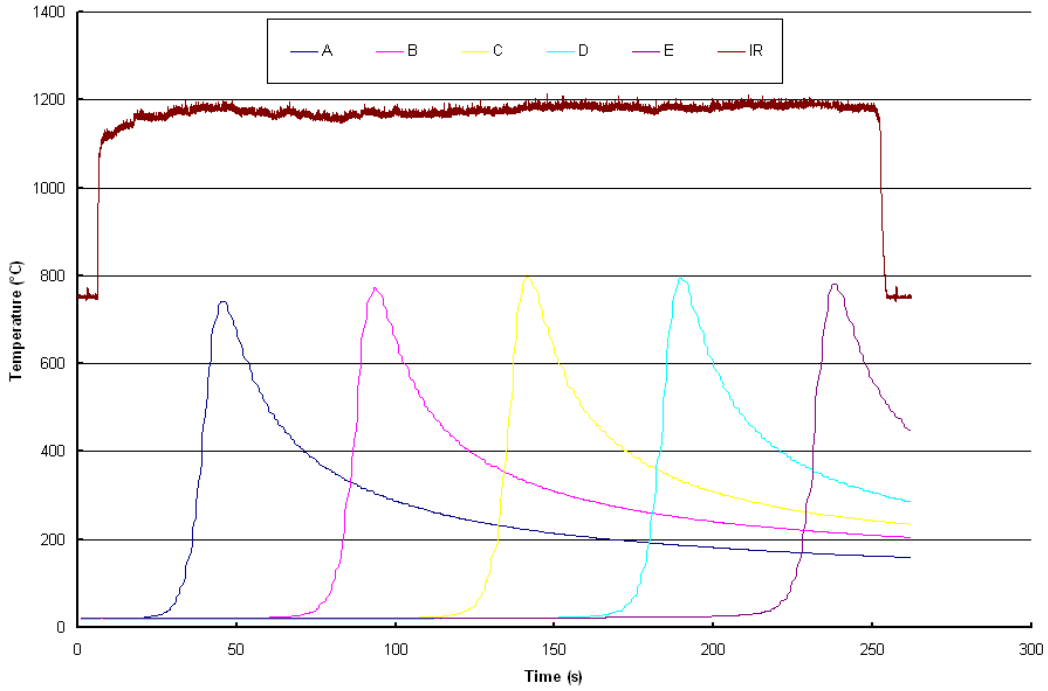

Figure H-1. Trial 2

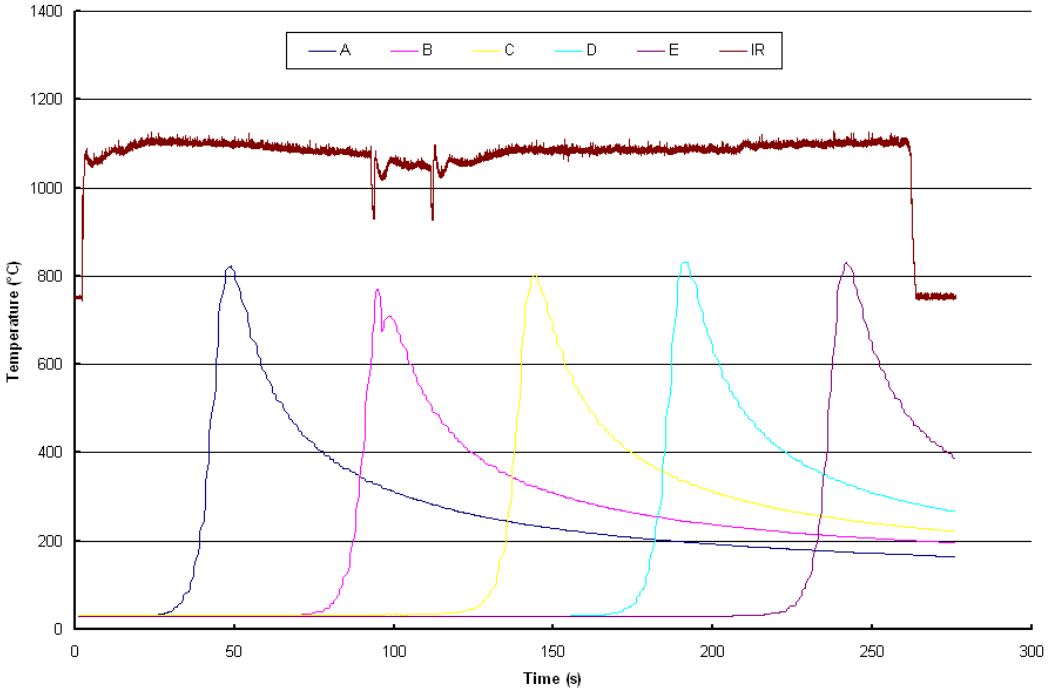

Figure H-2. Trial 3

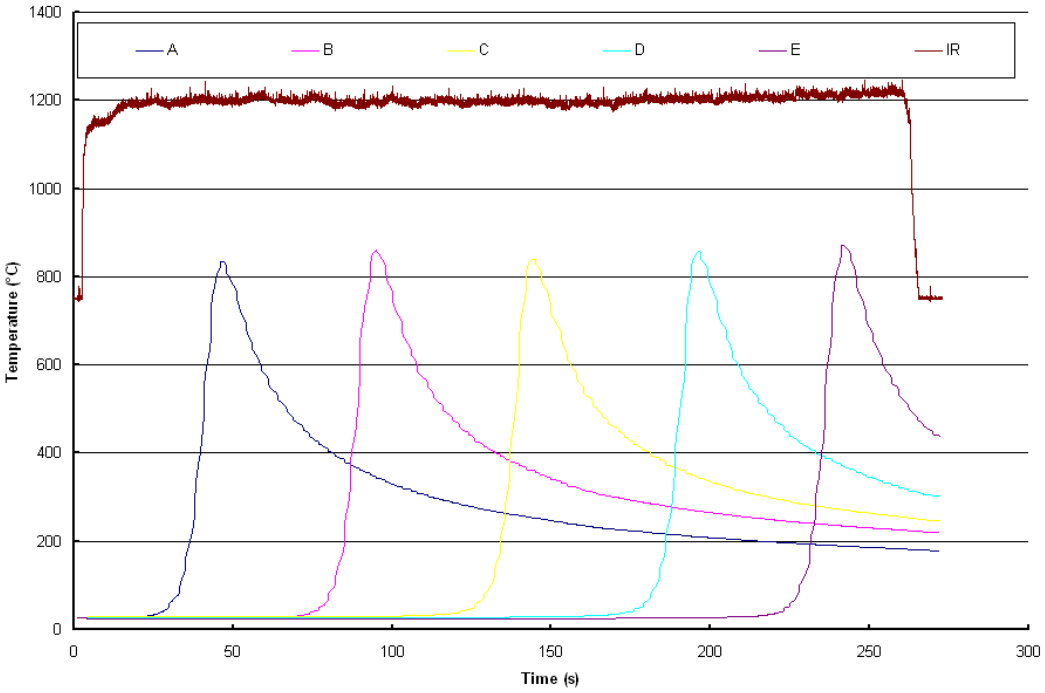

Figure H-3. Trial 4

4

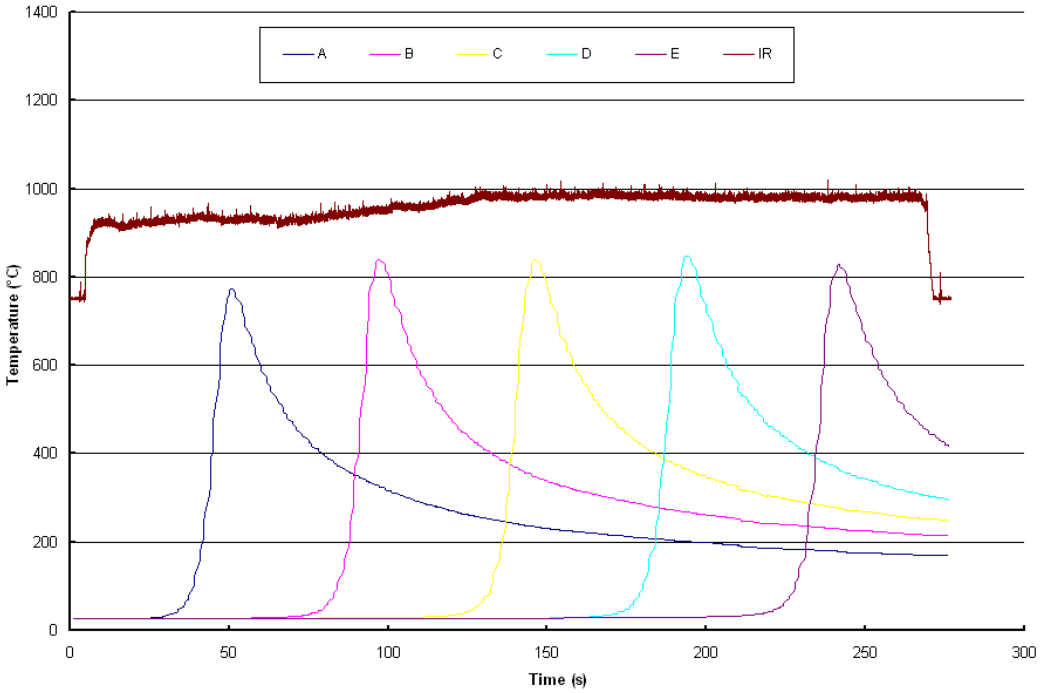

Figure H-4. Trial 5

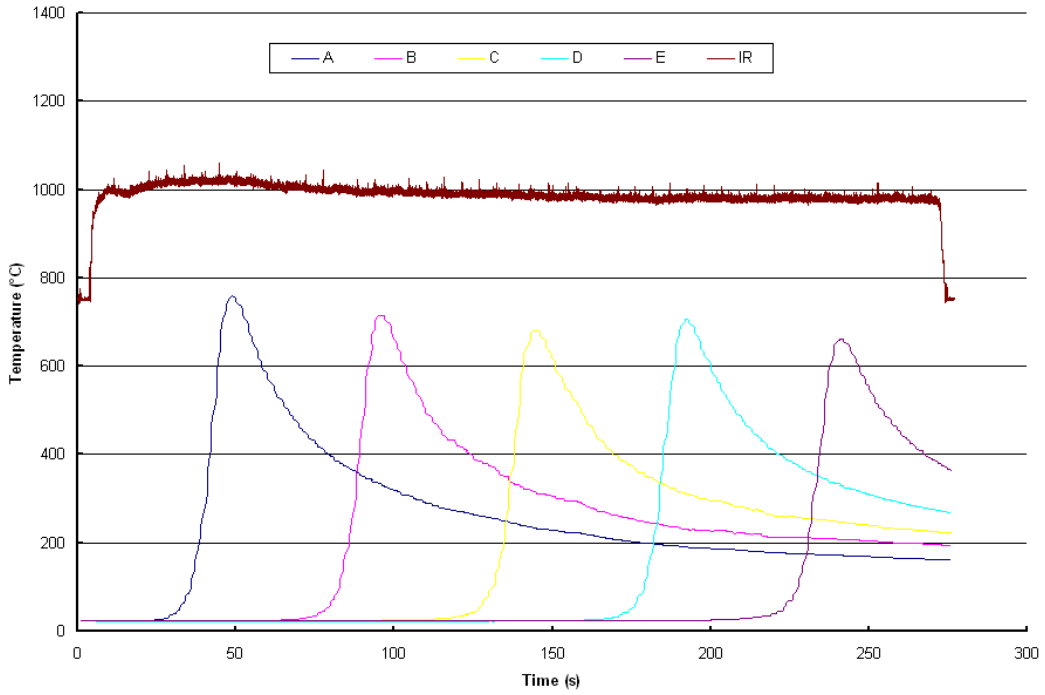

Figure H-5. Trial 6

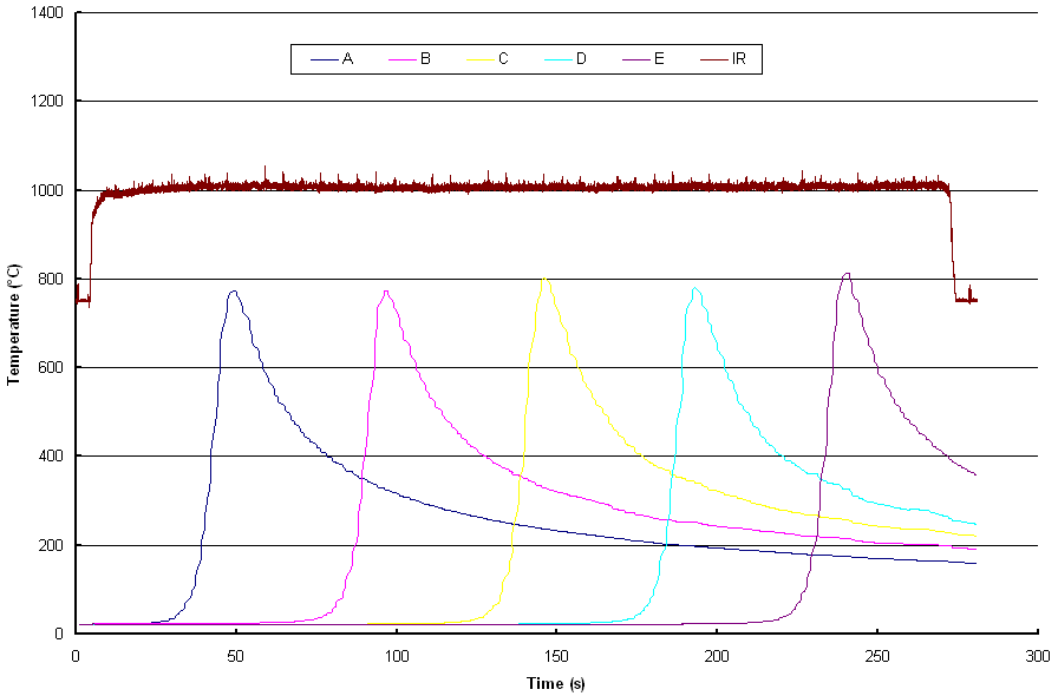

Figure H-6. Trial 7

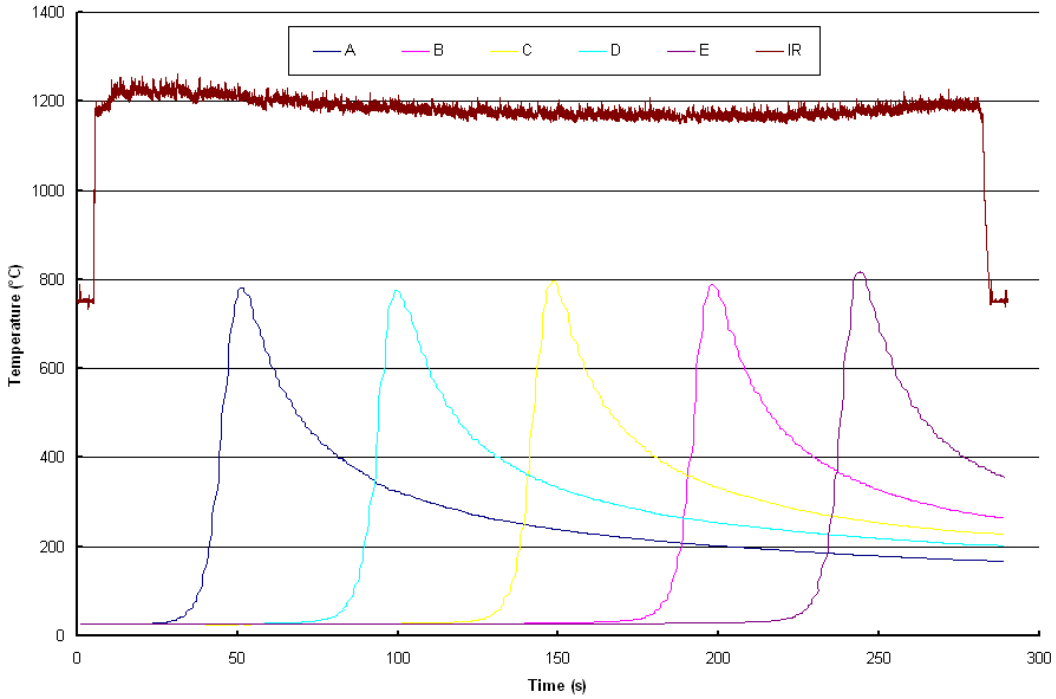

Figure H-7. Trial 8

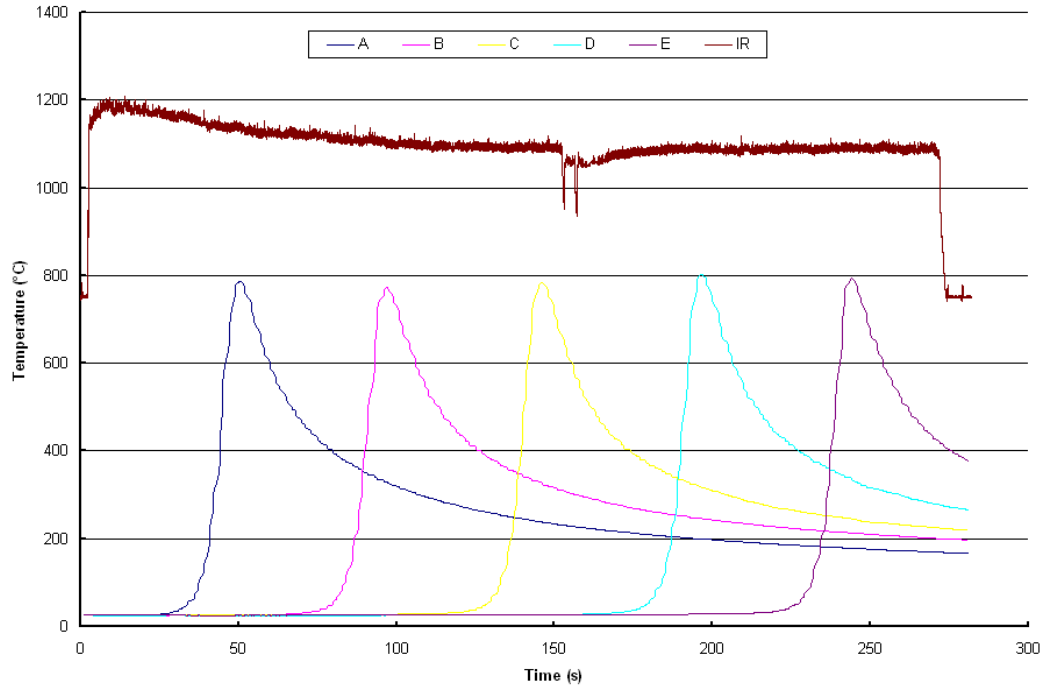

Figure H-8. Trial 9

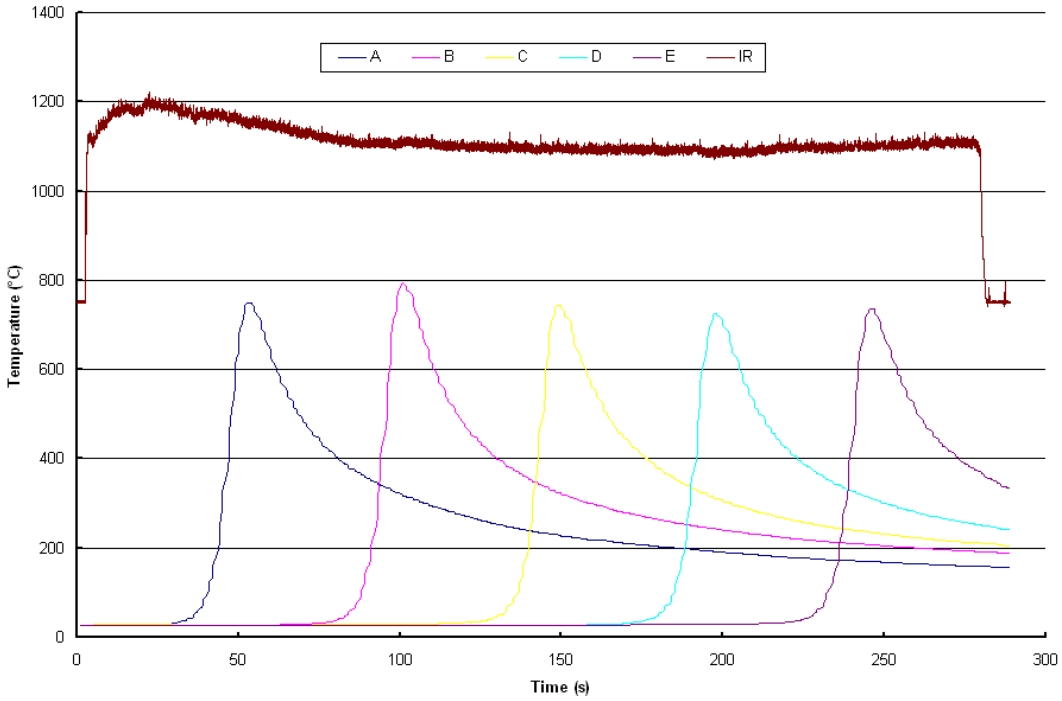

Figure H-9. Trial 10

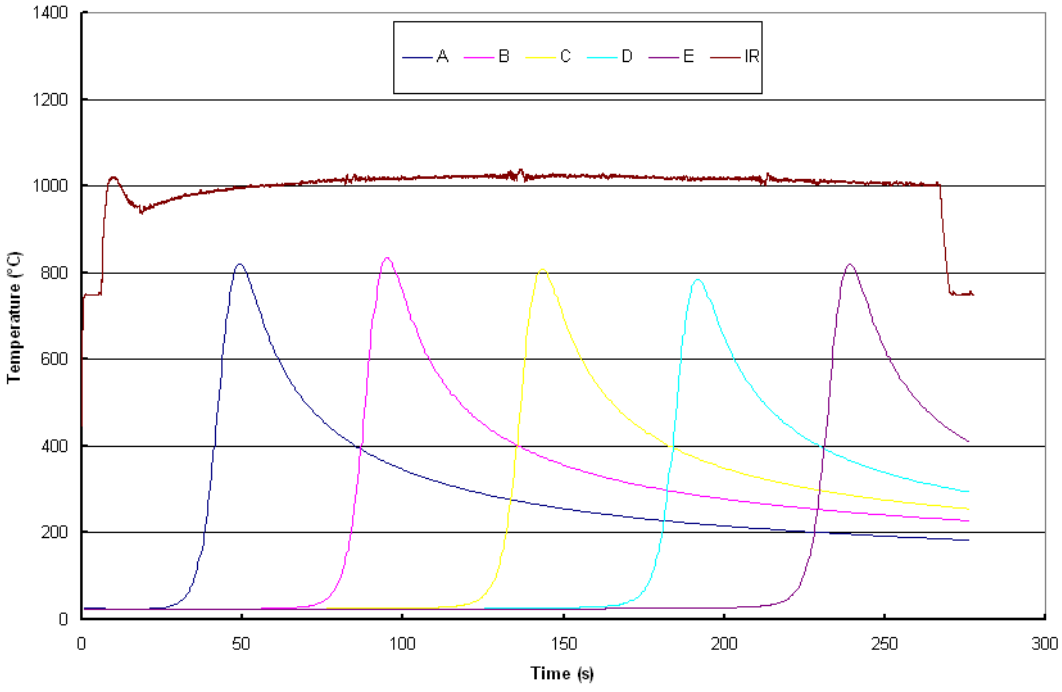

Figure H-10, Trial 14

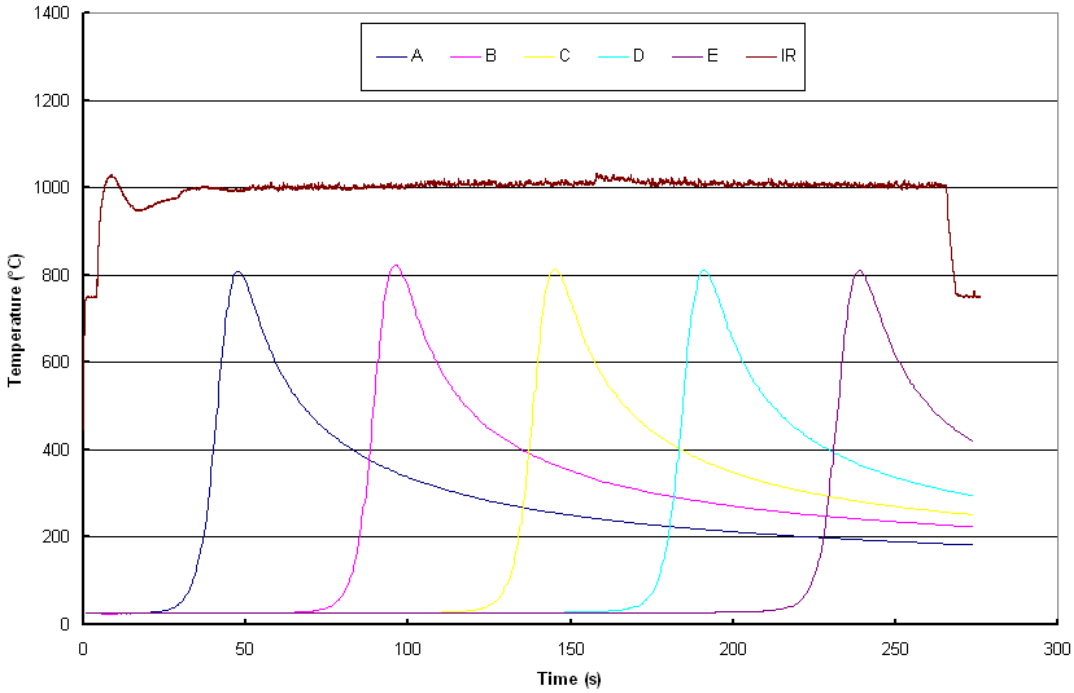

Figure H-11. Trial 15

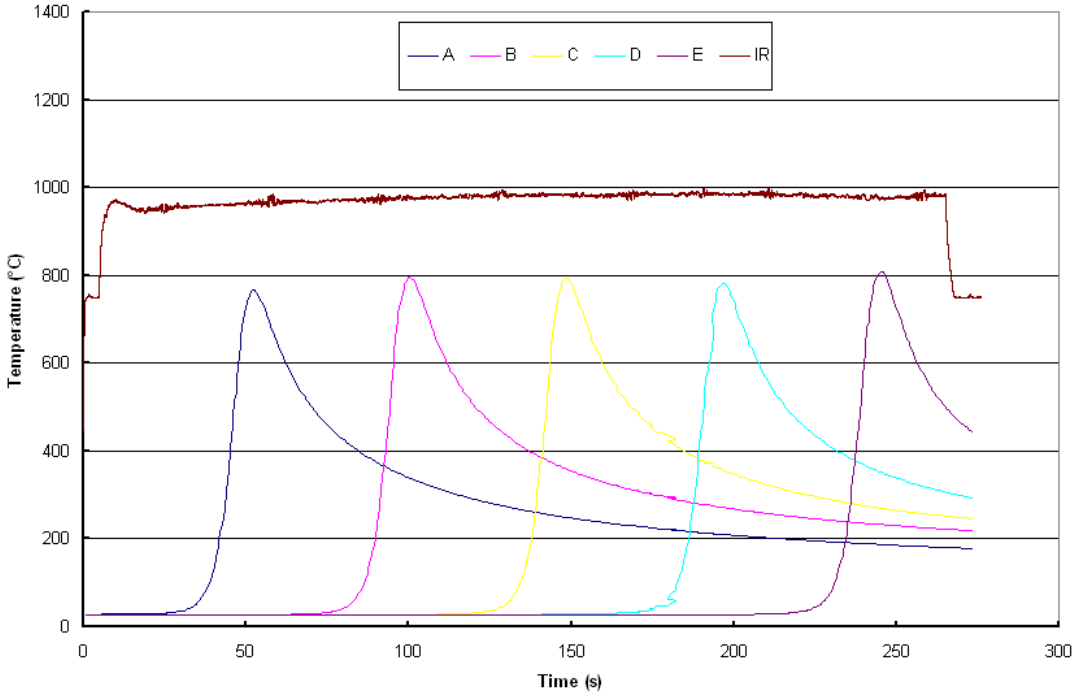

Figure H-12. Trial 16

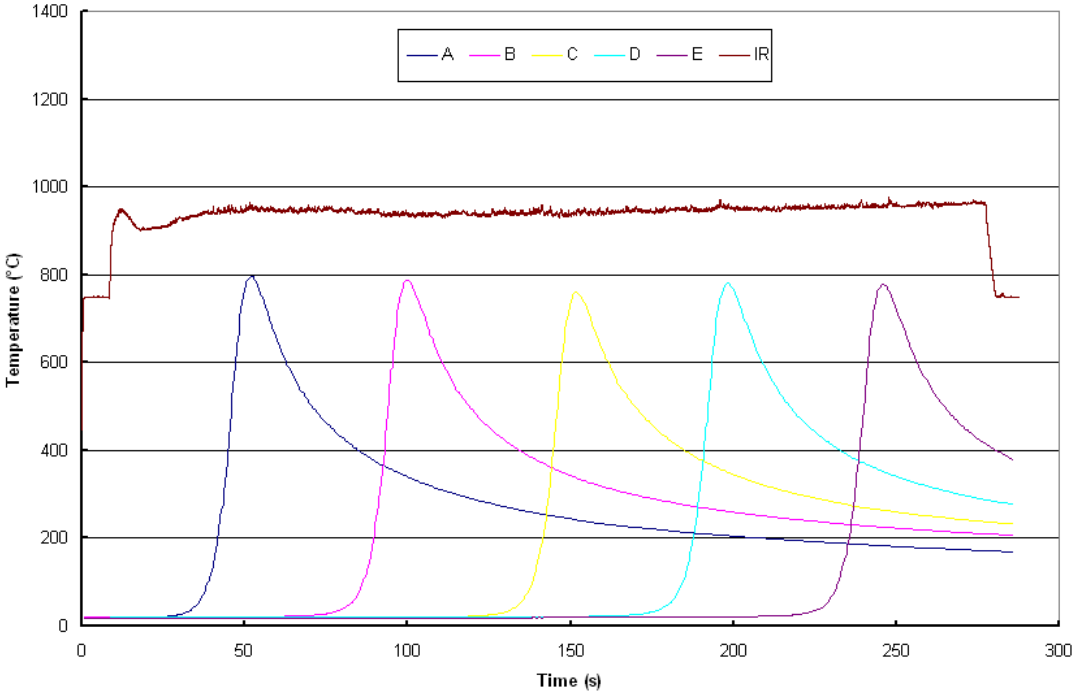

Figure H-13. Trial 17

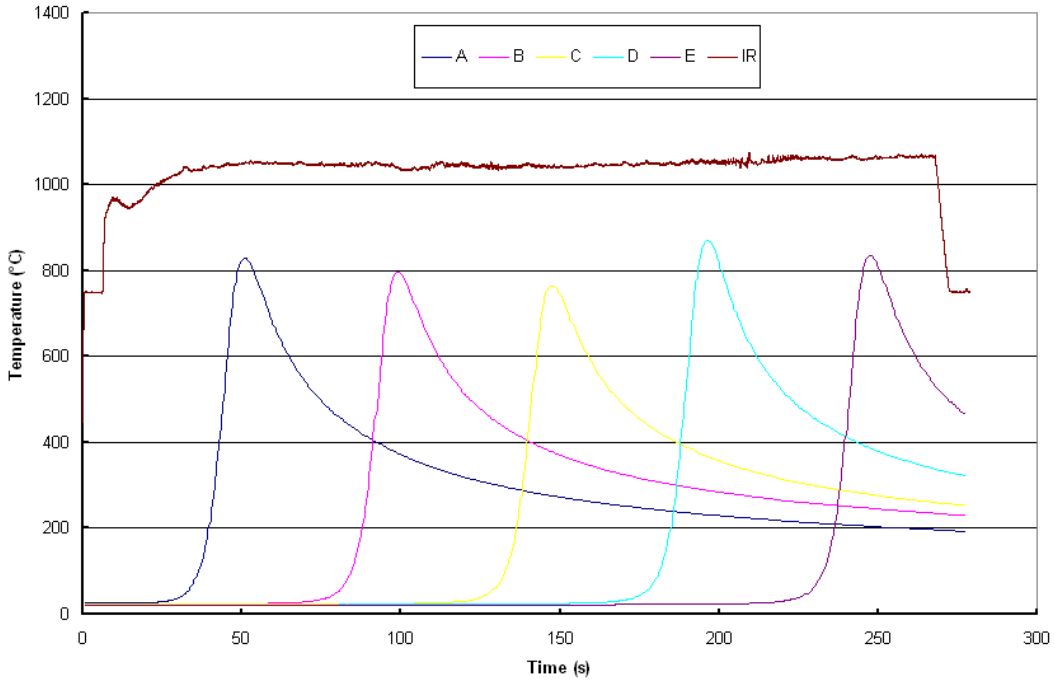

Figure H-14. Trial 18

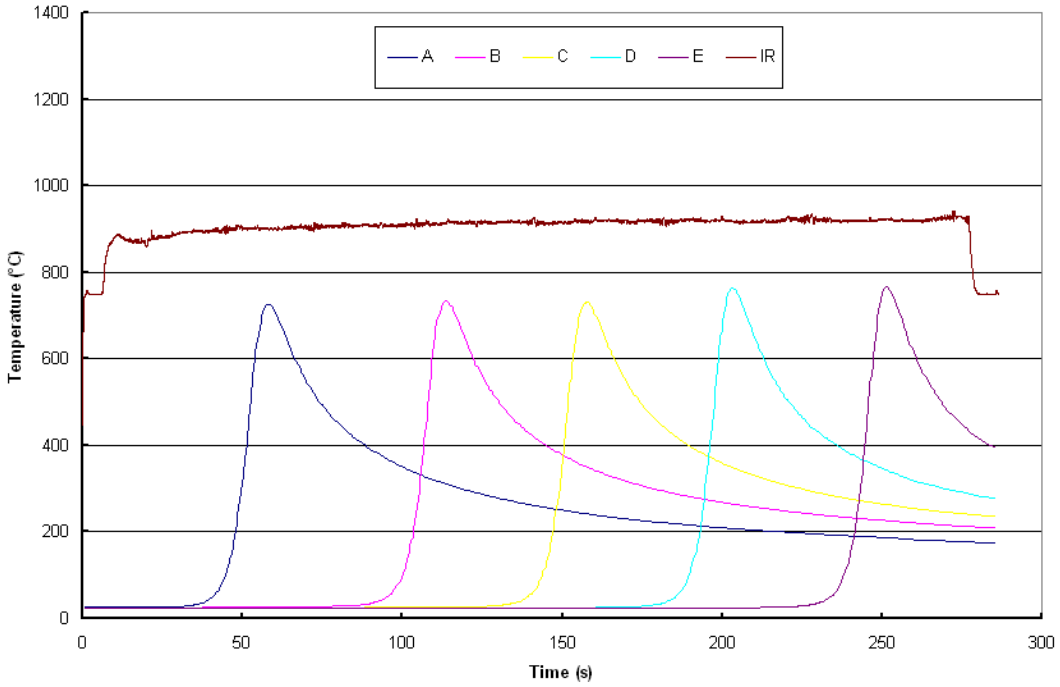

Figure H-15. Trial 19

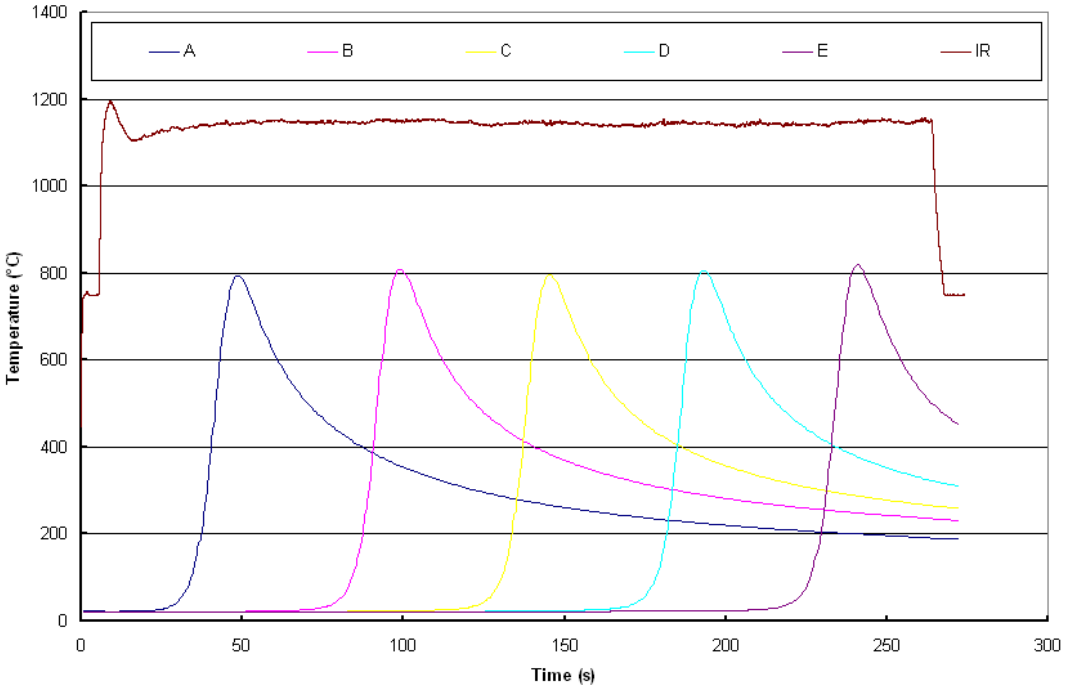

Figure H-16. Trial 20

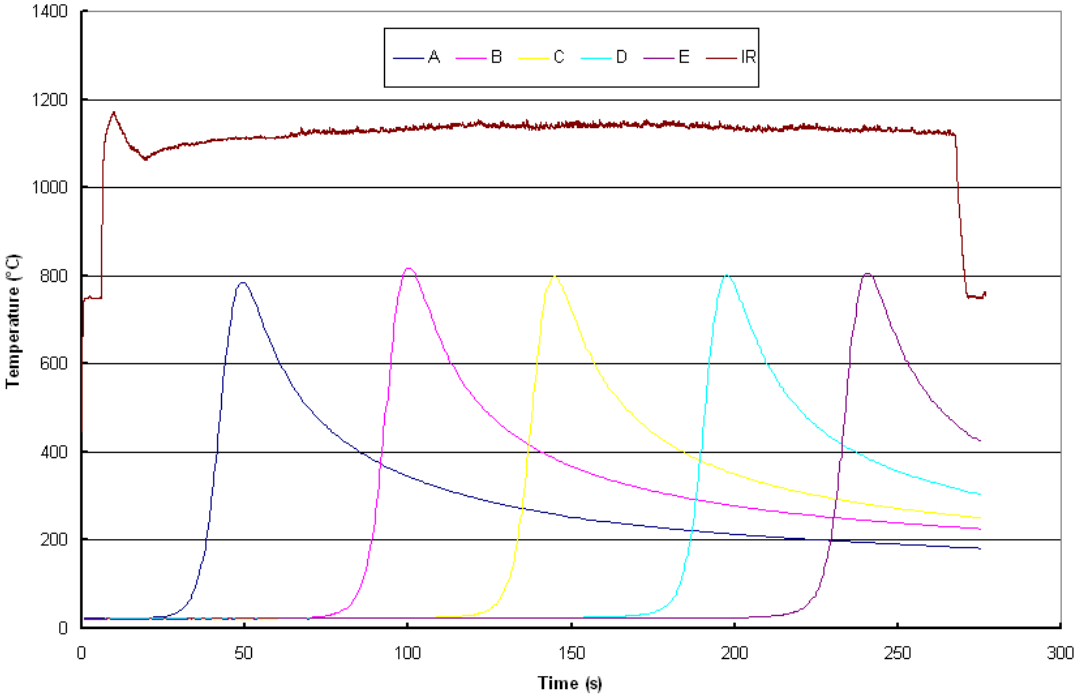

Figure H-17. Trial 21

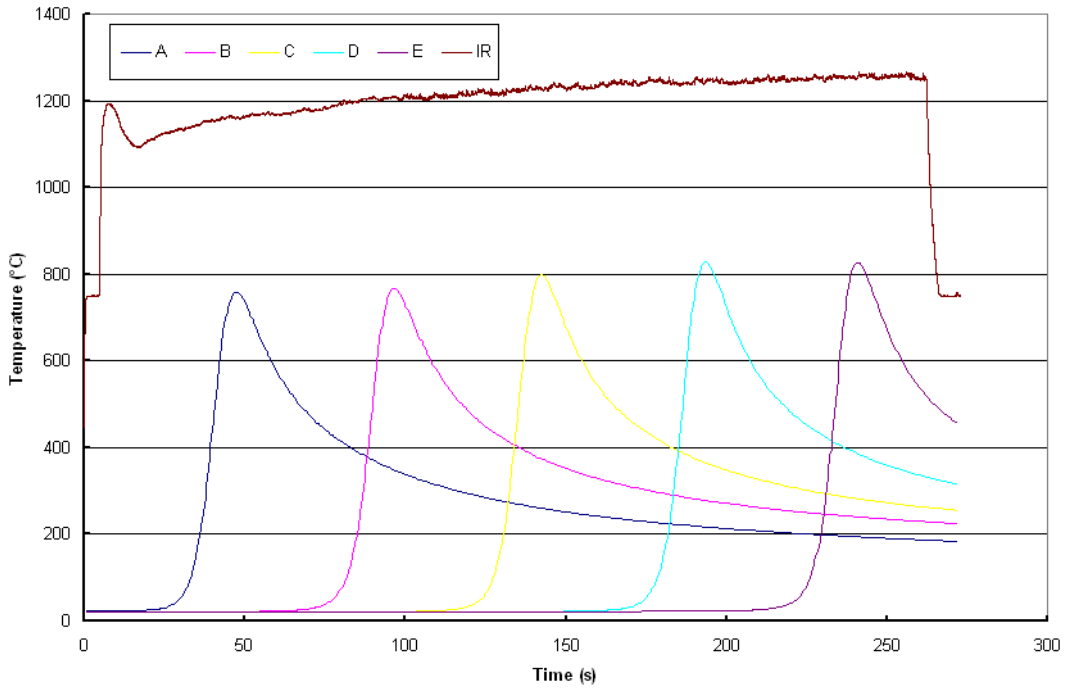

Figure H-18. Trial 22

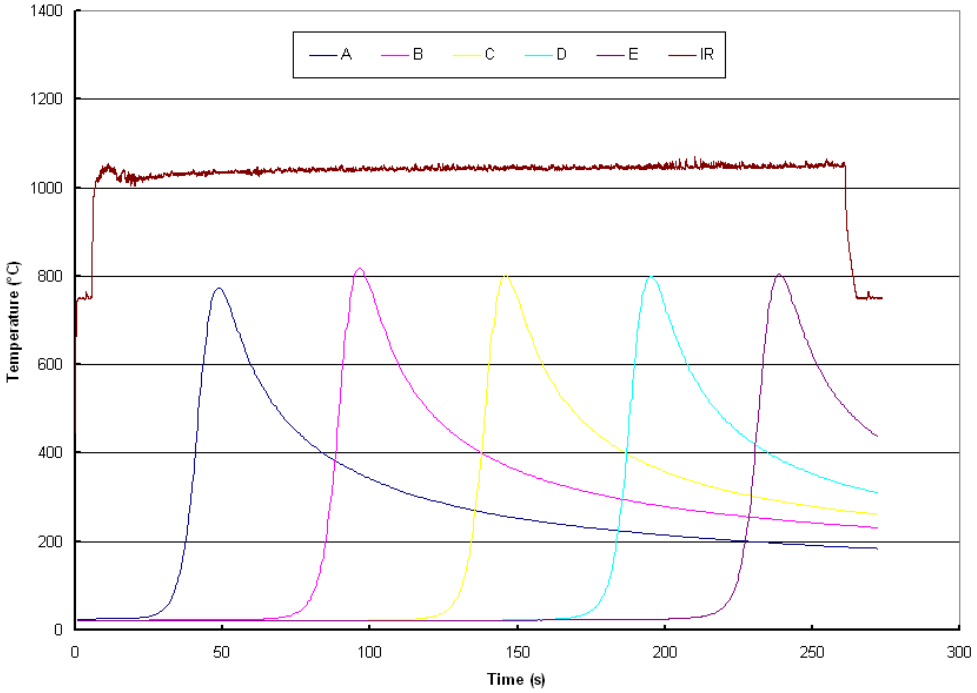

Figure H-19. Trial 23

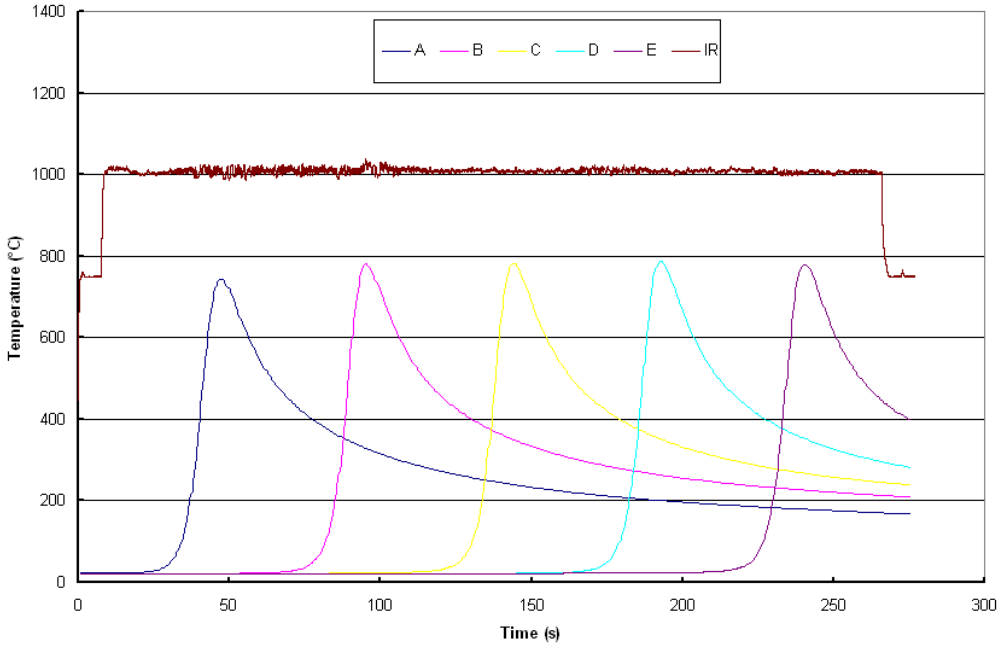

Figure H-20. Trial 24

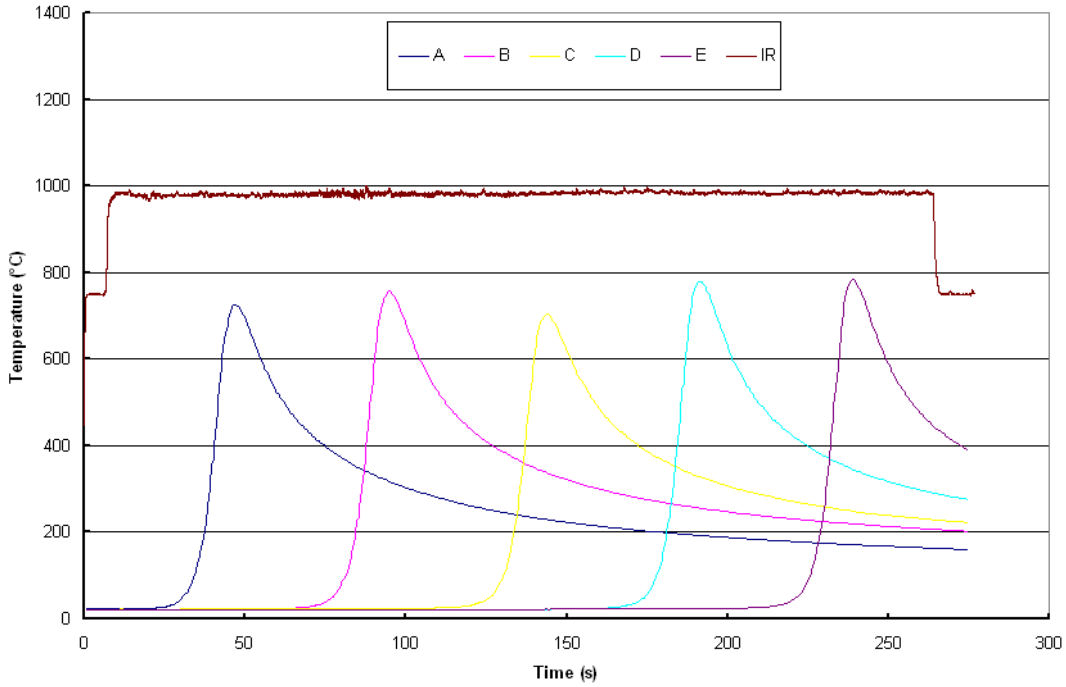

Figure H-21. Trial 25

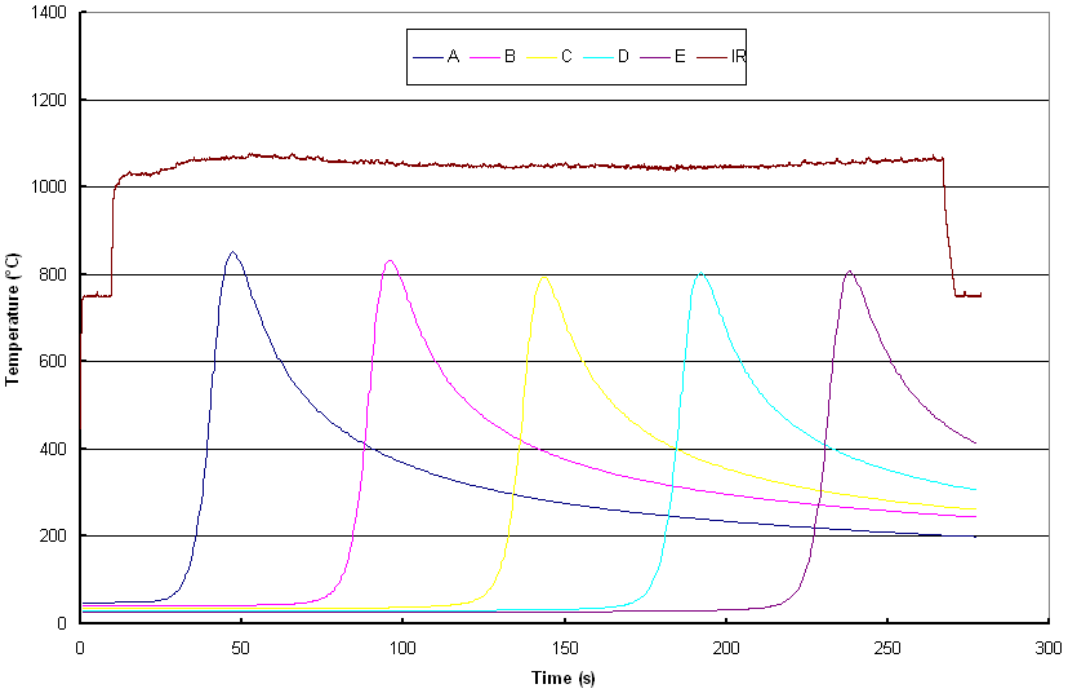

Figure H-22. Trial 26

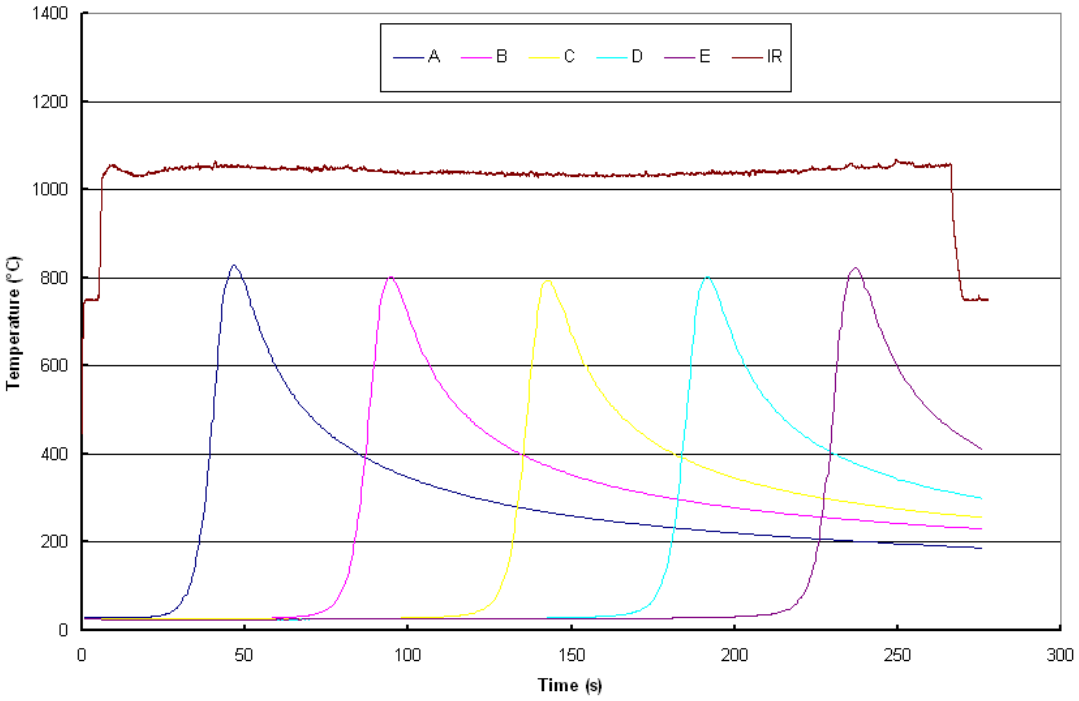

Figure H-23. Trial 27

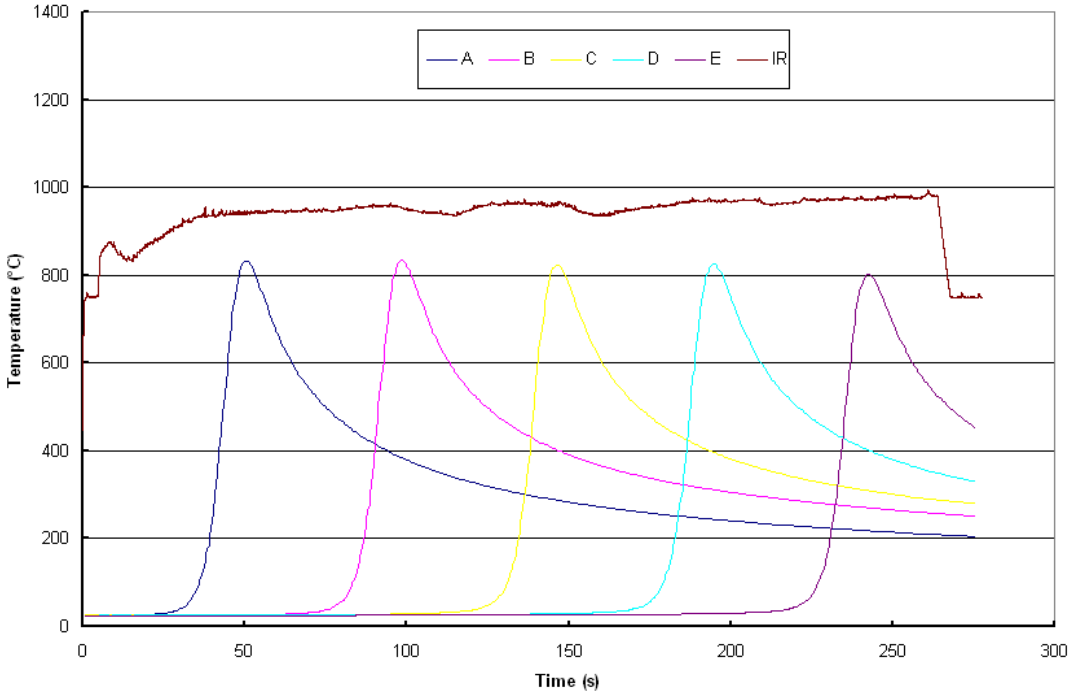

Figure H-24. Trial 28

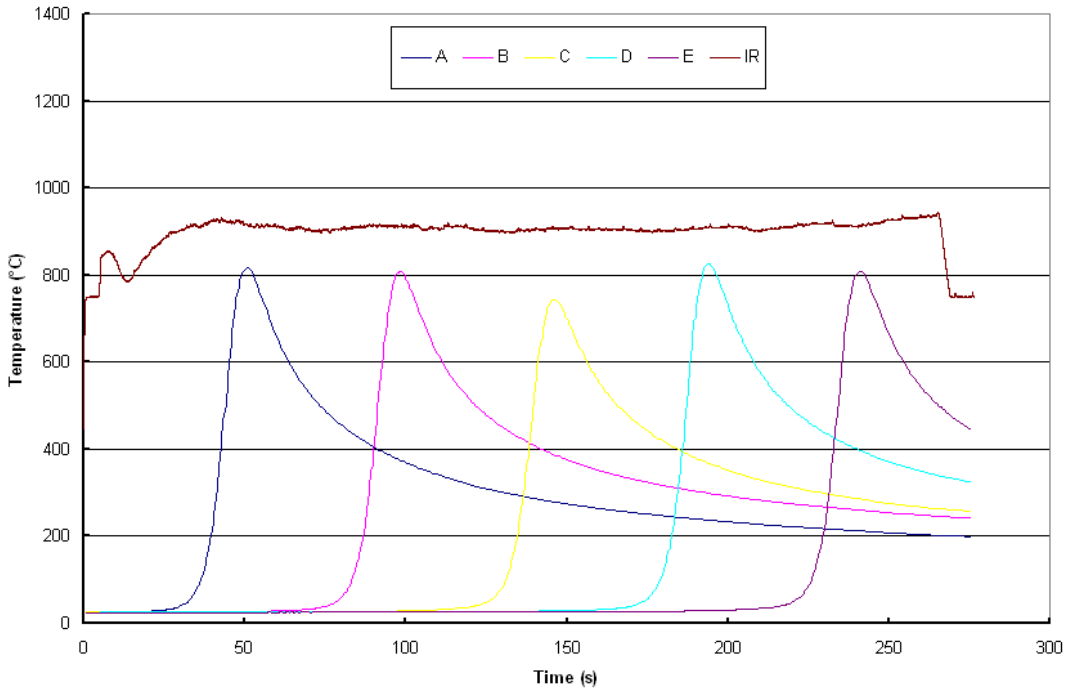

Figure H-25. Trial 29

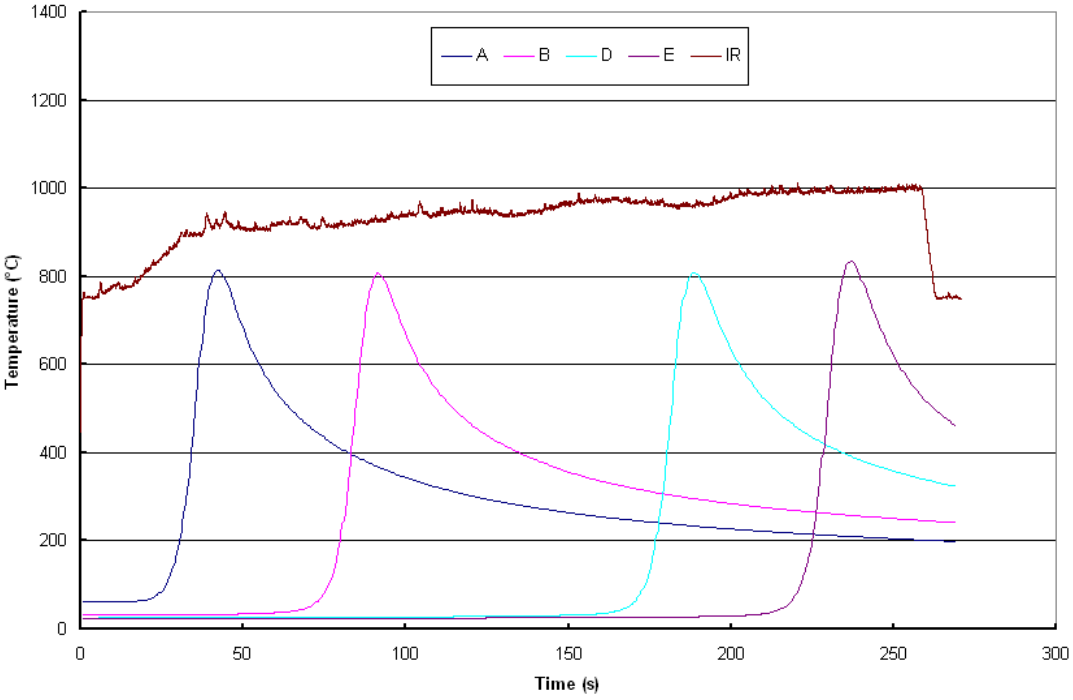

Figure H-26. Trial 30

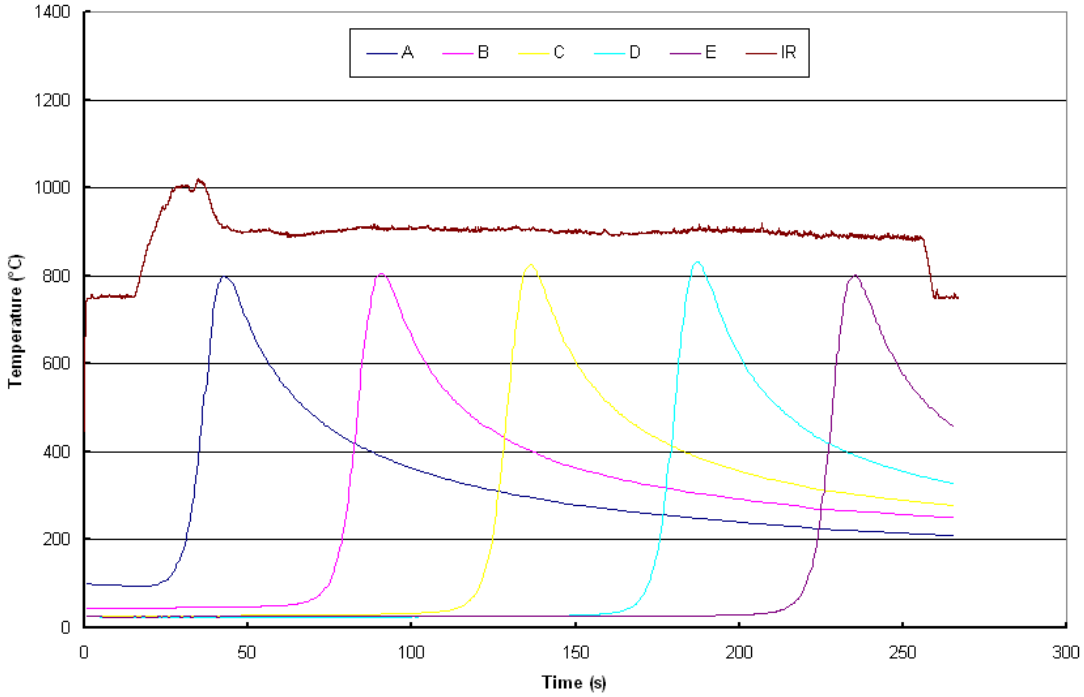

Figure H-27. Trial 31

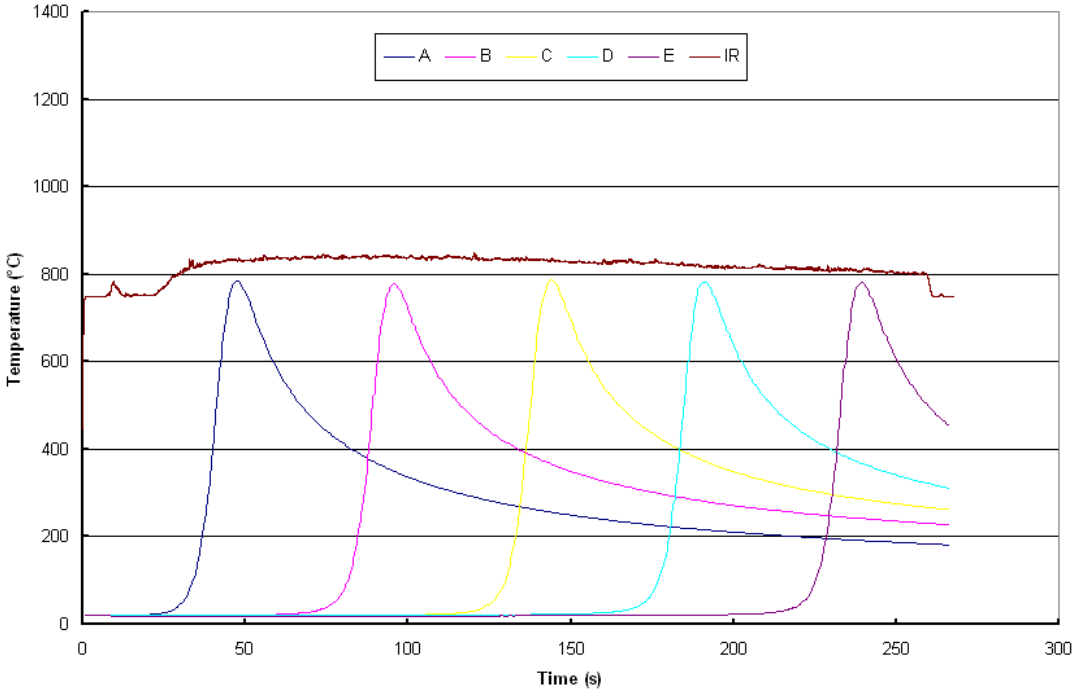

Figure H-28. Trial 33

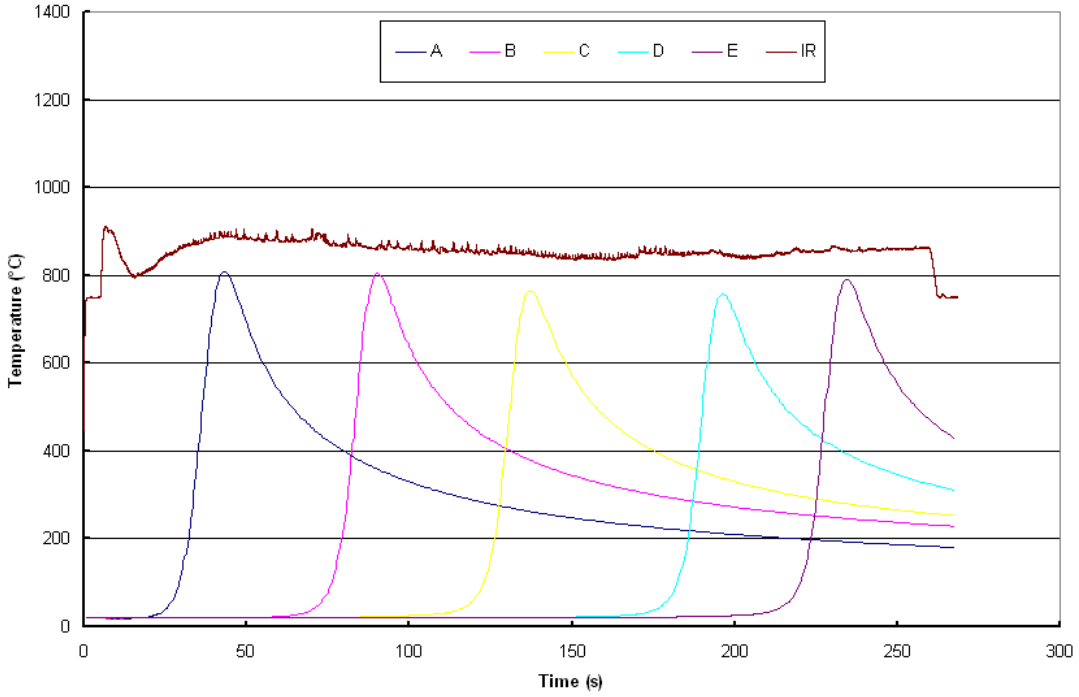

Figure H-29. Trial 34

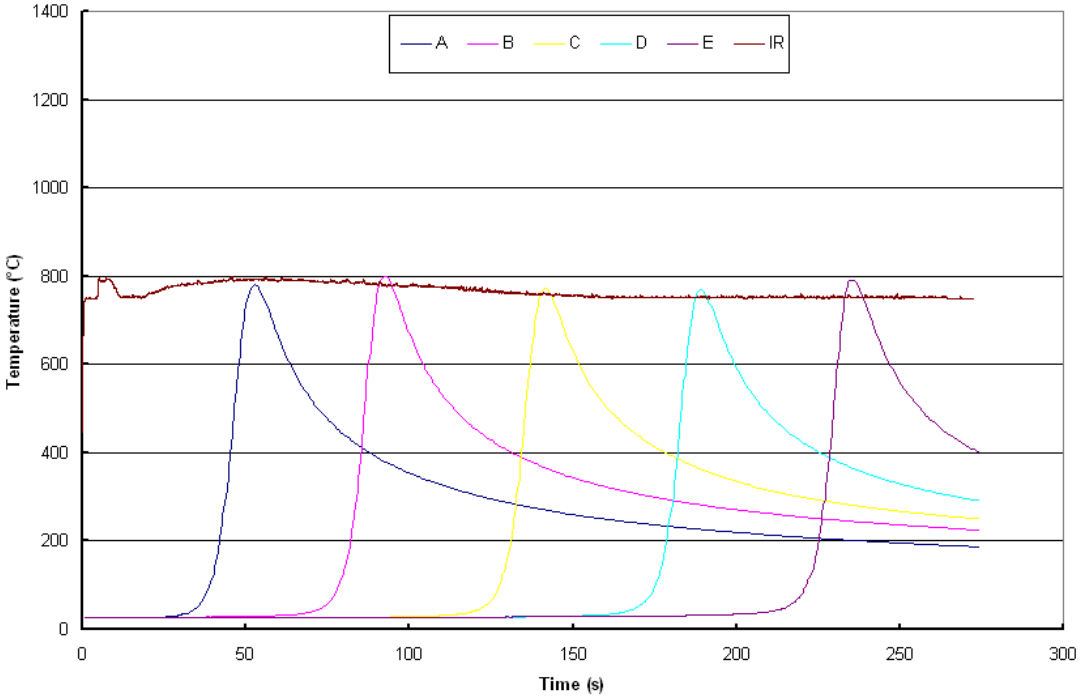

Figure H-30. Trial 35

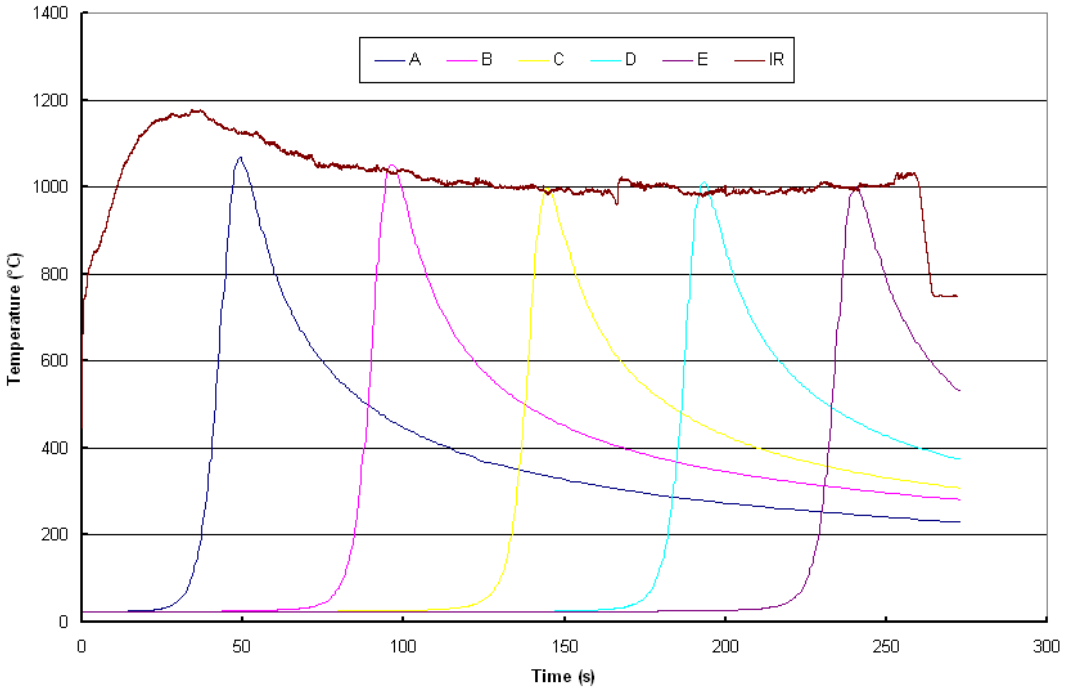

Figure H-31. Trial 36

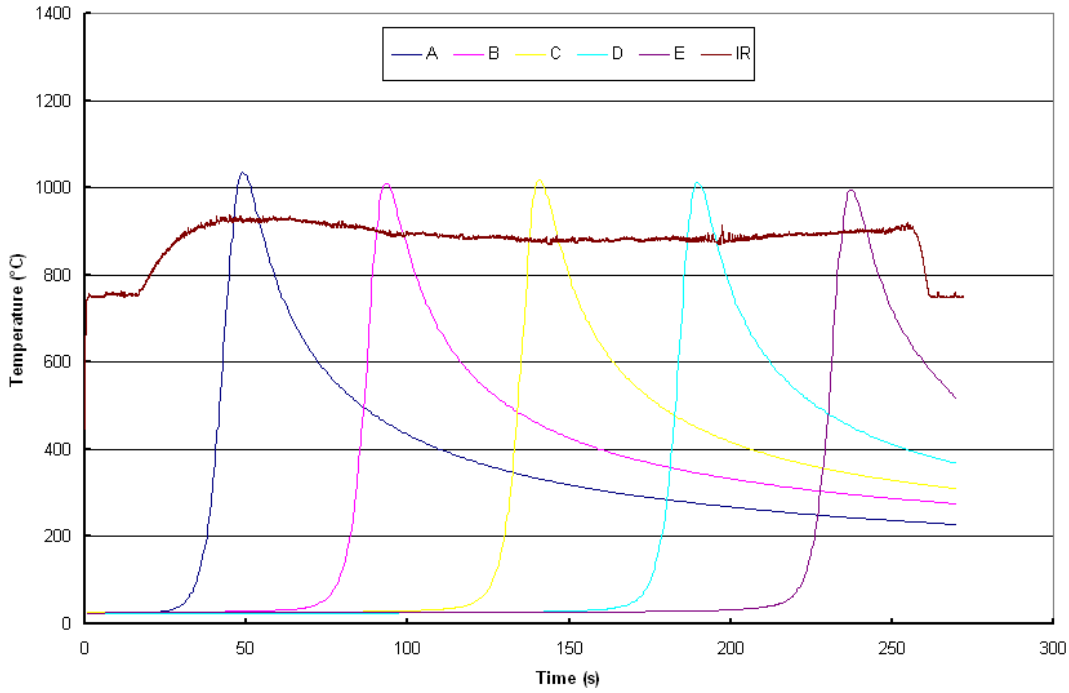

Figure H-32. Trial 38

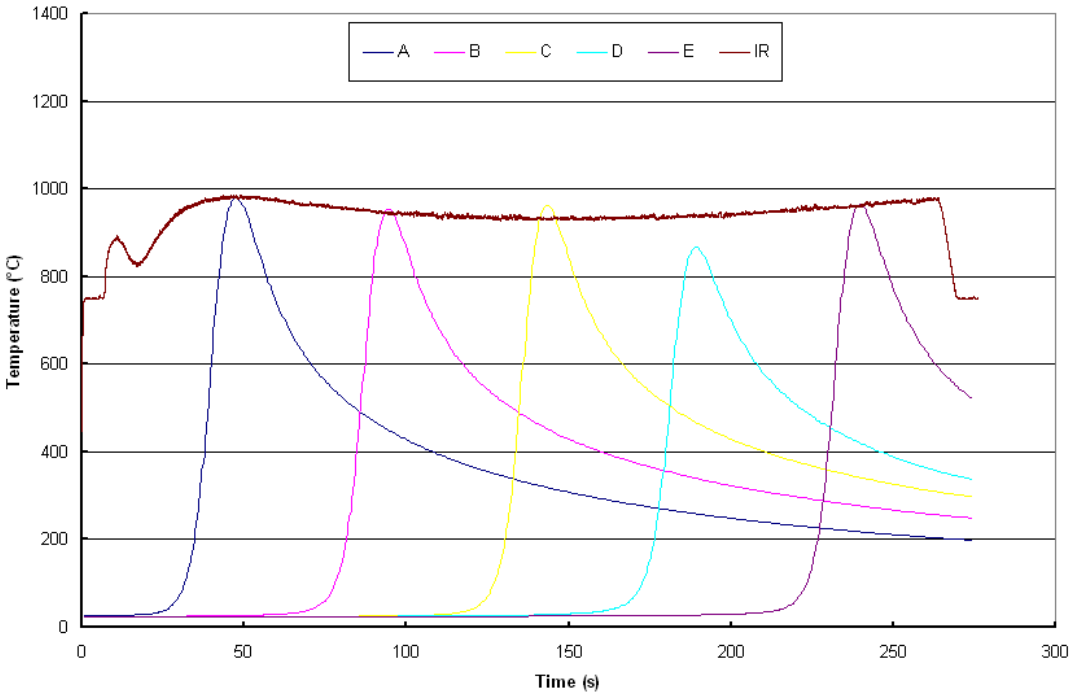

Figure H-33. Trial 39

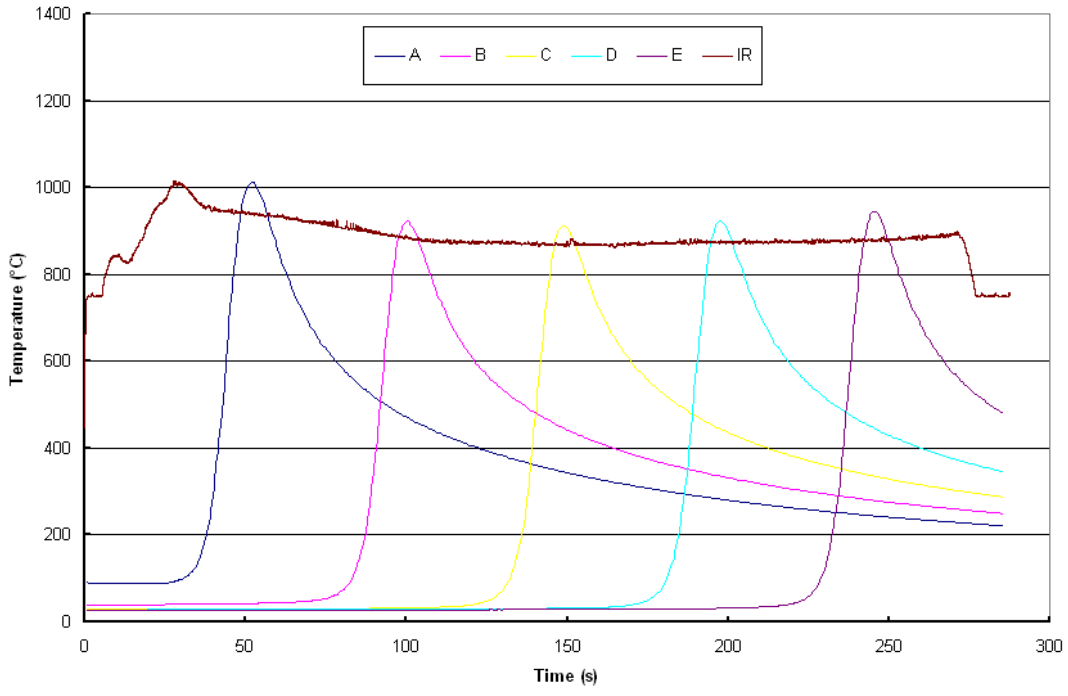

Figure H-34. Trial 40

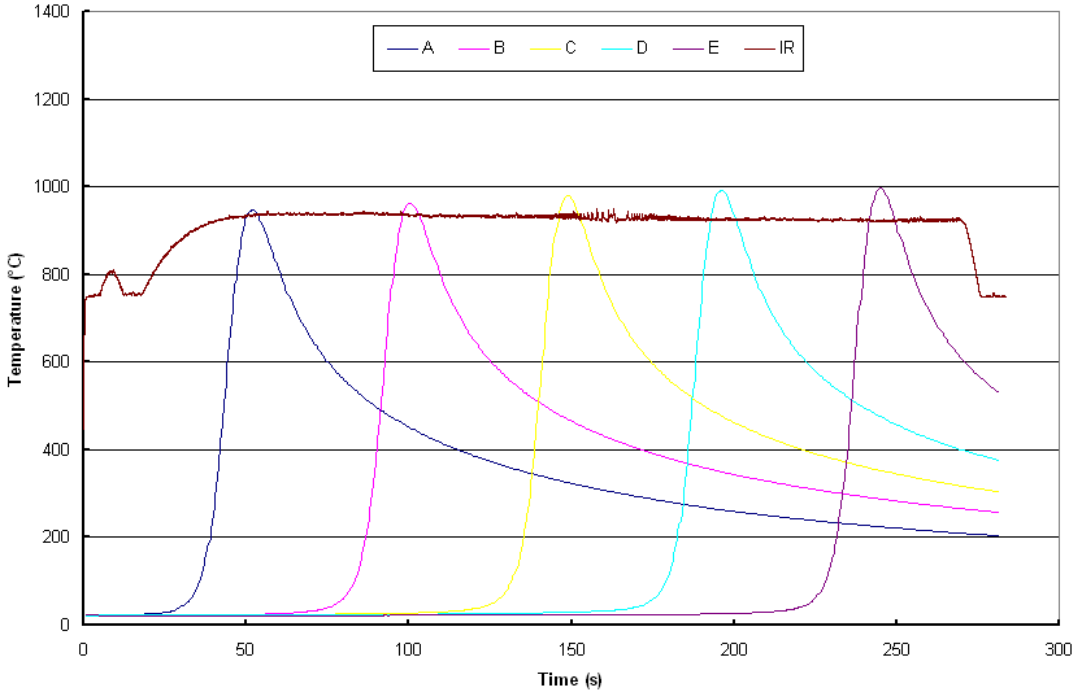

Figure H-35. Trial 42

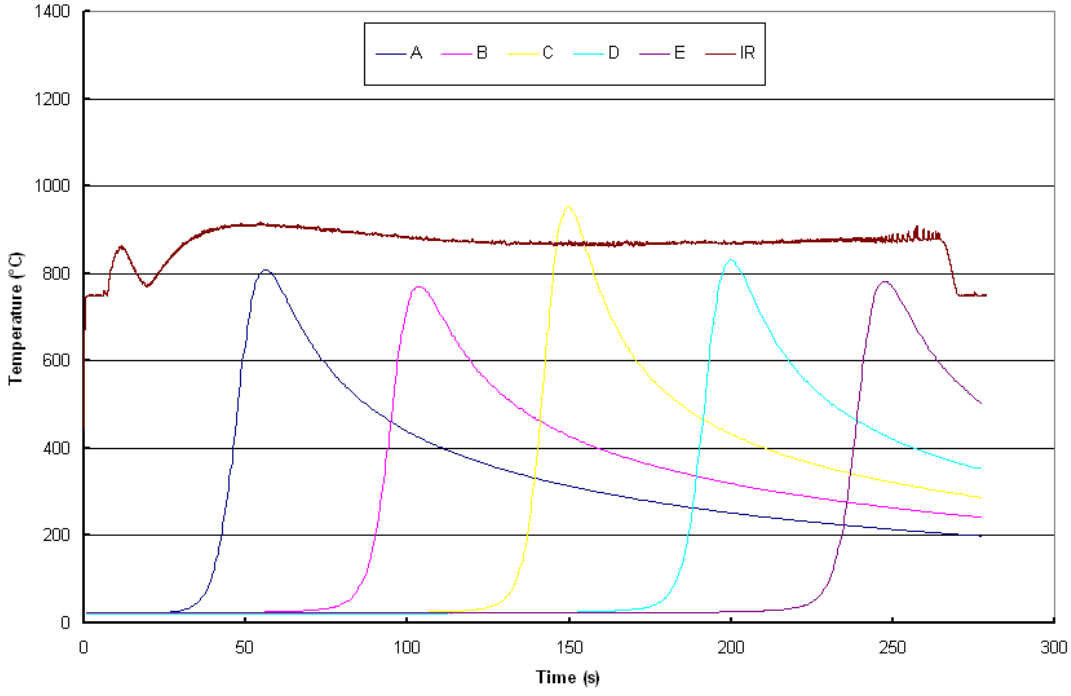

Figure H-36. Trial 43

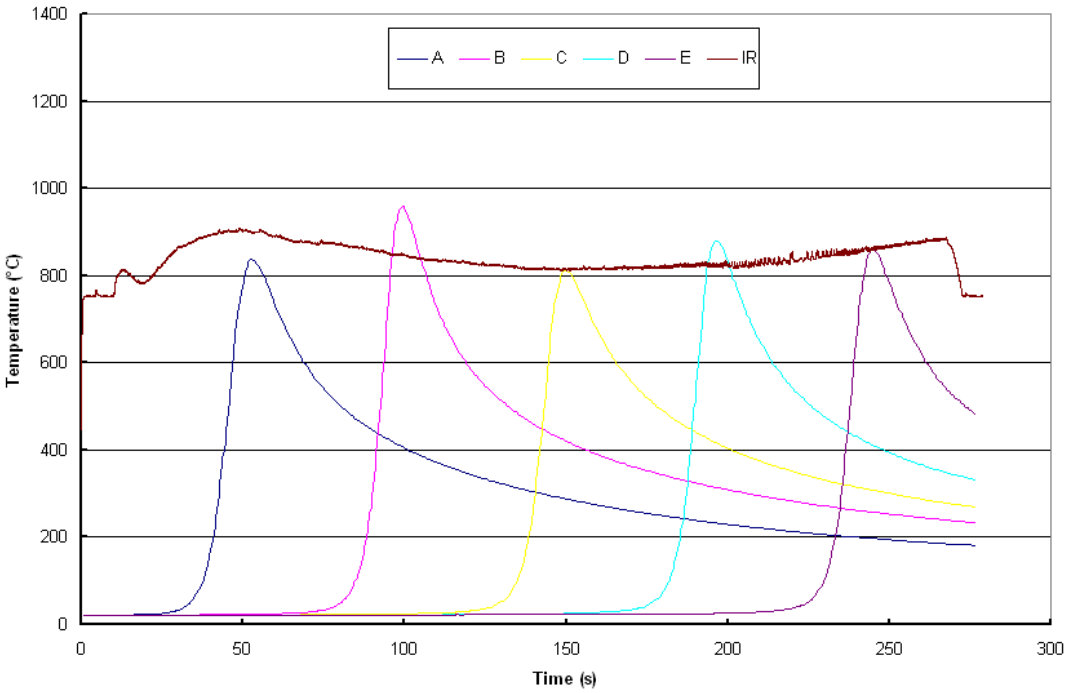

Figure H-37. Trial 44

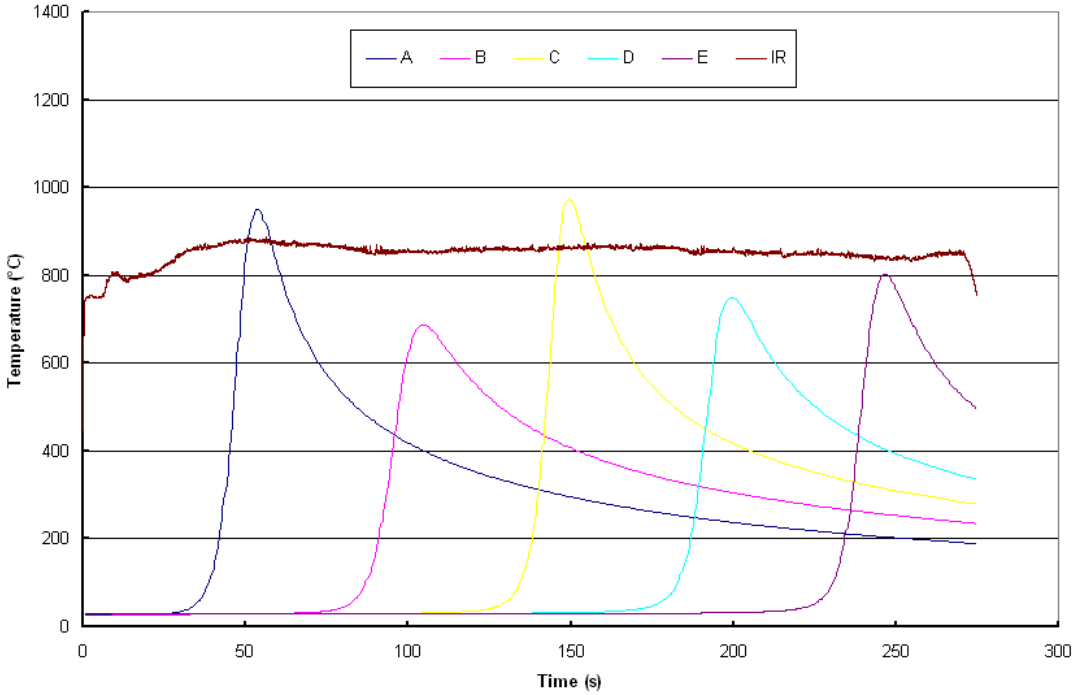

Figure H-38. Trial 45

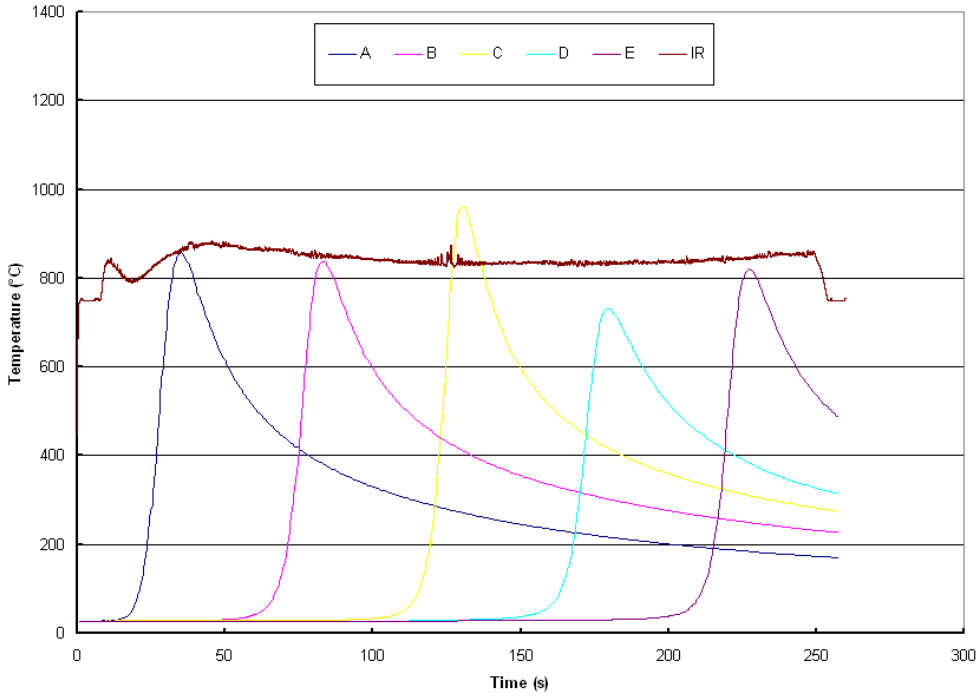

Figure H-39. Trial 46

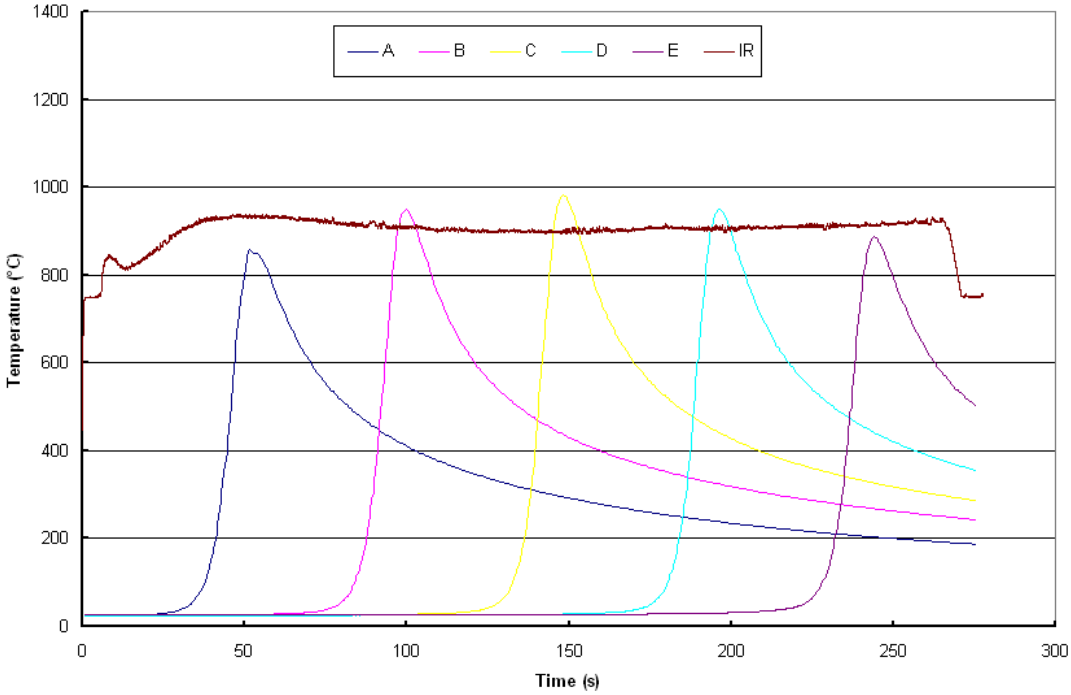

Figure H-40. Trial 47

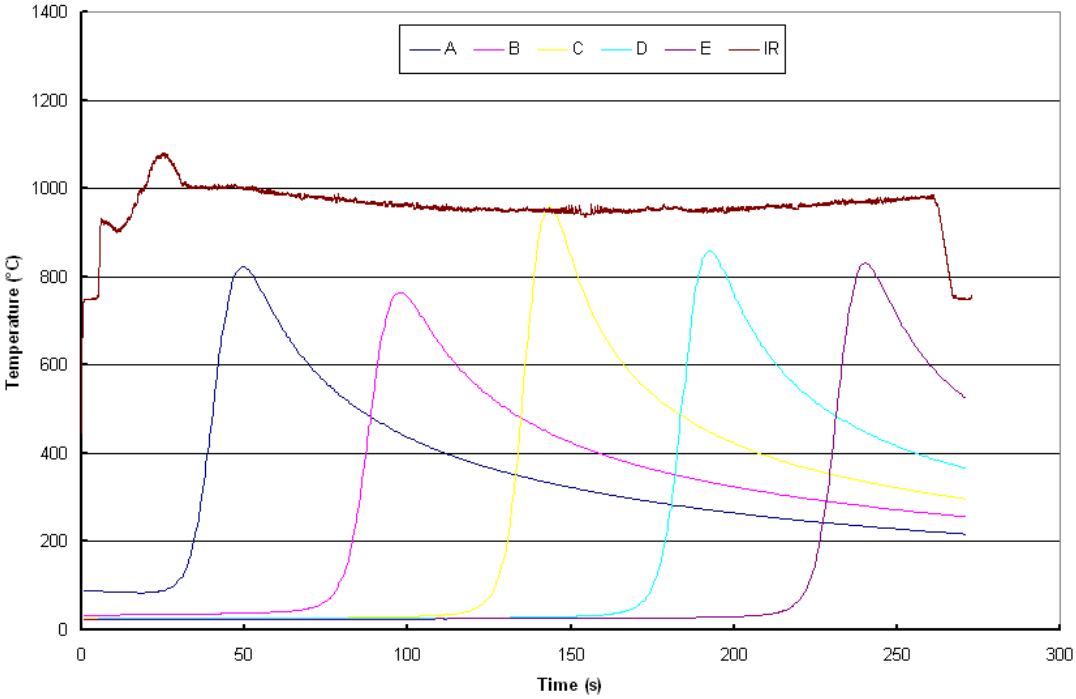

Figure H-41. Trial 48

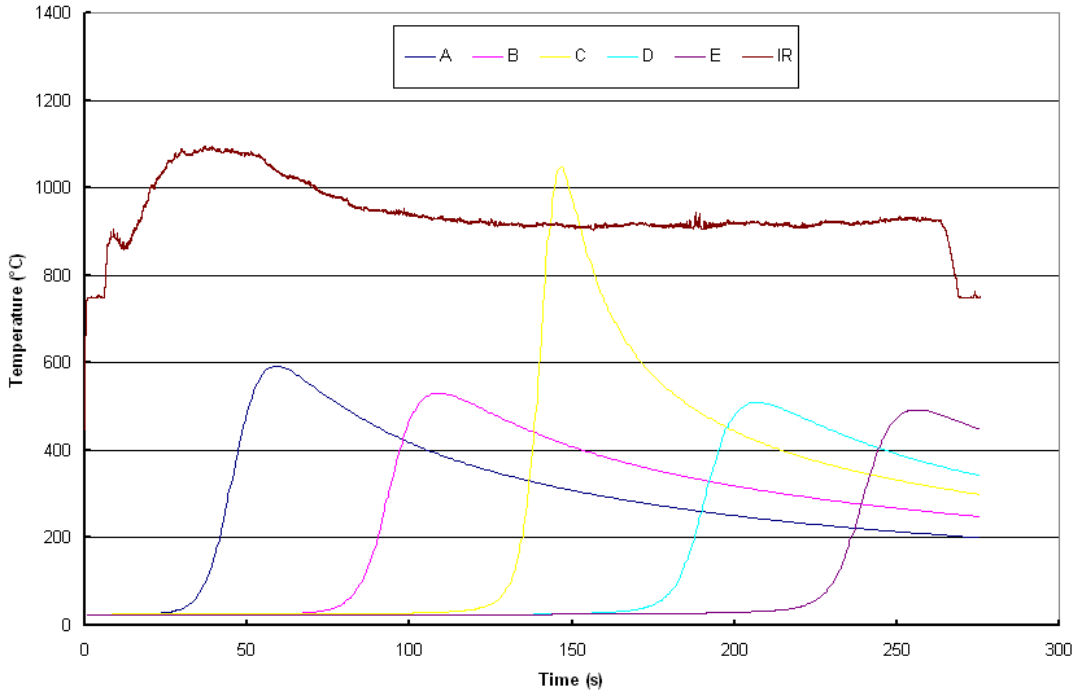

Figure H-42. Trial 49

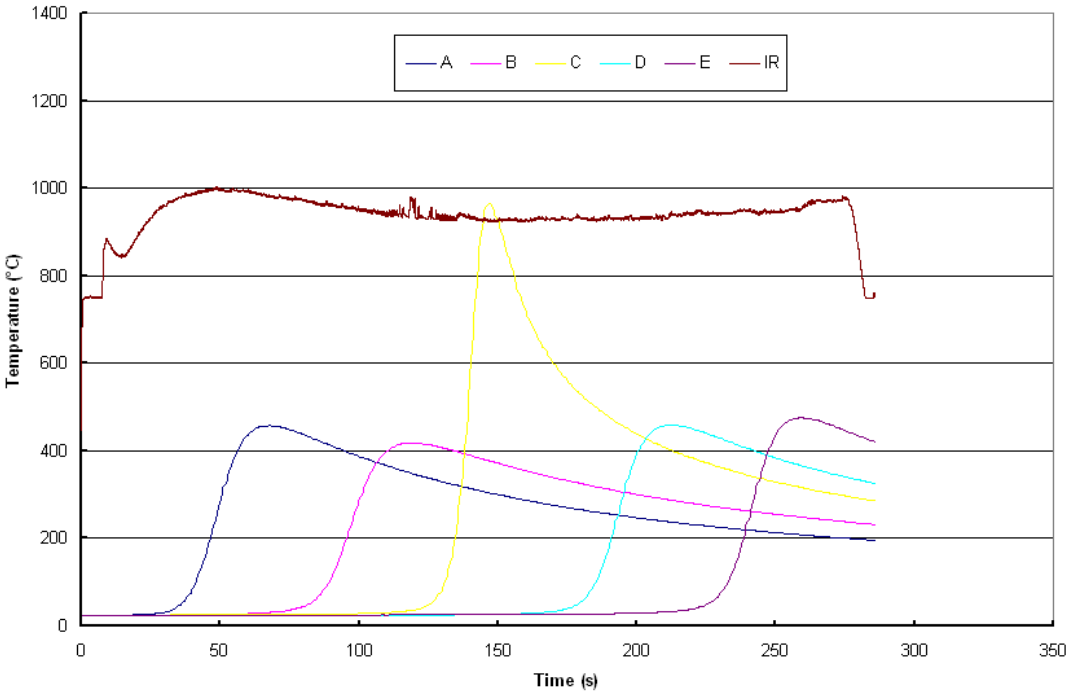

Figure H-43. Trial 50

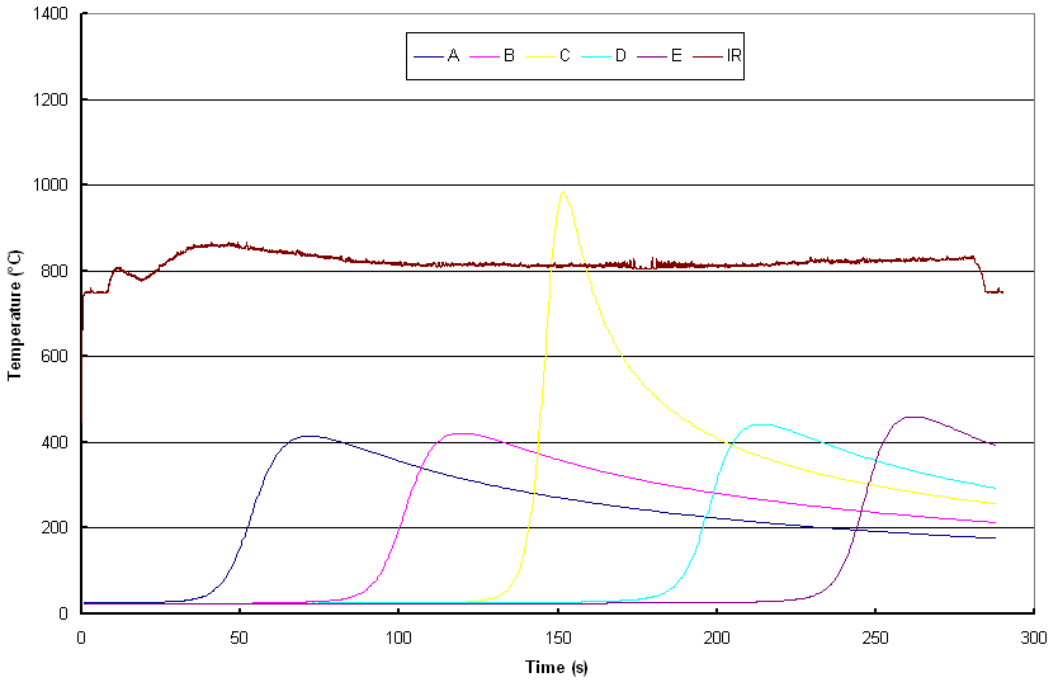

Figure H-44. Trial 51

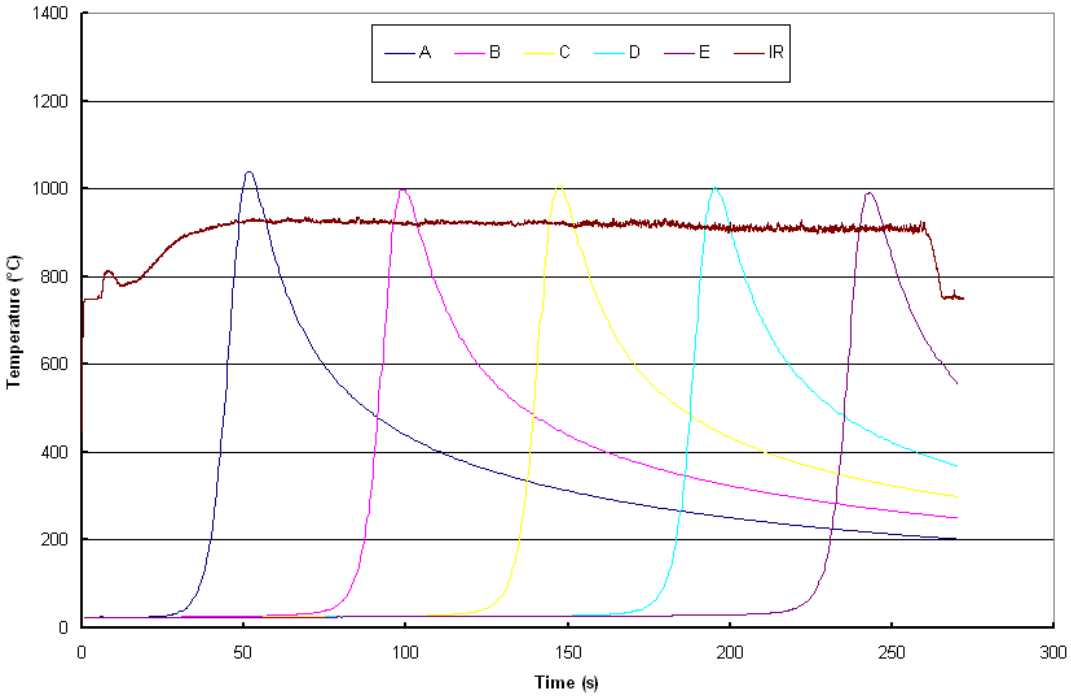

Figure H-45. Trial 52

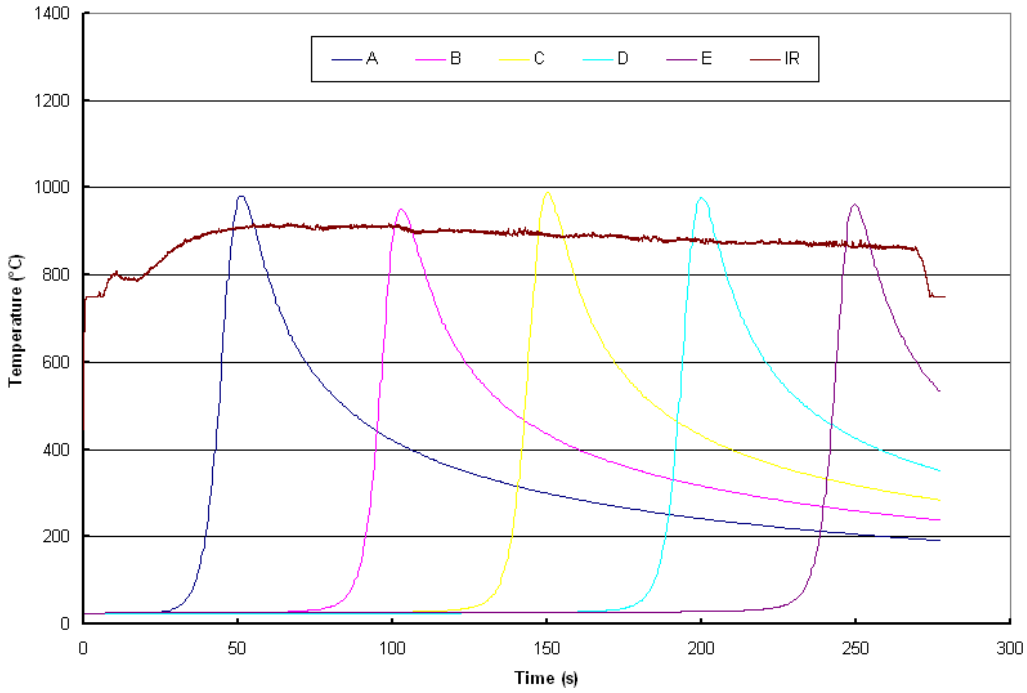

Figure H-46. Trial 53

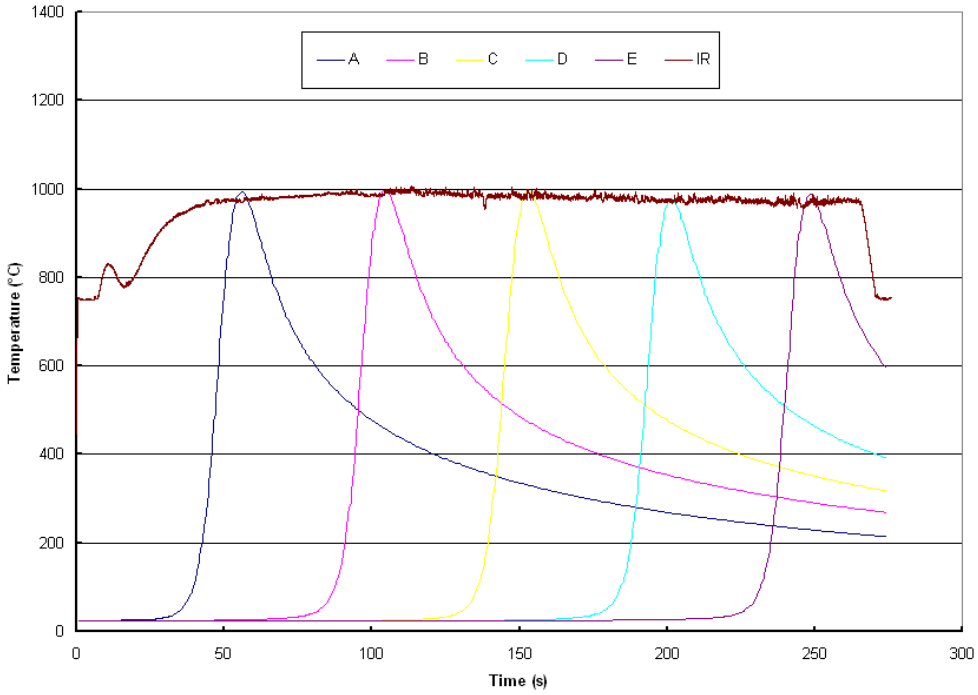

Figure H-47. Trial 54

54

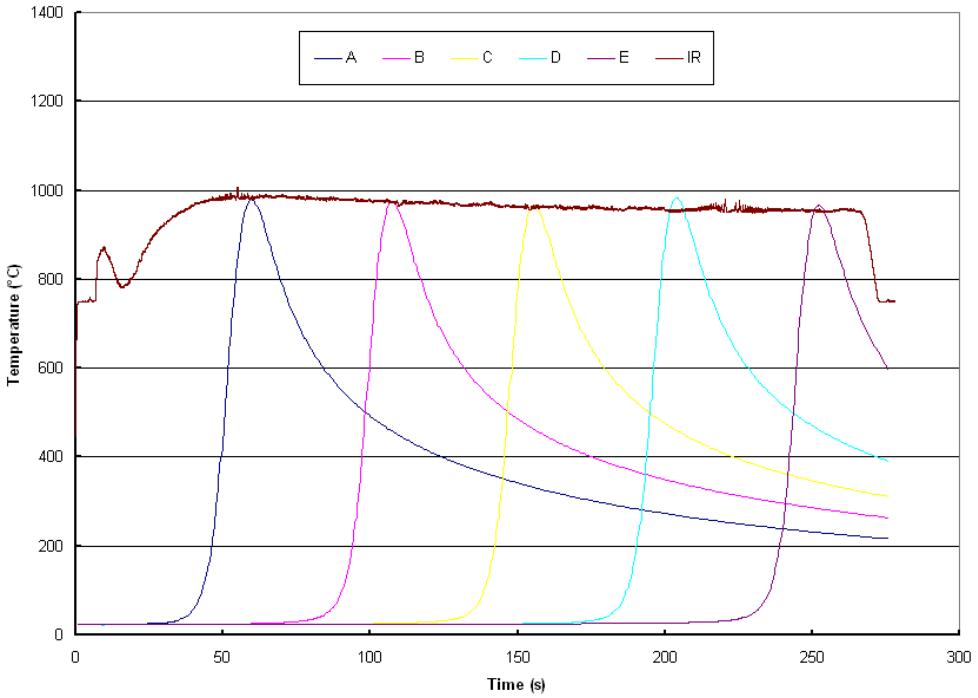

Figure H-48. Trial 55

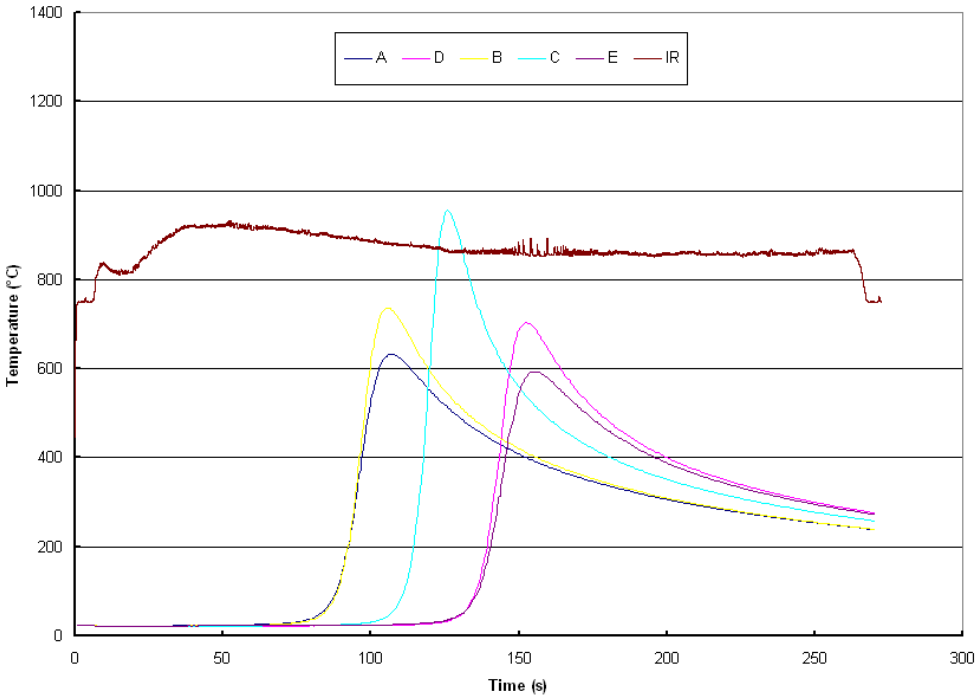

Figure H-49. Trial 56

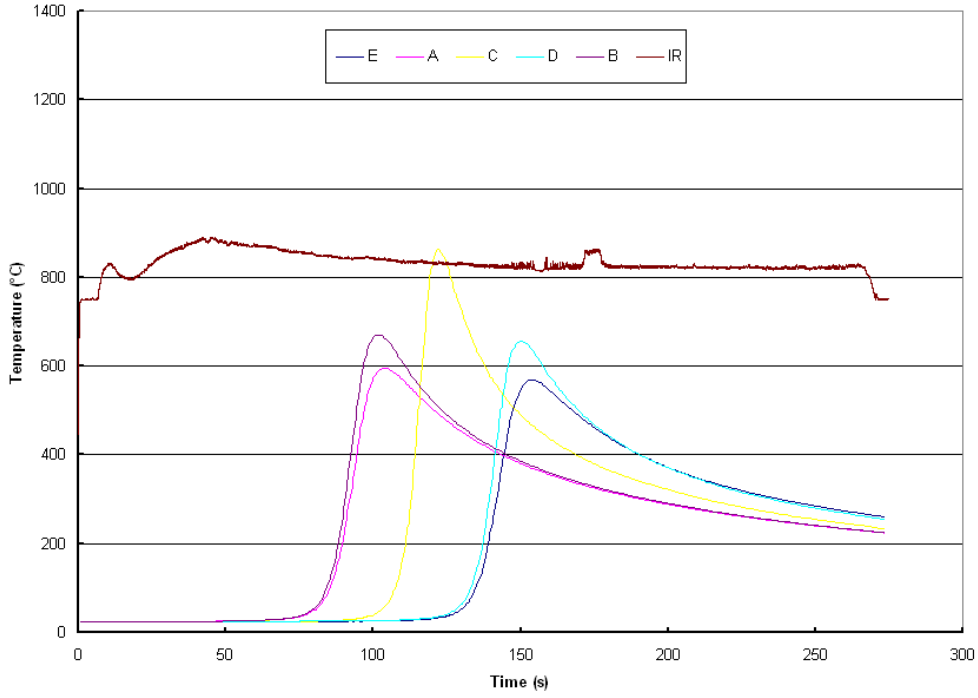

Figure H-50. Trial 57

57

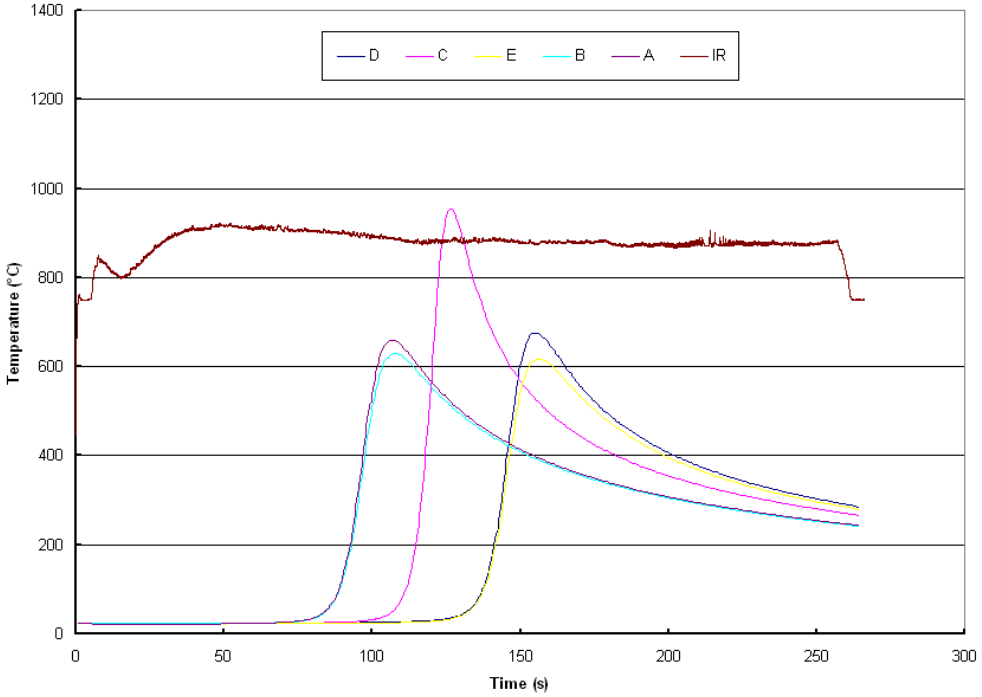

Figure H-51. Trial 58

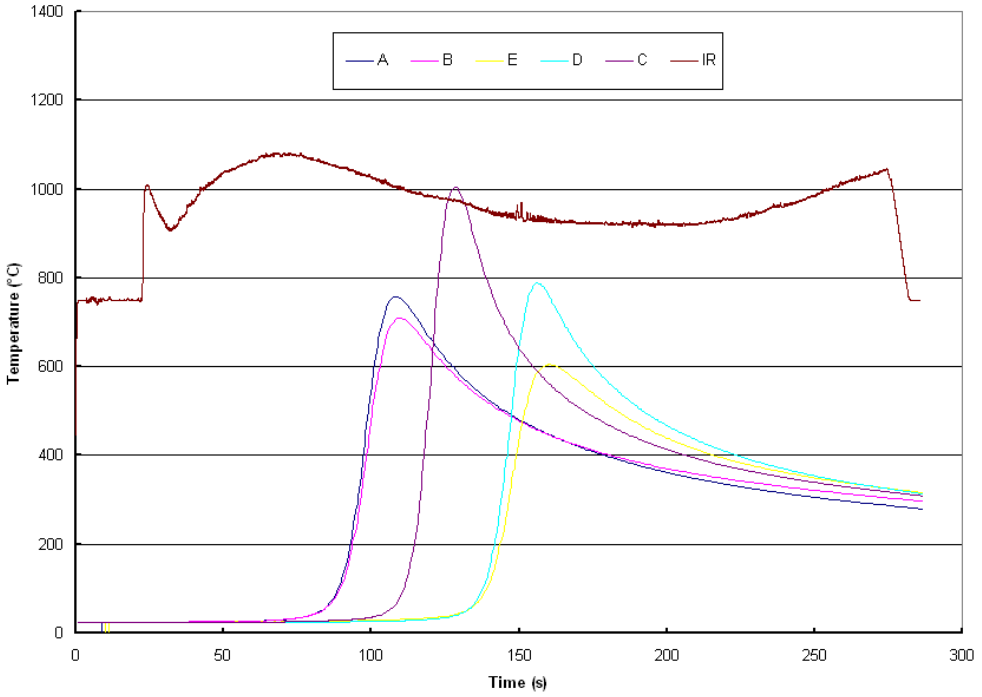

Figure H-52. Trial 59

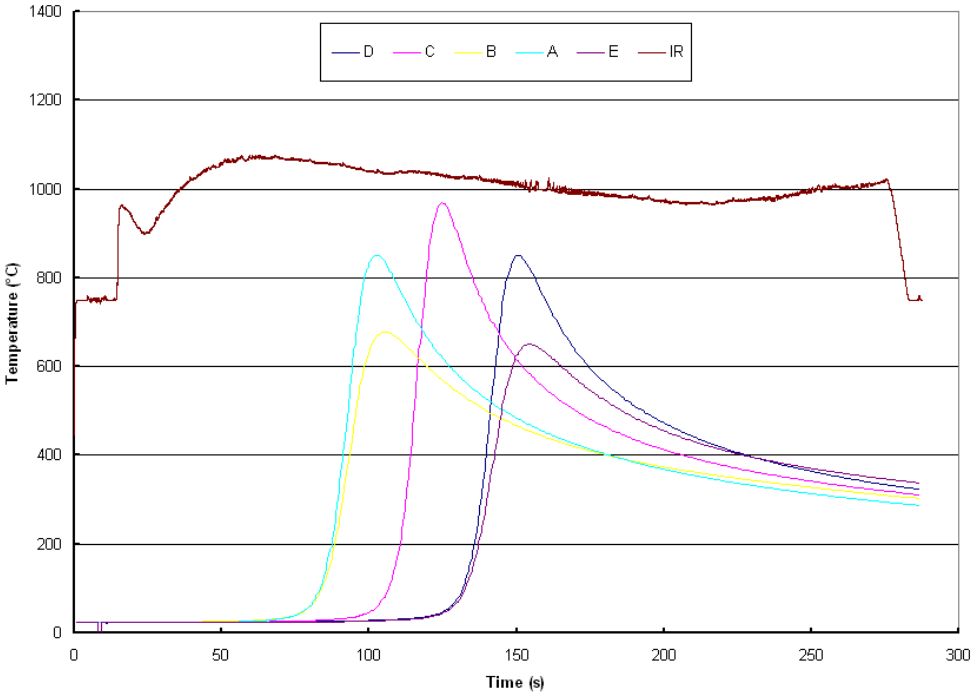

Figure H-53. Trial 60

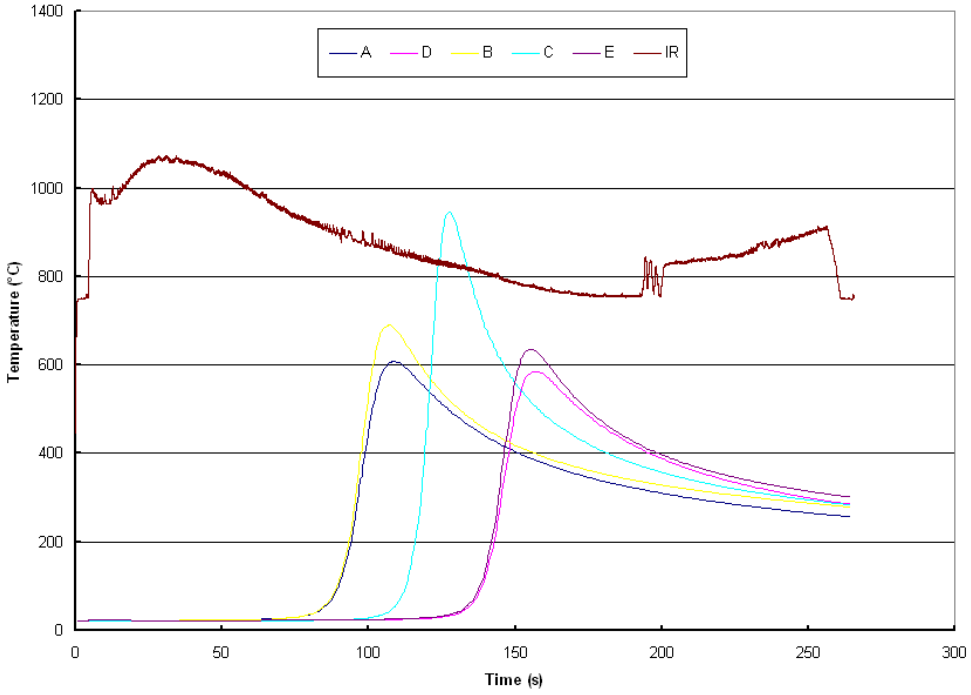

Figure H-54. Trial 61

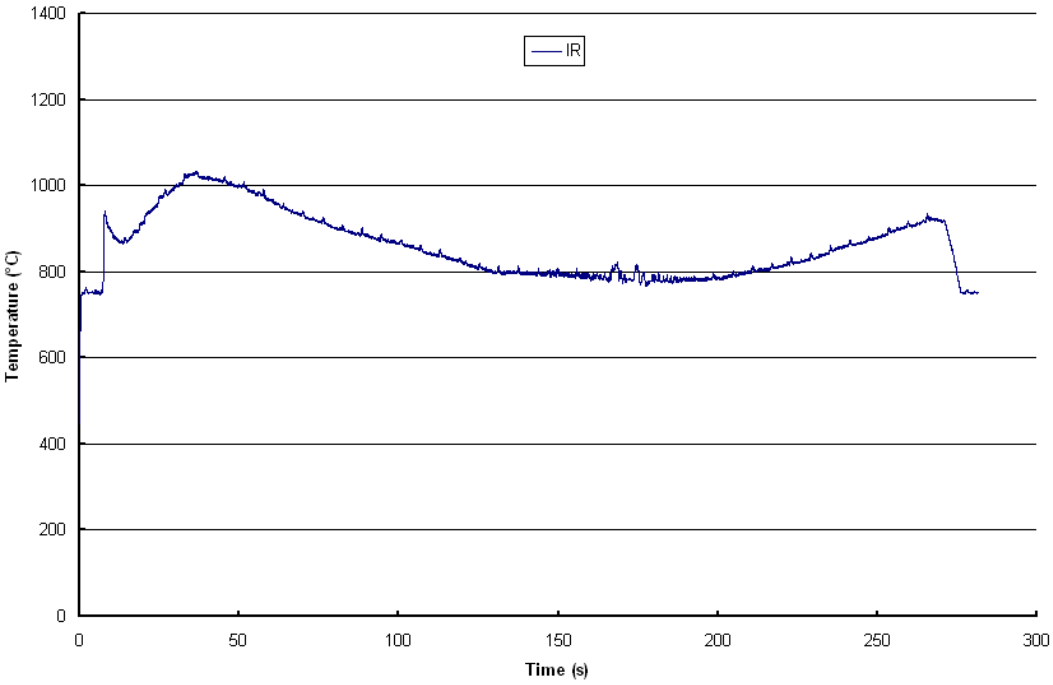

Figure H-55. Trial 62

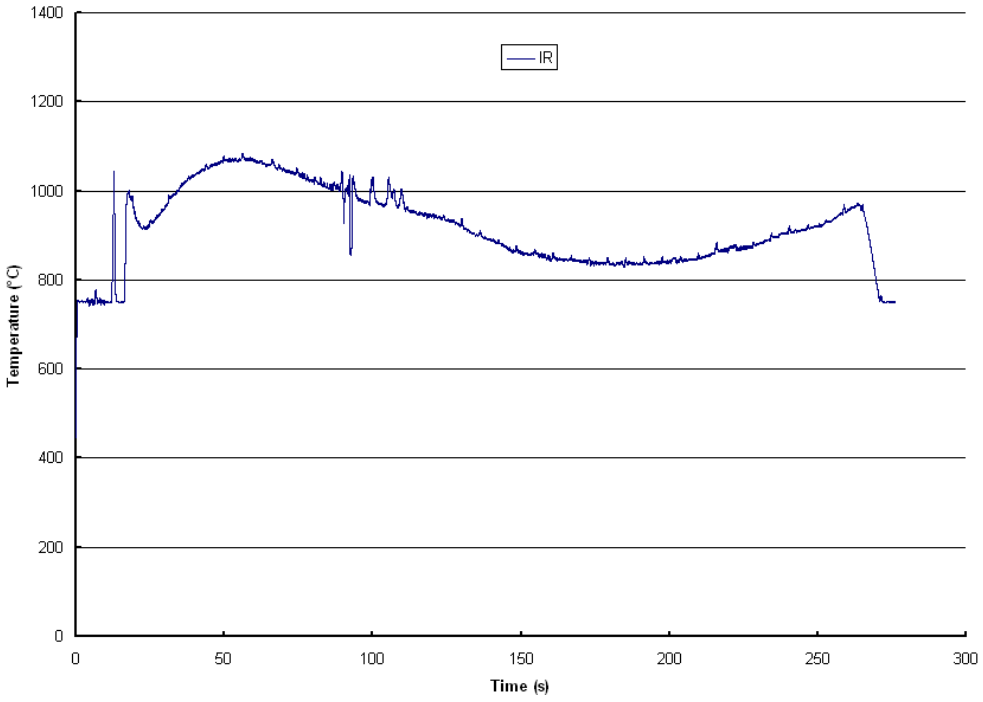

Figure H-56. Trial 63

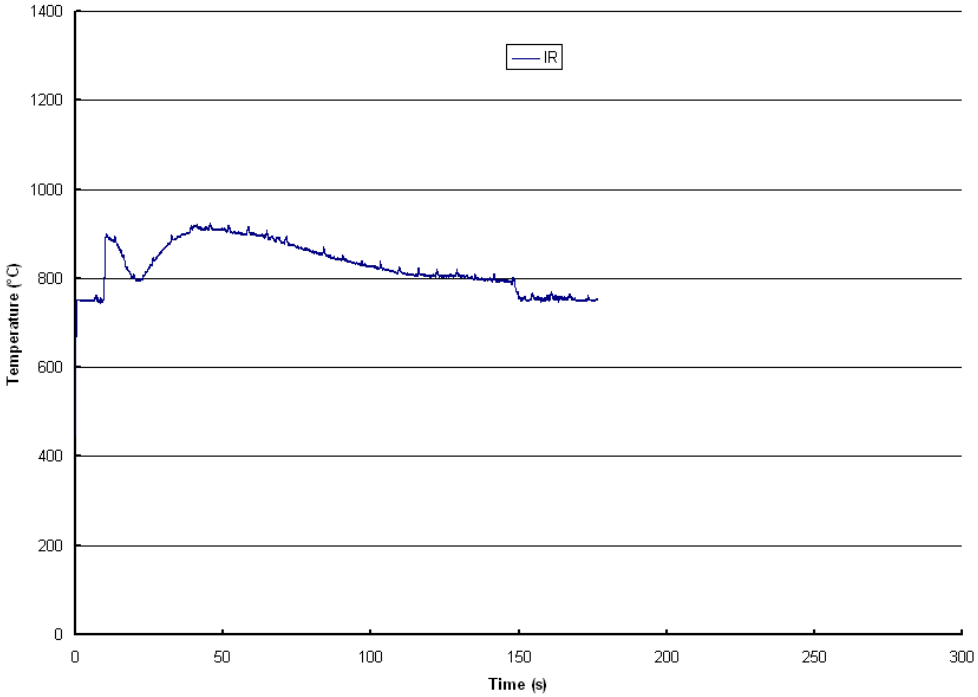

Figure H-57. Trial 64